The Interaction between Soil and Buried Bent Pipelines

by

Junaid Abdul Wahid Siddiqui

A Thesis Presented to the

FACULTY OF THE COLLEGE OF GRADUATE STUDIES

KING FAHD UNIVERSITY OF PETROLEUM & MINERALS

DHAHRAN, SAUDI ARABIA

In Partial Fulfillment of the
Requirements for the Degree of

MASTER OF SCIENCE

In

CIVIL ENGINEERING

May, 2000

INFORMATION TO USERS

This manuscript has been reproduced from the microfilm master. UMI films the text directly from the original or copy submitted. Thus, some thesis and dissertation copies are in typewriter face, while others may be from any type of computer printer.

The quality of this reproduction is dependent upon the quality of the copy submitted. Broken or indistinct print, colored or poor quality illustrations and photographs, print bleedthrough, substandard margins, and improper alignment can adversely affect reproduction.

In the unlikely event that the author did not send UMI a complete manuscript and there are missing pages, these will be noted. Also, if unauthorized copyright material had to be removed, a note will indicate the deletion.

Oversize materials (e.g., maps, drawings, charts) are reproduced by sectioning the original, beginning at the upper left-hand corner and continuing from left to right in equal sections with small overlaps.

Photographs included in the original manuscript have been reproduced xerographically in this copy. Higher quality 6" x 9" black and white photographic prints are available for any photographs or illustrations appearing in this copy for an additional charge. Contact UMI directly to order.

Bell & Howell Information and Learning
300 North Zeeb Road, Ann Arbor, MI 48106-1346 USA
800-521-0600

UMI®

THE INTERACTION BETWEEN SOIL AND BURIED BENT PIPELINES

BY

JUNAID ABDUL WAHID SIDDIQUI

A Thesis Presented to the

DEANSHIP OF GRADUATE STUDIES

KING FAHD UNIVERSITY OF PETROLEUM & MINERALS

DHAHRAN, SAUDI ARABIA

In Partial Fulfillment of the
Requirements for the Degree of

MASTER OF SCIENCE

In

CIVIL ENGINEERING

MAY 2000

KING FAHD UNIVERSITY OF PETROLEUM AND MINERALS
DHAHRAN 31261, SAUDI ARABIA

DEANSHIP OF GRADUATE STUDIES

This thesis, written by

JUNAID ABDUL WAHID SIDDIQUI

under the direction of his Thesis Advisor and approved by his Thesis Committee, has been presented to and accepted by the Dean of Graduate Studies, in partial fulfillment of the requirements for the degree of

MASTER OF SCIENCE IN CIVIL ENGINEERING.

THESIS COMMITTEE:

16-2-1421
20-5-2000
Dr. Hamdan N. Al-Ghamedy, Chariman

Prof. Dr. Sahal N. Abduljauwad, Co-Chairman

Dr. Naser A. Al-Shayea, Member

Dr. Ibrahim M. K. Asi, Member

5-20-2000
Chairman, Civil Engineering Department

Dean of Graduate Studies

DEANSHIP OF GRADUATE STUDIES

Date: 21/5/2000

To my Late **MOTHER**

who is the source of my spiritual strength

ACKNOWLEDGEMENTS

I am most grateful to **ALLAH** the Almighty for providing me this opportunity and giving me the strength and capability to complete this task. All praise for ***Prophet Mohammad*** (peace be upon him) who guided us to the right path.

Acknowledgments are due to King Fahd University of Petroleum and Minerals for providing the support for this work. This work is part of an extensive study on buried pipelines carried out at the Civil Engineering Department and sponsored by the Saudi Arabian Oil Company (Saudi Aramco).

I am greatly indebted to my major advisor Dr. Hamdan Al-Ghamedy for his careful guidance, constructive criticism and generous time throughout the work. I always found him ready to help me whenever I needed it. I am grateful to the co-chairman of the committee Dr. Sahal Abduljauwad for his advice and great interest throughout the work. I would also like to express my appreciation for the committee members Dr Naser Al-Shayea and Dr. Ibrahim Asi for their comments and careful review of the thesis.

The companionship of Rashid Bashir during the work is something invaluable for me. It helped me a lot during the work. I am also appreciative of Mohammad Balah whose tips passed me through at a number of occasions, when I was stuck at some point.

I would like to express my profound gratitude to my parents for their love, affection, and sacrifices, which made this mark possible. I am also thankful to my wife who was behind me all the time and showed a remarkable level of understanding and patience.

I would also like to thank all my fellow students at the department and at KFUPM as a whole, which include Zaki Siddiqui, Noman Zaheer, and, a number of others. They were the source of great moral support for me during my stay at the university.

TABLE OF CONTENTS

LIST OF TABLES

LIST OF FIGURES

THESIS ABSTRACT

THE INTERACTION BETWEEN SOIL AND BURIED BENT PIPELINES

Temperature variation, Poisson's effect of internal pressure, and differential settlement may cause significant longitudinal forces in the buried pipelines. A pipeline bend moves in the transverse direction due to these longitudinal loads. The confining soil resists the transverse movement of the bend. The strength of soil is therefore important to keep a buried pipe bend structurally safe and adequately restrained against excessive deformation.

The classical methods used for the analysis and design of buried pipe bends have proven to be inadequate in modeling the actual field behavior of the pipe-soil system. Numerical methods based on improved modeling techniques are occasionally used, but their application is limited for the practical purposes because of the effort required in modeling the complex pipe-soil composite system.

The objective of this research is to study the buried pipe bend behavior using the finite element method and then to recommend procedures that may assist in the analysis and design of soil restraint at buried pipe bends. Three-dimensional finite element analyses are carried to investigate the soil strength requirements on the horizontal and vertical buried pipe bends. Tables, graphs and charts are developed using the results of the parametric study. The results are analyzed and the importance of various parameters is discussed.

MASTER OF SCIENCE
King Fahd University of Petroleum and Minerals

Junaid Abdul Wahid Siddiqui
Major Field: Structural Engineering
May 2000

خلاصة الرسالة

التفاعل بين التربة والأنابيب المدفونة والمنحنية

إن تغـــيرات الحرارة والتأثير الجانبي للضغط الداخلي والهبوط المتفاوت من الممكن أن تتسبب في نشؤ قـــوى طوليـــة مهمة في الأنابيب المدفونة. إن الأنابيب المنحنية تتحرك في الاتجاه العرضي نتيجة لتلك القـــوى الطوليـــة. كما أن التربة المحيطة بالأنبوب تقاوم الحركة العرضية للانحناء. لذلك فإن قوة التربة مهمة في حفظ سلامة الأنابيب المنحنية والمدفونة إنشائيا وتقييده ضد التشوهات المفرطة.

إن الطـــرق التقـــليدية المستخدمة في تحليل وتصميم الأنابيب المنحنية والمدفونة أثبتت أنها غير كافية في محاكـــاة الســـلوك الحقـــلي لـــنظام التربة والأنبوب. إن الطرق العددية المبنية على تقنية محاكاة محسنة تســـتخدم أحيانـــا، لكن تطبيقاتها محدودة في التطبيقات العملية وذلك بسبب الجهد المطلوب في محاكاة النظام المركب للتربة والأنبوب.

أن الغـــرض مـــن هـــذا البحث هو دراسة سلوك الأنابيب المنحنية والمدفونة باستخدام طريقة الأجزاء المحـــدودة، ومن ثم اقتراح إجرآت من الممكن أن تسهم في تحليل وتصميم تقييد التربة المحيطة بالأنابيب المنحـــنية والمدفونة. لقد تم استخدام برنامج العناصر المحدودة الثلاثية الأبعاد لبحث متطلبات قوة التربة عـــلى الانحناءات العمودية والأفقية للأنابيب المدفونة. لقد تم تبويب النتائج المحصلة من هذه الدراسة في جداول ورسومات بيانية. كما تم تحليل ومناقشة هذه النتائج لبيان أهمية كافة العناصر.

درجة الماجستير في العلوم

جامعة الملك فهد للبترول المعادن

جنيد عبدالواحد صديقي

مجال التخصص : هندسة الإنشآت

مايو ٢٠٠٠

CHAPTER 1
INTRODUCTION

1.1 Overview

The prime media of transporting fluids are pipelines. Pipelines that are used to transport a fluid between two distant stations usually run underground through most of their length. These pipelines are used to transport water, petroleum, natural gas and several other fluids. Pipelines are also used as utility corridors. The loading on these pipelines depends on the installation technique, site conditions and the intended use. The load to be resisted by a buried pipe is shared by both the pipe and the surrounding soil depending on the ratio of the stiffnesses of the two components.

Field conditions usually do not allow straight pipeline routes. Horizontal and vertical bends are, therefore, provided to run a pipeline along any given route. The structural behavior of an underground pipeline at these bends is quite different from that within its straight sections. In certain loading cases, such as temperature change, longitudinal forces are developed along a pipeline; and these forces are resisted by lateral earth pressure at a bend section (Figure 1-1). Curved geometry, therefore, causes a buried pipe bend to respond to such a load so that it moves laterally against the soil. This movement of a pipe against soil may cause failure of the soil cover.

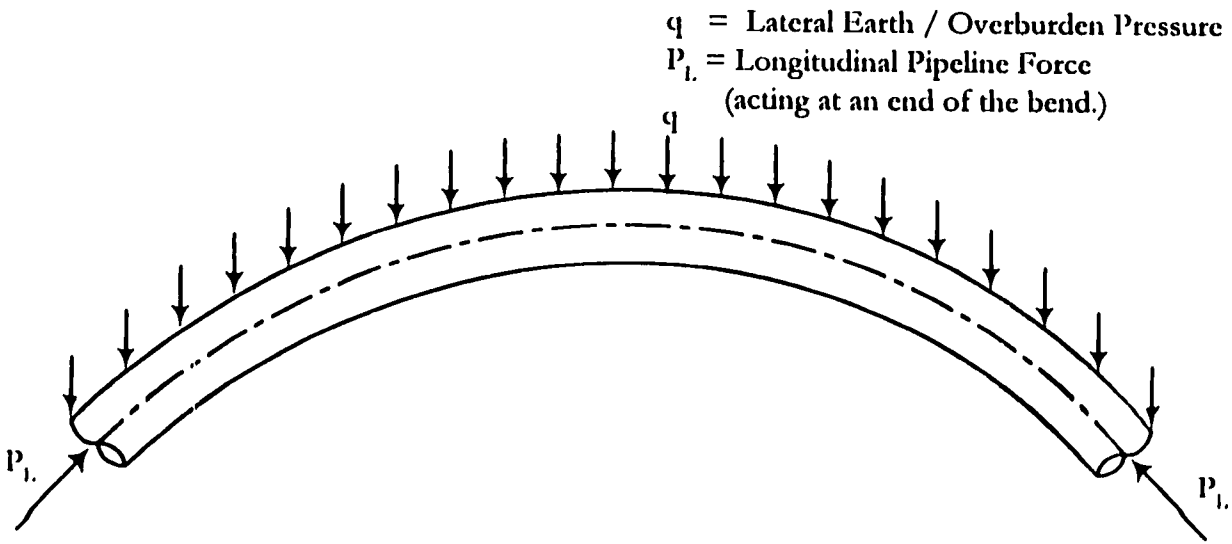

Figure 1-1 Lateral / overburden earth pressure resists buried pipe bend movement

The restraint provided by the soil at a bend is vital for the integrity and serviceability of a pipeline. Therefore, it is important to study the requirements of soil covers over buried pipe bends for their adequate restraint against excessive deformation.

1.2 Mechanics of Buried Pipe Bends

Gravity and surface loads at a buried pipe bend do not create significant longitudinal stresses if the pipe is installed carefully such that the bedding provides a continuous support to the pipe. The structural response of a buried pipe under such vertical loads is primarily two-dimensional in nature. As pointed out by Watkins (1985), the analysis and design of a buried pipe for these loading conditions is directed towards ring performance, i.e. radial and circumferential stresses, strains and deflection of a two-dimensional transverse cross-section.

In the case of restrained buried pipelines, i.e., pipelines with welded joints, the change in the temperature may cause significant longitudinal deformations. This deformation is counter-acted by the pipe-soil friction along a straight pipe, the weight of the pipe and its contents, and by lateral soil pressure at a pipe bend. At a horizontal bend, gravity loads act in the vertical plane, while lateral earth pressure acts along a horizontal plane. The displacement field generated by the movement of a vertical bend lies in a vertical transverse plane while the structural response of the bend itself is in the longitudinal direction. The response of a buried pipe bend system is therefore three-dimensional with respect to both geometry and loading.

1.2.1 Buried pipe cross-sectional response under vertical loads

The pipe-soil structural system is a statically indeterminate nonlinear problem in which the pressure of the soil on the pipe produces deflections that in turn determine the soil pressure. Therefore, the load imposed on a pipe buried in the soil depends on the ratio of the stiffness of both pipe and soil.

The term *arching* is used for the phenomenon of load transfer between pipe and soil. Arching is considered as the transfer of load to or away from a buried structure as a result of the difference in stiffness properties of the structure with its surrounding soil. Although several expressions have been proposed to quantify the arching, one of the simple expressions quantifying arching is,

$$A = 1 - \frac{p_i}{p_v} \qquad (1\text{-}1)$$

Where, A is arching factor,

p_i is the vertical pressure on a buried pipe at the crown,

p_v is the free-field vertical stress at the elevation of the pipe crown = γH_c,

γ is the unit weight of the soil, and

H_c is depth of the pipe crown below ground surface.

If the deformation characteristics of the pipe are the same as those of the soil, then $p_i = p_v$ and $A = 0$, which is a state of no arching. If the pipe is not as stiff as the soil

then $A > 0$ and arching is said to be positive. Conversely, if the pipe is stiffer than the soil then $A < 0$ and the arching is negative.

Pipes are usually broadly classified as either 'rigid' or 'flexible'. In general, all underground pipes support the load applied on them by two sources: first, the inherent strength of the pipe ring; second, the lateral pressure of the soil at the sides of the pipe ring. A rigid pipe may be defined as the one, which under its maximum load, does not deform sufficiently to produce a significant amount of passive restraint at the sides from the soil, and basically relies on the inherent strength of the pipe ring to resist the applied load. A flexible pipe, on the other hand, has relatively little inherent strength and its sides deform outward under external load to such an extent that lateral passive soil pressure is mobilized (Figure 1-2). This lateral pressure enables the pipe to resist the external loads. The high stiffness of rigid pipes therefore results in negative arching while the low ring stiffness of the flexible pipes result in the positive arching state of stress in the surrounding soil.

1.2.2 Behavior of pipe bends

A pipe bend subjected to end moments is shown in Figure 1-3(a). It is said to be in the state of positive bending if the direction of end moments is such that it cause the bend to become more sharply curved. Conversely, for negative bending the bend becomes less sharply curved (straightens). The circular cross-section of the pipe along the bend deforms into an oval shape in response to the end moments. In the case of positive bending, the section deforms such that the major axis of the elliptical

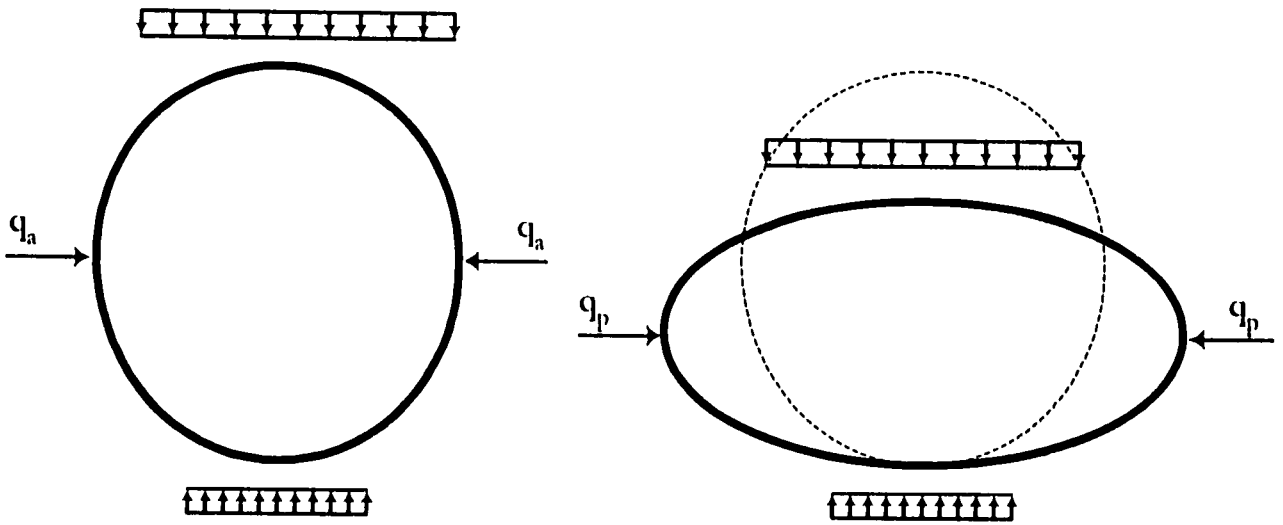

Figure 1-2 Sides of a flexible pipe deform outward to an extent to mobilize passive earth pressure.

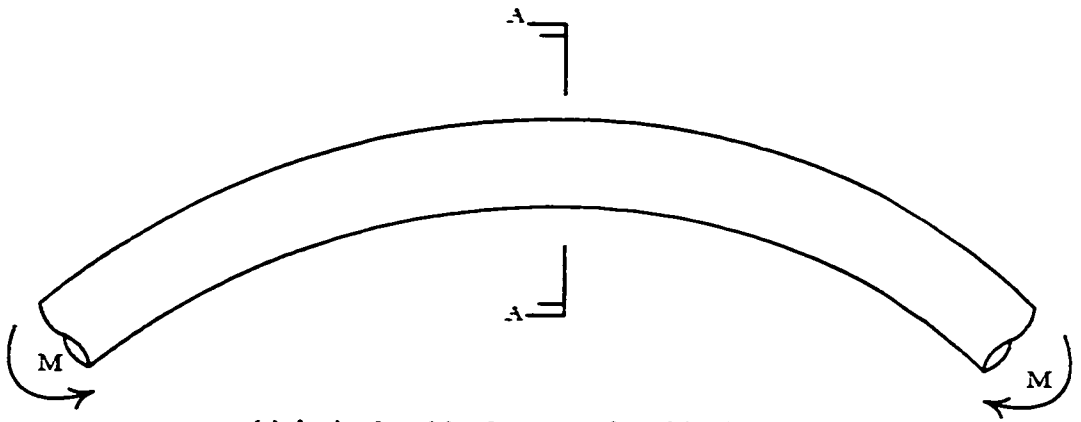

(a) A pipe bend in the state of positive bending

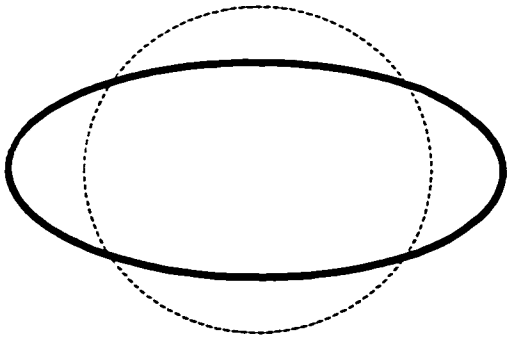

(b) Ovalization of Section -AA under positive bending

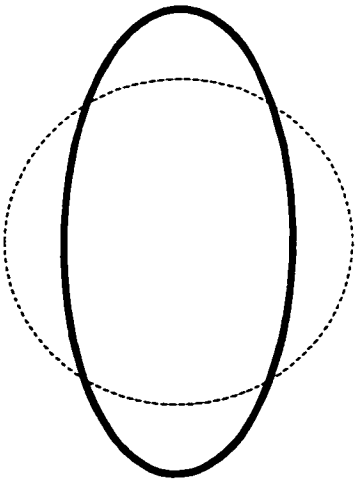

(c) Ovalization of Section -AA under negative bending

Figure 1-3 Pipe bend with end moments

deformed shape lies out of the plane of the bend, while in the case of negative bending the major axis lies in the plane of the bend as shown in Figure 1-3(b & c).

As a result of the ovalization, the flexibility of the bend changes. For positive bending the flexural stiffness of the bend decreases with the increasing ovalization, while for negative bending the flexural stiffness increases with increasing ovalization and bending moment (Gresnight and van Foeken, 1995). In pipe design codes such as ASME B31.4 (1992), this geometrically non-linear flexural behavior of a pipe bend is recognized by the use of the terms *flexibility factor* (k) and *stress intensification factor* (i). The flexibility factor is defined as the ratio of the flexural rigidity of a straight pipe to the flexural rigidity of a smooth pipe bend of the same length and cross-section. The stress intensification factor is the ratio of the maximum stress in a smooth pipe bend to the maximum stress in a straight pipe subjected to the same bending moment as that on the bend. The moment for this purpose is determined by the simple beam theory. If EI is the flexural rigidity of a straight pipe then for the whole length of a pipe bend of the same section the flexural rigidity is EI/k (Hose and Kitching, 1993). This concept thus allows carrying out a geometrically linear analysis of a pipe bend while including the bending ovalization effects using the flexibility and stress intensification factors.

The internal pressure in a straight pipe is globally self-equilibrating and does not produce any unbalanced force on the pipe. The change in the direction at a bend

however results in an unbalanced force due to the internal pressure as shown in Figure 1-4. In unrestrained buried pipelines, i.e., pipelines with expansion joints, thrust blocks are provided at a bend to resist the pressure thrust force. The thrust force in restrained pipelines is however resisted by the pipe-soil friction and thrust block is usually not required.

1.2.3 Longitudinal forces along a straight buried pipe

There are several possible reasons for the longitudinal stresses in a pipeline. They include the beam bending of the pipe when the pipe is not continuously supported on the bedding because of the hard or high spots in the bedding. However the stresses caused by beam bending of the pipe can be reduced considerably by proper installation of the pipe so that the pipe is supported continuously on its bedding and thus the beam bending of a pipe is neglected in the design.

Temperature change causes the pipe to contract or expand. This movement is resisted by the pipe-soil friction and thus results in the generation of longitudinal stresses in the pipe. The longitudinal stresses induced by temperature change can be significant in a restrained pipe. The temperature stress in the longitudinal direction of a fully restrained pipe, σ_T, can be calculated by the equation;

$$\sigma_T = E \alpha \Delta T \qquad (1\text{-}2)$$

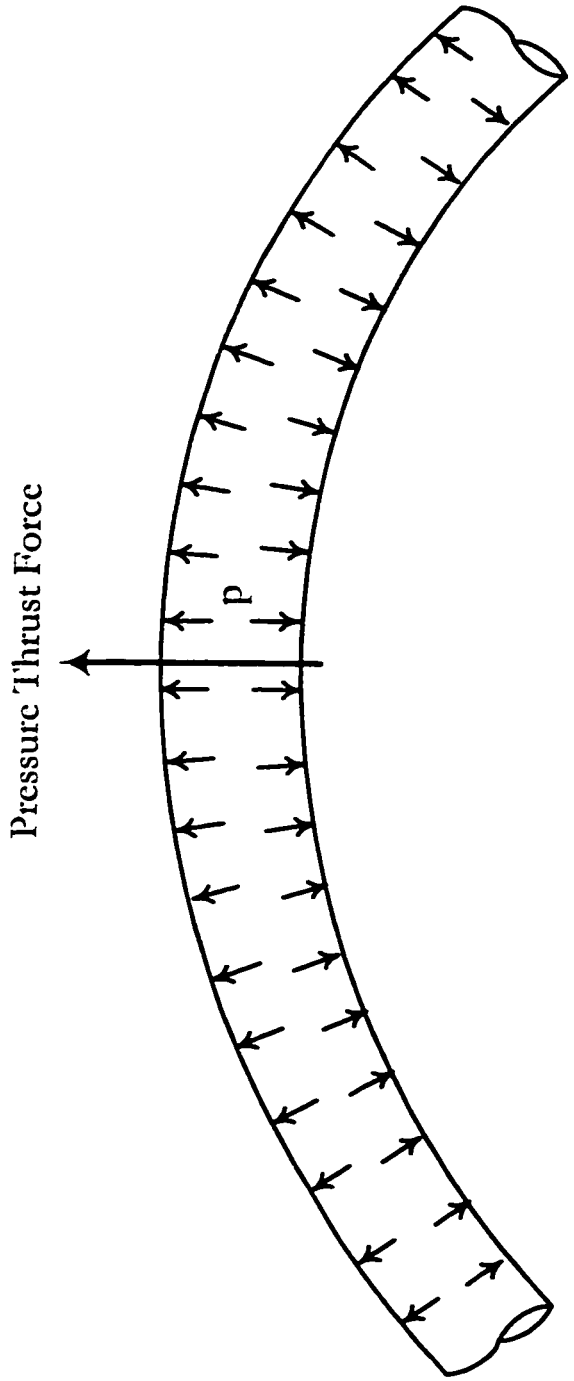

Figure 1-4 Pressure thrust at a pipe bend

Where, σ_T is the temperature stress taken positive in compression.

E is the modulus of elasticity of the pipe material,

α is the coefficient of thermal expansion of the pipe material, and

ΔT is temperature change.

The restrained pipe is also subjected to the longitudinal tensile stress due to internal pressure. When a pipe is inflated by the internal pressure it results in the reduction of the pipe length by the Poisson's ratio effect. The longitudinal stress thus induced in a restrained pipe is often called the Poisson's effect. It can be obtained by multiplying the circumferential stress due to internal pressure obtained using Barlow's formula with the Poisson's ratio, and thus can be expressed as:

$$\sigma_p = -\frac{\nu p r}{t} \tag{1-3}$$

Where, p is the pipe internal pressure,

ν is the Poisson's ratio of the pipe material,

r is the radius of pipe, and

t is the thickness of the pipe wall.

The friction at the pipe-soil interface causes the passive resistance of soil to the axial movement of a pipe. The friction is a function of the confining pressure and the coefficient of friction between the pipe and the backfill material. Friction forces exist only where there is actually or impending slippage between the pipe and the soil. The

maximum friction force per unit length of a pipe, *f*, can be calculated by the equation:

$$f = \mu(W_s + W_p) \tag{1-4}$$

Where, μ is the coefficient of friction between the soil and the pipe material,

W_p, is the weight of a pipe and its contents per unit length of the pipe, and

W_s, is the earth load per unit length carried by a pipe.

1.2.4 Buried pipe bend system

A typical buried pipe bend is shown in Figure 1-5. The bend has a radius R_b and an angle θ. When a straight pipe connected to a bend expands under temperature change, it causes the bend apex to move laterally. This results in the longitudinal movement of the straight pipe relative to the soil that is resisted by the friction between pipe and soil. The maximum value of pipe-soil friction force, *f*, within the length can be expressed by Equation 1-4. The maximum longitudinal movement along the straight portion of the pipeline occurs where it is connected to the bend. The movement reduces further ahead on the straight pipe due to pipe-soil friction up to a point beyond which there is no movement of the pipe relative to soil. This point is called the *virtual anchor*. The presence of a bend thus has an effect on a length of straight pipe up to the virtual anchor and this length must be included in the analysis of a buried pipe bend. The pipe beyond the virtual anchor is fully restrained, and the

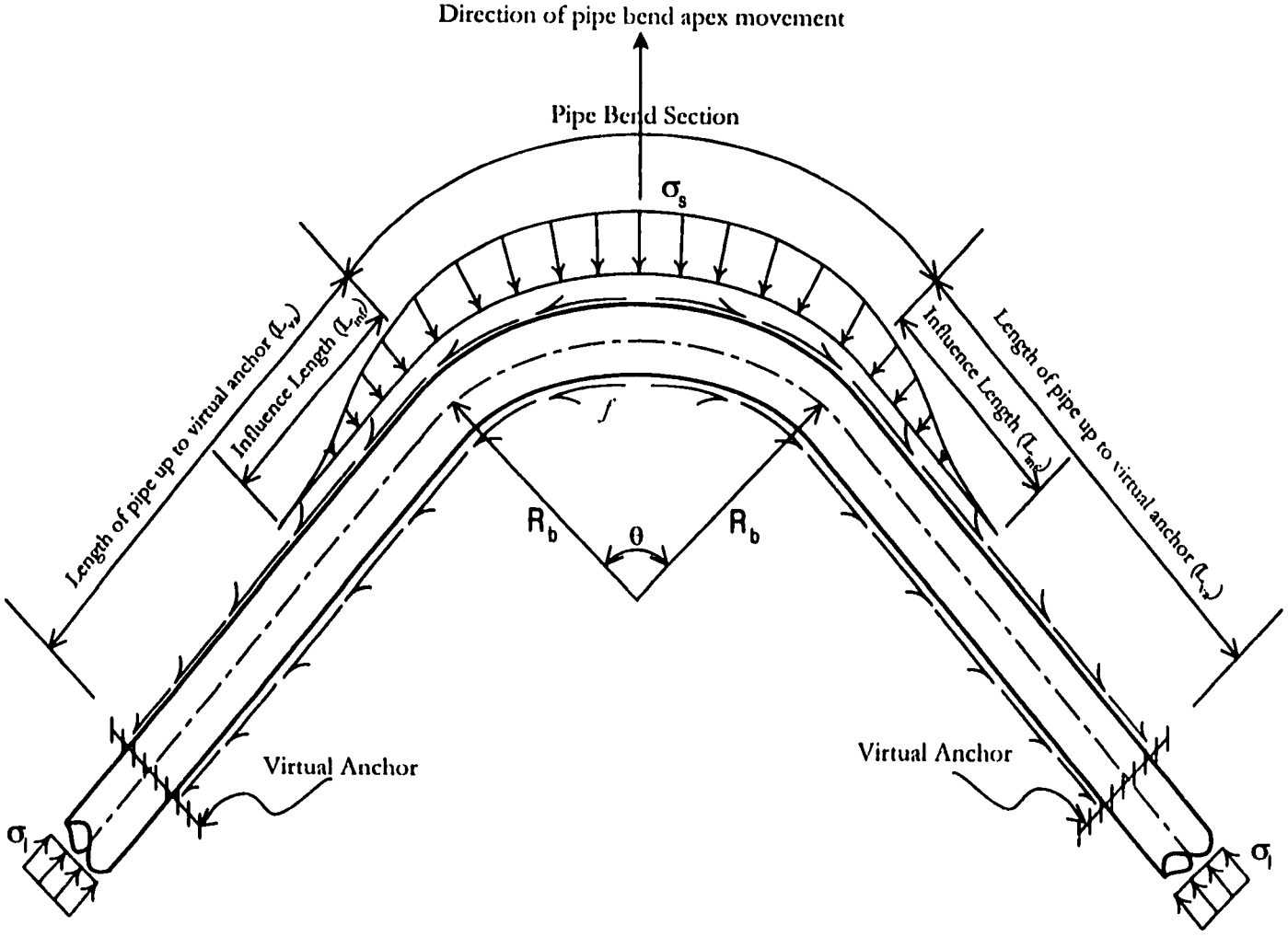

Figure 1-5 Soil forces developed at a typical buried pipe bend in response to the longitudinal movement of the pipeline

longitudinal stress (σ_l) within this fully restrained length can be expressed by adding Equation (1-2) and Equation (1-3), which gives:

$$\sigma_l = E\alpha\Delta T - \frac{\nu pr}{t} \qquad (1\text{-}5)$$

The lateral/uplift movement of a horizontal/vertical pipe bend is resisted by the passive/overburden soil pressure σ , as shown in Figure 1-5. At a buried vertical bend the vertical movement of the bend apex is resisted by the weight of the soil cover and the shear strength of the soil as shown in Figure 1-6(a). In the case of a horizontal bend the pipe moves laterally in a horizontal direction. The passive soil pressure and the shear strength of the soil resist this movement. When a buried pipe is moved horizontally, the soil displacement field around the pipe causes it to move in an upward direction as shown in Figure 1-6(b). The movement of a buried pipe is also counteracted by the weight of the pipe and its contents along with the resistance given by the soil.

In addition to the bend, a length of the straight pipe also moves transversely relative to the soil and this length is called the *influence length* as shown in Figure 1-5. The lateral movement along the influence length is caused by the in-plane bending moment transferred by the bend to the straight pipe. This length is equal to $\frac{3\pi}{4\beta}$, the length at which the hyperbolic function given by Hetenyi (1964) approaches to unity.

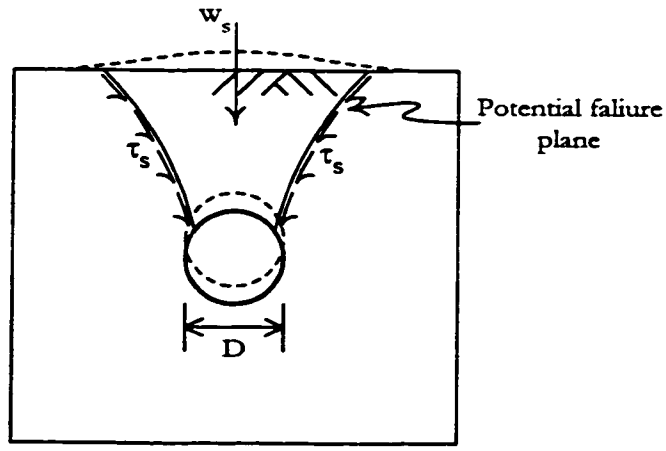

(a) Pipe moving up relative to the soil

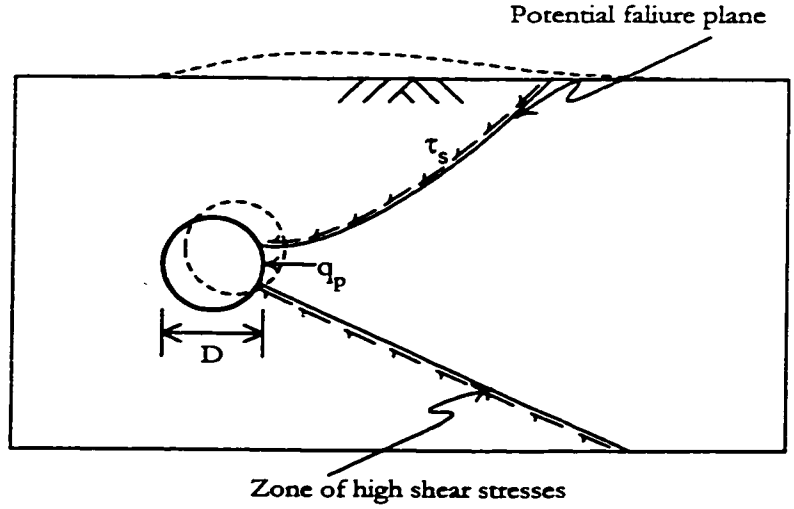

(b) Pipe moving horizontally relative to the soil

Figure 1-6 Soil reaction against movement of buried pipe

Here β is a parameter that depends on the modulus of subgrade reaction and the pipe stiffness.

The buried pipe bend structural system thus consists of a pipe bend with some length of straight pipe connected at each of its ends. The other end of the straight pipe section is constrained against longitudinal movement. The passive lateral and frictional soil force along with the weight of the pipe and its contents resist the thermal deformation of the system.

1.3 Problem Statement

Temperature variation and Poisson's effect of internal pressure may cause significant longitudinal deformations in restrained buried pipelines. The earth pressure of the confining soil at a bend contributes in resisting this longitudinal movement. The strength of soil is therefore important to keep a buried pipe bend adequately restrained against excessive deformation.

Methods based on classical theories are currently being used for the analysis and design of soil restraint at a buried pipe bend. For example in one approach, forces acting at the ends of a bend are projected at a plane parallel to the chord of the bend and this distributed load is compared with the passive earth pressure that may develop at that soil depth. Approaches like this have, however, proven to be inadequate in modeling the actual field behavior of the pipe-soil system. Because of this low level of confidence, these approaches may lead to a very conservative

design, which increases the cost. Numerical methods based on improved modeling techniques are occasionally used, but their application is limited for practical purposes because of the effort required in modeling the complex pipe-soil composite system.

A great deal of research has been carried out that has allowed better modeling of the structural systems like buried pipelines. The finite element method (FEM) is a method that has proven to be capable of modeling buried pipelines satisfactorily. The soil strength requirement on the horizontal and vertical buried pipe bends is investigated in this study using the three-dimensional finite element analyses. It also helped in improving the understanding of the structural behavior of buried pipe bends.

1.4 Objectives

The primary objective of this research is to study buried pipe-bend behavior using suitable finite element software and then to recommend procedures that may assist in the analysis and design of soil restraint at buried pipe bends. The specific objectives of this research are as follows:

- Review the literature, published to date, related to the structural behavior of buried pipe bends.

- Set up and validate a FEM model that is capable of modeling vertical and horizontal buried pipe bend systems.

- Carry out the analysis of the buried pipe bend system using the FEM model for the various possible combinations of the parameters that influence the behavior of buried pipe bends.

- Develop tables, graphs, and charts using the results obtained by the FEM analysis, to study the relation between various variables. These charts can also be used as design aids.

1.5 Thesis Organization

The thesis is divided into six chapters followed by three appendices. Chapter 1 gives an introduction to the thesis. The mechanics of the pipe-soil system is explained. The various structural phenomena that exist along a pipeline, i.e., the response of a buried pipe under vertical loads, ovalization at a bend, and the longitudinal response of a buried pipe are discussed first. The mechanics of a buried pipe bend system as a whole is then described. The problem statement and the objects of the thesis are also given in Chapter 1.

Chapter 2 presents the review of the literature on the subject. The literature discussed includes the work on the empirical models of the early 20th century to the recent finite element modeling of buried pipes. The work on the modeling of the

longitudinal behavior of buried pipes and the determination of soil spring rates is also discussed

The modeling of buried pipelines using the finite element method is described in Chapter 3. A finite element program called SMAP-3D is used in this study. Its capabilities are discussed and are validated by comparing its results with the results of the published studies and models. Chapter 4 explains the data file preparation process for SMAP-3D and discusses in detail the process of mesh generation for the buried pipe bend systems.

Chapter 5 gives the details of the parametric study of the buried pipe bends. The effects of the various parameters on a buried pipe bend behavior are investigated in the study. The finite element analysis results obtained for different combinations of the parameters are listed in the form of tables. The plots of the results are included and they are discussed in detail. Chapter 6 gives a summary of the work followed by a discussion of the results and the recommendations for further research. The main interest of this work is to study the soil restraint at buried pipe bends. The tables and graphs of the pipeline stresses obtained by the FEM analysis are, therefore, presented in the first two appendices.

The third appendix describes the Microsoft Excel macros, developed to automate the process of data file preparation and post-processing for the finite element analysis.

CHAPTER 2
LITERATURE REVIEW

2.1 General

Buried pipelines are used for many different applications. It includes sewers, drains, water mains, gas-lines, culverts, and for transportation of petroleum products. These kinds of pipelines transport fluids either by gravity or under pressure.

Underground structures of this kind have been found among the earliest examples of the subterranean activities of man. However it has been possible to design a pipeline on a rational basis only from the early years of the 20th century. Anson Marston was among those who began work on the problem. The paper by Marston and Anderson (1913) gave a foundation to the theory of loads on pipes in ditches and studied cement and clay drain tiles and sewer pipes. A series of bulletins was issued from then on, written mostly by Marston. Spangler, a former student of Marston, who wrote the most comprehensive review of this work (1948), carried the work forward. The work of Marston and Spangler provided the basis for the later research. Spangler and Handy (1982) has given a good summary of this work. A great deal of progress has been made since then in understanding the various aspects and behavior of pipe-soil systems and improving the design of buried pipes. Jeyapalan (1990) wrote a good

review of these advances in pipeline material and design. Mouser (1979) and recently Antaki (1997) have also reviewed and summarized the methods used for the analysis of buried pressure piping.

2.2 Strength of the Pipe Ring

The whole study of Marston was focused on rigid pipes because most of the pipes used at that time were of the rigid type. Marston carried out extensive experimental and analytical studies and presented empirical relationships for underground pipe design. Among the many bulletins he published, perhaps the most useful was a review of the theories of external loads on closed conduits (Marston, 1930). His theories are still heavily relied upon for the design and laying of rigid pipes. Both analytical and experimental studies followed the work of Marston.

[illegible] and Dabaghian (1967) considered a rigid circular culvert as a transducer. Hoëg (1968) investigated the magnitude and distribution of static normal stress against horizontal cylinder buried in a homogeneous deposit of dry sand. He carried out laboratory tests and demonstrated the application of mathematical models and the theory of elasticity to identify significant variables and their effects. Dar and Bates (1974) presented a set of equations based on classical theory of elasticity concerning the behavior of a cylinder within an elastic medium. These equations were general enough to be used for rigid and flexible pipes. They concluded that the flexibility and the modulus of surrounding medium control the stresses within a cylinder. Chua and Lytton (1989) obtained a linear visco-elastic solution by

transforming Hoëg's elastic solution. They demonstrated the time-dependent nature of the pipe-soil system.

The analysis of the behavior of thin-walled flexible pipes must take into account the need to know the change in the horizontal diameter and the ultimate strength of the pipe in terms of the buckling of the pipe wall. Spangler (1941) was the first to examine the problem of horizontal deflection in depth. The results of some of his experiments led him to propose that lateral pressure distribution at the sides of a pipe is parabolic (Figure 2-1(a)). Using this concept he developed mathematical expressions for moment, thrust and deflection. Lucher (1966) used the concept of a thin cylindrical tube surrounded by an annular ring of soil and presented expressions to estimate its buckling strength. The equations of Spangler and Lucher are still used by the flexible pipe industry in spite of all the criticism that these equations have received due to various reasons (Moore, 1989; Jeyapalan, 1990).

ATV (1988) and Gerbault (1985) proposed improved assumptions for the lateral soil distribution at the sides of pipe bends. They proposed a sum of a parabolic distribution similar to Spangler's model and a uniform pressure distribution corresponding to 0.2 to 0.3 of the geostatic load as shown in Figure 2-1(b). Gerbault (1995) has indicated that assumption of a given shape of lateral stress distribution is not always appropriate. He also proposed pipe ring models supported by linear and non-linear springs to account for the soil pressure around the pipe ring.

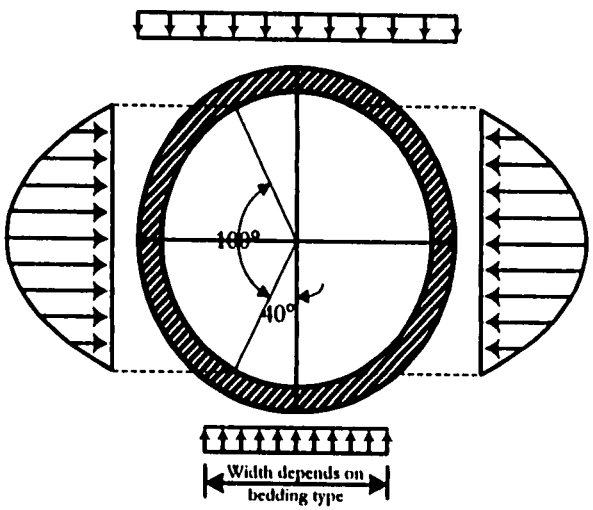

(a) Spangler's Earth Pressure Distribution

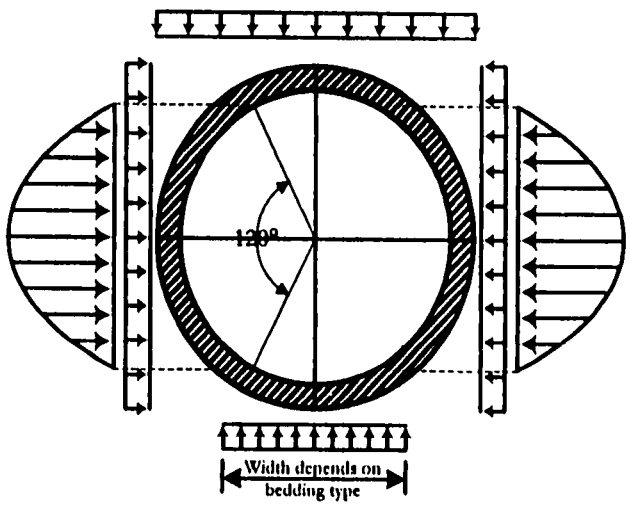

(b) A'TV's Earth Pressure Distribution

Figure 2-1 Proposed earth pressure distributions around a flexible pipe

The use of flexible pipes has increased in recent decades and a lot of research has been carried out to study the behavior of the pipe-soil system. Einstein and Schwartz (1979) proposed a linear model while Duncan (1979) and Moore and Booker (1987) presented rigorous non-linear models for a buried pipe system. Chua and Lytton (1985) and Jeyapalan et al. (1987) used finite elements and presented results for strain values of various pipe installations. These are only some of the published papers, which proposed different approaches for the design of flexible pipes. The great deal of confusion about the relative merits of the various design methods has led to reports and articles that have reviewed and compared various aspects of different approaches. Moore (1989) and Prevost and Kienow (1994) have unified these different methods for the benefit of the design practice of buried flexible pipes.

2.3 Pipe-Soil Modeling

As discussed previously, the early research on pipe-soil systems used field observations and developed empirical relations for the design of buried pipes. Laboratory tests were also used for this purpose to reduce the high cost involved in the field testing. The application of these empirical relations is reliable for those cases, which lie within the range of data using which these relations were developed. But their use outside the range of data is not that reliable.

The real behavior of the coupled pipe-soil system is usually not taken into account sufficiently in standard design procedures. Rather simplified models are used based on predefined stress or deformation patterns. This approach is appropriate for

practical design since a sufficiently high factor of safety is associated with the application of these approaches. If, however, the safety factor has to be quantified, or the exact value of the in-situ stress or strain are of interest, then more accurate models should be used. Efforts were made to come up with mathematical models based on the theory of mechanics, which could predict the general behavior of the pipe-soil system.

Pipe cross-sectional effects are analyzed by modeling a pipe ring in a 2-D semi-infinite soil space. This 2-D system is assumed to be in a plane-strain state. Initially both pipe and soil were modeled as linear elastic materials. Burns and Richards (1964) presented such a model. Hoëg (1968) presented a model in which he showed that the flexibility and compressibility of the cylinder and the depth of the soil cover significantly influence its behavior in an elastic soil medium. Dar and Bates (1974) and Einstein and Schwartz (1979) presented similar models. The real behavior of soil is, however, not elastic. Materials that are used for pipe construction are not linear elastic either. It is rarely feasible to obtain an analytic solution for these kinds of material models. Numerical methods are, therefore, used to obtain solutions for these types of models. Chua and Lytton (1985) and Jeyapalan et al. (1987) used finite elements analysis to study the behavior of buried flexible pipes. Seed and Duncan (1985) analyzed earth pressure and surface load effects on buried pipes using a plane-strain finite element code designed for an incremental non-linear analysis of soil-structure interaction. Jeyapalan et al. (1989) used the non-linear FEM analysis for Reinforced Plastic Mortar (RPM) pipes. Mohri et al. (1990) demonstrated that the

behavior of a pipe ring-soil system can be assessed by a non-linear elastoplastic finite element analysis. Altae et al. (1996) presented similar finite element analysis results for a laterally displaced pipeline. Abduljauwad (1999) carried out a full-scale field test, centrifuge laboratory model tests and the nonlinear finite element analysis of buried pipes to investigate the effect of soil cover on the structural response. He compared the results obtained by the three methods, which showed a close agreement of the nonlinear finite element analysis results with the field test results.

The stresses that develop in a buried pipe depends on the stiffness of the surrounding soil and it is important that the soil model used in a finite element analysis is capable of modeling the actual soil stiffness as closely as possible. The real stress-strain curve of soil is not linear and the stress-strain modulus depends on the value of the confining pressure. The soil model that incorporates this soil behavior is the hyperbolic soil model that was first proposed by Kondner and Zelasko (1963). In addition to the stress-strain modulus, a second elasticity parameter is required to define a material's mechanical properties. Poisson's ratio was initially used as the second parameter but it is usually very difficult to estimate its value for soil with confidence. Bulk modulus was therefore incorporated in the hyperbolic soil model first by Duncan et al. (1980) and later improved by Selig (1988). There are many programs currently available, such as Culvert ANalysis and DEsign (CANDE) (Katona et al., 1976) and SPIDA (Heger et al., 1985), which have included this model for the pipe-soil analysis. Leonards et al. (1985) compared various soil models available in the CANDE program and showed significant differences in the pipe

stresses obtained by each of the models. They also demonstrated the importance of properly simulating the actual construction sequence in the analysis of buried pipes. They found out that the requirements for good predictions of the buried pipes include using the hyperbolic soil model with the appropriate selection of parameters, accounting for the slip at the pipe-soil interface, and starting the analysis when the backfill is at the pipe invert and following the sequence of soil layer placement closely.

An analysis of longitudinal effects along pipe-soil system is often required. One of the most famous simplified models to carry out this analysis was first proposed by Winkler (1867). In the Winkler model, the soil is modeled as a series of springs, which provide resistance to the structure resting on the soil. Many improvements to this model have been proposed for its application to various kinds of soil-structure systems. Rajani et al. (1996) developed a simplified Winkler model to simulate the response of jointed water mains subjected to temperature change and water pressure. Soil interface elements for the FEM analysis presented by Badie and Salmon (1997) and Karadeniz (1997) are also based on the Winkler model.

The boundary-element method has also been used for modeling the semi-infinite space of soil because it requires less modeling and computational effort than the finite element method. Chiou and Chi (1993) used boundary elements to model the soil as an inelastic medium characterized by the Mohr-Coulomb and the Drucker-

Prager yield criteria. Shinokawa and Mitsui (1993) showed that the boundary-element method can be efficiently applied in practical geotechnical problems.

2.4 Strength of Pipe Bends

As discussed in section 1.2.2, the application of bending moment results in a change of pipe bend stiffness. Karman (1911) presented the first theoretical solution for smooth unrestrained bends with end moments and internal pressure. Numerous publications followed, which extended his work to include other forms of loading. These publications include those by Vigness (1943), Kafka and Dunn (1956), Rodabaugh and George (1957), and Findlay and Spence (1979). Initially solutions were presented for long bends without end restraints, i.e., without tangent pipes or flanges. Later investigations showed that the end restraints may have an important influence on the flexibility and stress. For many years the best available information on end restrains was that by Pardue and Vigness (1951). But after sometime more investigations were made such as that by Thomson and Spence (1983) who presented some new analytical solutions. Whatham (1986) used the thin shell theory to present a solution without any simplifying assumptions. Recently Gresnight and van Foeken (1995) presented an analytical model for the elastic and plastic design of pipe bends using the theory of minimum potential energy. In this model they explicitly incorporated the soil load that may act on a buried pipe bend.

The finite-element method has also been used to analyze the geometrically nonlinear behavior of pipe bends. Among others, Natarajan and Blomfield (1975), Ohtsubo

and Watanabe (1977), Weiß et al. (1996) used finite elements and developed diagrams, charts and other design aids. Natarajan and Blomfield (1975) examined several forms of end constraints over a fairly wide range of parameters. They concluded that the significance of the tangent depends on the bend angle to radius ratio. Weiß et al. (1996) demonstrated the use of the finite-element method for the design of pipe bends with respect to fatigue strength and load carrying capacity. Several pipe bend elements have been proposed that can be broadly divided into two categories: beam-shell elements, and shell-ring elements. Beam-shell elements are those in which shell type ovalization-deformation is superposed on a curved beam element. Hibett (1974), Bathe and Almeida (1982), and Mackenzie and Boyle (1992) have presented beam-shell type of elements. Shell-ring type of elements are wholly based on the thin shell theory. Ohtsubo and Watanabe (1977) have presented a shell-ring element. De Melo and De Castro (1992) also presented a pipe element, derived from the arch bending theory, for the analysis of in-plane bending of curved pipes.

2.5 Soil Restraint on Buried Pipes

The restraint offered by soil against movement of a buried pipe is called the *subgrade reaction*. Generally, the soil restraint is divided into its vertical and horizontal components and quantified as the coefficient of vertical and horizontal subgrade reaction, k_v and k_h, respectively. These coefficients, expressed in units of stress per unit length, do not represent any real physical soil property, but are convenient mathematical parameters describing the rate of change of soil pressure with

displacement. The concept of the elastic modulus of subgrade reaction was first introduced by Winkler (1867) and later investigated by various researchers like Hetenyi (1946). In the numerical analysis of soil-pipe interaction, the soil surrounding a pipe can be modeled by a set of perpendicular springs as shown in Figure 2-2. The stiffness of the soil springs is calculated using the coefficients of subgrade reaction.

A lot of work has been carried out to estimate reliable values for the coefficient of subgrade reaction for different types of soils. Vesić (1971) computed the uplift capacity of cylinders on the basis of the pressure required to expand a cavity to the surface. Audibert and Nyman (1977) performed tests on the horizontal movement of pipes. They proposed a relation for soil spring rates for the horizontal movement of pipes. These test results showed a hyperbolic relationship between the displacement and the passive restraining forces. There have also been some studies to quantify soil restraint against oblique motion of pipelines such as that by Nyman (1984) and Hsu (1996).

Troutmann et al. (1985 a & b) carried out an extensive lab study of the uplift and lateral movement of buried pipes. They compared the results with the previous experimental and analytical studies including those related to the movement of anchor plates and piles. They found out that the analytical studies give a wide range of values for the uplift capacity of buried pipe in similar conditions. The Vesić (1971) cavity expansion model and the Row and Davis (1982) finite element model were

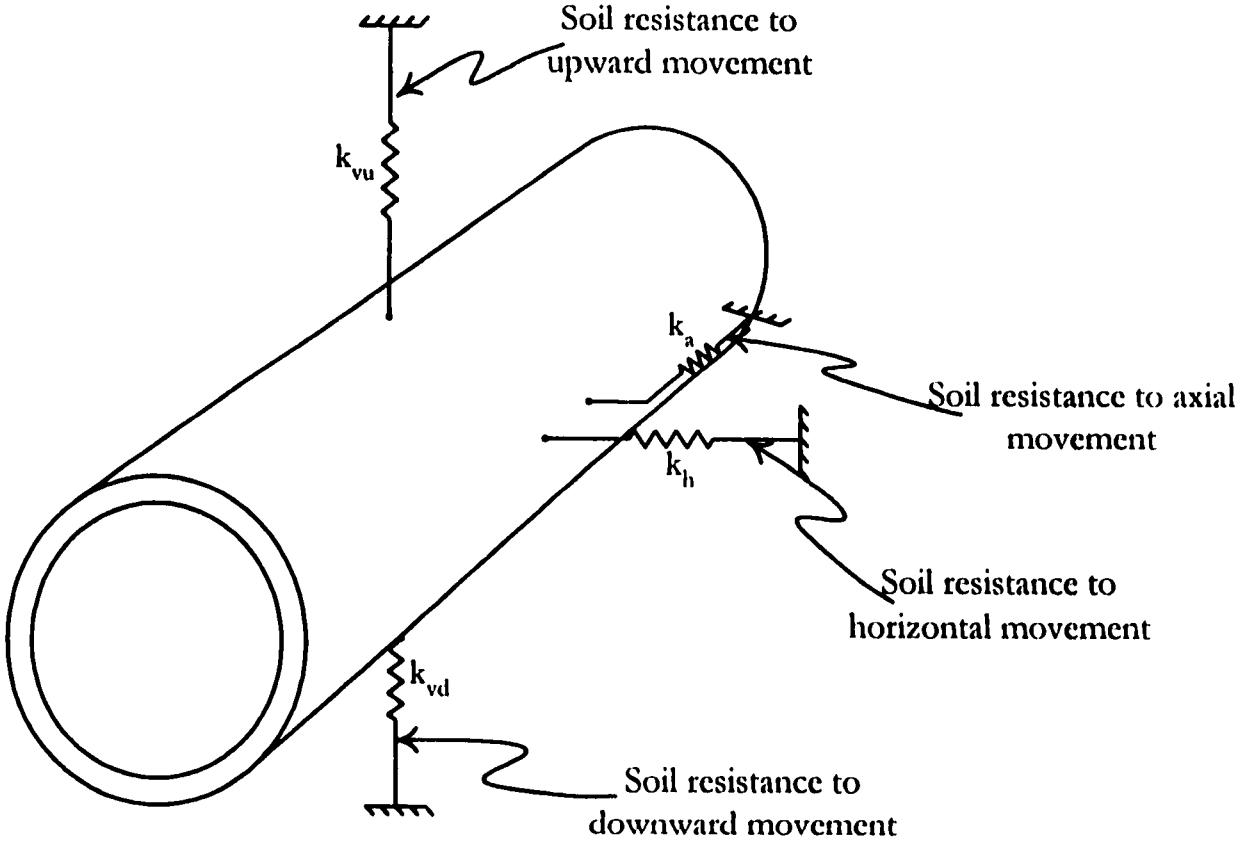

Figure 2-2 Winkler model used to analyze the effects of a buried pipe movement

found to most closely predict the pipe uplift forces in medium and dense sand. In the case of lateral movement capacity of buried pipes, the models of Ovesen (1964) and Row and Davis (1982) were found to agree closely with the lab test results for medium and dense sand. The experimental data from Audibert and Nyman (1977) was also found to be matching with the lab test results. Dickin (1994) carried out a centrifuge model study and agreed with the Troutmann et al. (1985 a) findings that the uplift resistance of buried pipelines is essentially the same as that of the equivalent strip anchor. Hsu (1993) studied the velocity effects on the lateral soil restraint of pipelines and concluded that the maximum soil restraint factor and its corresponding displacement exhibit the power law relationship (a standard mathematical relationship) with the pipe velocity.

The lateral pipe-soil interaction has also been studied in clays. Poorooshasbh et al. (1994) studied lateral pipeline-soil interaction using centrifuge modeling and determined the value of the interaction factor. Yin et al. (1993) compared finite element analysis with the centrifuge modeling results. They concluded that the comparison is encouraging but there are limitations and improvements can be made in the finite element modeling. Altaee and Boivin (1995) performed finite element analysis for slightly overconsolidated clays. Altaee et al. (1996) extended the work for highly overconsolidated clays and studied the effect of rate of movement and the location of the ground water table.

Restrained underground pipes are those in which longitudinal stress is transferred to the soil by an anchor or soil friction. Temperature change and Poisson's effect of internal pressure contribute to the longitudinal stress in a restrained pipe. Peng (1978) published guidelines for calculating stresses, including approximate equations for estimating passive soil bearing and friction reactions. The Power piping code of ASME-B31.1 (1992) contains procedures for the design of restrained underground piping in appendix VII. It includes guidelines for analysis of a restrained pipe system using simple computer models. Goodling (1997) reviewed appendix VII of ASME B31.1 code and offered some guidelines in estimating soil spring rates to be used in the computer modeling. Ng at al. (1997) proposed a two-stage analysis technique for modeling laterally loaded pipelines. The first stage uses a 2-D plane strain finite element analysis to predict the restraining effect of the soil as a function of pipe displacement. These predictions are then used in stage 2, which models the behavior of the pipeline using the Winkler model.

The method of calculating required soil cover over buried pipe bends is discussed in the SAES-L-051 (1996) specifications of the Saudi Aramco Engineering Standards. The specifications give some very simplified methods to find the cover height. The use of a program called PIPECOVR, developed by Saudi Aramco, is also demonstrated in the specifications, which calculates the minimum cover height required for the buried pipe bends. The program uses an approximate and simplified method in which the buckling equation of straight buried pipes is used to find the minimum cover height.

The continuous long buried pipes may experience relatively large deformations due to temperature change or other reasons. These longitudinal deformations are considered acceptable for a pipeline lying in the open field. However in certain cases even small movement of a pipe cannot be accommodated such as near the point of its entry in a plant. Anchor blocks are provided in such conditions to restrict any longitudinal movement of a buried pipe. These anchor blocks are usually constructed by welding anchor steel plates with the pipe. These steel plates, with or without stiffeners, are then surrounded by massive cast-in place concrete blocks. The absence of a clear and practical method for the analysis and design of these steel anchor plates led Al-Ghamedy (1997) to investigate the behavior of such systems. He suggested a simple and practical analysis and design method for the pipeline stiffened-anchor plates.

2.6 Summary

A great deal of research has been carried out about the structural behavior of pipe bends, and its theory is now well established. There have been attempts to quantify the soil restraint on buried pipes, and various sources are available which estimate a reliable value of soil spring rates. However, the soil restraint at a buried pipe bend has not been explicitly studied yet.

The current trend in the study of structural systems, like buried pipes, is to use numerical methods particularly the finite-element method. The reason for the popularity of the finite-element method is its capability to model composite systems

that are characterized by different non-linear material behaviors. Time dependent effects like creep and stress relaxation can also be incorporated in the model. The finite-element method is now well developed for its application to geotechnical problems. Its predictions about the structural behavior of a soil-structure system are considered quite reliable. The need to carry out expensive field-testing has now been reduced considerably, and finite-element analysis is usually carried out to study systems like buried pipelines.

CHAPTER 3
SOFTWARE SELECTION AND VALIDATION

3.1 Overview

The analysis of buried pipe bends using the finite-element method requires a program that has appropriate elements to model the pipe-soil system, and should be capable of modeling the response of the system with reasonable accuracy. In the case of vertical bends, the bend apex moves upward in the plane of the bend, and as a result of this movement the soil cover fails in a plane that lies normal to the plane of the bend. Similarly the lateral movement of a horizontal bend results in the failure of soil cover which occurs in a vertical plane. The structural response at a pipe bend is therefore three dimensional in nature and requires for its analysis a finite element program that has appropriate 3D modeling capabilities.

The structural system of buried pipe bends consists of the pipe bend, straight pipes up to virtual anchors and the surrounding soil. The element usually used to model the pipe in a 3D model is a shell element that has both in-plane and bending stiffnesses. The semi-infinite soil domain surrounding the pipe can be modeled by 3D continuum elements. The pipe-soil interface requires especial consideration,

because the movement of a pipe bend at its apex results in the debonding of pipe soil interface at the intradose of the bend.

If pipe stresses are of prime interest then a soil model capable of modeling the non-linear soil stiffness should be incorporated, because buried pipe stresses are greatly influenced by the soil stiffness. In addition, the bending ovalization of pipe has a significant effect on the pipe stresses, and the finite element model should be capable of incorporating this large deformation behavior. However, the prime interest of this study is to determine the capacity of the soil cover in resisting the lateral/uplift movement of the pipe bends. This requires that the element used for soil is capable of modeling the strength of the soil.

There are numerous programs commercially available for the analysis and design of structures and foundations. NASTRAN, ANSYS and STRUDL are general-purpose FEM programs, and are quite popular for common structural analysis. These programs, however, do not include all the features required for a geotechnical analysis due to their generality. CANDE-89 is one of the most popular software for the pipe-soil interaction analysis but it is only capable of carrying out 2-D plane strain analyses.

Taking into account the modeling requirements of buried pipe bends, the most appropriate software found is the Structure Medium Analysis Program (SMAP-3D) (1999). It has a continuum soil element that can be characterized by a number of

available soil models. It also has elements to model the pipe and the pipe-soil interface.

3.2 Introduction to SMAP-3D

SMAP-3D is an advanced three-dimensional finite element computer program developed to analyze geometrically and materially nonlinear soil-structure interaction problems. It is a general-purpose program for the static, consolidation, and dynamic analysis of geomechanical problems.

It contains a three-dimensional 8-noded isoparametric continuum element that can be used to model soils, rocks, and concrete media. Dry, saturated, and partially saturated porous media can be modeled by the continuum elements. The yielding of the material can be incorporated by choosing an appropriate material model. The material models available in the program are:

- Von Mises Model
- Mohr-Coulomb Model
- In Situ Rock Model
- Generalized Hoek and Brown Model
- Single Hardening Elasto-Plastic Model
- JWL Explosive Source Model
- Modified Cam-Clay Model
- Engineering Model

- Hyperbolic Model

The joint element available in the program can be used to model joints, faults and interfaces. A joint face has to be specified for the element along which the slipping takes place when the shear stress exceeds the shear strength or the debonding occurs when the tension across the face exceeds the specified value for tensile strength.

The shell element provided in the program can be used to model slabs, shear walls, tunnel linings, pipe wall, etc. It is a linearly elastic element that has membrane, bending and torsional stiffnesses. Surface loads including pressure can be specified for the element.

The loads that can be specified include nodal force time history, velocity time history, gravity load, base acceleration time history, and temperature differential time history.

3.3 Validation of SMAP-3D for Modeling Buried Pipe Bends

A buried pipe problem can be modeled in SMAP-3D using continuum elements for soil, shell elements for pipe, and joint elements for pipe-soil interface. Among the material models available in SMAP-3D, the Mohr-Coulomb criterion is chosen to characterize the soil elements, which is commonly used to model sand. The strength parameters required for the model, i.e., the angle of internal friction and cohesion, can be easily and reliably determined in the lab. The tensile strength of the material

can be also specified for the model, which is zero for dry sand. The lumped nonlinear joint model available in SMAP-3D is selected to model the pipe-soil interface, which has better performance than the other available joint models as given in the SMAP-3D manual.

As mentioned in the literature review, no previous study of the soil restraint at a buried pipe is available which could be used to validate the response of a buried pipe bend modeled in SMAP-3D as outlined above. The model can however be validated for individual structural phenomena that occur in response to the loads acting on the buried pipe structural system. These phenomena include the load distribution or arching in the soil around a pipe, the soil resistance to the uplift movement of a straight pipe and the soil resistance to the horizontal movement of a straight pipe. These phenomena are modeled in SMAP-3D. The results and the comparison with the available analytical and experimental results are given in the subsequent sub-sections.

3.3.1 Modeling of buried pipe under gravity load

Marston and Anderson (1913) gave formulas based on the theory of arching to calculate earth pressure on buried pipes (Figure 3-1) and are called Marston formulas. As discussed in chapter 1, pipes are categorized as being *rigid* or *flexible* depending on the ratio of the stiffnesses of the pipe and the soil. Marston gave separate equations

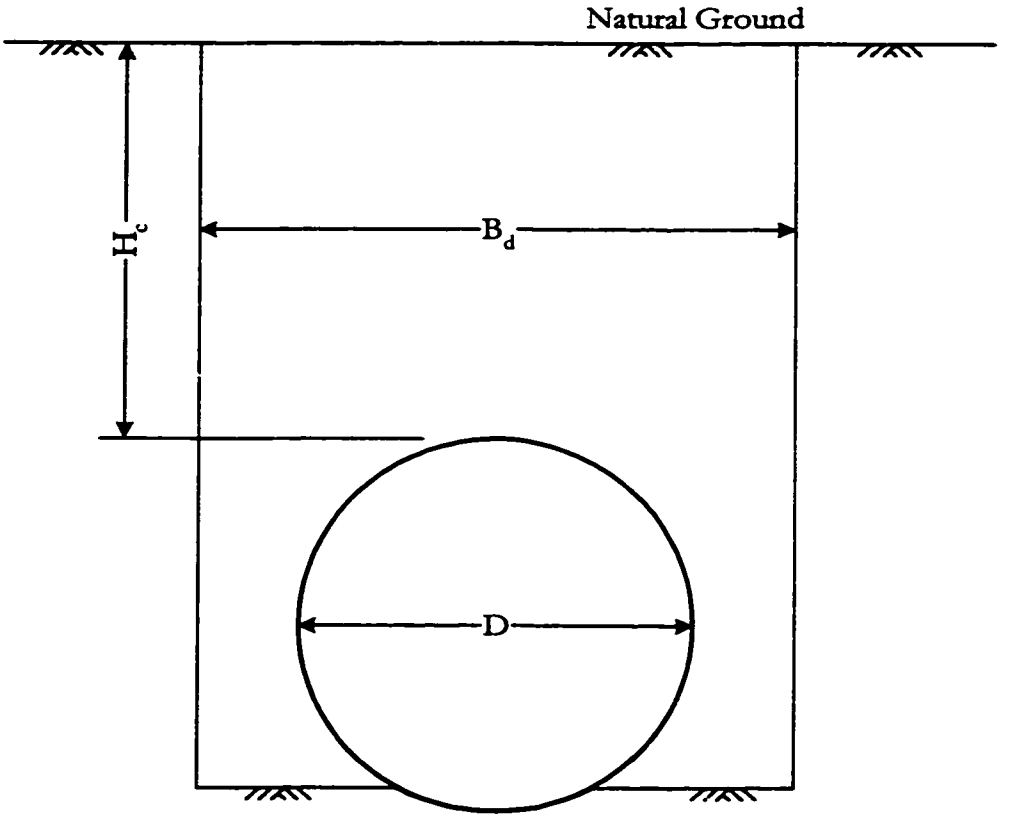

Figure 3-1 Cross-section of a typical buried pipe.

for both pipe types, which are:

$$W_s = C_d \gamma B_d^2 \quad \text{(Marston – Rigid Pipes)} \tag{3-1}$$

$$W_s = C_d \gamma D B_d \quad \text{(Marston – Flexible Pipes)} \tag{3-2}$$

The weight of the soil prism above a buried pipe can be calculated as:

$$W_s = \gamma H_c D \tag{3-3}$$

Where, W_s is earth load per unit length of the pipe,

C_d is Marston's soil load coefficient (Spangler and Handy, 1982),

γ is unit weight of the soil,

H_c is depth of the pipe crown below ground surface,

B_d is the width of the trench, and

D is the outside diameter of the pipe.

These three equations are compared with the SMAP-3D by modeling the buried pipe in SMAP-3D for the following parameters:

In-Situ Soil:	E = 9000 psi (62.1 MPa),	ϕ = 43°,	γ = 120 lb/ft^3 (18.9 kN/m^3)
Trench Soil:	E = 7000 psi (48.3 MPa),	ϕ = 38°,	γ = 110 lb/ft^3 (17.3 kN/m^3)
	B_d = 60 in (1524 mm)		

Pipe: D = 48 in (1219 mm)

Rigid:	$E = 29 \times 10^6$ psi, (200 GPa)	$\nu = 0.3$,	t = 6 in (152 mm)
Felxible:	$E = 1 \times 10^5$ psi, (690 MPa)	$\nu = 0.3$,	t = 0.25 in (6.35 mm)

The solution of SMAP-3D is obtained for four cover depths, which are H_c = 30 in., 42 in., 60 in., 90 in.

A comparison of the results is shown in Figure 3-2. If the pipe is rigid and unyielding relative to the columns of the soil at the sides of the pipe, then the entire soil load is carried by the pipe itself with little contribution of the soil stiffness. The Marston's rigid pipe equation thus gives a good estimate of the earth load, which is the total soil load on a horizontal plane through the top of the pipe and between the sides of the ditch. The SMAP-3D rigid pipe curve therefore lies close to the Marston's rigid pipe equation curve. The slight difference is because of the reason that the Marston's equation does not explicitly consider the stiffness of the system while SMAP-3D model directly incorporates the stiffnesses of the pipe and the soil. The Marston's formula for flexible pipes does not directly consider the pipe and the soil stiffnesses either, but it assumes that the pipe and the soil columns on each side of the pipe take the soil load in proportion to their width D/B_d. This assumption results in a conservative estimate of the soil loads and that is why the Marston's flexible pipe equation curve lies noticeably higher than the corresponding SMAP-3D curve.

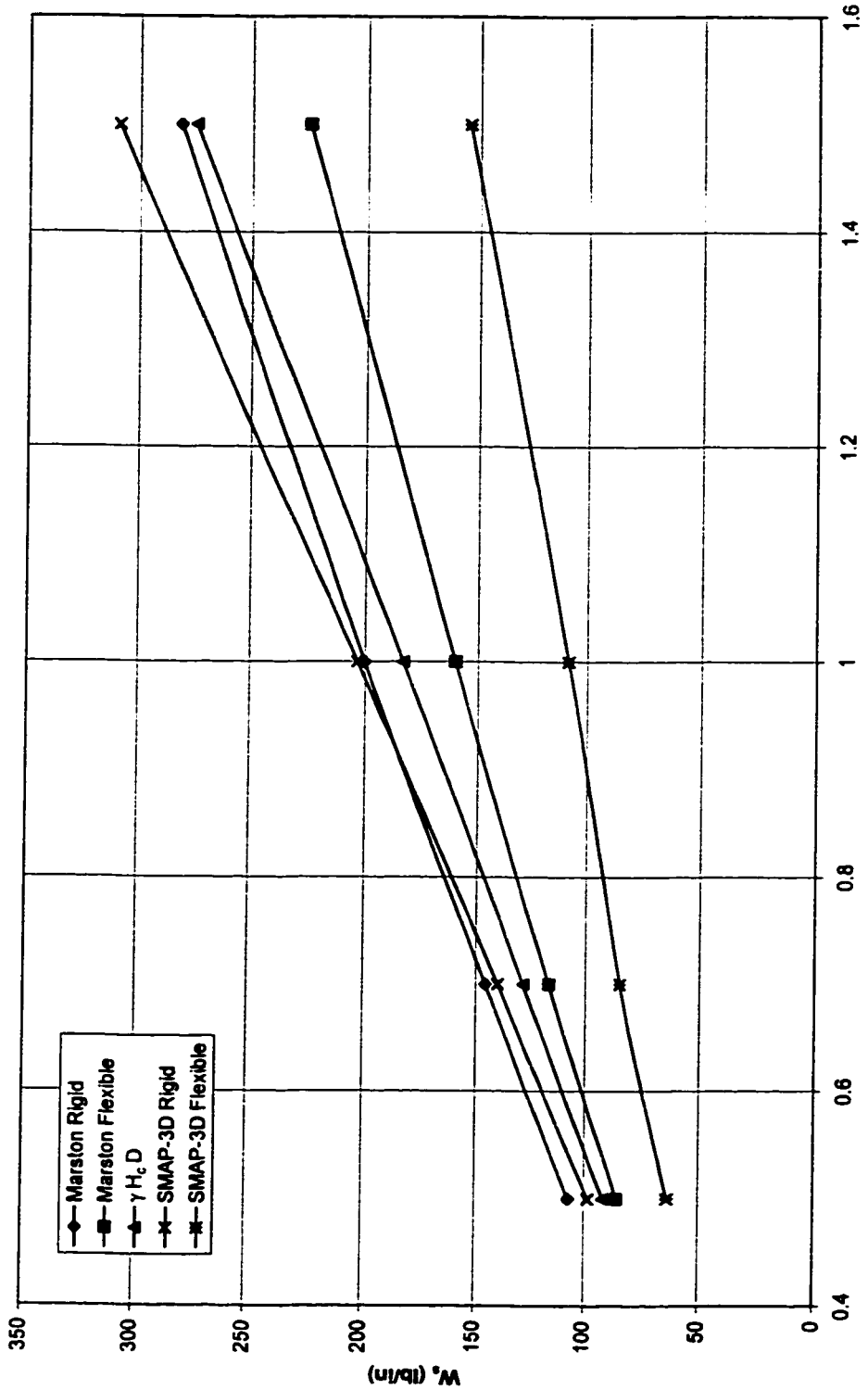

Figure 3-2 Comparison of SMAP-3D results with Marston's equation

The deformed shape of a rigid pipe is shown in Figure 3-3 (a). The high stiffness of the pipe results in a smaller settlement above the pipe crown as compared to the free-field settlement of the grade. On the other hand, the low stiffness of the flexible pipe gives rise to a greater settlement of the grade above the pipe crown as shown in Figure 3-3(b).

The vertical stress contours in the soil medium are shown in Figure 3-4. It can be noticed that the vertical stress increases at the crown and the invert of a rigid pipe, but it decreases in the vicinity of the springline. Conversely, the presence of a flexible pipe causes a reduction of vertical stress above and below the pipe. These vertical stresses are compared with the free field stress (yy) in Figure 3-5. The stresses at the pipe crown and at a depth of $H_c/2$ are plotted in the figure. In the case of rigid pipes, the maximum stress occurs at the pipe crown, which then decreases at a sharp gradient on each side of the crown. The minimum stress occurs at a distance slightly greater than the pipe radius from the pipe centerline on each side of the pipe. The vertical stress the increases from its minimum value away from the pipe center until it becomes equal to the free field stress. A similar but opposite distribution of vertical stresses occurs above a flexible pipe as shown in Figure 3-5(b). It can be noticed that the presence of the flexible pipe can cause a reduction of vertical stress at the crown of the pipe such that the stress at the crown can become smaller than the stress at a depth of $H_c/2$.

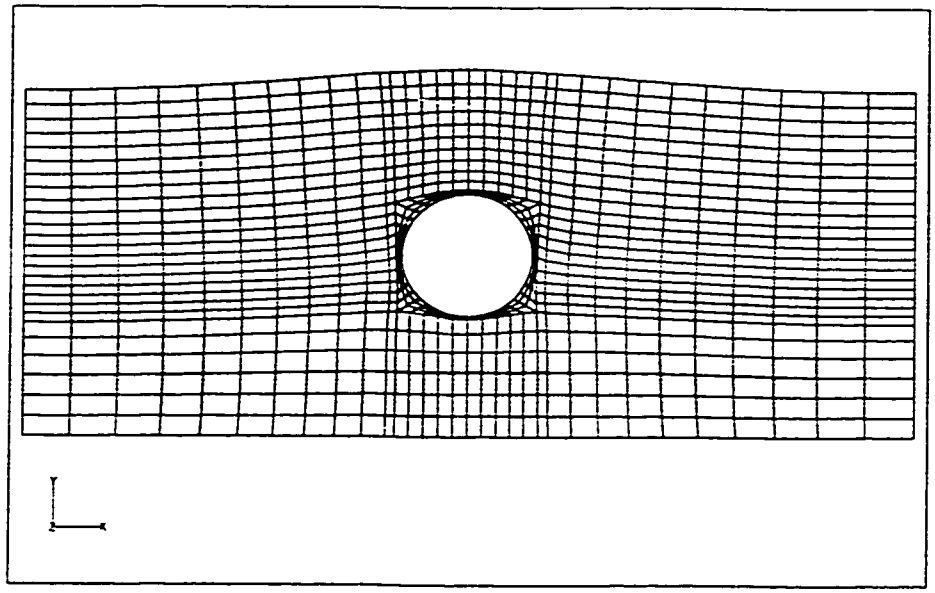

(a) Rigid pipe (Deformation 800 times magnified)

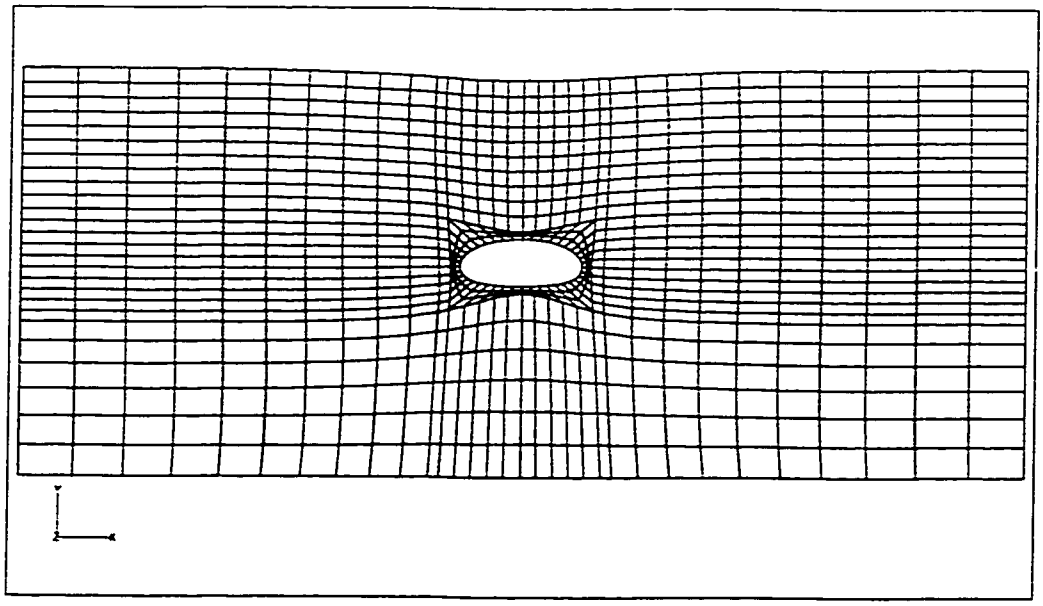

(b) Flexible pipe (Deformation 500 times magnified)

Figure 3-3 Typical deformed shapes obtained by the SMAP-3D analysis

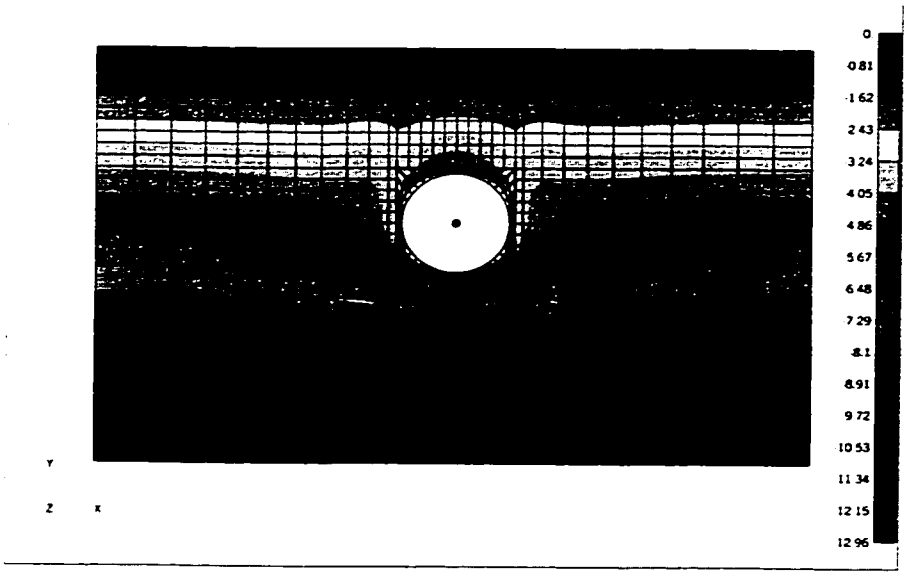

(a) Rigid pipe

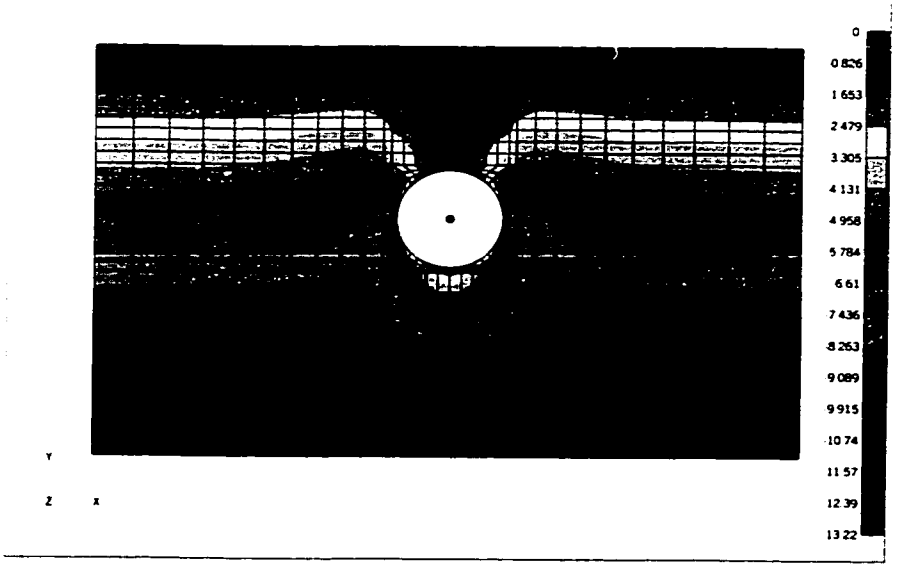

(b) Flexible pipe

Figure 3-4 Typical vertical stress contours obtained by the SMAP-3D analysis

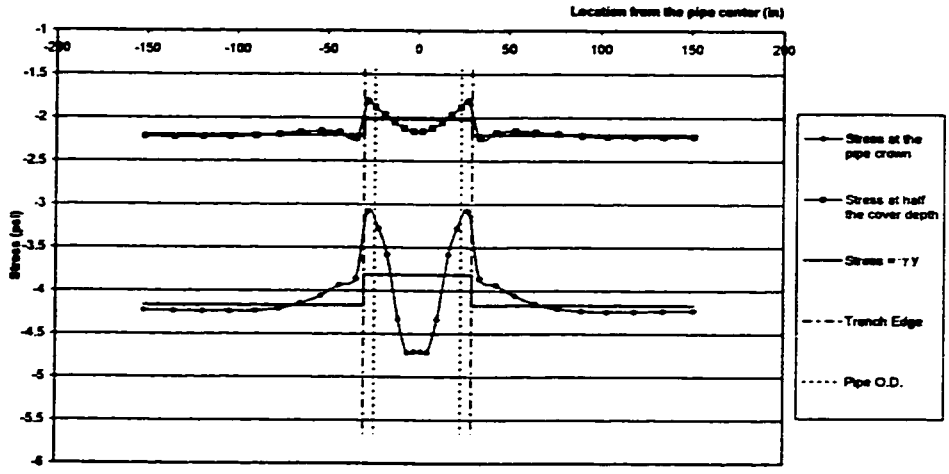

(a) Rigid pipe

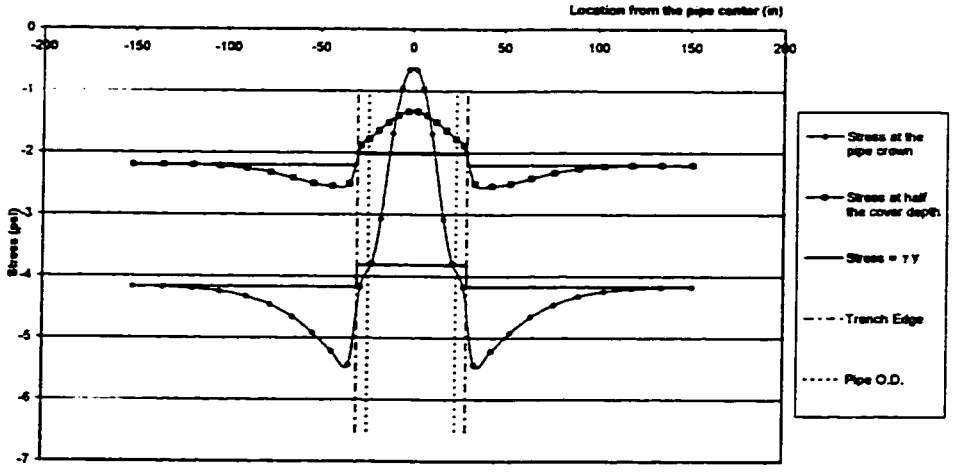

(b) Flexible pipe

Figure 3-5 Vertical stress distribution obtained by the SMAP-3D analysis

The low deformation in the rigid pipe as compared to the settlement of the soil on its sides results in the reduction of the lateral confining earth pressure above the pipe as apparent in Figure 3-6(a). The converse is true for the flexible pipe as shown in Figure 3-6(b).

3.3.2 Modeling of buried pipe uplift

In continuation with the validation process of SMAP-3D, the uplift movement of buried pipes is analyzed. The data selected for the comparison with the SMAP-3D model for verification is the one obtained by Trautmann et al. (1985 a) through a full-scale lab test. The study is widely recognized and the use of its findings for design purposes has been recommended in various publications such as ASME-B31.1 (1992) and by CGL (1984).

A typical load-deformation curve for a pipe moving up relative to the soil is shown in Figure 3-7. The vertical load on a buried pipe comes from the weight of the soil cover and the pipe with its contents. The pipe transfers this load to the soil at the pipe invert. Once the pipe starts to move up, the reaction at the pipe invert decreases and the pipe system starts to carry the vertical load directly. The load-deformation curve stays straight until the contact between the pipe and the soil breaks at the pipe invert. In the case of shallow buried pipes, the break of the contact is closely followed by the mobilization of shear strength of the soil against the uplift movement along a plane as shown in Figure 1-6(a), and the peak of the curve is obtained. However for deeply buried pipes the soil does not reach its shear strength

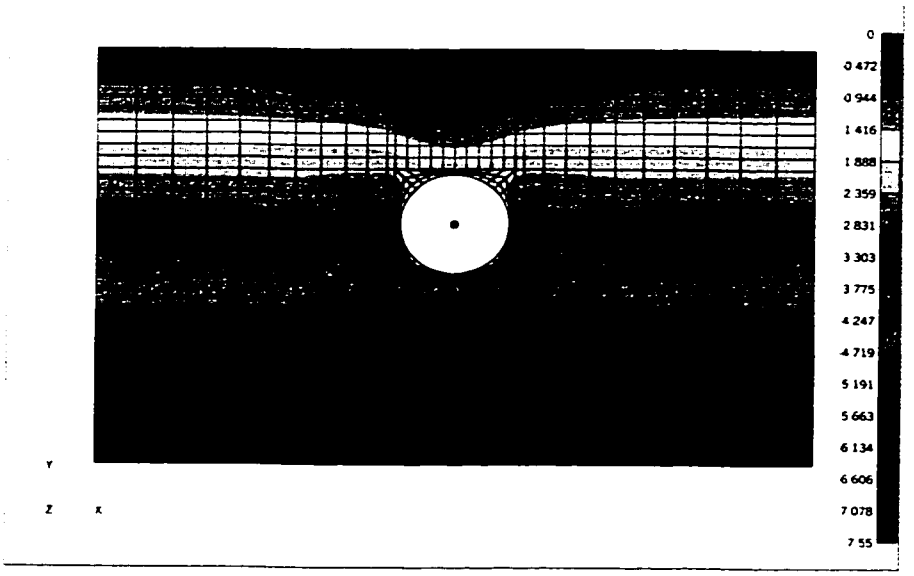

(a) Rigid pipe

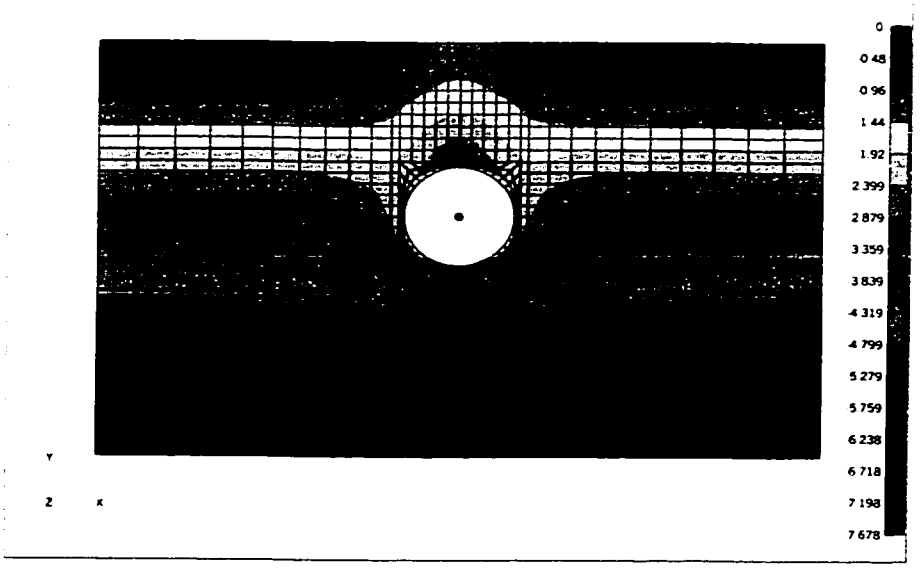

(b) Flexible pipe

Figure 3-6 Typical horizontal stress contours obtained by the SMAP-3D analysis

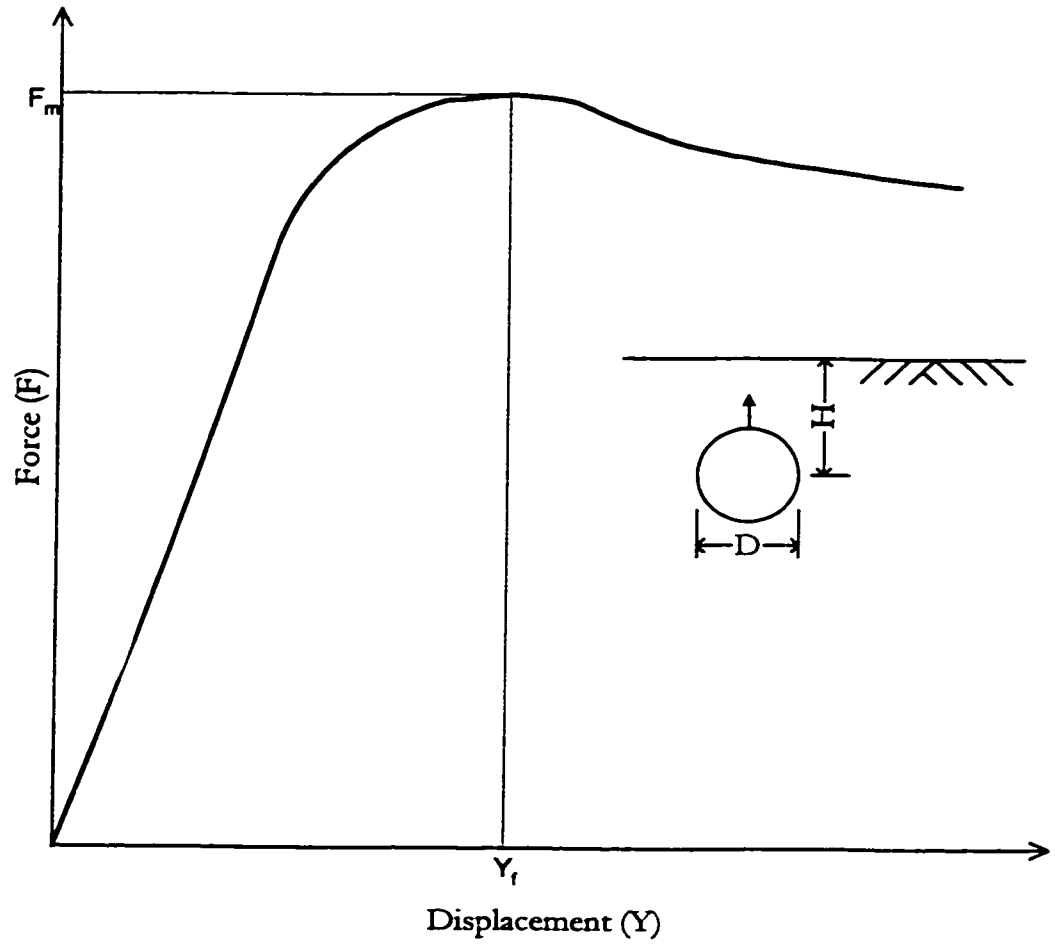

Figure 3-7 A typical load-displacement curve for uplift of buried pipes

just at the break of pipe-soil interface at the pipe invert and continues to give some resistance to the pipe movement until it reaches its shear strength. The maximum peak force (F_m) and the corresponding displacement (Y_f) are shown in Figure 3-7.

The uplift movement behavior of the buried pipes is modeled in SMAP-3D and compared with the Trautmann et al. (1985 a) study for the following parameters:

Pipe outer diameter D = 4 in

Pipe wall thickness t = 0.25 in

Four cover depths (H) are used: 6 in, 16 in, 32 in, and 52 in.

Three types of soils are investigated:

- Loose sand (γ = 94.2 pcf (14.8 kN/m^3), ϕ = 31°)
- Medium sand (γ = 104.4 pcf (16.4 kN/m^3), ϕ = 36°)
- Dense sand (γ = 112.7 pcf (17.7 kN/m^3), ϕ = 44°)

The analysis is carried out using displacement control. Taking advantage of the symmetry, only one half of the mesh is used. The domain idealization is shown in Figure 3-8. The mesh is prepared such that reasonable mesh density and element aspect ratios are obtained. The two-dimensional mesh is thus prepared in a manner as described in detail in Chapter 4.

The load-deformation curves obtained by the SMAP-3D analysis are shown in Figure 3-9. The maximum force F_m has been located on the curve by the arrows as

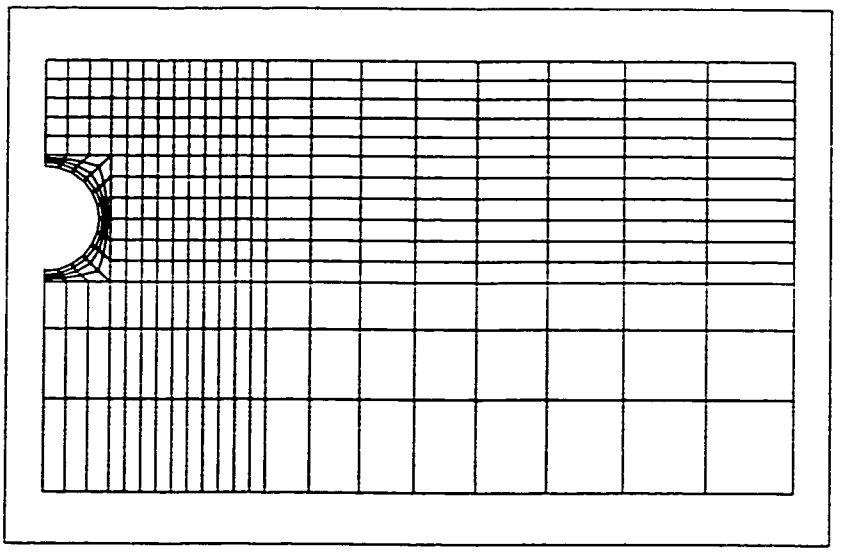

(a) Typical mesh

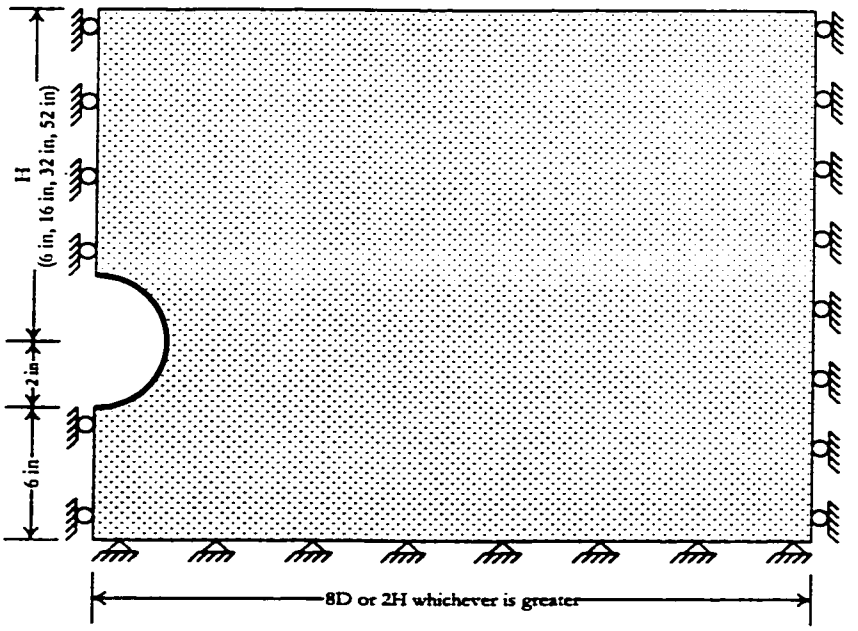

(a) Dimensions and boundary conditions of the mesh

Figure 3-8 Domain idealization used to model the uplift of a buried pipe

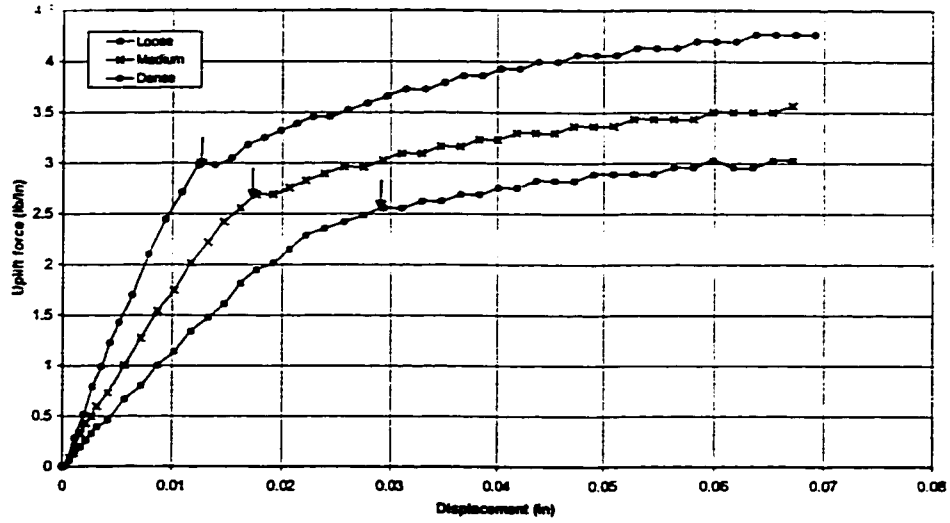

(a) H = 6 in (H/D = 1.5)

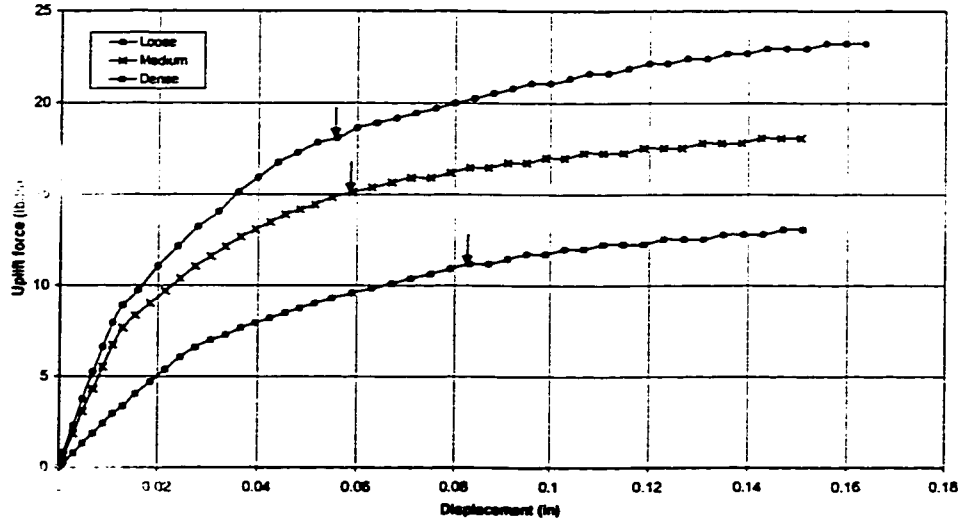

(b) H = 16 in (H/D = 4)

Figure 3-9 Load-deformation curves obtained by the SMAP-3D analysis for the uplift of buried pipes.

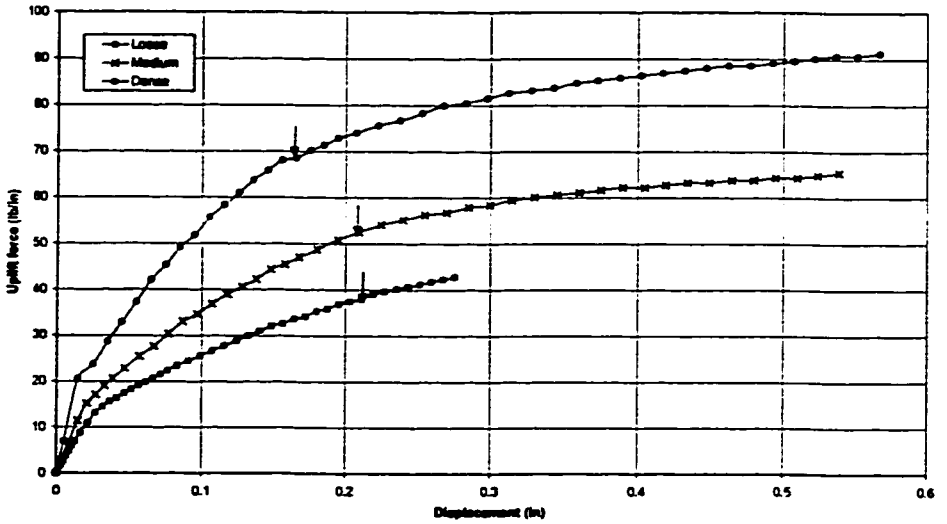

(c) H = 32 in (H/D = 8)

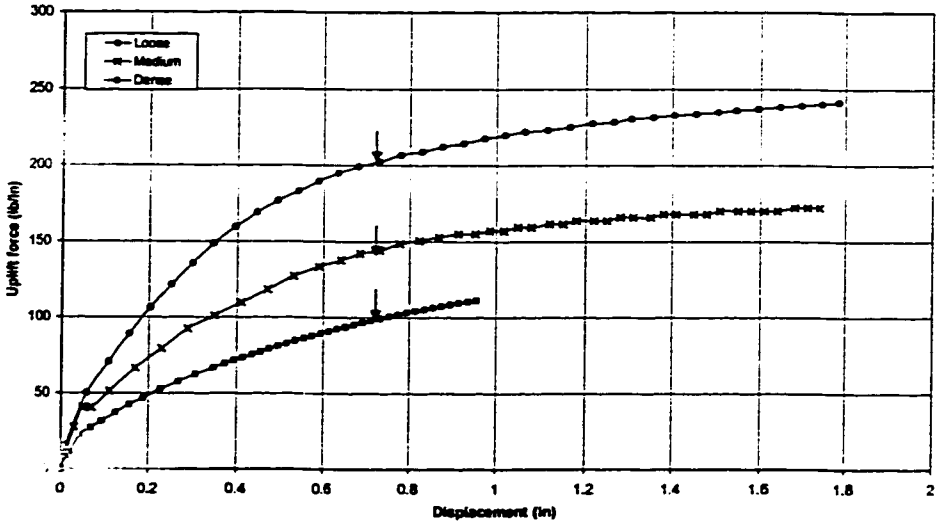

(d) H = 52 in (H/D = 13)

Figure 3-9 (Contd.)

the points where the curve starts to become flat. The point of maximum force is relatively easy to be identified for smaller cover depths, and it can be noticed that the range of corresponding Y_f is small for these curves. The identification of the point of maximum force is especially difficult on the curves of loose soil with large cover depths. Based on the small range of the value of Y_f, the point on these curves for loose soil has been located at a displacement equal to that obtained for the curve of medium soil plotted above them.

The strength of soil against the uplift movement of a buried pipe is usually quantified by a dimensionless factor N_γ that can be expressed as,

$$N_\gamma = \frac{F_m}{\gamma HDL} \tag{3-3}$$

Where, N_γ is the dimensionless factor for the strength of a buried pipe against uplift,

F_m is the maximum force against uplift of a buried pipe,

γ is the unit weight of the soil,

H is the depth of the pipe center below ground surface,

L is the length of the pipe, and

D is the outside diameter of the pipe.

Trautmann et al. (1985 a) calculated the value of N_γ after subtracting the weight of the pipe from the value of F_m. The value of N_γ thus quantifies the maximum soil resistance to the uplift movement of a pipe. The values of N_γ are calculated

accordingly for the SMAP-3D results, and a comparison with the results of Trautmann et al. (1985 a) is shown in Figure 3-10. The SMAP-3D results compared well for all soils for small cover depths. SMAP-3D is found to slightly over predict the strength of medium and dense soils for larger cover depths. The difference is as high as 40% for the largest cover depth. A noticeable discrepancy occurs for deep pipes in loose sands. This discrepancy is also found with the analytical model of Vesić (1971) and the finite element solution of Row and Davis (1982). Trautmann et al. (1985 a) mentioned that a punching mechanism develops during the uplift of a deeply buried pipe in loose sand. They described the reason of this discrepancy as the inability of analytical models to account for the contractive behavior during shear. The high porosity of loose sands results in the large volume change, and this effect is not taken into account by the analytical model.

A typical deformed shape and the stress contours obtained by the analysis at a post soil yield stage are shown in Figure 3-11. The uplift of the cover along with the pipe and the separation of the pipe-soil interface (stretching of joint elements below the pipe) at the pipe invert are apparent in the deformed shape. The separation of pipe-soil interface has resulted in the reduction of vertical stresses beneath the pipe (Figure 3-11(b)). The zone of reduced vertical stress continues from the pipe invert to the earth surface and thus outlines the plug of soil cover taken up by the pipe. The vertical stress at the pipe crown increases as the pipe pushes the soil while moving up (Figure 3-11(b)). The confining stress increases at the pipe crown and decreases from there on so that a zone of reduced horizontal stress develops near the earth

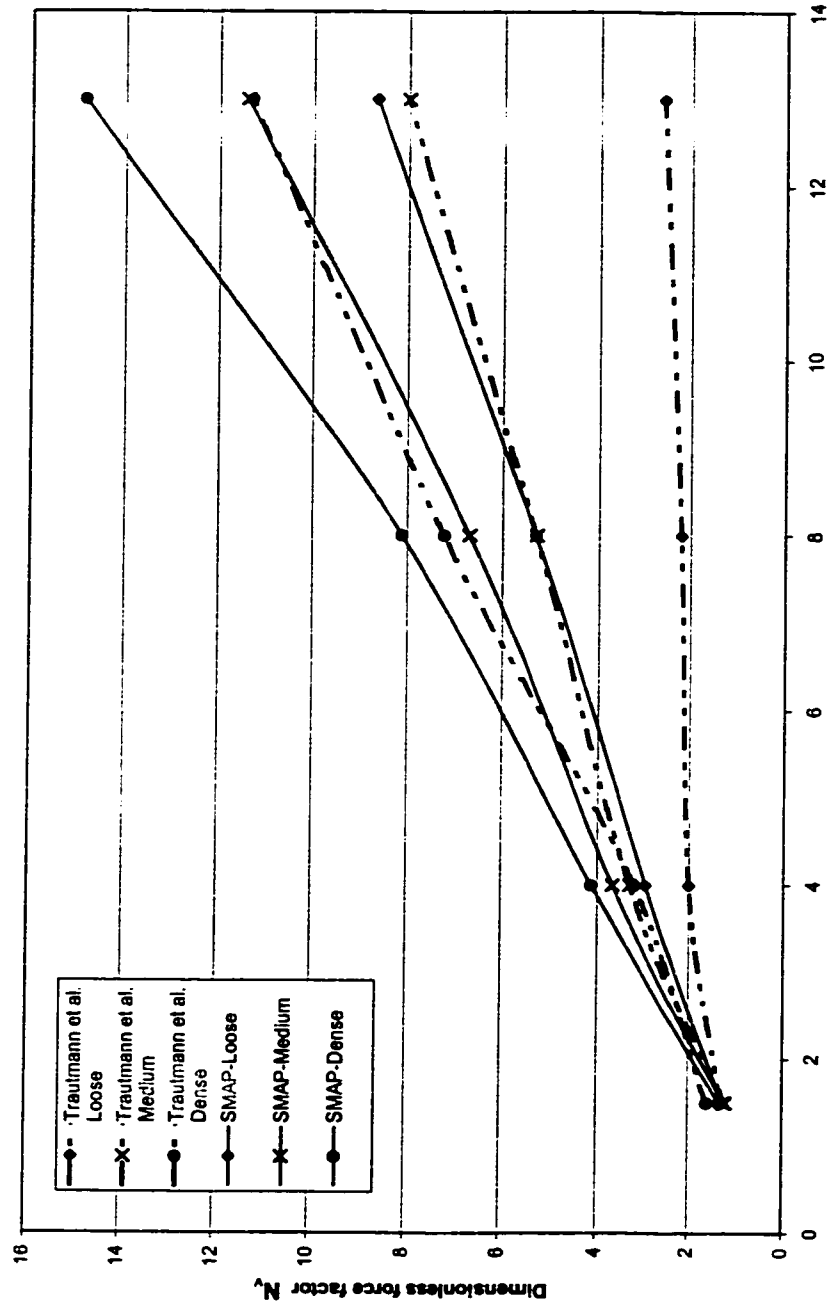

Figure 3-10 Comparison of SMAP-3D and lab test results for uplift movement of pipe

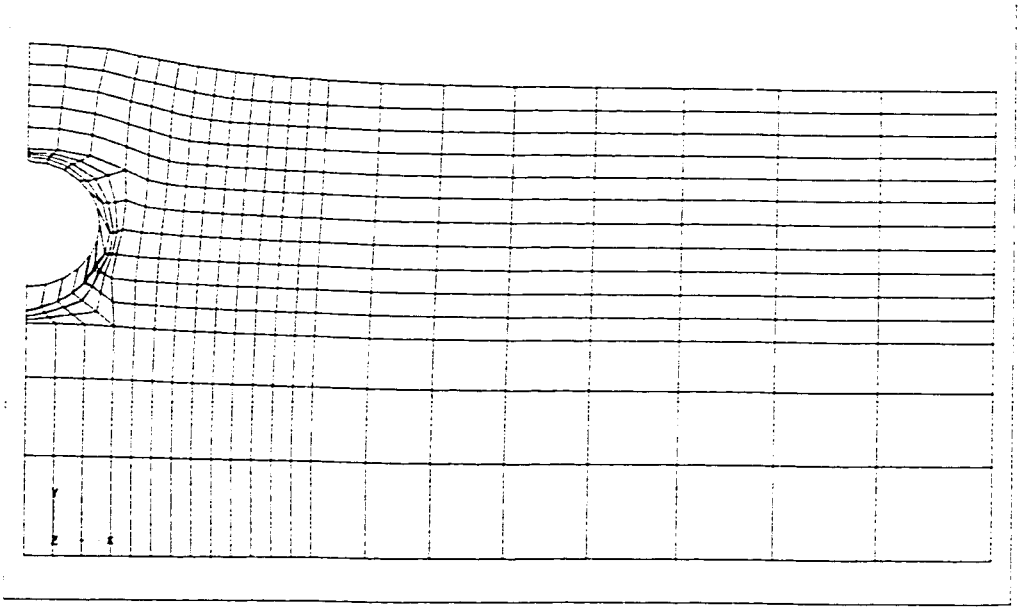

(a) Deformed shape (Deformation 20 times magnified)

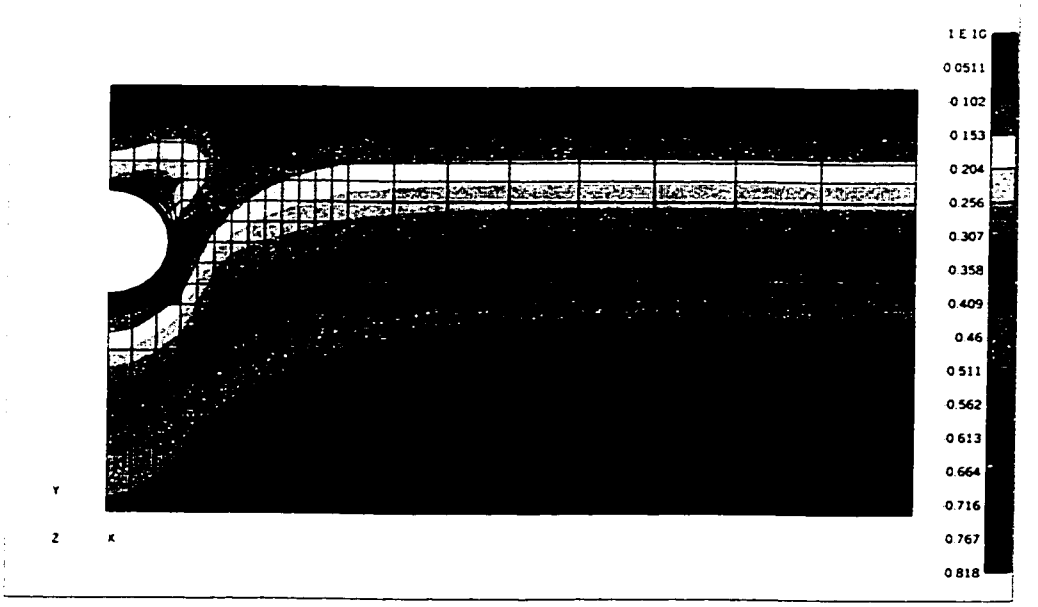

(b) Vertical stress contours

Figure 3-11 Plot of the results of pipe uplift analysis obtained by SMAP-3D analysis at a post soil yield stage

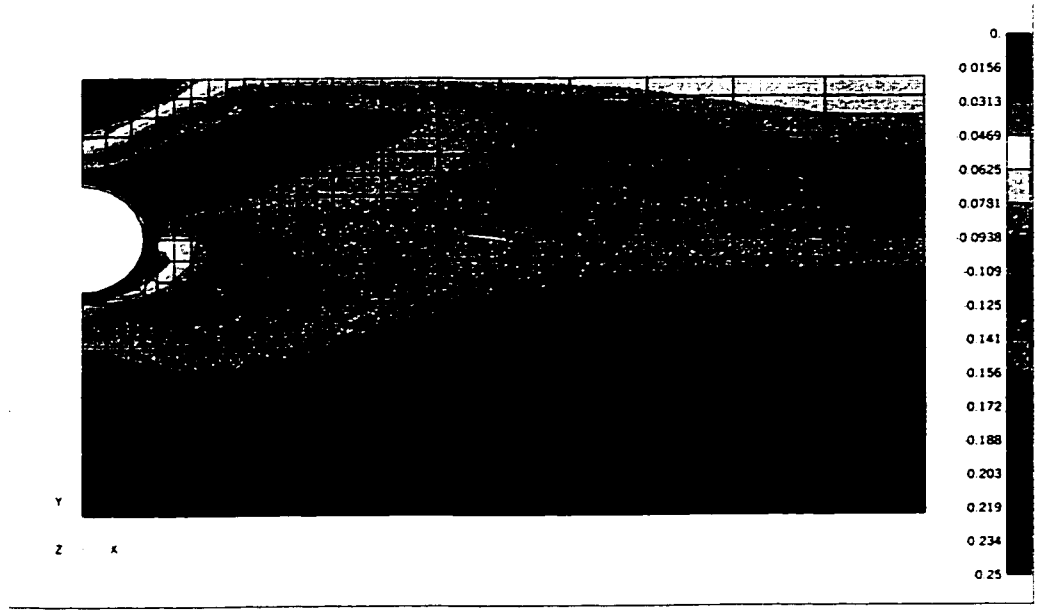

(c) Horizontal stress contours

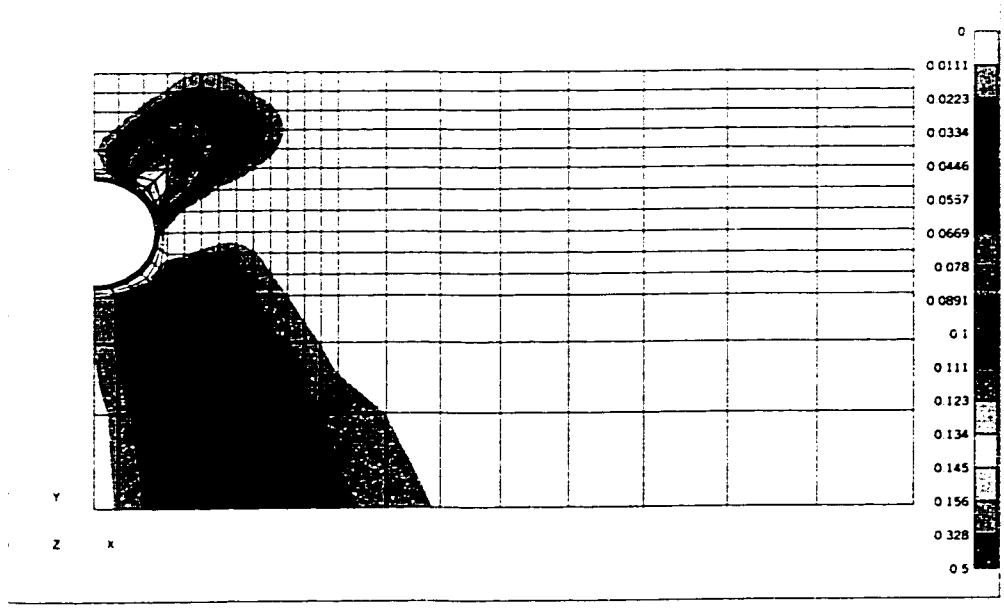

(d) Shear stress contours

Figure 3-11 (Contd.)

surface above the pipe crown (Figure 3-11(c)). The horizontal stress distribution above the pipe crown is similar to the distribution of normal stress in a flexural member. The tensile strength of the sand is zero. This zero tensile strength is specified in the SMAP-3D model, and therefore instead of a zone of tensile stress, a zone of zero stress is visible in Figure 3-11(c). The shear stress contours, as shown in Figure 3-11(d), outlines a plane of maximum shear above the pipe as shown in Figure 1-6(a). A zone of shear stress is also visible beneath the pipe. This zone is generated because the presence of the pipe changes the settlement of the soil column beneath the pipe relative to the settlement of the adjoining soil.

Solution difficulties were encountered while solving the runs of the uplift of buried pipes using SMAP-3D. A number of runs were performed to investigate the reasons of the solution instability, and it was found that the values of joint element properties highly affect the solution stability. The debonding and sliding that occurs along the joint element due to the uplift of a buried pipe make it a highly nonlinear problem. It is found that, among all the other joint element properties, its thickness affects the solution stability the most in the case of the uplift of buried pipes. Stable and converged solutions are obtained only when the thickness of the joint element is taken equal to or larger than a certain minimum value. It is also found that the size of the load increment also affects the stability of the solution. The load is therefore required to be specified in an enough number of steps so that the load increment in a step is sufficiently small. Each of the runs, therefore, has to be solved a number of time by varying the joint element properties and the number of solution steps until

stable and converged results are achieved. The experience gained during the solutions of the uplift of buried pipes helped a lot in the solutions carried out later, in quickly achieving their stable, smooth, and converged solutions.

3.3.3 Modeling of horizontal movement of buried pipes

To further validate the model for horizontal bend problems, the lateral movement of pipe is analyzed using SMAP-3D. Trautmann and O'Rourke (1985 b) carried out a study of the lateral movement of buried pipes, along with the study of pipe uplift movement. The study of buried pipes lateral movement is as well recognized as their study of buried pipe uplift. The data obtained by the study of Trautmann and O'Rourke (1985 b) is therefore selected for comparison with the SMAP-3D model.

A typical load–deformation curve of pipe moving laterally relative to the soil is shown in Figure 3-12. The curve initially has a high slope with little change of the gradient and is almost straight. The curve however starts to change its slope rapidly when the resistance of soil against the lateral movement of pipe reaches its capacity, i.e., passive earth pressure state. The curve then becomes relatively flat and not much resistance is further added against the lateral movement of the pipe. The maximum force generated against the lateral movement of the pipe thus basically depends on the passive earth pressure of the soil. The maximum peak force (F_m) and the corresponding displacement (Z_f) are shown in Figure 3-12.

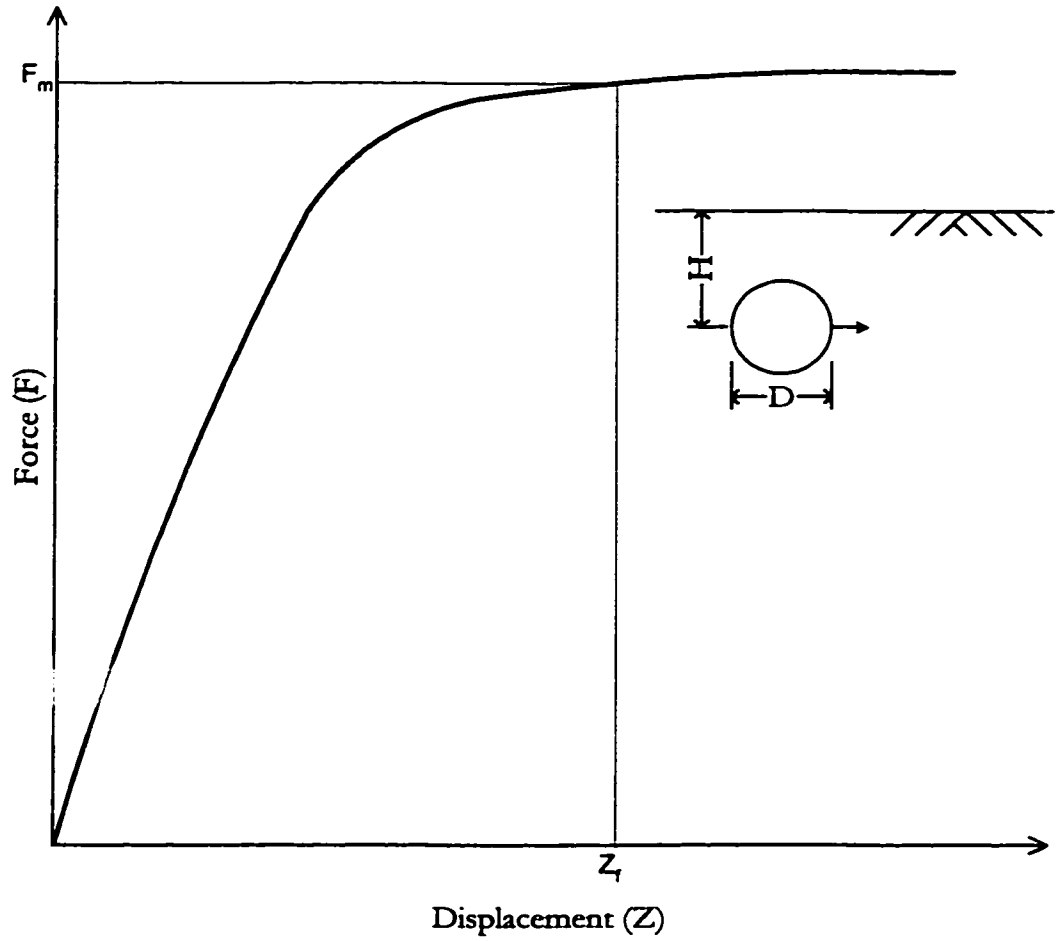

Figure 3-12 A typical load-displacement curve for horizontal movement of buried pipes

The lateral movement of buried pipes is modeled in SMAP-3D for the following parameters:

Pipe outer diameter D = 4 in

Pipe wall thickness t = 0.25 in

Four cover depths are used: H = 6 in, 14 in, 32 in, and 44 in

Three types of soils are investigated:

- Loose sand (γ = 94.2 pcf (14.8 kN/m^3), ϕ = 31°)
- Medium sand (γ = 104.4 pcf (16.4 kN/m^3), ϕ = 36°)
- Dense sand (γ = 112.7 pcf (17.7 kN/m^3), ϕ = 44°)

The analysis is carried out using displacement control. It is found that as the pipe moves laterally, a void is created behind it, which creates instability in the FEM solution. To overcome this difficulty, linear elastic elements are used just behind the pipe. The elasticity parameters and the weight of these elements behind the pipe are kept the same as the rest of the soil. The domain idealization is shown in Figure 3-13. The mesh is prepared such that reasonable mesh density and element aspect ratios are obtained. The two-dimensional mesh is thus prepared in a manner as described in detail in Chapter 4. As discussed for the buried pipe uplift validation runs above, each of the runs have to be solved a number of time by varying the joint element properties and number of solution steps until stable and converged results are achieved.

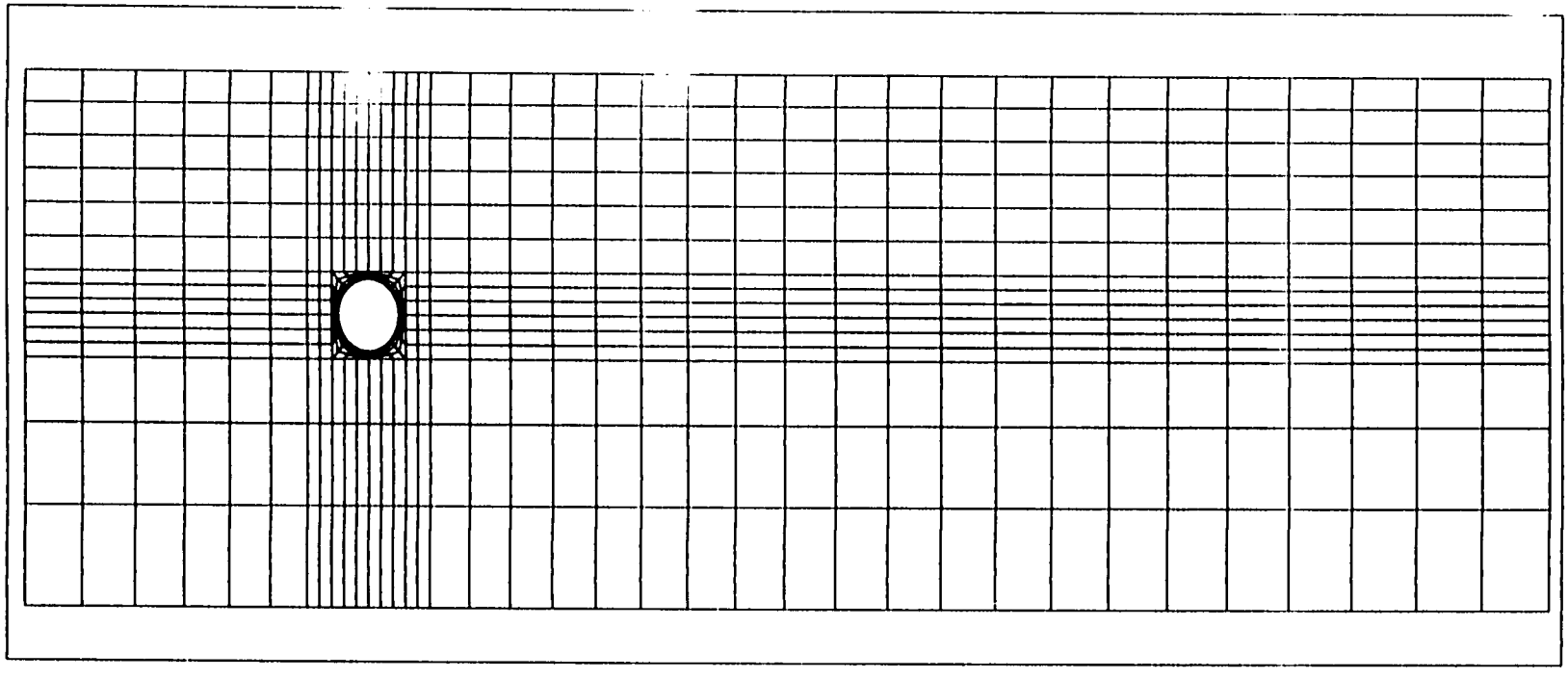

(a) Typical mesh

Figure 3-13 Domain idealization used to model the horizontal movement of a buried pipe

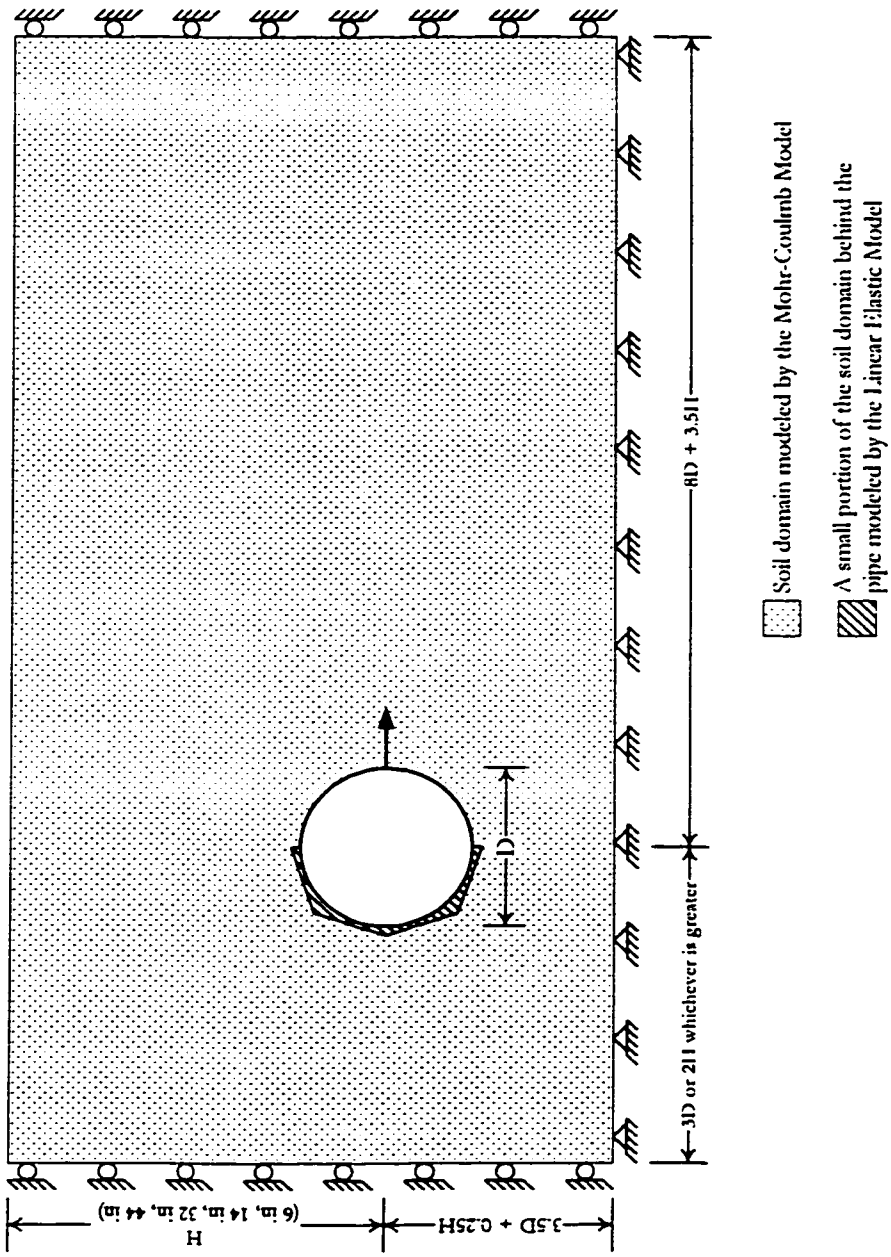

(b) Dimensions and boundary conditions of the mesh

Figure 3-13 (contd.)

The load-deformation curves obtained by the SMAP-3D analysis are shown in Figure 3-14. The maximum force F_m is located on the curve by the arrows at the point beyond which the curve becomes relatively flat.

The strength of soil against the lateral movement of a buried pipe is usually quantified by a dimensionless factor N_h that can be expressed as,

$$N_h = \frac{F_m}{\gamma HDL} \tag{3-3}$$

Where, N_h is the dimensionless factor quantifying the strength of a buried pipe against the horizontal movement,

F_m is the maximum force against horizontal movement of a buried pipe,

γ is the unit weight of the soil,

H is the depth of the pipe center below ground surface,

L is the length of the pipe, and

D is the outside diameter of the pipe.

The dimensionless quantity N_h has a similar relationship with buried pipes as the coefficient of passive earth pressure K_p has with earth retaining structures. The values of N_h are calculated accordingly from the SMAP-3D results and its comparison with the results of Trautmann and O'Rourke (1985 b) is shown in Figure 3-15. The SMAP-3D results compared well for loose and medium soils. The over prediction for larger cover depths is because of the fact that analytical models like

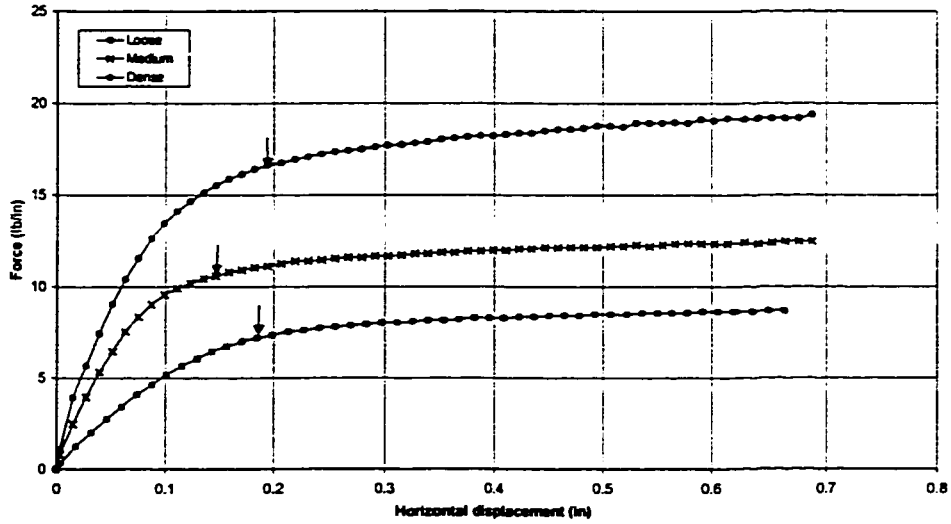

(a) H = 6 in (H/D = 1.5)

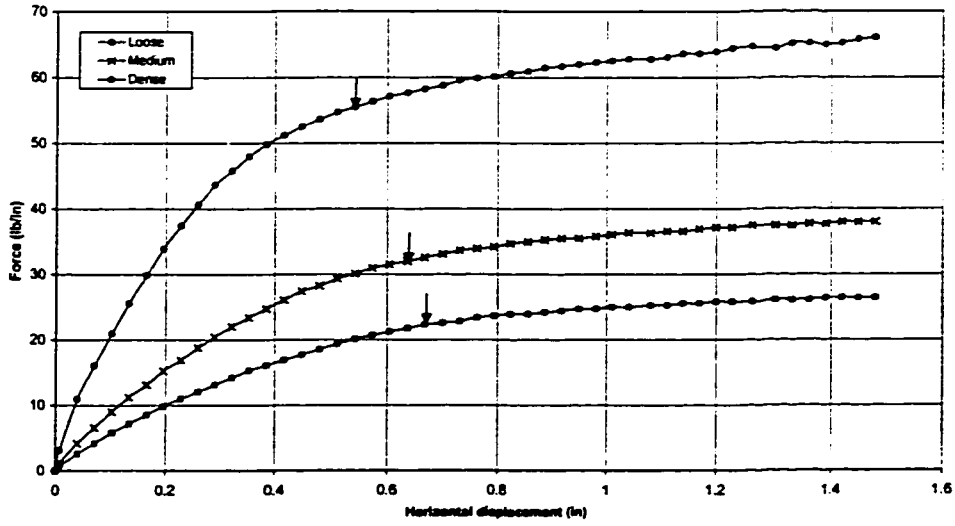

(b) H = 14 in (H/D = 3.5)

Figure 3-14 Load-deformation curves obtained by the SMAP-3D analysis for the lateral movement of buried pipes.

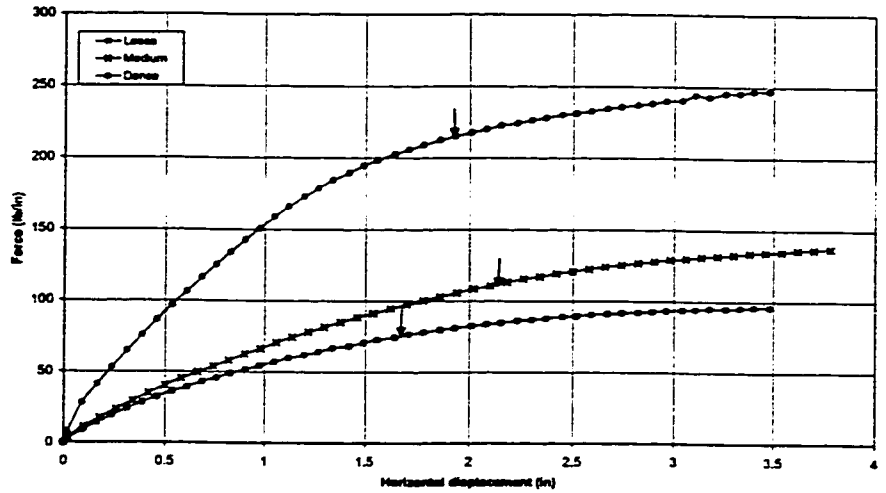

(c) H = 32 in (H/D = 8)

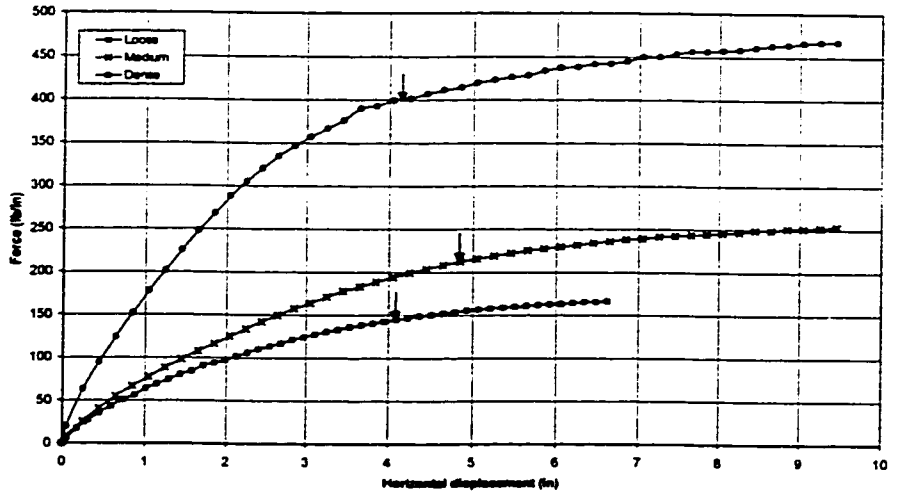

(d) H = 44 in (H/D = 11)

Figure 3-14 (Contd.)

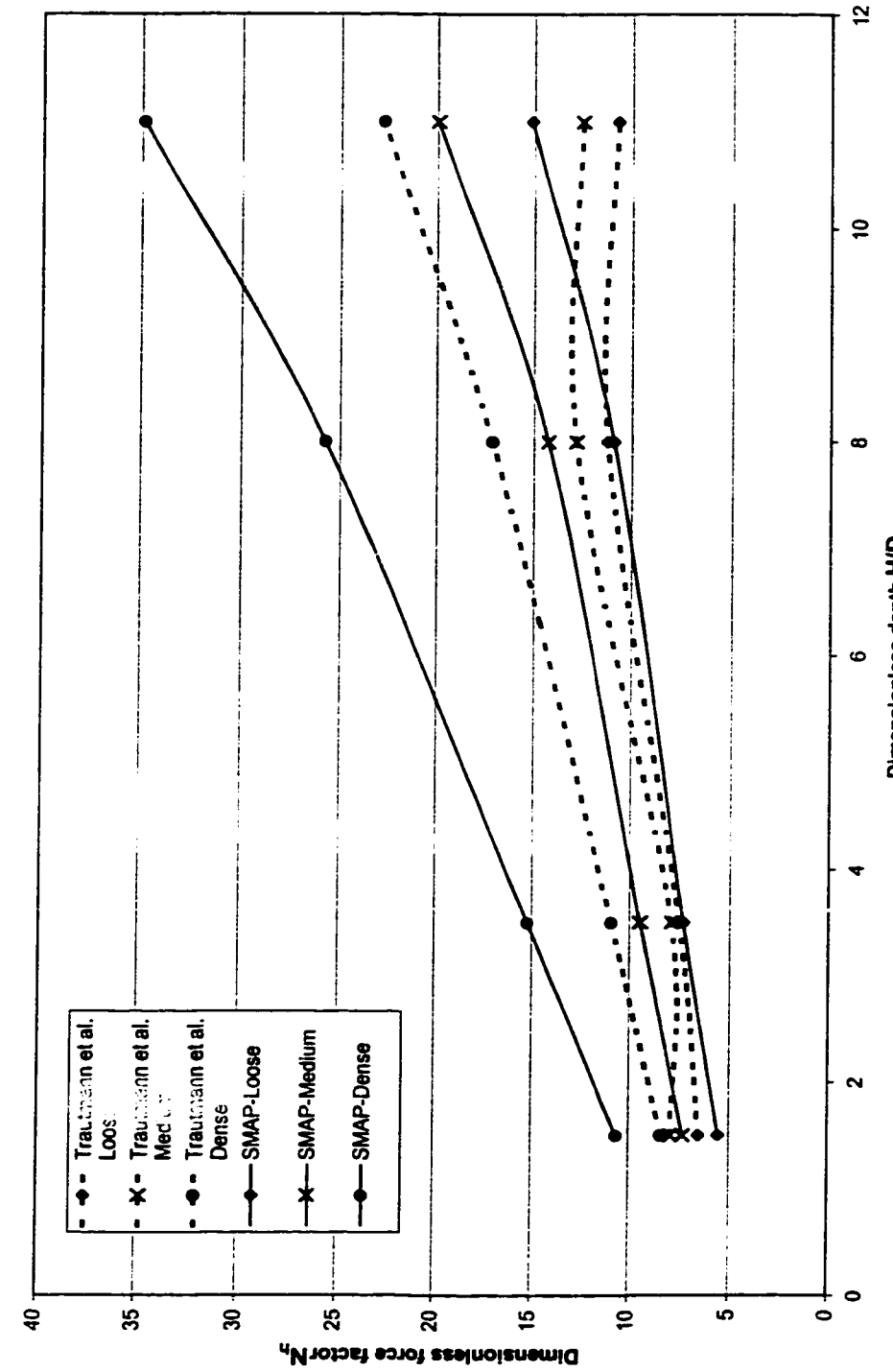

Figure 3-15 Comparison of SMAP-3D with lab test results for lateral movement of pipe

SMAP-3D can not account for the large volume reductions that occur during shear. SMAP-3D is also over predicting the results for dense sand. One of the possible reasons for this discrepancy is that the value $\phi = 44°$ for dense sand as reported by Trautmann and O'Rourke (1985 b) is determined using direct shear test. Triaxial test results are however more appropriate for use with the 3 dimensional analysis of SMAP-3D. The angle of internal friction obtained from a triaxial test can be 1 to 5 degrees smaller than that obtained from a direct shear test.

A typical deformed shape and the stress contours obtained by the analysis at a post soil yield stage are shown in Figure 3-16. The confinement of the soil above the pipe is always less than the infinite confinement provided by the soil domain below the pipe. Therefore, when a pipe moves laterally it also displaces in the upward direction. This oblique motion of the pipe and the separation at the pipe-soil interface behind the pipe (stretching of joint elements) are apparent in Figure 3-16(a). The cover goes up along with the pipe and the deformation in soil above the pipe is also visible in the deformed shape. The separation of pipe-soil interface has resulted in the reduction of vertical stresses behind the pipe (Figure 3-16(b)). There is an increase in vertical stress between the pipe invert and the front springline of the pipe. This resistance to the pipe lateral movement is however not available between the crown and the front springline and that is why pipe rolls up while moving horizontally. The passive stress induced in the soil in response to the pipe lateral movement is shown in horizontal stress contours (Figure 3-16(c)). The shear stress contours as shown in Figure 3-16(d) outlines a plane of maximum shear stress as shown in Figure 1-6(b).

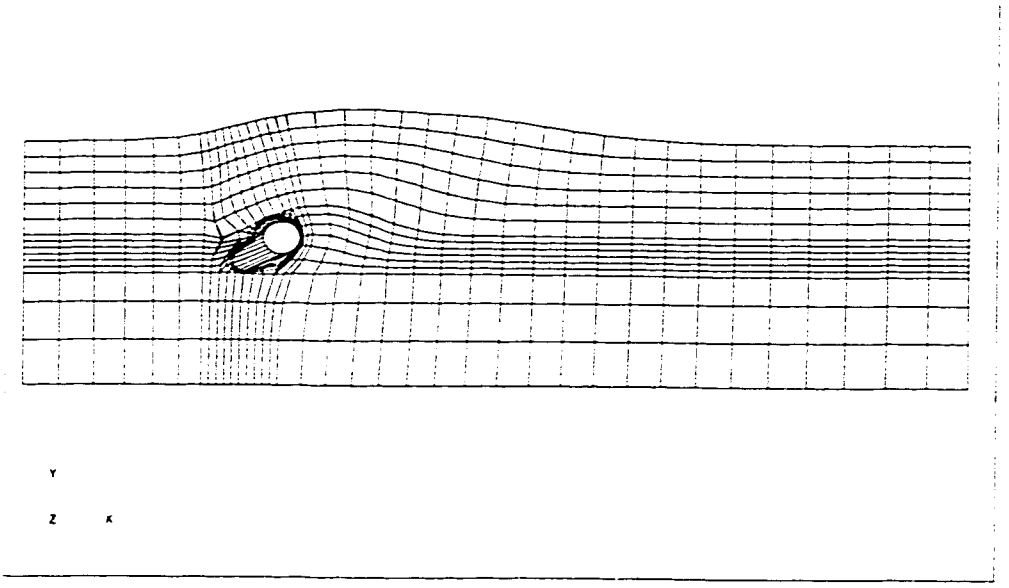

(a) Deformed shape (Deformation 3 times magnified)

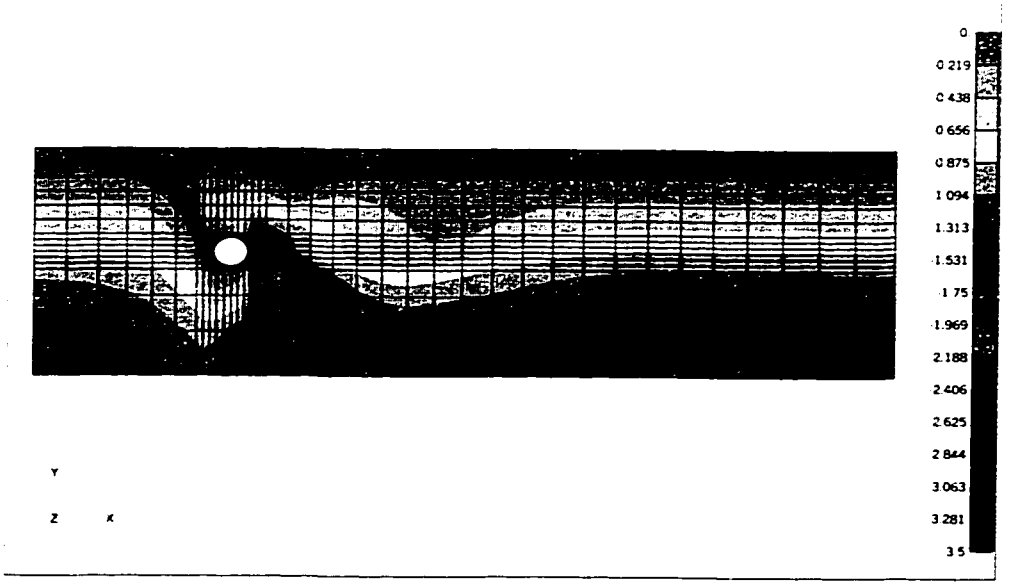

(b) Vertical stress contours

Figure 3-16 Deformed shape and contours of pipe lateral movement obtained by SMAP-3D analysis at a post soil yield stage.

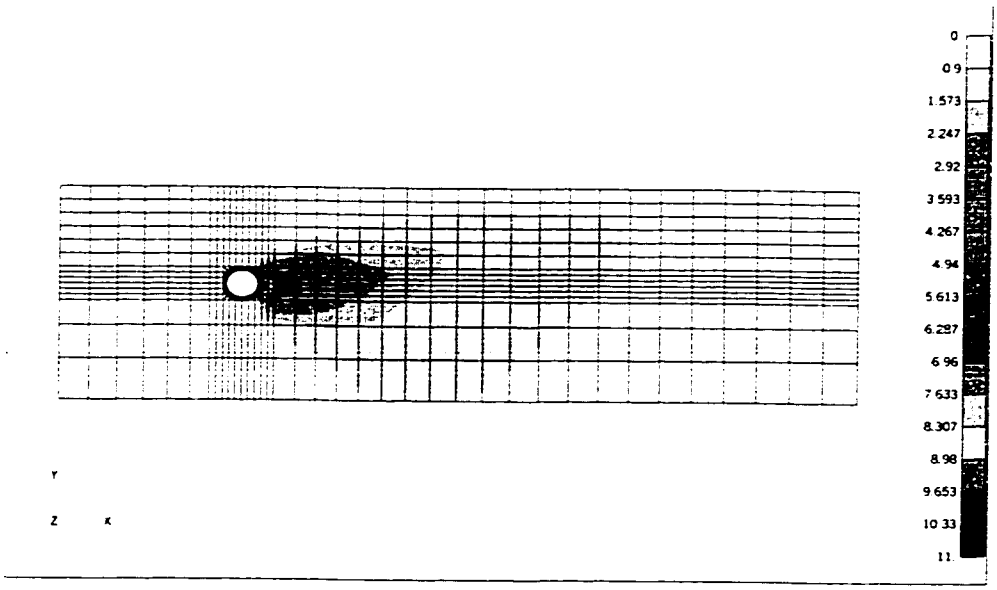

(c) Horizontal stress contours

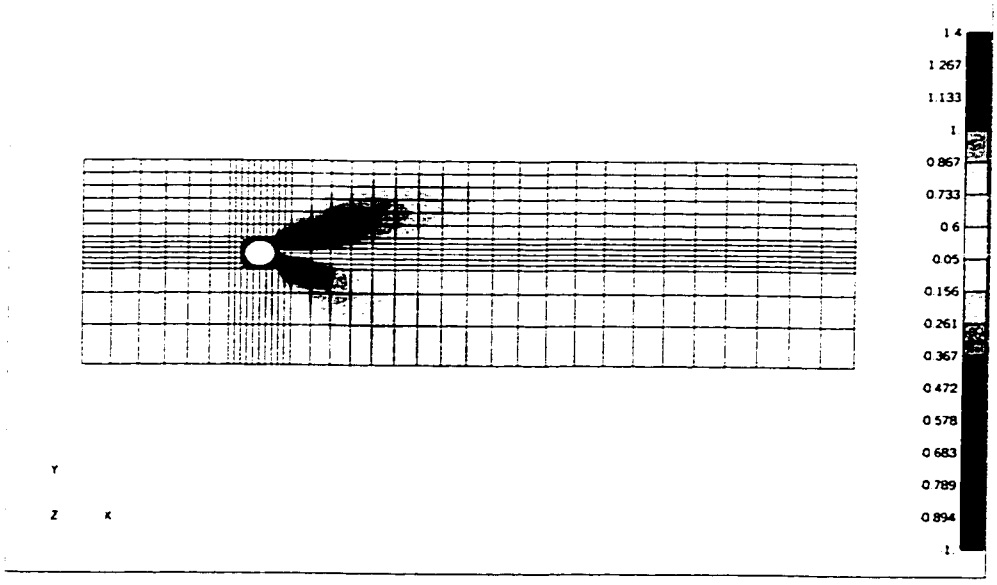

(d) Shear stress contours

Figure 3-16 (Contd.)

The state of passive earth pressure is attained when a curved plane of shear stresses is developed beginning in between the pipe crown and the front springline of the pipe and reaching up to the ground surface.

3.4 Summary

The feasibility of using SMAP-3D (1999) for the analysis of three-dimensional buried pipe systems is investigated. SMAP-3D has continuum soil elements along with shell elements to model the pipe. The pipe-soil interface can be modeled using the joint element available in the software. The capability of the program to model structural behavior of buried pipe systems is validated by comparing its results with the well-recognized available models and the lab test results. The structural phenomena investigated for this purpose include the load distribution or arching in the soil around a pipe, the strength of soil against the uplift movement of a pipe and the strength of soil against the horizontal movement of a pipe. SMAP-3D is therefore found suitable for the analysis of the three-dimensional structural system of buried pipe bends.

The SMAP-3D results compared well with the Marston formula of earth load on buried pipes. The SMAP-3D results show that it is capable of modeling soil arching and the earth load transfer mechanism at the buried pipes, which depend on the ratio of the stiffnesses of pipe and the soil. SMAP-3D results show positive arching for flexible pipes and negative arching for rigid pipes.

SMAP-3D is found to over predict the soil strength against the uplift and lateral movement of pipes for high cover depths and loose soils. The current study of buried pipe bends is however focused towards shallow buried pipes, where the H/D ratio is mostly less than 2.5. The SMAP-3D results compared well with the published results for small H/D ratios for all soils. Thus SMAP-3D is well suited for the purpose of the current study.

CHAPTER 4
DATA FILE PREPARATION AND MESH GENERATION

4.1 Introduction

The main task in modeling a structure in SMAP-3D is to generate the mesh of the structure and prepare the data file. The data file prepared to model a structure in SMAP-3D has the following main sections:

1) System control and title of the problem
2) Analysis type information, i.e., static or dynamic, linear or nonlinear, etc.
3) Computational parameters including number of load steps, number of iterations, and other nonlinear analysis parameters
4) Nodal indices, their boundary conditions, and coordinates
5) Continuum elements with sub-sections for:
   - Material properties
   - Element indices and their nodal connectivity
   - Initial stress and surface traction
6) Beam elements
7) Truss elements
8) Element Activity

9) Loads, with sub-sections for:
   - Gravity load
   - Concentrated nodal forces
   - Specified and initial velocity
   - Specified base acceleration
   - Transmitting boundary
10) Requested Output
11) PLTDS plot information
12) PLTXY plot information
13) FEMAP plot information

The details of these sections are given in the user's manual of SMAP-3D (1999) in which each of the sections as described above is referred to as a *card* of the data file. Some of the important aspects of the input required by SMAP-3D and the data file structure are discussed below.

The continuum element of SMAP-3D can be defined as an eight-noded brick element or a 6-noded wedge element. It is a general element that has the capability of modeling two-phase fluid-grain medium. The material property data required for the continuum elements therefore includes fluid, grain, elasticity, and yield criterion parameters. The shell element has been included as a special continuum element in SMAP-3D, and its data is defined along with the continuum element data. It can be defined as a four-noded quadrilateral or a three-noded triangular. The joint element

is also defined as a continuum element, however its thickness is defined by the value given in the material data section of joint elements. SMAP-3D modifies the coordinates of nodes connected to the joint face of a joint element according to its specified thickness.

Most of the loading data is specified in card 9 of the data file. The temperature history data file is however prepared separately with the file name *Eltemp.dat*.

After processing, a given data file SMAP-3D can generate its output for three post-processing programs. PLTDS and PLTXY are two utilities that come as part of the SMAP-3D package. PLTDS is a program for plotting meshes their deformed shapes and stress contours. PLTXY is used to get graphs for the various structural responses. These graphs can be made with respect to solution increments (time history) or with respect to distance across the mesh (snapshot). Finite Element Modeling And Postprocessing (FEMAP) (1996 a) is a third party general-purpose pre and post-processing program, which can plot deformed shapes, stress contours, and graphs of the results of a finite element analysis. SMAP-3D develops the neutral file after a solution, which can be used with FEMAP for post processing. The user can define the details of structural responses of his interest in the last three data cards for each of the corresponding three post-processing programs. The output can also be obtained in the form of text files according to the data furnished in data card 10.

The process of mesh generation includes the establishment of nodal coordinates, element connectivity, boundary conditions, and the definition of concentrated and distributed loads. The proper definition of these parameters is very significant in modeling a structure using finite elements. Mesh generation is the most time consuming task of the data file preparation process. The SMAP-3D package comes with various routines that facilitate the generation of the mesh data. However the powerful pre and post-processing program FEMAP is utilized in this study for the generation of meshes. A neutral file can be obtained after the generation of the mesh in FEMAP. A translation program available with the SMAP-3D package then translates the mesh data from the neutral file of FEMAP to a format suitable for the SMAP-3D data file.

The basic data of a structure, i.e., the physical dimensions and the material properties must be available before the preparation of the data file. The components of a buried pipe bend system are the pipe bend, the length of the straight pipe up to the virtual anchor connected at each end of the bend, and the surrounding soil. The independent parameters of a buried pipe bend structural system thus are:

- Diameter, wall thickness, and material properties of the pipe
- Burial depth of the pipe
- Radius and angle of the pipe bend
- Surrounding soil material properties
- Loading, which includes pipe internal pressure, soil, pipe, and pipe contents weight, and pipe temperature differential.

The other parameters are calculated using the values of these independent parameters. The dependent parameters include the soil domain truncation limits where the boundary of the mesh is defined, the distance of the virtual anchor, and the influence length along the straight pipe. Thus for a given set of independent parameters, the dependent parameters are calculated, the mesh is generated, and the data file is compiled for analysis on SMAP-3D.

Before making a data file, all the data required to generate the mesh and prepare the data file is summarized on a data sheet to improve the efficiency of the data file preparation process. The sample data sheets for vertical and horizontal bends are shown in Table 4-1. The title and date are followed by the data of pipe and its burial depth in the data sheet. As discussed later in this chapter, the three-dimensional mesh of a buried pipe bend is generated by extruding a two-dimensional mesh. The data of the 2D mesh is also furnished in the data sheet. The values of the parameters related to the location of the virtual anchor are then given followed by the pipe bend, load, material properties, and the analysis data. The fluid/grain properties data specified at the end of data sheet has to be furnished in the SMAP-3D data file, which requires the data due to its general two-phase media analysis capabilities. The analyses carried out in this study however included elements modeling dry sand, joint elements, and shell elements, which are defined using single-phase media continuum elements. The values given in the fluid/grain properties data section for single-phase media are used by SMAP-3D for material's weight calculations only. For eight noded continuum elements the weight is calculated by the equation:

Table 4-1 Sample data sheets

(a) Vertical bend problem

Title	Sample run for a vertical bend						*Date*	Nov 29,1999
Geometry	Pipe outer dia. (D)	24 in		Center line dia.	23.52 in			
	D/t	50	t 0.48 in	Pipe x-section steel area	35.467 in^2			
	H (Pipe center to ground)	24 in		H/D	1			
	CH (Pipe crown to ground)	12 in						
2D mesh data	No. of pipe elements along x-section	24		Element aspect ratio for soil cover	1			
	In-situ gravity width			84 in				
	In-situ extra width for uplift/lateral			192 in				
	Element aspect ratio for in-situ width			3				
	Bottom width			60 in				
Virtual anchor	C	500	N 1.14	Trench width	60 in			
	C_d	0.23		Pipe - soil friction factor	0.3			
	Virtl. anchor length L_{va}	19500 in		Influence length L_{inf}	350 in			
	Elements in L_{va}-L_{inf}	79		Element length in L_{inf} (2.5 D)	60 in			
Bend data	Bend type	[x] Vertical	[ ] Horizontal					
	Bend radius	700 ft (8400 in)		Bend angle	20°			
	Element length along bend (2D)	48 in						
	Bend extradose apex node number	2082		Bend intradose apex node number	2070			
Loads	Total temperature differential ΔT	120°F						
	Pipe internal pressure	150 psi		γ_{fluid}	0			
Material properties	*In-situ Soil*							
	γ	99.1 pcf	ϕ 35	porosity	0.403			
	E	1000 psi	v 0.3	Shear strength ratio K	0.679			
	C	0	Tensile strength 0	ST Normal	1000	ST Shear	100	
	Joint Element (Pipe - Soil)							
	Joint type	2	E 1000 psi	G	25 psi			
	Thickness t	0.6 in	C 1.00E-08	ϕ	16.7°			
	Shell Element (Pipe Steel)							
	E	$29x10^6$ psi	v 0.3	α	$6.5x10^{-6}$ /°F			
Analysis	No. of load steps	20	No. of gravity steps 5	ΔT for each step	8°F			
	No. of nodes	20760	No. of elements 18460	Execution time	15 Hr 40 Min			
	SMAP-3D file name	n1nxxnnn.001		FEMAP file name	n1nxxn.mod			
Fluid / grain properties	Water unit weight	0.03613 pci		Gravity constant	386.1 in/sec^2			
	Grain blk. modulus	$5x10^6$ psi		Grain sp. gravity*	2.66			
	Fluid blk. modulus	290,000 psi		Fluid sp. gravity	1			
	Permeability coef.	0.01		Mlt. fctr. for perm.	1			

* For shell elements used to model pipe (steel), use 7.85

Table 4-1 (Contd.)

(b) Horizontal bend problem

Title	Sample run for a horizontal bend					*Date*	Dec 13,1999
Geometry	Pipe outer dia. (D) 24 in			Center line dia. 23.52 in			
	D/t 50	t 0.48 in		Pipe x-section steel area 35.467 in^2			
	H (Pipe center to ground) 36 in			H/D 1.5			
	CH (Pipe crown to ground) 24 in						
2D mesh data	No. of pipe elements along x-section 24			Element aspect ratio for soil cover 1.5			
	In-situ gravity width			72 in			
	In-situ extra width for uplift/lateral			318 in			
	Element aspect ratio for in-situ width			6			
	Bottom width			93 in			
Virtual anchor	C_k 20		N 5.05		Trench width 60 in		
	C_d 0.38			Pipe - soil friction factor 0.3			
	Virtl. anchor length L_{va} 19500 in			Influence length L_{inf} 525 in			
	Elements in L_{va}-L_{inf} 31			Element length in L_{inf} (2.5 D) 60 in			
Bend data	Bend type [ ] Vertical			[x] Horizontal			
	Bend radius 50 ft (600 in)			Bend angle 15°			
	Element length along bend (2D) 48 in						
	Bend extradose apex node number 2027			Bend intradose apex node number 2039			
Loads	Total temperature differential ΔT 120°F						
	Pipe internal pressure 150 psi			γ_{fluid} 0			
Material properties	*In-situ Soil*						
	γ 99.1 pcf	ϕ 35		porosity 0.403			
	E 1000 psi	ν 0.3		Shear strength ratio K 0.679			
	C 0	Tensile strength 0		ST Normal 1000		ST Shear 100	
	Joint Element (Pipe - Soil)						
	Joint type 2	E 1000 psi		G 25 psi			
	Thickness t 0.6 in	C 1.00E-08		ϕ 16.7°			
	Shell Element (Pipe Steel)						
	E $29x10^6$ psi	ν 0.3		α $6.5x10^{-6}$ /°F			
	Joint Element (Skew boundary)						
	Joint type 3	E $1x10^{30}$		G 0			
	Thickness t 1	C 0		ϕ 0			
Analysis	No. of load steps 20		No. of gravity steps 5		ΔT for each step 8°F		
	No. of nodes 14184	No. of elements 12900		Execution time 29 Hr 45 Min			
	SMAP-3D file name nnnnnnnn.H01			FEMAP file name nnnnnH.mod			
Fluid / grain properties	Water unit weight 0.03613 pci			Gravity constant 386.1 in/sec^2			
	Grain blk. modulus $5x10^6$ psi			Grain sp. gravity* 2.66			
	Fluid blk. modulus 290,000 psi			Fluid sp. gravity 1			
	Permeability coef. 0.01			Mlt. fctr. for perm. 1			

* For shell elements used to model pipe (steel), use 7.85

$$\gamma = \gamma_w G_s (1-n) \qquad (4\text{-}1)$$

Where, γ is the unit weight of the material,

γ_w is the unit weight of water,

G_s is specific gravity of the material, and

n is the porosity of the material.

The weight, γ_s, of a shell element, which is included as a special continuum element, is calculated using equation:

$$\gamma_s = \gamma_w G_s \qquad (4\text{-}2)$$

4.2 Calculation of Parameters

4.2.1 Mesh limits

The soil system comprises of a semi-infinite domain extending infinitely in horizontal direction and downward. A point in this soil domain is confined all around and moves only vertically down under the action of gravity in the free field or the geostatic state. The presence of any structure such as a pipe in the soil however affects the soil displacement field and stresses. The soil may move both vertically and laterally in the vicinity of the buried structure. This effect of the presence of a structure however exists only for a finite distance around the buried structure, beyond which the soil exists in the geostatic state.

One of the important aspects of making a mesh for the analysis of a buried structure is to truncate the mesh in the semi-infinite domain of soil at a place where geostatic condition exists. The nodal constraints at a vertical boundary thus located can easily be specified, since the only deformation is the vertical direction along the boundary. The horizontal boundary below the structure is located where there is no lateral movement of the soil and the nodes at this boundary are fully constrained. The vertical deformation of all nodes in the mesh is relative to the fixed horizontal boundary at the bottom of the mesh.

The limits that are used for the mesh dimensions and specify the geostatic condition at the boundary are shown in Figure 4-1. The use of the limits shown for buried pipe under gravity load only is quite common. The dimensions used for Level-2 CAN1 mesh in CANDE (1989) are also the same as shown in Figure 4-1(a). There is however no generally accepted criteria for the mesh dimensions of buried pipes moving laterally and upwards. Row and Davis (1982) took a mesh with the dimensions 8 times the anchor plate width on sides and bottom of its center. The mesh used by Altaee et al. (1996) however had much larger dimensions. They did not specify the exact dimensions of the mesh used. Due to lack of clear guidelines, some runs with large mesh dimensions were made for buried pipe movement analysis, along with the validation runs discussed in Chapter 3. It was found that the extent at which the geostatic condition begins depends on the pipe burial depth in addition to the pipe diameter. The dimensions shown in Figure 4-1 (b & c) are conservatively

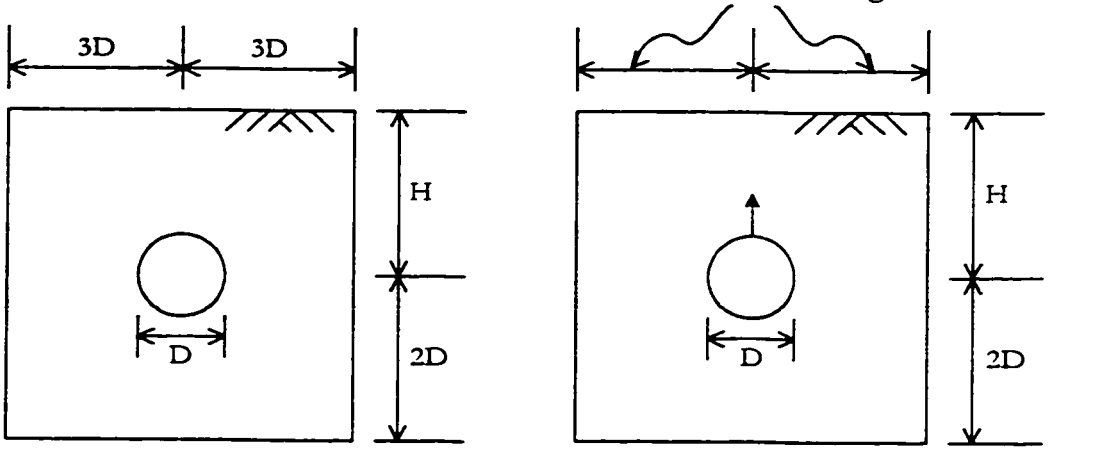

(a) Limits for pipe under gravity loading (b)Limits for pipe moving under uplift forces

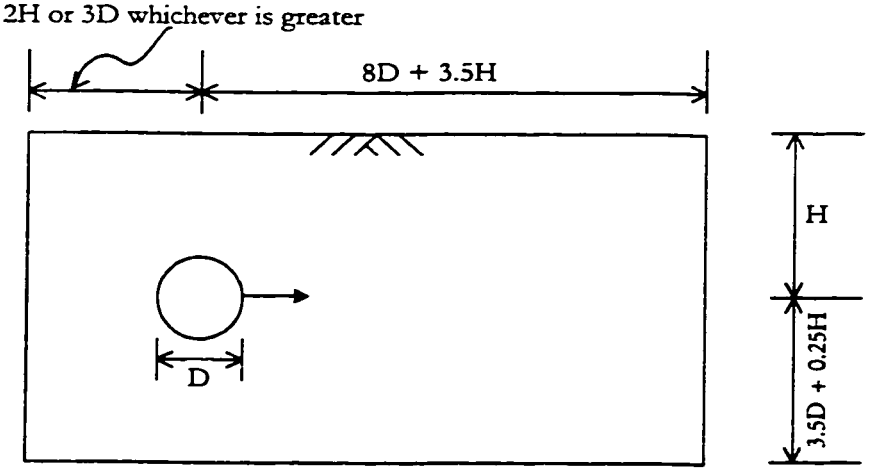

(c) Limits for pipe moving under lateral forces

Figure 4-1 Location of mesh boundaries

established using the observations of the large mesh runs and the values found in the published finite element studies.

4.2.2 Virtual anchor location and influence length

The location of the virtual anchor, defined in Chapter 1, is required to provide appropriate boundary conditions for the three-dimensional mesh of a buried pipe bend. The lateral movement of a buried pipe bend occurs along the bend and the influence length, as discussed in Chapter 1. The determination of the influence length is therefore required so that the mesh dimensions could be defined accordingly. The location of the virtual anchor and the influence length are calculated using the method given in ASME B31.1 (1992). The method is described below according to the specific characteristics of the buried pipe bends.

The process of calculating the virtual anchor length begins with the determination of the value of the subgrade reaction, k. The value of horizontal or vertical subgrade reaction (k_h or k_v) is used depending on the direction of the movement of pipe bend apex. The value of k_h is therefore used for horizontal bends and the value of k_v is used for vertical bends.

There are several analytical methods available to estimate a value for the horizontal subgrade reaction. The equation recommended in ASME B31.1 (1992) is:

$$k_h = C_k N_h \gamma D \qquad (4\text{-}3)$$

Where, C_k is an empirical factor, which depends on soil type,

N_h is a dimensionless factor for the strength of buried pipe against horizontal movement,

γ is the unit weight of the soil, and

D is the outside diameter of the pipe.

This equation is originally recommended by Trautmann and O'Rourke (1985 b). They recommended the values of C_k as shown in Table 4-2. They gave the values of N_h based on the model of Ovesen (1964) as a function of H/D. The values of N_h have been plotted in Figure 4-2. Trautmann et al. (1985 a) recommended a similar expression for uplift subgrade reaction, which is:

$$k_v = 500\, N_v\, \gamma\, D \qquad (4\text{-}4)$$

Where, N_v is a dimensionless factor to for the strength of buried pipe against uplift,

γ is the unit weight of the soil, and

D is the outside diameter of the pipe.

They recommended the use of Vesić (1971) model for the determination of N_v. However the values of N_v for Vesić (1971) model are available only for $H/D \leq 5$ as shown in Table 4-3. For the larger values of H/D they recommended to use the vertical slip surface model recommended by Kulhawy et al. (1983), which defines the value of N_v by equations:

Table 4-2 Factor for estimating horizontal soil stiffness (Trautmann and O'Rourke, 1985 b)

Soil Density	Loose $\phi < 32^{o}$ $\gamma < 16$ kN/m^3 (100 pcf)	Medium ϕ 32°-40° γ 16-20 kN/m^3 (100-130 pcf)	Dense $\phi > 40^{o}$ $\gamma > 20$ kN/m^3 (130 pcf)
C_k	20	30	80

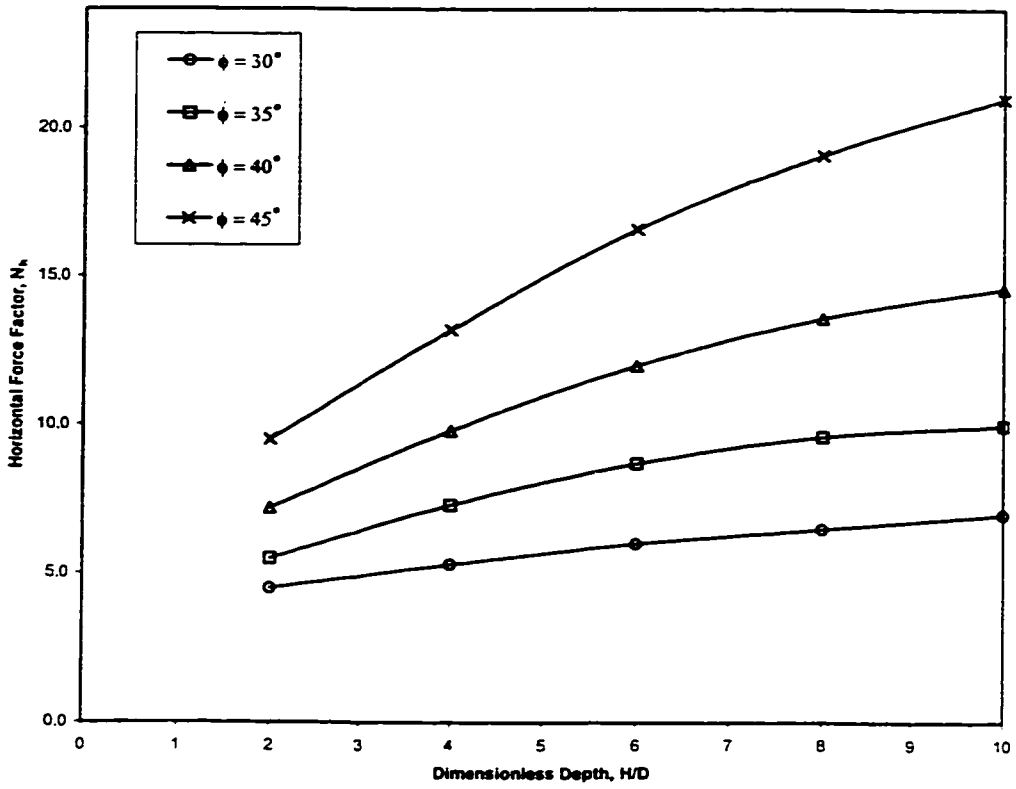

Figure 4-2 Plot of N_h versus H/D

Table 4-3 Values of N_v based on Vesić (1971) model

H/D	ϕ (Degrees)		
	30°	40°	50°
1.0	1.08	1.19	1.25
1.5	1.45	1.61	1.70
2.5	2.03	2.30	2.44
5.0	3.30	3.83	4.12

$$N_v = 1 - \frac{\pi D}{8H} + K \tan\phi \frac{H}{D} \qquad (4\text{-}5a)$$

Where, K is coefficient of lateral soil stress,

ϕ is the angle of internal friction of soil,

H is the depth of pipe center, and

D is the outside diameter of the pipe.

Kulhawy et al. (1983) recommended upper limit on the value of N_v for deeply buried pipes in loose sand. The above equation can therefore be modified for loose sand and H/D > 6 and thus can be written as:

$$N_v = 1 - \frac{\pi}{48} + 6K \tan\phi \qquad (4\text{-}5b)$$

Trautmann et al. (1985 a) have provided the suitable values of K for use in equations 4-5. These values are shown in Table 4-4.

The other quantity required in the calculations of the virtual anchor length is the pipe-soil friction force per unit length of the pipe (f). It is calculated by the equation:

$$f = \mu (P_c A_c + W_p) \qquad (4\text{-}6)$$

Where, μ is the coefficient of friction between the soil and the pipe material,

P_c is the confining pressure of soil weight on the pipe,

Table 4-4 Values of K for use in the calculations of N_v using vertical slip surface model (Trautmann et al., 1985 a)

ϕ	30°	31°	36°	44°	50°
K	0.5	0.5	0.65	0.75	1

For $\phi < 30^\circ$, $\quad K \sim K_o = 1 - \sin \phi$

A_c is the surface area per unit length of a pipe, and

W_p is the weight of a pipe and its contents per unit length of the pipe.

ASME B31.1 (1992) recommends calculating the confining pressure of the backfill on the pipe, P_c, required in the above equation using the following modified Marston equation:

$$P_c = C_d \gamma B_d \tag{4-7}$$

Where, C_d is the Marston's soil load coefficient,

γ is the unit weight of the soil, and

B_d is the trench width at the grade level.

The pipe beyond the location of virtual anchor is fully constrained. The maximum axial force, F_{max}, therefore developed at the virtual anchor due to a temperature change is given by:

$$F_{max} = \alpha \Delta T E A_s \tag{4-8}$$

Where, α is the coefficient of thermal expansion of the pipe material,

ΔT is the temperature change,

E is the modulus of elasticity of pipe material, and

A_s is the cross-sectional area of the pipe.

ASME B31.1 (1992) gives following equations to calculate pipe/soil system characteristic parameter, β, and effective length parameter, Ω.

$$\beta = \sqrt[4]{\frac{k}{4EI}} \tag{4-9}$$

$$\Omega = \frac{A_s E \beta}{k} \tag{4-10}$$

The value of the influence length, which is the length at which the hyperbolic function in the Hetenyi's (1964) equation approaches unity, can now be calculated using the equation:

$$L_{inf} = \frac{3\pi}{4\beta} \tag{4-11}$$

The location of the virtual anchor along the pipe is calculated using the equation:

$$L_{va} = \Omega\left[\sqrt{1+\frac{2F_{max}}{f\Omega}}-1\right] \tag{4-12}$$

4.3 Mesh Generation

The task of generating a three-dimensional mesh of the buried pipe bend system for a given problem is accomplished using the FEMAP program. As pointed out in FEMAP (1996 b), the restrictions on the volume generation capability of FEMAP

make its use limited. The basic strategy, therefore, used in FEMAP is to first generate a two-dimensional mesh along the pipe cross-section. The two-dimensional mesh is then extruded along the pipeline longitudinal axis to get the full three-dimensional mesh.

4.3.1 Two-dimensional mesh of a typical cross-section

First consider the case of the buried pipe vertical bend. The process of mesh preparation starts with the generation of a two-dimensional mesh, as shown in Figure 4-3. Taking advantage of the symmetry, only half of the mesh is used. The process of 2D-mesh generation starts with defining the pipe elements using line elements. The rest of the mesh is then generated in segments around the pipe elements using four-noded plane elements. These mesh segments are added in a sequence, as shown in Figure 4-3.

The joint elements are added using the FEMAP menu command *Generate-Region*. This command can be used to generate two-dimensional elements connected with pre-defined nodes. The thickness of the joint element occupies the region, which is physically taken up by soil. It is, therefore, desirable to keep the thickness of the joint element as small as possible. However, as discussed in Chapter 3, it is found during the validation runs that the solution does not converge if a very small value for the thickness of the joint element is used. Each of the validation runs is, therefore, solved a number of times by changing the value of the joint element thickness, until the stable solution is obtained for the smallest possible value of the joint thickness.

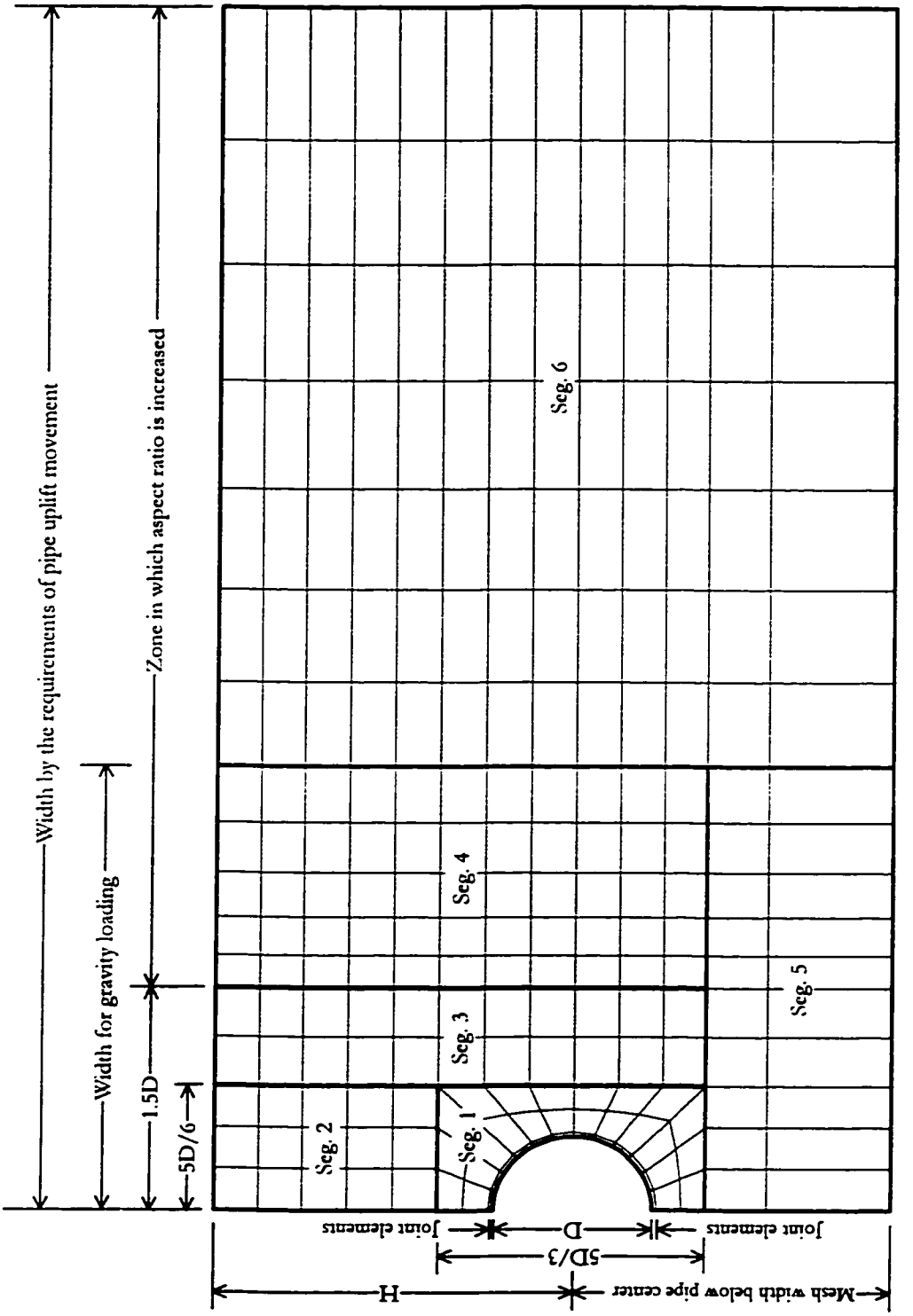

Figure 4-3 Two-dimensional mesh made to extrude to a vertical bend mesh

This trial procedure to obtain a suitable joint thickness is, however, not feasible for the analysis of three-dimensional buried pipe bend systems. Based on the values of joint thickness found during the validation runs, it is concluded that a suitable value of joint element thickness, which does not cause any solution problems, is D/40. Trial runs were carried out initially for the vertical bend problems and it was found that apart from joint thickness, the value of the joint element parameter, G, is also significant in achieving stable results because of the longitudinal movement of the pipe relative to the soil. Stable and converged results are achieved when the value of G does not exceed a certain limit. A value of 25 psi came out to be most appropriate when a cover depth, H_c, of 12 in or more is used. A smaller value of G has to be used in some cases where a very small cover depth is used.

Segment 1 of the mesh is also generated using the menu command *Generate-Region*. Segment 1 is the only segment in which the elements do not have sides at right angles. The minimum angle within the region is 45°. The segment provides a straight edge so that rectangular elements could be generated around it. It was tried to keep the average lengths and breadths of the elements as close to each other as possible within the segment. The size of the sides of the segment is, therefore, decided after varying its value and checking the range of element aspect ratios. The values of the aspect ratios of elements e_1, e_2, e_3 and e_4, shown in Figure 4-4, are 0.93, 0.67, 1.78, and 1.23 respectively. This range of aspect ratios, obtained for a size of 5D/6 of the octant side, is found to be closest to 1 after varying the size of the side for different

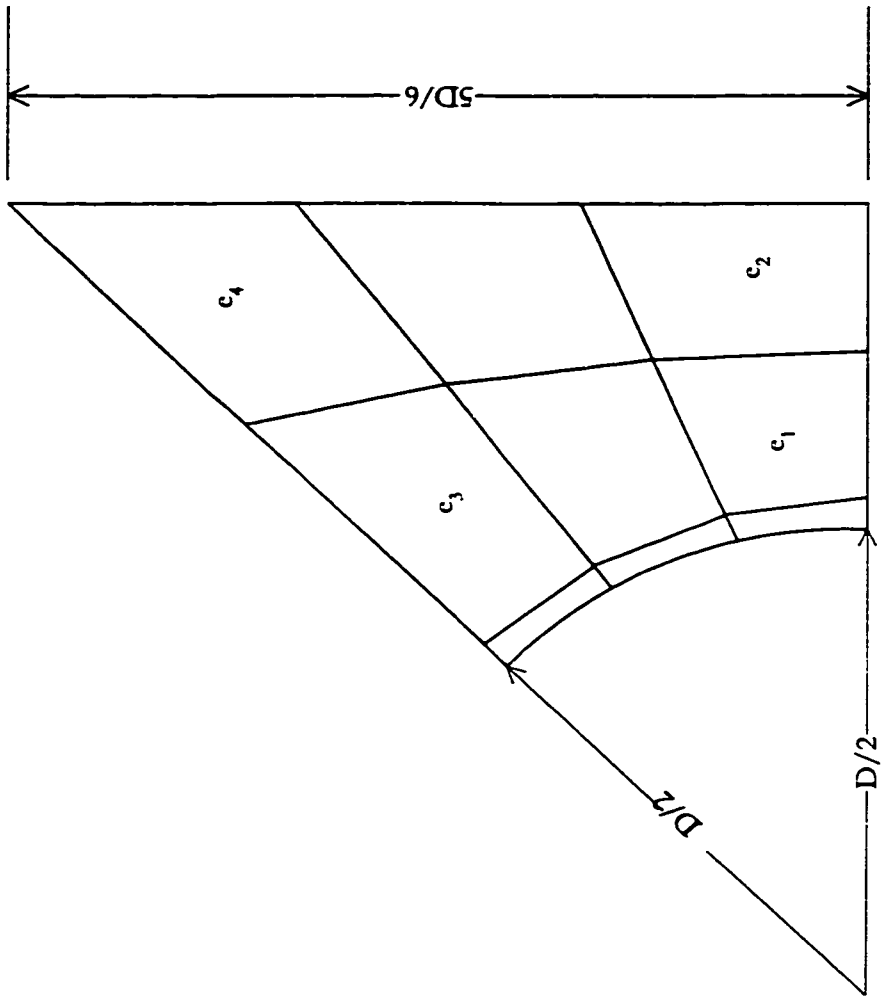

Figure 4-4 Octant of the pipe and the mesh of segment 1

values. Therefore if twelve line elements are used around the pipe semi-circle, then it is concluded that a suitable size of the octant sides is 5D/6.

All other segments are added using the menu command *Generate-Region* except segment 2, which is added using the simplified menu command *Generate-Between* because the segment is generated along a straight edge, which has equidistant nodes.

The aspect ratio is kept 1 for the elements lying within a width 1.5D from the pipe center, i.e., elements within segments 2 and 3. Beyond the width of 1.5D and up to the geostatic boundary, the element aspect ratio is increased gradually. It becomes 3 at the farther edge of the mesh. This scheme allows for a satisfactory mesh density near the pipe while at the same time keeping the problem size relatively small. To examine the effect of mesh density, buried pipes uplift is modeled using two meshes as shown in Figure 4-5. The fine mesh has an element aspect ratio of 1 in segments 2 to 6. The relatively coarse mesh is generated by the element aspect ratio variation procedure described above. A comparison of the results of the two meshes is shown in Figure 4-6. It can be seen that the two results are almost identical.

It will be discussed later that the mesh extruded from the end of the influence length to the virtual anchor has the smaller width as required by the gravity loading shown in Figure 4-1. Segment 4 is thus generated with the outer edge lying at a distance from the pipe center, which is required by the gravity loading geostatic boundary. The final segment 6 is generated with the outer edge located at a distance according

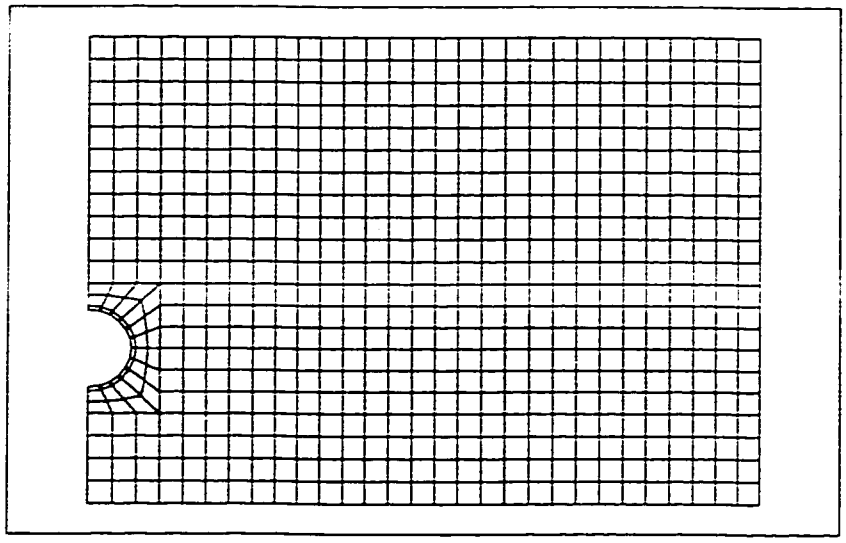

(a) Fine mesh

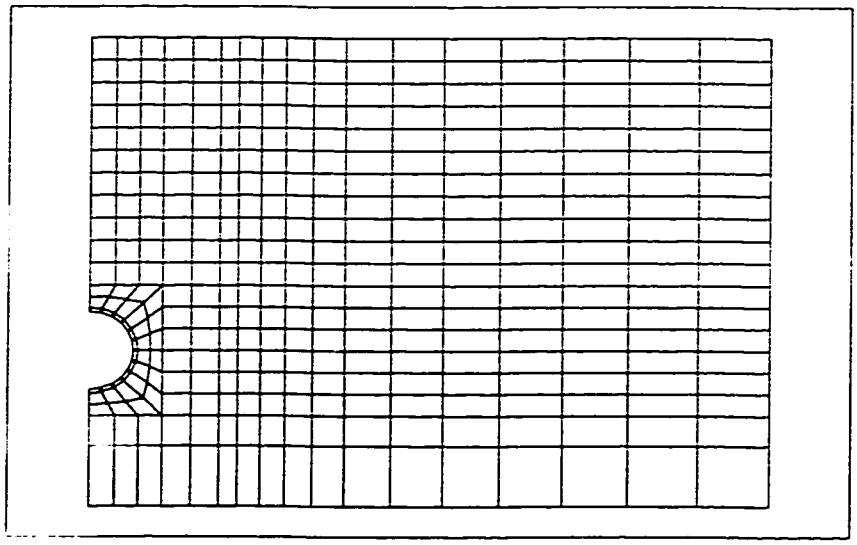

(b) Normal mesh

Figure 4-5 Meshes used to examine the effect of the mesh density for vertical bends

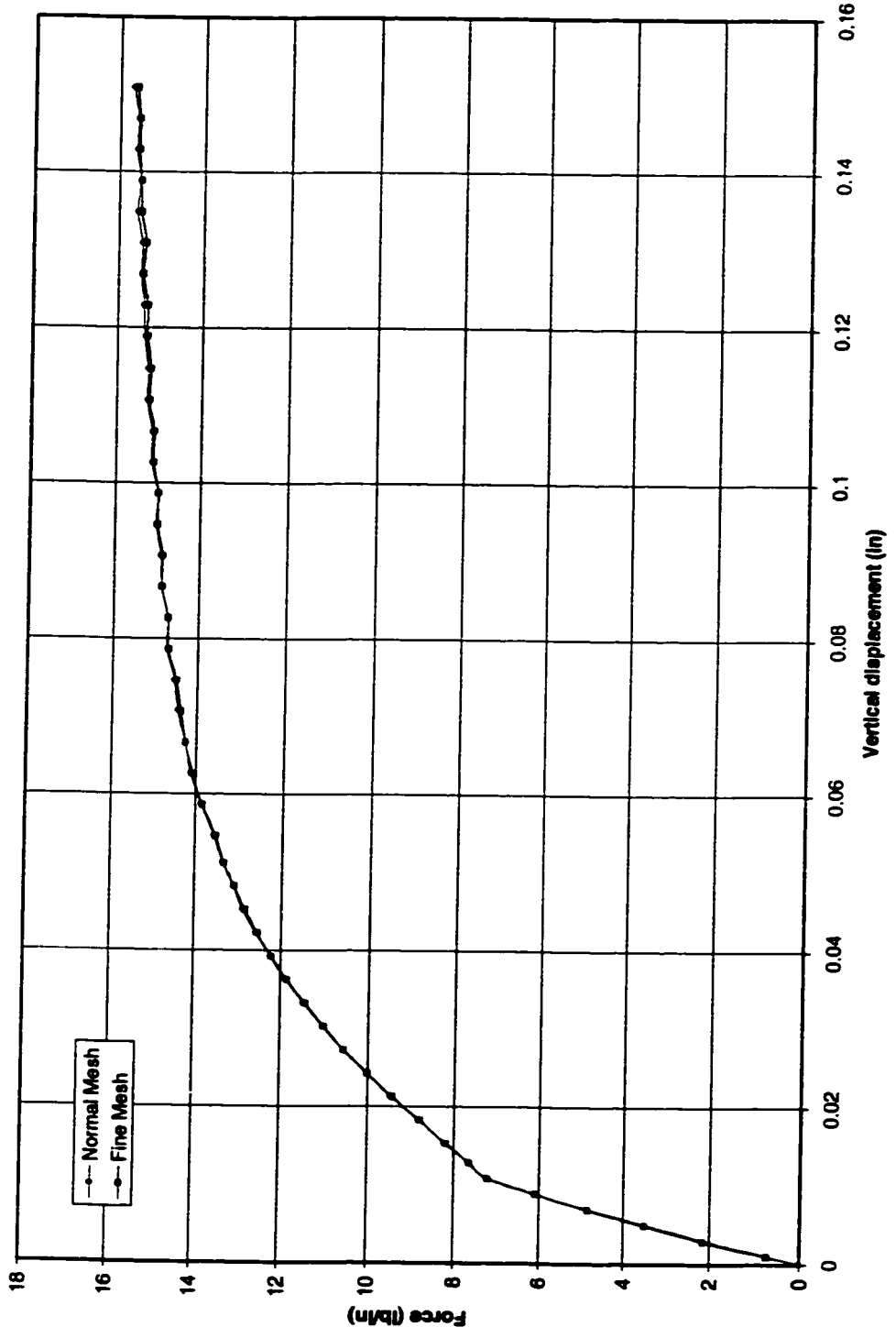

Figure 4-6 Effect of mesh density on the results of the uplift of buried pipes

to the pipe uplift movement requirements. The aspect ratio of the elements is varied within segment 4 and 6. To maintain the rate of change for the element aspect ratio from one segment to the other, the number of elements in the horizontal direction within each segment and the element bias are determined using the rules of arithmetic progression.

The two-dimensional mesh for the buried pipe horizontal bend mesh is prepared in a way similar to that of the 2D mesh for the vertical bends; as shown in Figure 4-7. The full mesh needs to be taken, as no line of symmetry exists in this case. As discussed in Chapter 3, all soil elements are characterized by Mohr-Coulomb model except a layer of elements just behind the pipe; it is assigned the linear elastic model. This is required because as the pipe moves laterally, a void is generated behind the pipe and it causes solution stability problems if Mohr-Coulomb model is used for these elements behind the pipe.

The aspect ratio scheme used for the horizontal pipe bend meshes is similar to that described above for the vertical bends in most of the cases. The horizontal pipe bend model, however, requires a very large-size mesh. In certain cases, the mesh size becomes larger than the capacity of SMAP-3D, which is about 30,000 nodes. Larger element aspect ratios have to be used for such large horizontal bend meshes. An element aspect ratio of up to 2 is used within the soil cover above the pipe. The aspect ratio of the elements along the farther vertical boundary is taken as 5 or above. To examine the effects of mesh density, the buried pipe horizontal movement

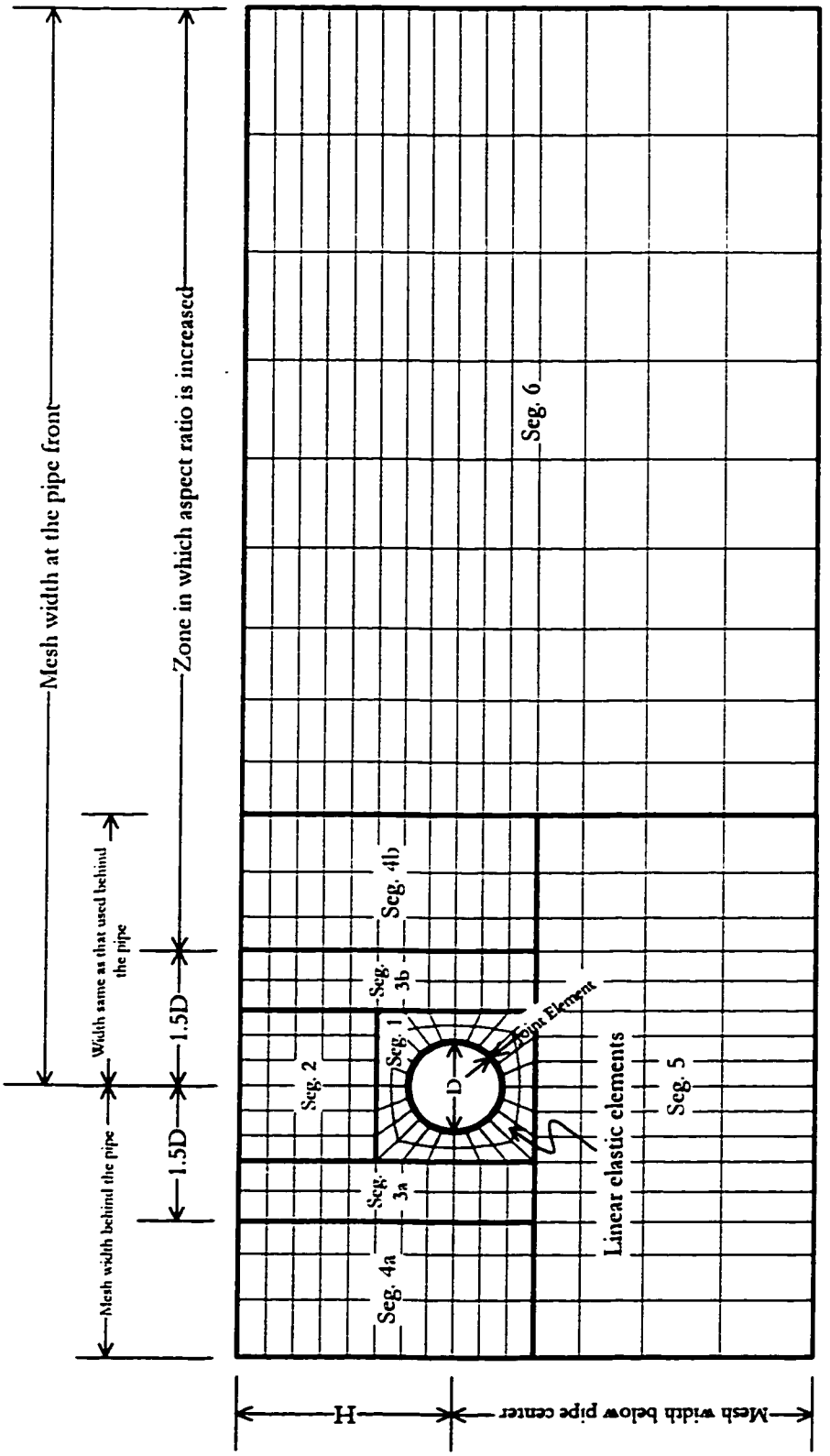

Figure 4-7 Two-dimensional mesh made to extrude to a horizontal bend mesh

is modeled using four meshes, as shown in Figure 4-8. The fine mesh has an element aspect ratio of 1 in segments 2 to 6. The other meshes are generated by the element aspect ratio variation procedure described above. The comparison of the results of the meshes is shown in Figure 4-9. It can be seen that the results of the normal mesh, which has the aspect ratio of the elements at the left vertical boundary (ARVB) as 5 and the aspect ratio of the elements within the soil cover (ARSC) as 1, are almost identical to the fine mesh. The results of the other two coarse meshes slightly deviate from the fine mesh results. This deviation is, however, very small.

The dimensions of the 2D mesh extruded to a horizontal bend mesh are determined using the values shown in Figure 4-1. The width behind the pipe is taken as the larger of that required by the gravity loading and that required for the pipe horizontal movement. The width below the pipe is similarly taken as the larger value obtained by each of the two requirements.

4.3.2 Extrusion of 2D mesh to 3D mesh

When the two-dimensional mesh is ready, it is positioned appropriately in the global coordinate system so that it could be extruded along the longitudinal axis to make the full three-dimensional mesh. The system is symmetric on each side of the pipe bend apex, therefore only half of the mesh is required to be considered. Before a 2D mesh could be extruded to a vertical or horizontal bend mesh, the pipe longitudinal axis needs to be located with respect to the global coordinate system of the FEM model (Figure 4-10). The mesh is located such that the position of the pipe

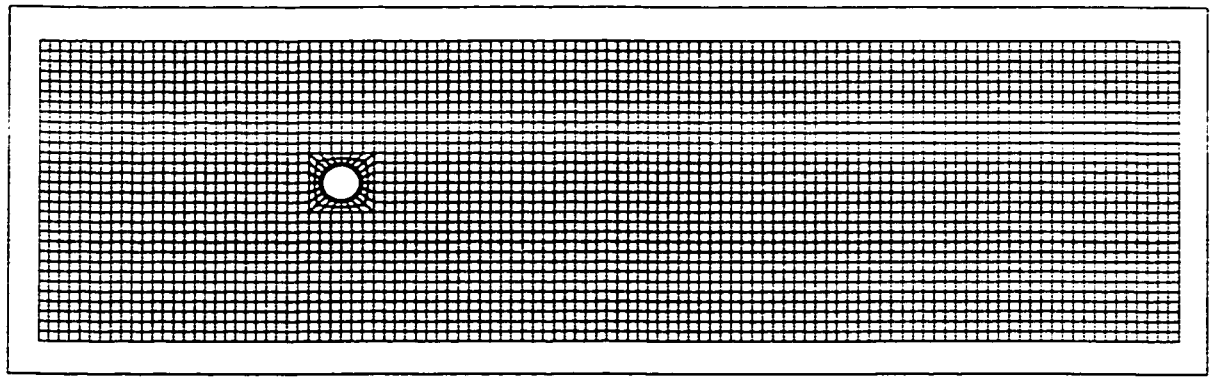

(a) Fine mesh

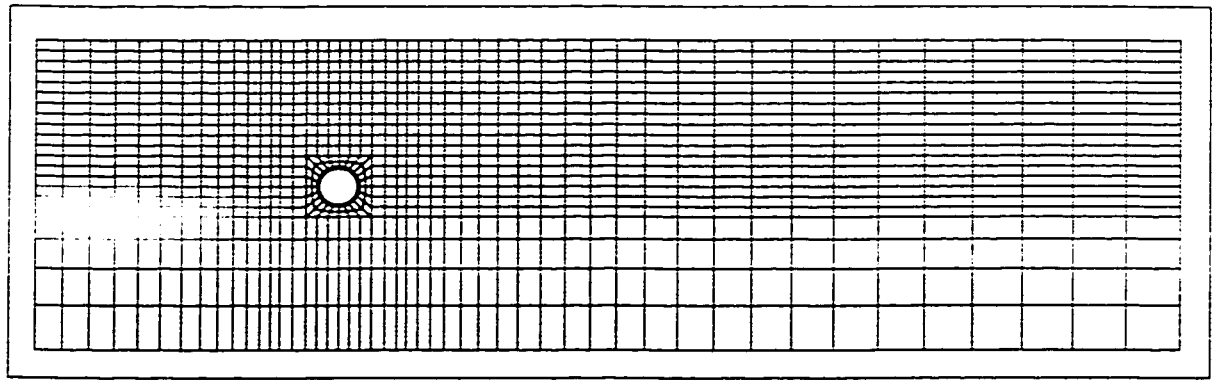

(b) Normal mesh (ARVB = 5 and ARSC = 1)

Figure 4-8 Meshes used to examine the effect of the mesh density for horizontal bends

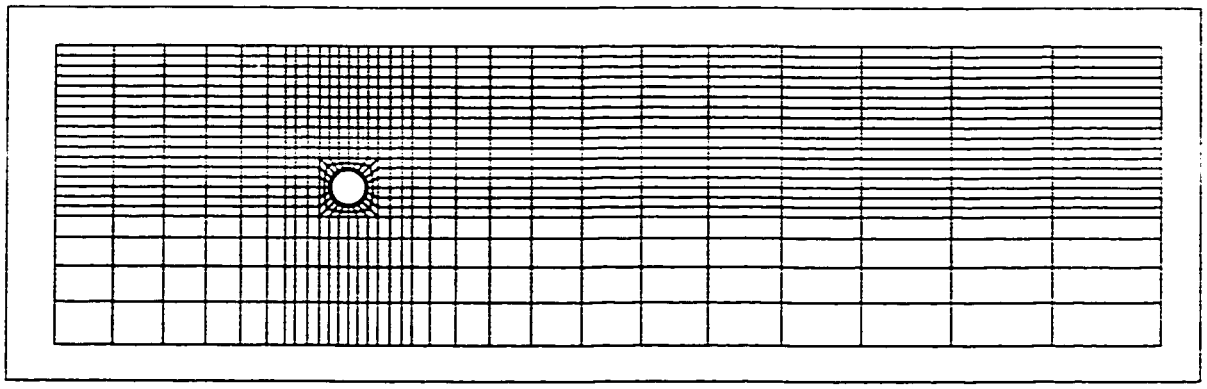

(c) Mesh with ARVB = 10 and ARSC = 1

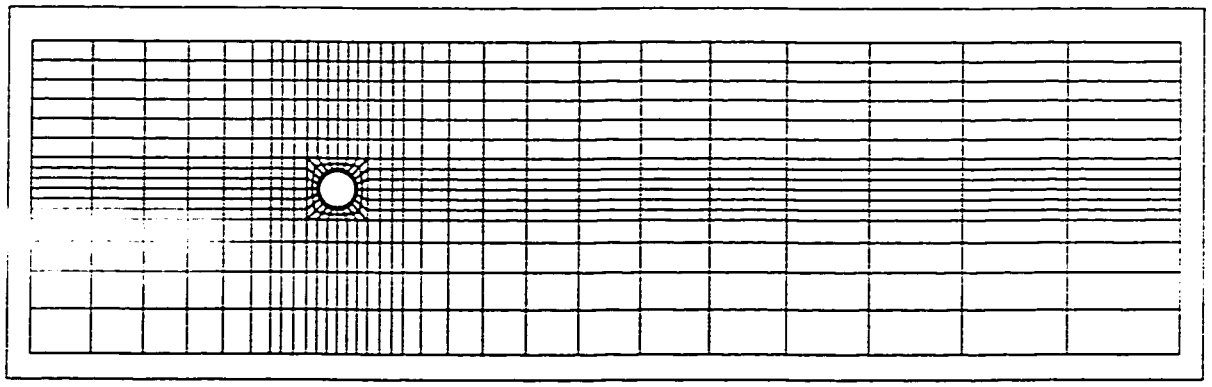

(d) Mesh with ARVB = 10 and ARSC = 2

Figure 4-8 (Contd.)

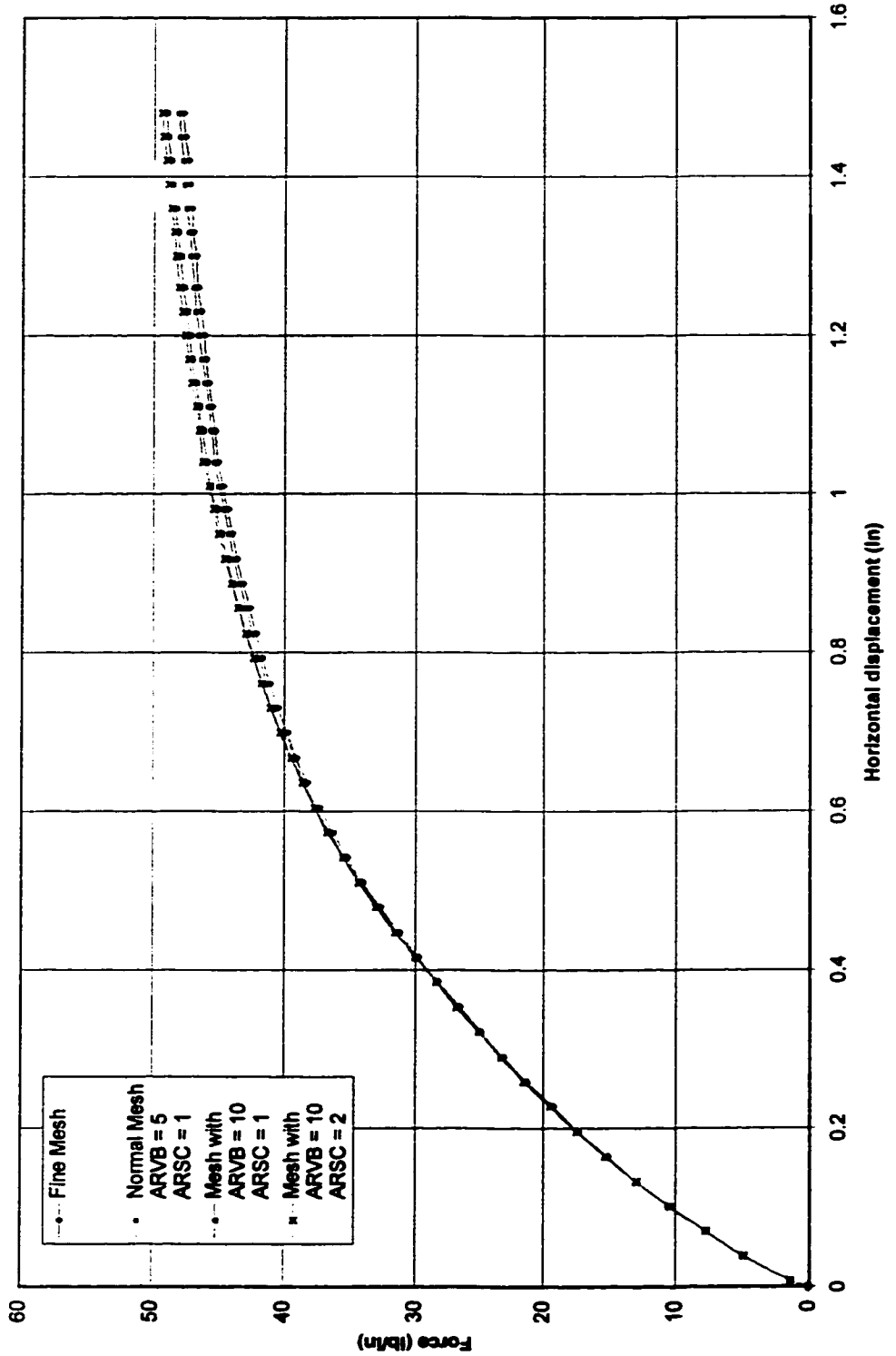

Figure 4-9 Effect of mesh density on the results of the horizontal movement of buried pipes

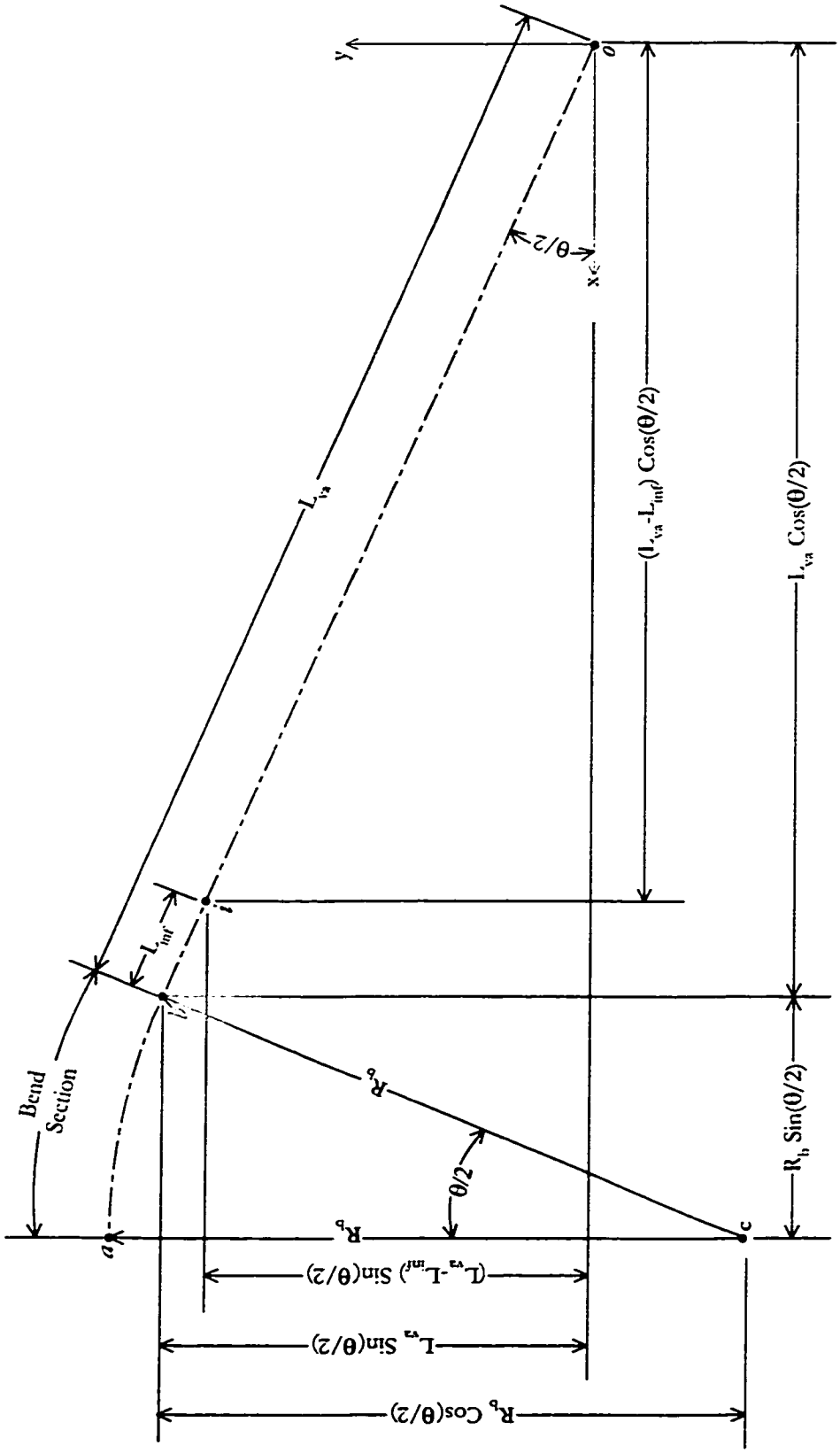

Figure 4-10 Locating buried pipe bend longitudinal axis with respect to global coordinate system of the finite element model

longitudinal axis at the virtual anchor lies at the origin, *o*, of the global coordinate system. The locations that are required to be determined before carrying out the extrusion of the 2D mesh are the center of the bend (*c*), the location where the bend joins the straight pipe (*b*), and the location at the end of the influence length (*i*). The coordinates of the center of the bend are calculated using the expressions:

$$x_c = L_{va} \text{Cos}(\theta/2) + R_b \text{Sin}(\theta/2) \quad (4\text{-}13a)$$

$$y_c = L_{va} \text{Sin}(\theta/2) - R_b \text{Cos}(\theta/2) \quad (4\text{-}13b)$$

The coordinates of the point where the pipe bend joins the straight pipe are:

$$x_b = L_{va} \text{Cos}(\theta/2) \quad (4\text{-}14a)$$

$$y_b = L_{va} \text{Sin}(\theta/2) \quad (4\text{-}14b)$$

The coordinates of the point at the end of the influence length are:

$$x_i = (L_{va} - L_{inf}) \text{Cos}(\theta/2) \quad (4\text{-}15a)$$

$$y_i = (L_{va} - L_{inf}) \text{Sin}(\theta/2) \quad (4\text{-}15b)$$

Once these coordinates are calculated, the two-dimensional mesh is extruded along the longitudinal axis of the pipe. The mesh for the vertical bend thus obtained is shown in Figure 4-11. Similarly, the mesh for the horizontal bend is shown in Figure 4-12.

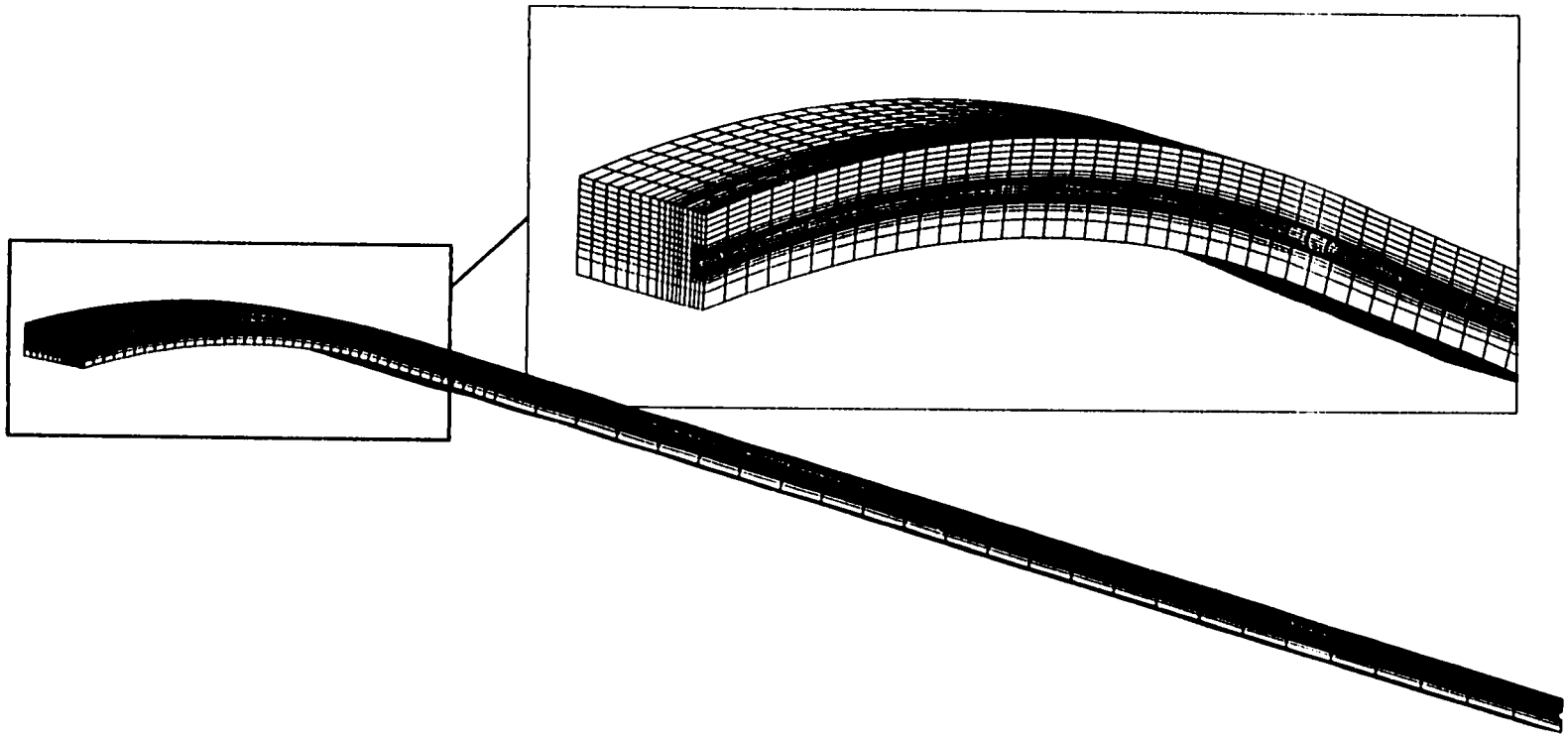

(a) Perspective view

Figure 4-11 Buried pipe vertical bend mesh

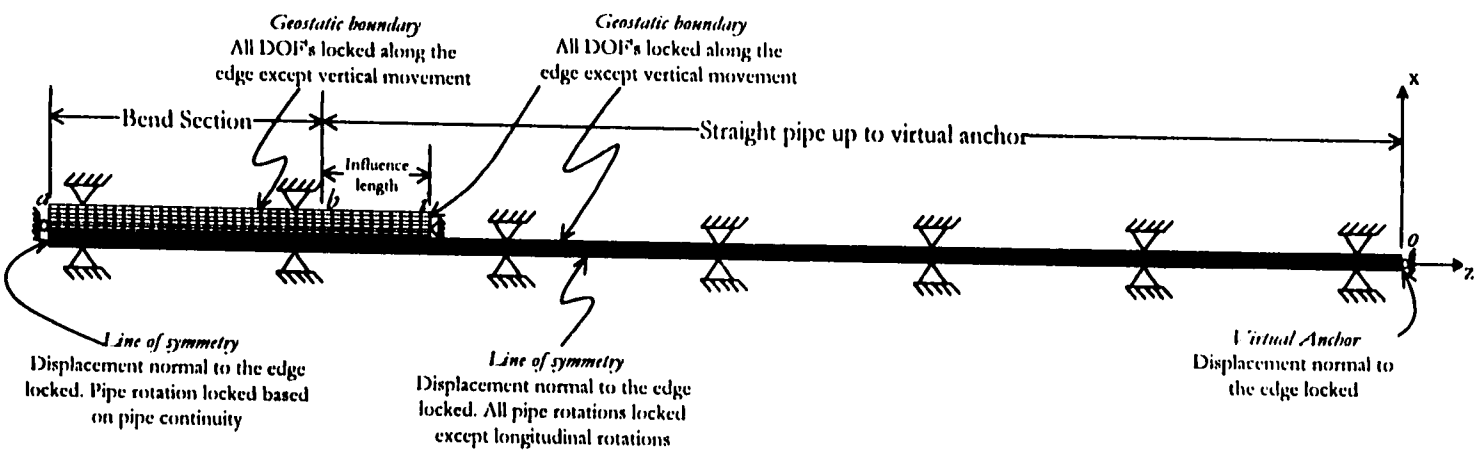

(b) Plan

Figure 4-11 (Contd.)

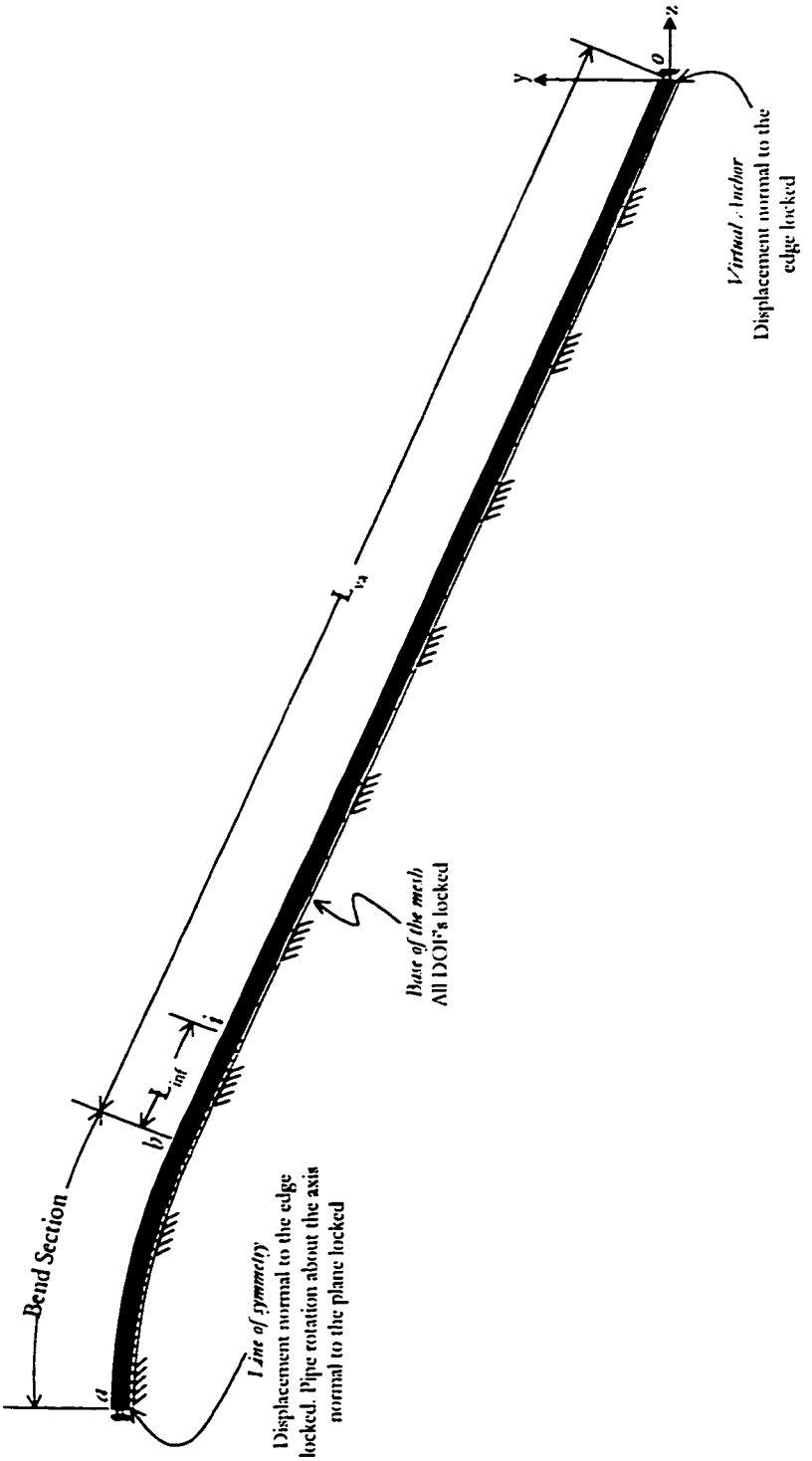

(c) Side view

Figure 4-11 (Contd.)

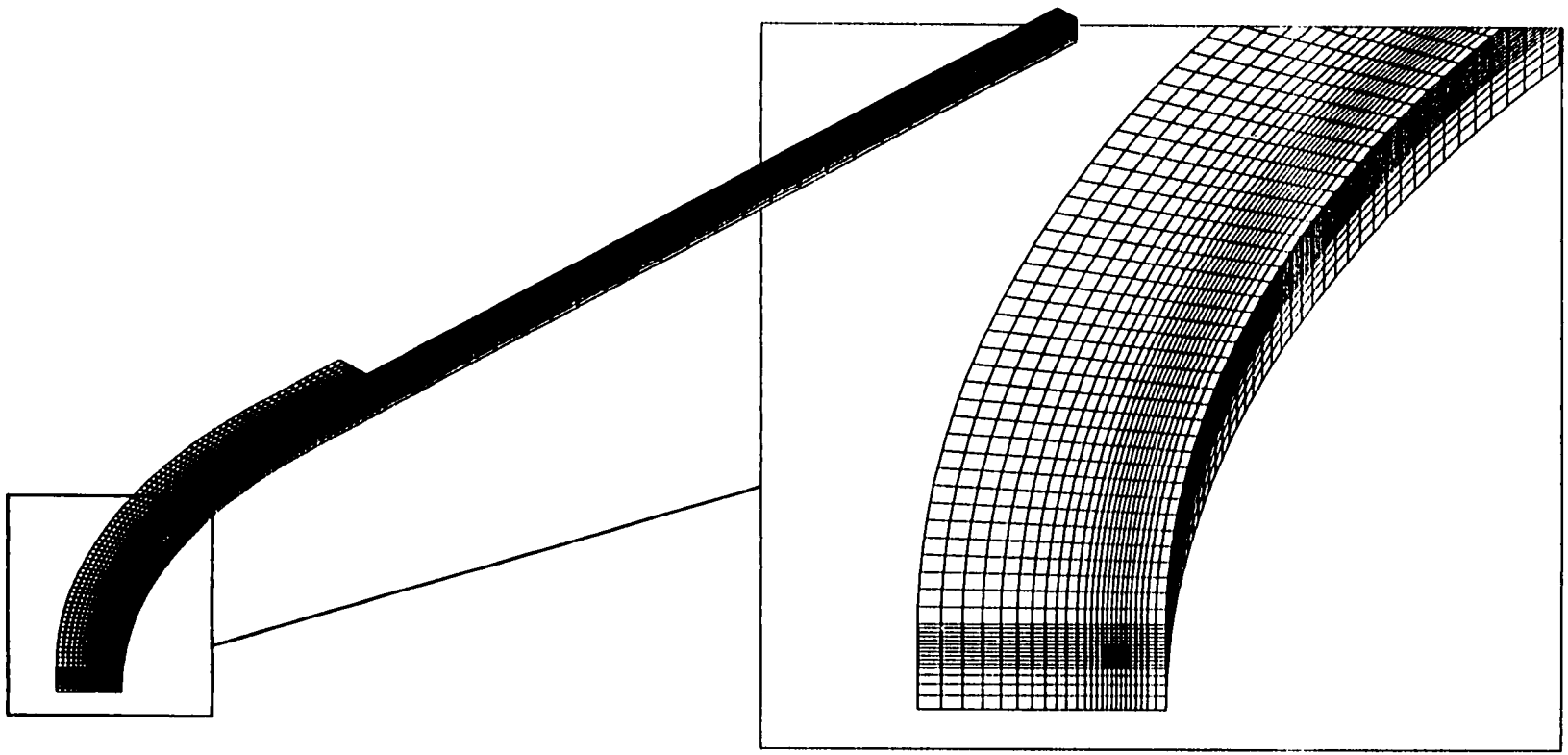

(a) Perspective view

Figure 4-12 Buried pipe horizontal bend mesh

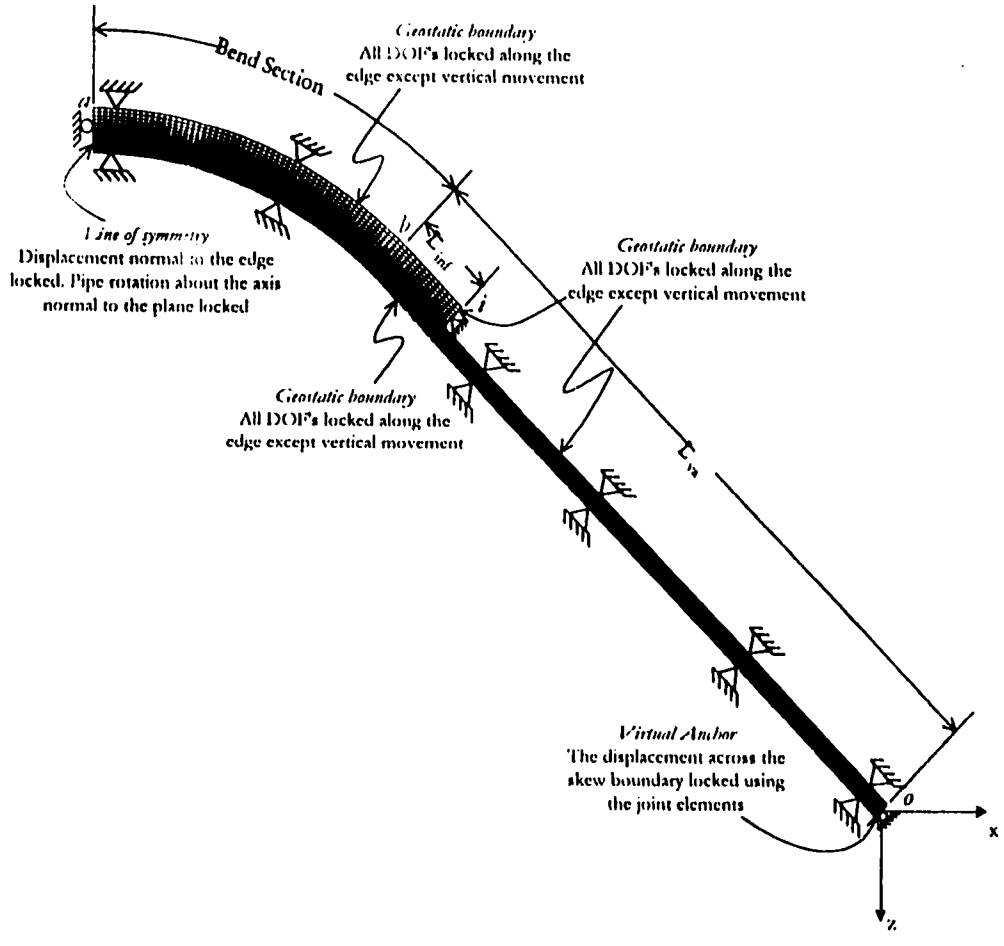

(b) Plan

Figure 4-12 (Contd.)

The region along the bend and the influence length requires a finer mesh because the pipe moves laterally within this region. The length of the elements is therefore taken as 2D along the bend and about 2.5D along the influence length. The longitudinal mesh configuration along the pipe length from the end of the influence length, *i*, to the virtual anchor, *o*, is not significant because there is no transverse movement of the pipe along the length. The element length is, therefore, taken as a constant (10D) or more if required for keeping the mesh size within the SMAP-3D limits.

The two-dimensional meshes shown in Figures 4-3 and 4-7 are extruded with their full widths along the bend and the influence length. From the end of the influence length, *i*, to the virtual anchor, *o*, the pipe does not move laterally and the mesh dimension as required for the gravity loading is enough for the boundary specification requirements. The extra side width (Seg. 6) is therefore not extruded within this length, which can be observed in Figures 4-11(b) and 4-12(b). Geostatic boundary condition exists along the face exposed due to the change of the mesh width. Appropriate boundary condition is specified along the exposed face. This and all other boundary conditions defined for the vertical and horizontal bend meshes are shown in Figures 4-11 and 4-12, respectively.

To specify the appropriate boundary conditions at the virtual anchor (*o*), and the bend apex (*a*) of a buried pipe vertical bend, a special mesh generation procedure is required. This mesh generation procedure is explained as follows. The condition at the virtual anchor is such that the nodes can move in the vertical and lateral

directions due to gravity load but they are constrained from movement in the pipe longitudinal direction (Figure 4-11). To specify the appropriate boundary condition, the plane of nodes at the virtual anchor should lie in a vertical plane normal to the plane in which longitudinal axis of the vertical bend system lies. It can be observed in Figure 4-11(c) that such a vertical plane lies in the X-Y plane of the global coordinate system. The two-dimensional mesh shown in Figure 4-3 is therefore oriented in the X-Y plan before it is extruded from the point of the virtual anchor (*o*) to point *i*.

The plane of nodes at the apex of the bend (*a*) should also lie in a vertical plane normal to the plane in which longitudinal axis of the vertical bend system lies, for the definition of the appropriate boundary conditions (Figure 4-11(c)). The plane at the apex will be vertical if the bend part of the mesh, $\widehat{ba}$, is extruded from a two-dimensional mesh at point *b* oriented at an angle of θ/2 from the vertical. The mesh along $\overline{oi}$ is, therefore, extruded such that the section at end *i* is oriented at an angle equal to θ/2 from the vertical. Now when the mesh along $\overline{ib}$ is extruded then the plane at point *b* is obtained oriented at an angle of θ/2 form the vertical as required.

It is now obvious from the above discussion that the extrusion process along $\overline{oi}$ is required to be carried out in such a way that the plane of nodes at the virtual anchor (*o*) is vertical, while the plane of nodes at the other end of extrusion (*i*) is oriented at an angle equal to θ/2 form the vertical. There is no direct procedure available in FEMAP that allows the orientation of the plane of nodes at one end of the extrusion

to be different from the orientation of the plane of nodes at the other end. The approach therefore used to obtain the required mesh is shown in Figure 4-13. After orientating the 2D mesh shown in Figure 4-3 in the X-Y plane, the 2D mesh is first extruded along a circular arc from point *o*. The arc, along which the mesh is extruded, passes through point *o*. The radial line to the arc at point *o* is vertical. While at the other end, the radial line to the arc makes an angle of $\theta/2$ from the vertical. The radius of the arc can be calculated using the expression:

$$R_e = \frac{L_{va} - L_{inf}}{\mathrm{Sin}\left(\frac{\theta}{2}\right)} \tag{4-16}$$

The mesh extruded along the arc is then moved to make it aligned with the actual longitudinal axis of the pipe. Consider a plane of nodes on the curved extruded mesh, which makes an angle ψ form the vertical (Figure 4-13). This plane of nodes is moved radially, for a distance of R_e-R_ψ, to make it aligned with the pipe longitudinal axis. The value of R_ψ can be calculates as:

$$R_\psi = R_e \frac{\mathrm{Cos}\left(\frac{\theta}{2}\right)}{\mathrm{Cos}\left(\frac{\theta}{2} - \psi\right)} \tag{4-17}$$

The desired mesh is obtained once all nodes are moved radially by R_e-R_ψ to make the mesh aligned with the pipe longitudinal axis.

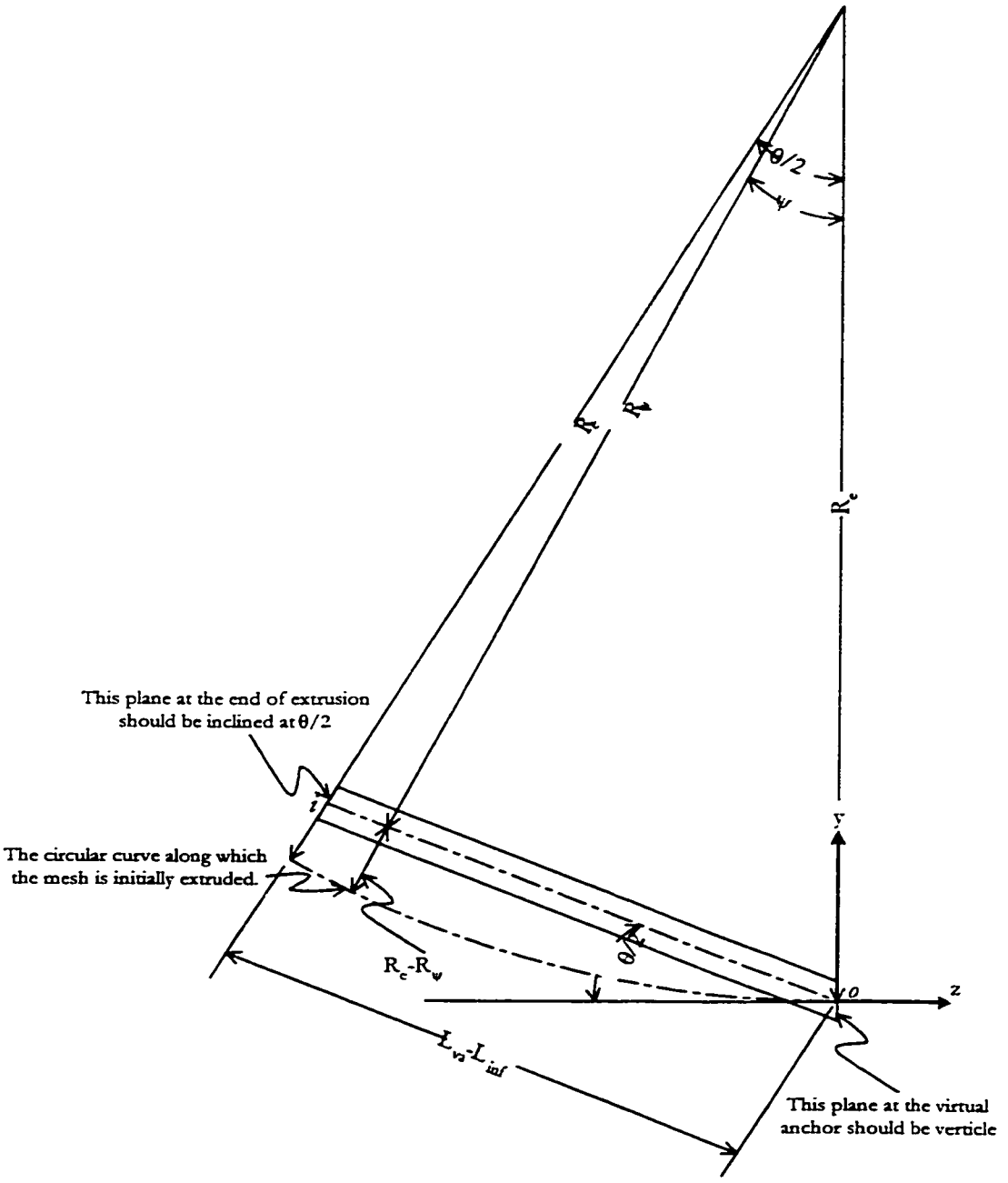

Figure 4-13 Extrusion along the length L_{va}-L_{inf} for a vertical bend mesh

Consider now the horizontal bend mesh (Figure 4-12). Mesh boundary conditions for the horizontal bend are similar to that of the vertical bend mesh. In the case of the horizontal bend mesh, the extrusion with ends at different orientations is not needed. To specify the appropriate boundary conditions, the mesh is oriented such that the nodes at the bend apex lie in a plane parallel to the Y-Z plane of the global coordinate system as shown in Figure 4-12(b). The boundary condition at the virtual anchor requires the plane of nodes at the location to be normal to the direction of the longitudinal axis at point *o*. This results in a boundary that is skewed with respect to the global coordinate system of the mesh. SMAP-3D does not have a provision to specify skew boundaries. The virtual anchor boundary condition at the skew boundary is modeled using the contact joint elements. A unit layer of joint elements having unit thickness is specified behind the skew boundary. The normal stiffness of the joint elements is specified with a very high value to simulate the boundary condition that the movement in the longitudinal direction is constrained. The contact joint element does not have any shear strength and, therefore, the in-plane vertical and lateral movements of nodes are allowed. The joint element therefore models the required boundary condition as specified at point *o* in Figure 4-12(b).

4.4 Application of Loads

The load on a buried pipe finite element model is specified in load steps or increments. Initially, the gravity load is applied. It is found that when joint elements are included in the model, the SMAP-3D results do not converge if the entire gravity

load is applied in one step. It was found that the solution converges if the gravity load is incremented in at least five load steps. The unit weights of the pipe and the soil increase in each increment until they attain their full values in the fifth increment. The temperature load is then applied starting from the sixth increment. Trial runs were carried out initially for the vertical bend problems and it was found that 20 load steps are optimum to specify the gravity and temperature loading. The results accuracy does not improve when more than 20 load steps are used while specifying a total temperature differential of 120°F.

The pipe internal pressure is defined as a surface pressure for the shell elements modeling the pipe. The weight of the pipe contents also affects the loading of the pipe bend system. The effect of the weight of the pipe contents is also included as a pressure applied on the pipe internal surface. The net pressure acting on the pipe internal surface is therefore the sum of the specified internal pressure and the pressure produced by the weight of the fluid inside the pipe. The vertical bend changes its elevation along its longitudinal axis and the pipe internal pressure changes along the pipe as shown in Figure 4-14(a). The horizontal bend, however, does not changes its elevation along its longitudinal direction and the pressure is only varied along the cross-section, as shown in Figure 4-14(b).

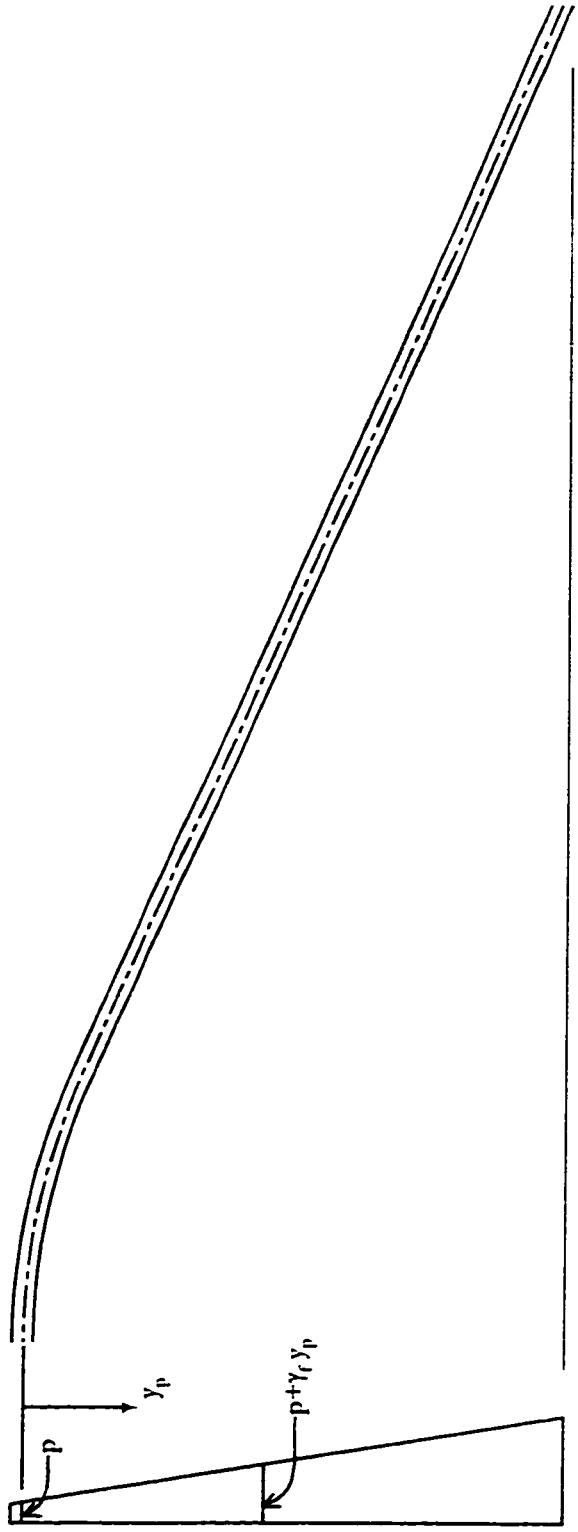

(a) Vertical bend

Figure 4-14 Variation of pipe internal pressure due to fluid weight

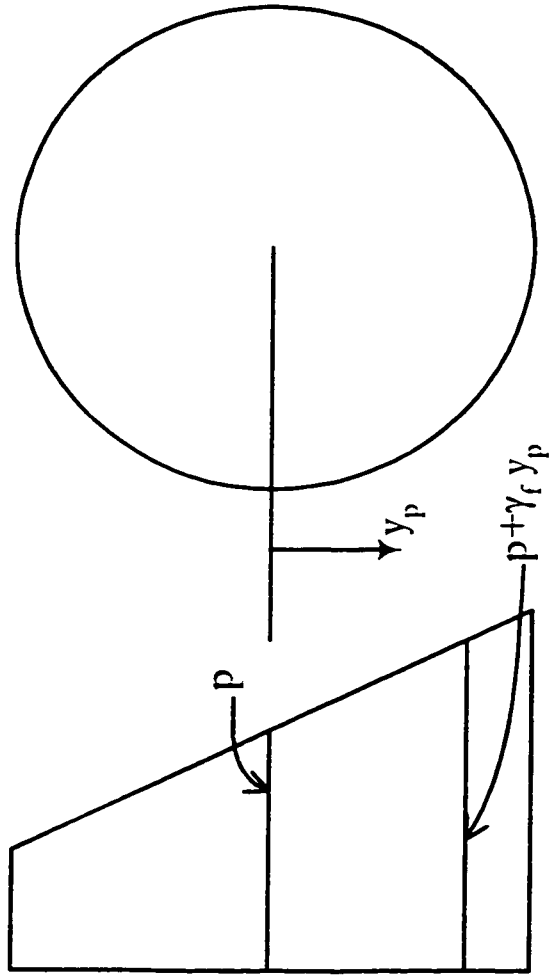

(b) A pipe cross-section along the horizontal bend

Figure 4-14 (Contd.)

CHAPTER 5
PARAMETRIC STUDY AND DISCUSSION OF RESULTS

5.1 Introduction

The structural response of a buried pipe bend depends on a number of parameters as discussed in Chapter 1. The effects of these parameters are investigated; the range of values covered in this study is shown in Table 5-1. Other values are also used in some random runs. Steel is used as the pipe material, since it is the most widely used material in cross-country pipelines. The soil considered in this study is loose sand, as this is the normal practice in large oil companies like the Saudi Arabian oil company (Saudi Aramco) to use loose sand for the soil cover. Similarly, the ranges that are shown in Table 5-1 for other parameters are those usually encountered in the field pipeline installations. The values of the parameters are varied within their limits, and various combinations are considered in order to obtain the effect of each of the parameter individually and the interaction of the parameters.

5.2 Vertical Bend Analysis

The gravity load along with the pipe internal pressure is first applied in the finite element model of the vertical buried pipe bend. The temperature increase of the shell elements is then specified in increments. The apex of the pipe bend extradose is the

Table 5-1 Parameters considered in the study of the buried pipe bends

(a) Vertical Bend

Factor	Minimum	Maximum
D	24 in.	60 in.
H_c	36 in.	60 in.
R_b	50 ft	700 ft
θ	8°	20°
D/t	50	100
p	0	1000 psi
G_f	0	1

(b) Horizontal Bend

Factor	Minimum	Maximum
D	24 in.	60 in.
H_c	24 in.	48 in.
R_b	50 ft	690 ft
θ	15°	90°
D/t	50	50
p	150 psi	150 psi
G_f	0	0

Pipe Material: Steel API 5L Grade X60

$E = 29 \times 10^6$ psi, $\nu = 0.3$, $\alpha = 6.5 \times 10^{-6}$ /°F, $\gamma_p = 490$ pcf, SMYS = 60 ksi, Allowable Stress = 0.72 SMYS = 43.2 ksi.

Soil Material: Loose Sand

$\phi = 35°$, $C = 0$, $\gamma = 99.1$ pcf, $E = 1000$ psi, $\nu = 0.3$

Temperature Specification:

Maximum operating temperature = 190°F, Tie in temperature = 70°F, $\Delta T = 120$°F

location on the pipe bend at which the effect of temperature change is most pronounced. This is the point, which moves the most in response to the temperature changes. A typical curve of the extradose movement versus load steps is shown in Figure 5-1. The curve initially shows a negative or downward movement under gravity load. The curve changes its direction when the temperature load begins to be applied. The curve initially stays straight with a relatively steep slope during temperature load steps. The slope of the curve decreases when the soil cover reaches its capacity because of the pipe uplift. The extradose apex of the bend moves rapidly on further increase of the temperature. A point is required to be located on the curve that defines the capacity of the buried pipe bend system against temperature increase. Two criteria are considered to define the buried pipe vertical bend capacity.

The first method, called the *Installation Condition Method* (ICM), requires that the upward movement of the bend under temperature change is restricted to the installation condition, where the installation condition is defined as the state of the trench before the pipe is laid. After the installation of the pipe, the whole system settles down under the weight of the pipe and the soil cover. Therefore, according to the ICM, the allowed upward movement of the bend apex is equal to the settlement caused by the weight of the pipe and the soil cover. This method restricts the pipe movement so that the pipe invert does not get separated from the trench bed as a result of the pipe uplift movement. The capacity of the vertical buried pipe bend against the temperature change can thus be calculated as shown in Figure 5-2. In this method the settlement of the mesh below the pipe under its own weight is

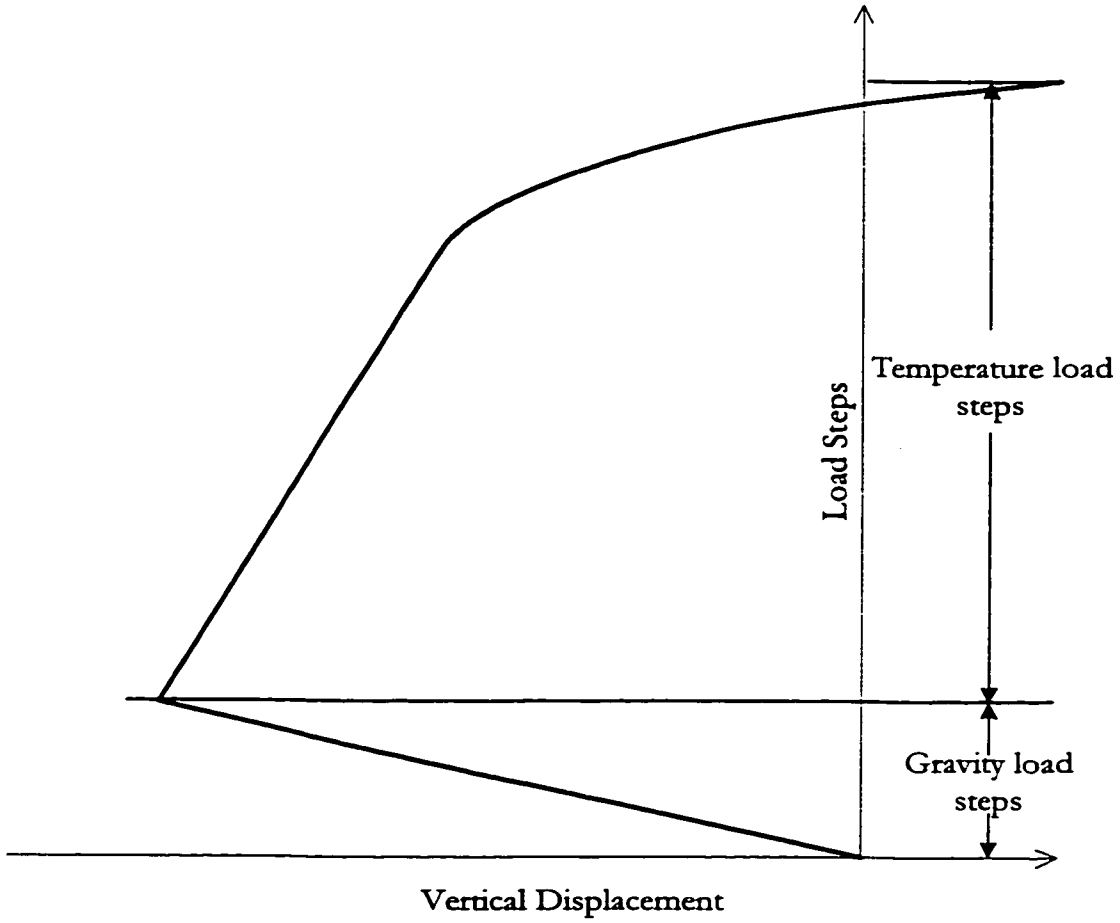

Figure 5-1 Typical load-steps versus displacement curve for a vertical bend extradose apex obtained by the finite element analysis

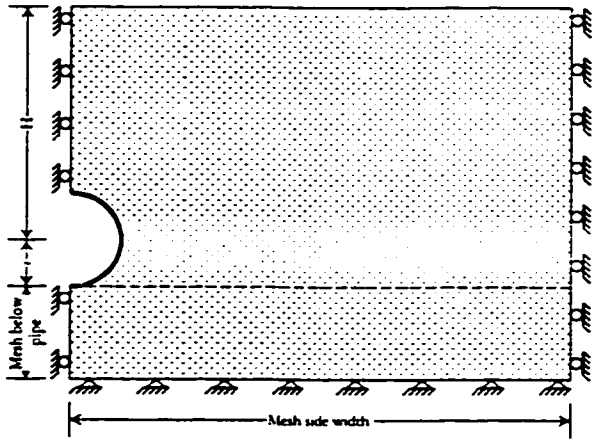

(a) The settlement of the mesh under its own weight below the pipe (dashed line) is subtracted from the total gravity load settlement

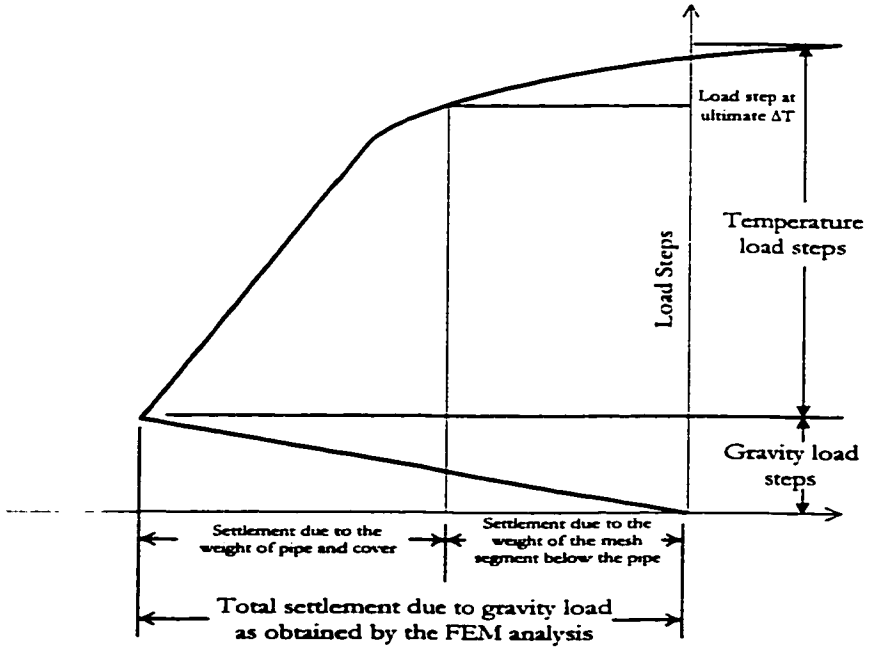

(b) Locating the capacity on the curve

Figure 5-2 Determination of the vertical bend capacity against the temperature change using the Installation Condition Method

subtracted from the total settlement of the pipe bend extradose apex to get the allowed uplift movement according to the method. The settlement of the mesh below the pipe under its own weight is calculated using the following equation:

$$Settelment = \frac{(thickness\ of\ the\ mesh\ below\ the\ pipe)^2 \gamma}{2\,E} \qquad (5\text{-}1)$$

The above expression can be easily derived by considering the axial deformation of a member under its own weight.

The other method, called the *Ultimate Temperature Method* (UTM), defines the capacity as the point where the slope of *temperature change – apex movement* starts to decrease. The change in the curve gradient from steep to flat is gradual, and it is difficult to visually select a point at which the curve becomes flat. The procedure used to define the capacity point on the curve is shown in Figure 5-3. The displacement is plotted relative to the condition when the total gravity load is acting. A line is drawn parallel to the initial tangent modulus of the curve at an offset of 0.2% of H (depth to the pipe center). The point at which this line intersects the curve is taken as the ultimate capacity point. This is one of the methods commonly used if a clear peak is not available on any elasto-plastic curve.

The two methods try to locate the same point on the curve theoretically, because the *temperature change – apex movement* curve starts to become flat when the pipe invert just leaves the trench bed due to its uplift. The offset value of 0.2% H used in UTM however results in a relatively higher value for the capacity, especially for the small

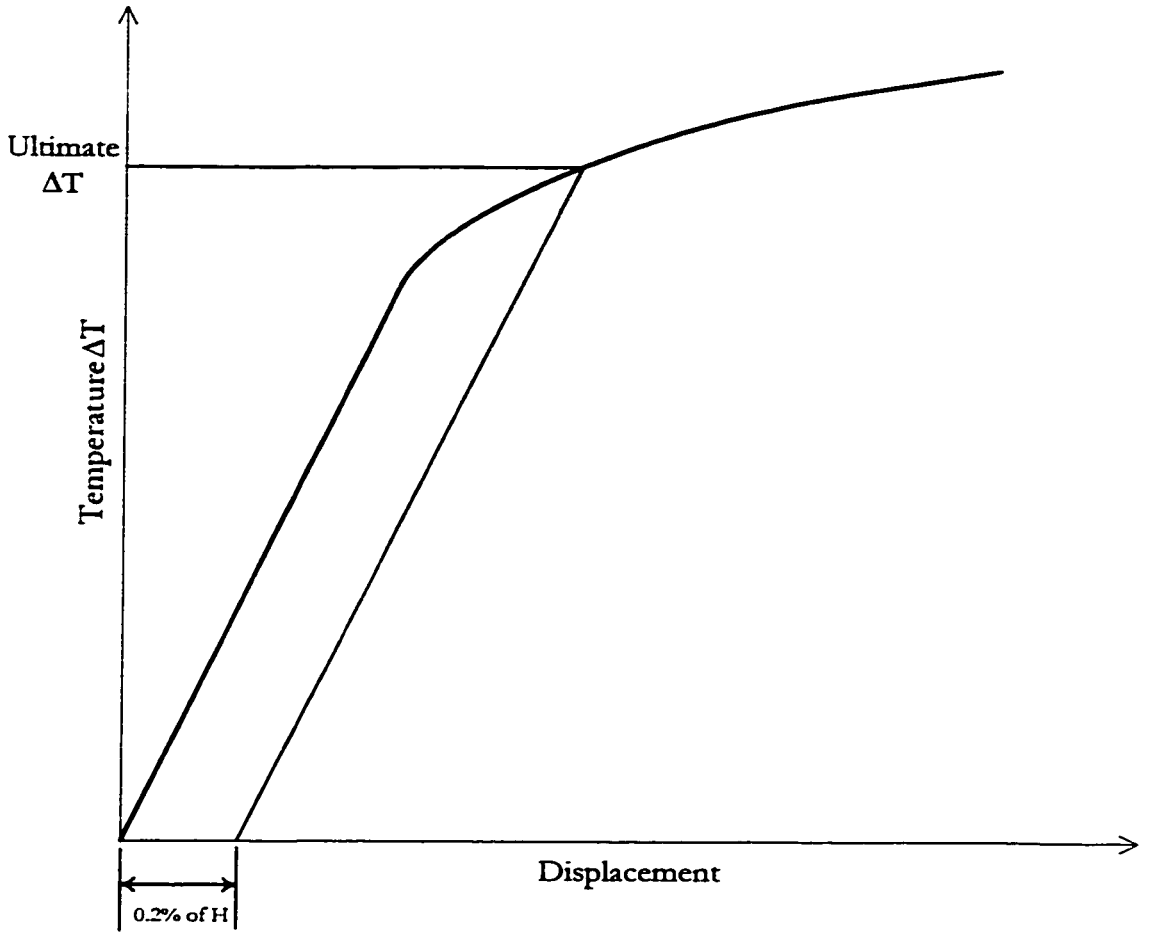

Figure 5-3 Determination of the vertical bend capacity against the temperature change using the Ultimate Temperature Method

diameter pipes, as the value of the displacement depends on the pipe diameter in addition to the cover height. On the other hand, subtracting the settlement value, as calculated by equation 5-1, from the total gravity settlement according to ICM gives a relatively conservative (lower) value for the vertical bend capacity. ICM is suitable if the displacements are of major concern. However, the full strength of the soil against the bend movement is obtained using UTM.

5.2.1 Capacity against temperature change

A number of runs are executed to find the capacity of buried pipe vertical bends against temperature change. A summary of the results of these runs is shown in Table 5-2. It is concluded using the trend obtained for the different combinations of parameters (with a certain fixed value of D/t, internal pressure and fluid specific gravity) that the runs shown in Table 5-2 are sufficient to draw solid conclusions. These runs are carried out to study the effect of the pipe diameter, cover height, bend radius and bend angle on the capacity of a buried pipe vertical bend against temperature change. Other parameters are kept constant and their values are also shown in Table 5-2. The capacity is determined from the results of each run using each of the two methods, i.e., ICM and UTM. The maximum temperature increase specified in all the runs is 120°F. For certain runs, the bend system did not reach its capacity even at the maximum specified temperature increase. If the capacity could not be found even for the 36 in cover depth, then few additional runs are made with smaller depths, this can be observed in Table 5-2. The values obtained by a program

Table 5-2 Vertical bend runs to study the effects of D, H_c, R_b and θ
($D/t = 50$, $p = 150$ psi, $G_f = 0$)

S. No.	D (in)	H_c (in)	R_b (ft)	θ (Degrees)	Ultimate Temperature °F		
					Installation Condition Method	Ultimate Temperature Method	PIPECOVR§ program
1	24	36	50	20	22.89	36.49	31.108
2	24	42	50	20	25.77	41.74	34.911
3	24	60	50	20	36.61	59.88	46.599
4	42	36	50	20	25.04	33.45	32.033
5	42	42	50	20	27.62	37.37	35.171
6	42	60	50	20	37.27	50.32	44.64
7	60	36	50	20	28.22	34.26	34.116
8	60	42	50	20	31.62	38.44	36.943
9	60	60	50	20	40.55	48.3	45.419
10	24	36	300	20	70.13	82.89	45.457
11	24	42	300	20	81.84	98.22	52.849
12	24	60	300	20	>120*	>120*	78.839
13	42	36	300	20	43.32	50.69	37.892
14	42	42	300	20	49.8	58	41.929
15	42	60	300	20	69.16	79.2	54.469
16	60	36	300	20	38.2	42.65	38.144
17	60	42	300	20	42.37	49.47	41.469
18	60	60	300	20	56.42	64.64	51.579
19	24	12	700	20	52.52	68.88	45.427
20	24	21	700	20	86.01	109.84	66.692
21	24	36	700	20	>120*	>120*	107.351
22	24	42	700	20	>120*	>120*	125.437
23	24	60	700	20	>120*	>120*	185.966
24	42	27	700	20	73.58	82.45	51.979
25	42	36	700	20	93.98	102.17	64.687
26	42	42	700	20	107.84	118.31	73.619
27	42	60	700	20	>120*	>120*	102.609
28	60	36	700	20	72.79	80.05	50.478
29	60	42	700	20	81.83	88.81	55.979
30	60	60	700	20	110.61	115.49	74.538

§ The temperatures are obtained by iterating the PIPECOVR program to get the desired value of H_c. The PIPECOVR program does not give the calculated value of H_c if $H_c < 36$. In the case of $H_c < 36$ the temperature was found by quadratic extrapolation.

* The bend system did not reach its capacity at the maximum specified temperature of 120°F

Table 5-2 (Contd.)

S. No.	D (in)	H_c (in)	R_b (ft)	θ (Degrees)	Ultimate Temperature °F		
					Installation Condition Method	Ultimate Temperature Method	PIPECOVR§ program
31	24	36	50	15	25.29	42.24	38.123
32	24	42	50	15	29.31	48.95	42.665
33	24	60	50	15	42.3	72	56.609
34	42	36	50	15	27.28	37.84	39.386
35	42	42	50	15	31.42	42.93	43.155
36	42	60	50	15	42.76	58.43	54.521
37	60	36	50	15	31.48	39.48	41.954
38	60	42	50	15	34.64	43.14	45.356
39	60	60	50	15	45.86	55.72	55.554
40	24	36	300	15	66.13	81.05	49.704
41	24	42	300	15	77.45	95.45	56.719
42	24	60	300	15	113.53	>120*	80.193
43	42	36	300	15	41.78	51.21	44.765
44	42	42	300	15	48.25	59.15	49.329
45	42	60	300	15	67.68	80.4	63.369
46	60	36	300	15	38.36	45.32	45.754
47	60	42	300	15	42.94	51.15	49.616
48	60	60	300	15	57.33	66.66	61.319
49	24	15	700	15	62.17	82.17	52.254
50	24	21	700	15	85.14	107.74	66.692
51	24	36	700	15	>120*	>120*	107.351
52	24	42	700	15	>120*	>120*	125.437
53	24	60	700	15	>120*	>120*	185.966
54	42	30	700	15	76.82	84.36	56.124
55	42	36	700	15	90.16	99.43	64.687
56	42	42	700	15	104.99	115.8	73.619
57	42	60	700	15	>120*	>120*	102.609
58	60	36	700	15	67.42	73.31	55.412
59	60	42	700	15	76.69	82.44	60.729
60	60	60	700	15	105.04	113.23	77.619

§ The temperatures are obtained by iterating the PIPECOVR program to get the desired value of H_c. The PIPECOVR program does not give the calculated value of H_c if $H_c < 36$. In the case of $H_c < 36$ the temperature was found by quadratic extrapolation.

* The bend system did not reach its capacity at the maximum specified temperature of 120°F

Table 5-2 (Contd.)

S. No.	D (in)	H_c (in)	R_b (ft)	θ (Degrees)	Ultimate Temperature °F		
					Installation Condition Method	Ultimate Temperature Method	PIPECOVR§ program
61	24	36	50	8	38.69	66.06	59.172
62	24	42	50	8	45.21	77.26	65.936
63	24	60	50	8	67.5	118.98	86.655
64	42	36	50	8	43.29	62.42	61.414
65	42	42	50	8	49.68	71.12	67.075
66	42	60	50	8	69.61	99.93	84.133
67	60	36	50	8	48.5	62.57	65.423
68	60	42	50	8	54.61	71.74	70.55
69	60	60	50	8	73.83	94.64	85.909
70	24	36	300	8	63.53	89.36	68.246
71	24	42	300	8	74.89	107.75	76.699
72	24	60	300	8	111.44	>120*	103.409
73	42	36	300	8	49.64	68.39	66.209
74	42	42	300	8	57.24	77.67	72.545
75	42	60	300	8	81.43	111.46	91.841
76	60	36	300	8	48.19	63.34	68.933
77	60	42	300	8	54.98	71.35	74.472
78	60	60	300	8	74.93	96.45	91.164
79	24	15	700	8	59.31	76.87	52.254
80	24	25	700	8	96.39	121	76.897
81	24	36	700	8	>120*	>120*	107.351
82	24	42	700	8	>120*	>120*	125.437
83	24	60	700	8	>120*	>120*	185.966
84	42	24	700	8	56.72	72.86	61.805
85	42	36	700	8	81.7	99.44	77.627
86	42	42	700	8	95.08	114.83	85.894
87	42	60	700	8	>120*	>120*	112.1199
88	60	36	700	8	66.1	80.38	76.192
89	60	42	700	8	74.83	90.1	82.679
90	60	48	700	8	85.13	99.97	89.281
91	60	60	700	8	104.74	>120*	102.549

§ The temperatures are obtained by iterating the PIPECOVR program to get the desired value of H_c. The PIPECOVR program does not give the calculated value of H_c if $H_c < 36$. In the case of $H_c < 36$ the temperature was found by quadratic extrapolation.

* The bend system did not reach its capacity at the maximum specified temperature of 120°F

called PIPECOVR are also included in the table for comparison purposes. As discussed in Chapter 2, the program is developed and used by Saudi Aramco to calculate required soil cover over buried pipe bends.

These results are plotted as shown in Figure 5-4. In all cases, the value of the ultimate temperature change, ΔT, increases with increasing cover height, showing that deeper covers increase the capacity of buried pipe vertical bends against the temperature increase. The results obtained by UTM are greater than those of ICM in all cases. The difference in the results is more noticeable for the smaller pipe diameters. The curves show that smaller diameter pipes reach their capacity at a greater temperature. The reverse trend is however apparent for the curves of ICM with a bend radius of 50 ft within the H_c range of 36 in to 60 in. It can be observed that all curves shown in Figure 5-4 are almost linear. The PIPECOVR program curves are mostly in between the curves of ICM and UTM for small diameter pipes, which show a close agreement of PIPECOVR program with the FEM analysis results. However in the cases of medium and large diameter pipes, the PIPECOVR results are relatively conservative than those of ICM and UTM. It can be noticed that for R_b = 50 ft, θ = 8°, D = 60 in, and H_c = 36 in (Figure 5-4(g)), the PIPECOVR result is slightly on the unconservative side as compared to ICM and UTM.

The maximum principal, longitudinal, and hoop stresses corresponding to the ultimate ΔT, as given in Table 5-2, are listed in Tables A-1 to A-3 (Appendix A). The values are the absolute maximum stresses anywhere in the modeled pipe. The

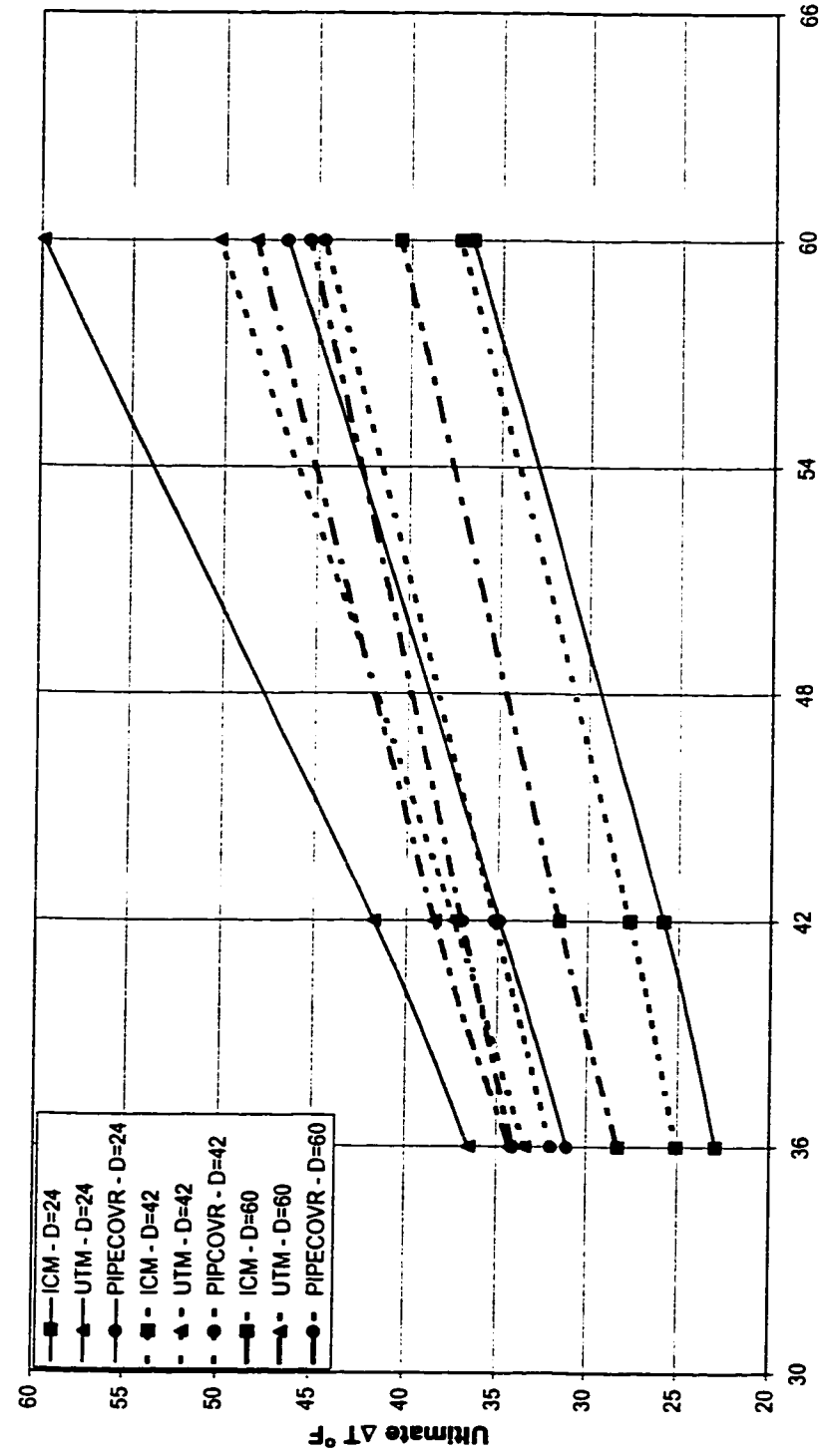

(a) R_b = 50 ft, $\theta = 20^{\circ}$

Figure 5-4 The effect of cover height on the ultimate ΔT

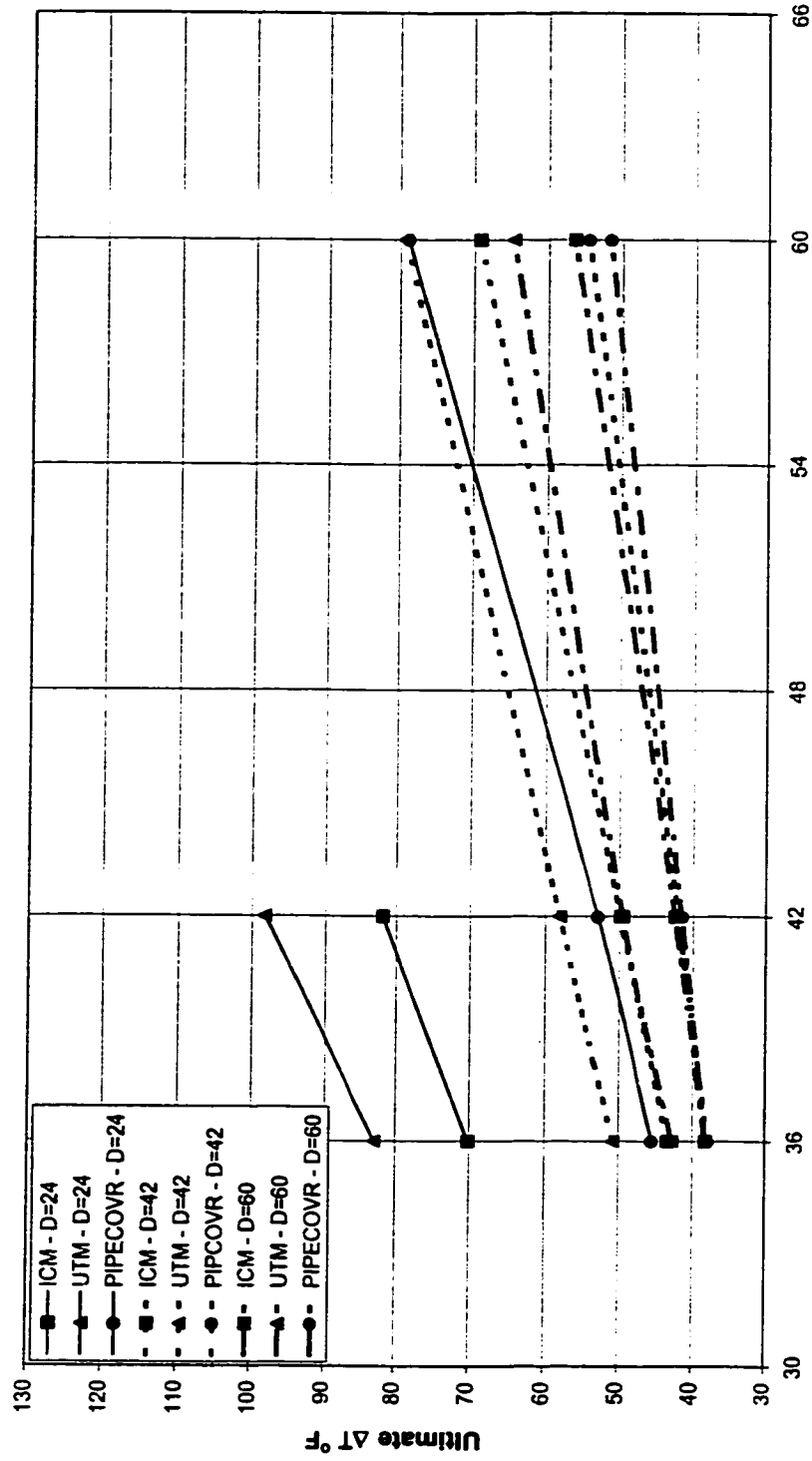

(b) R_b = 300 ft, $\theta = 20^\circ$

Figure 5-4 (Contd.)

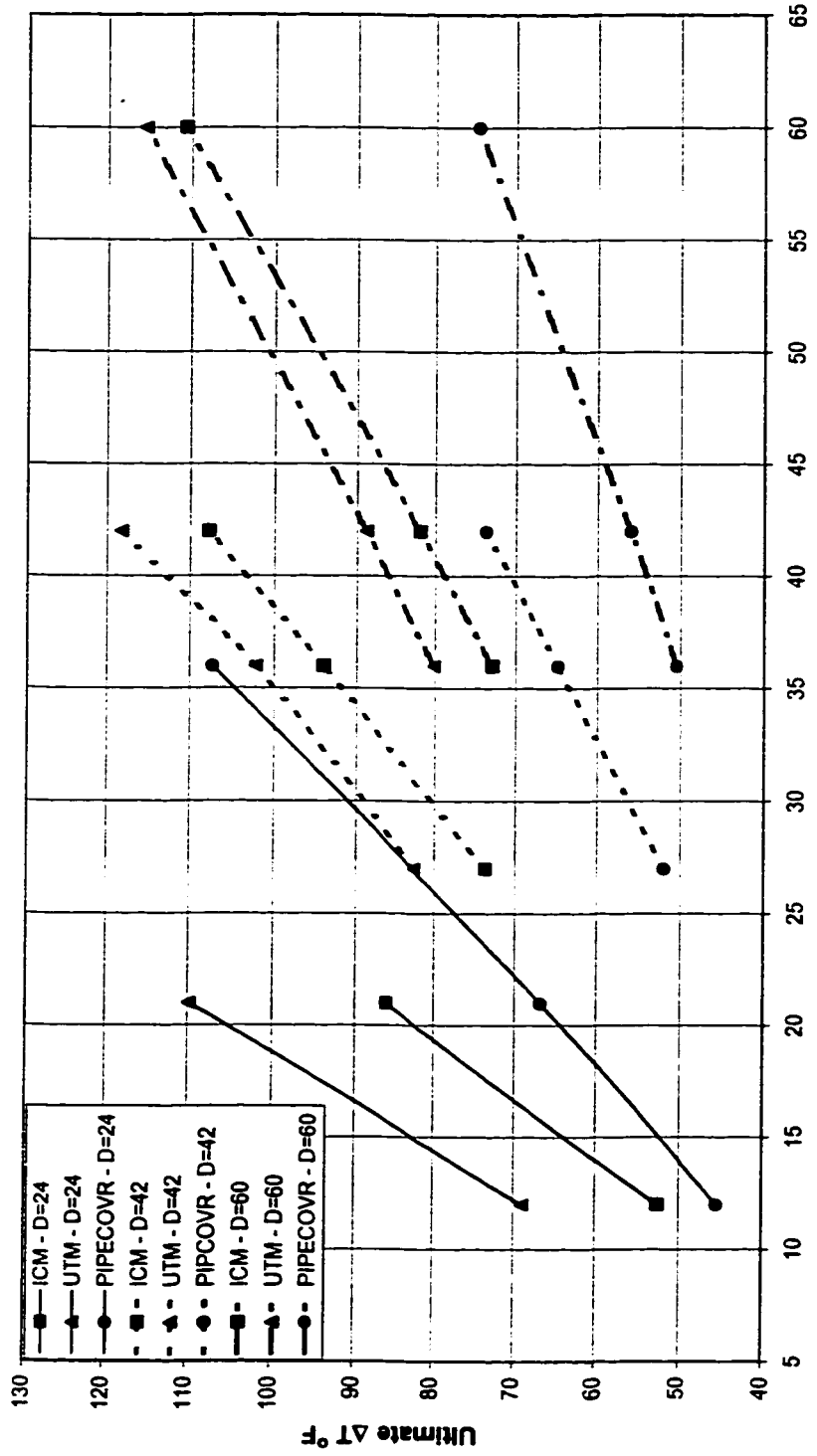

(c) R_b = 700 ft, θ = 20°

Figure 5-4 (Contd.)

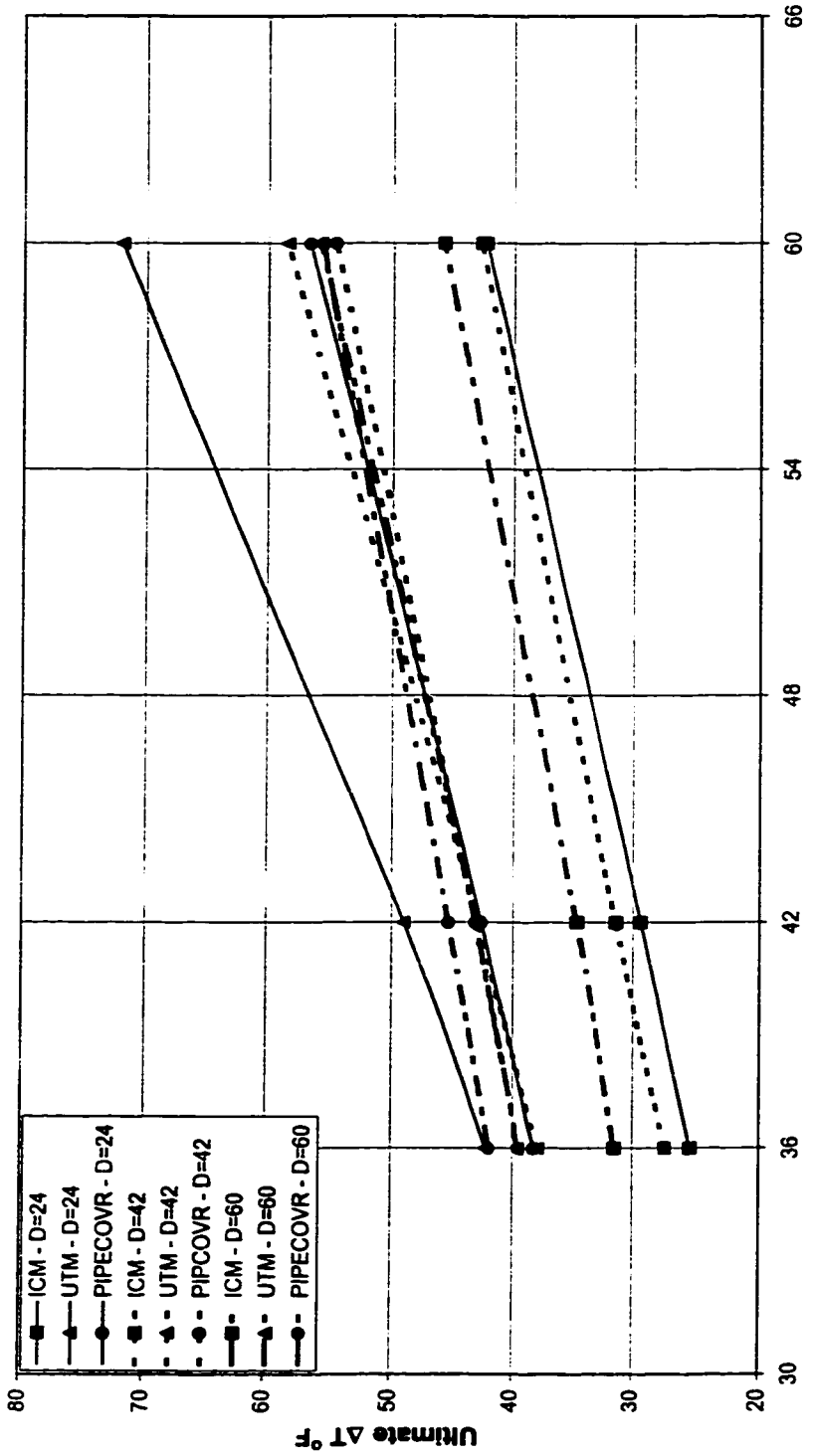

(d) R_b = 50 ft, θ = 15°

Figure 5-4 (Contd.)

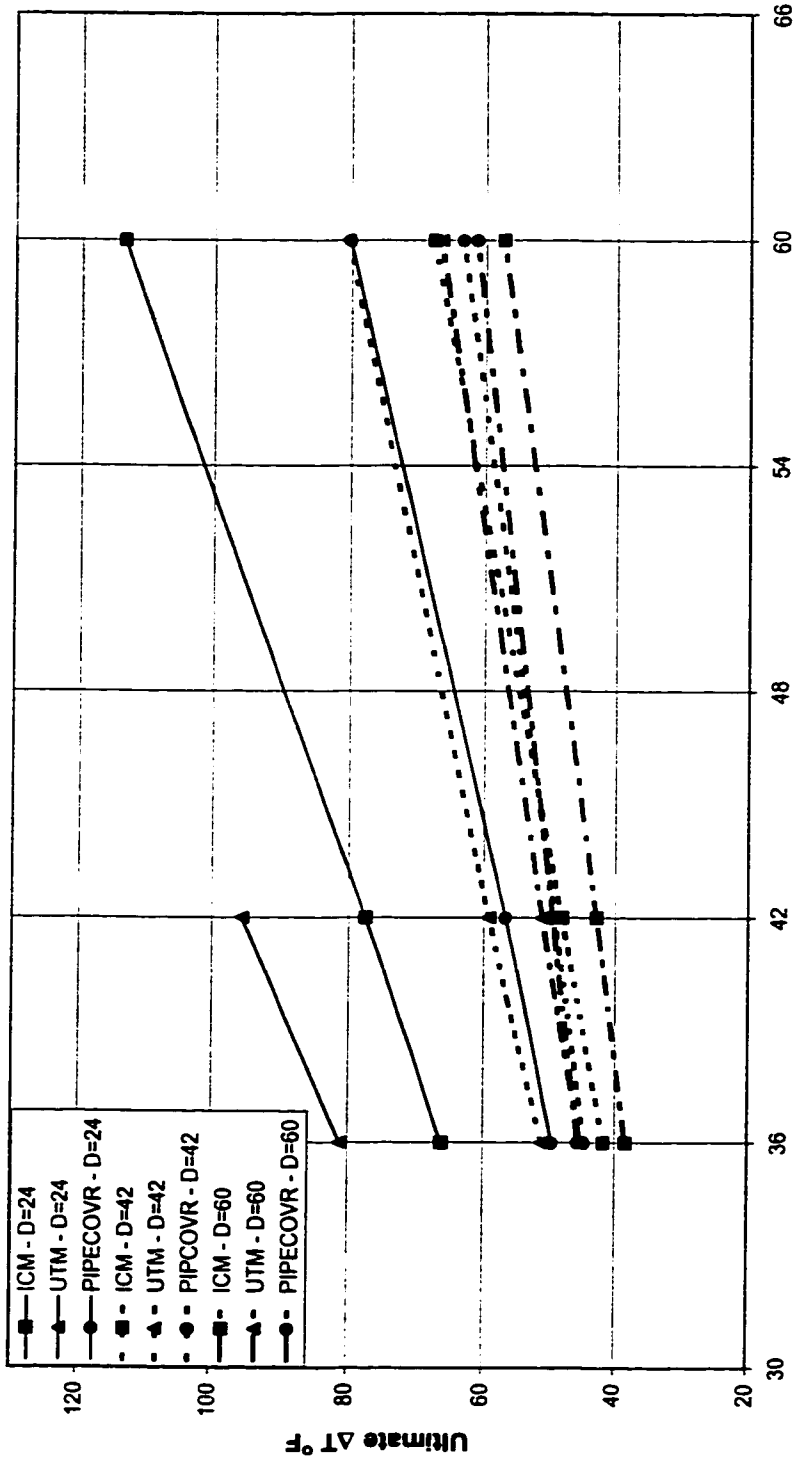

(e) R_b = 300 ft, θ = 15°

Figure 5-4 (Contd.)

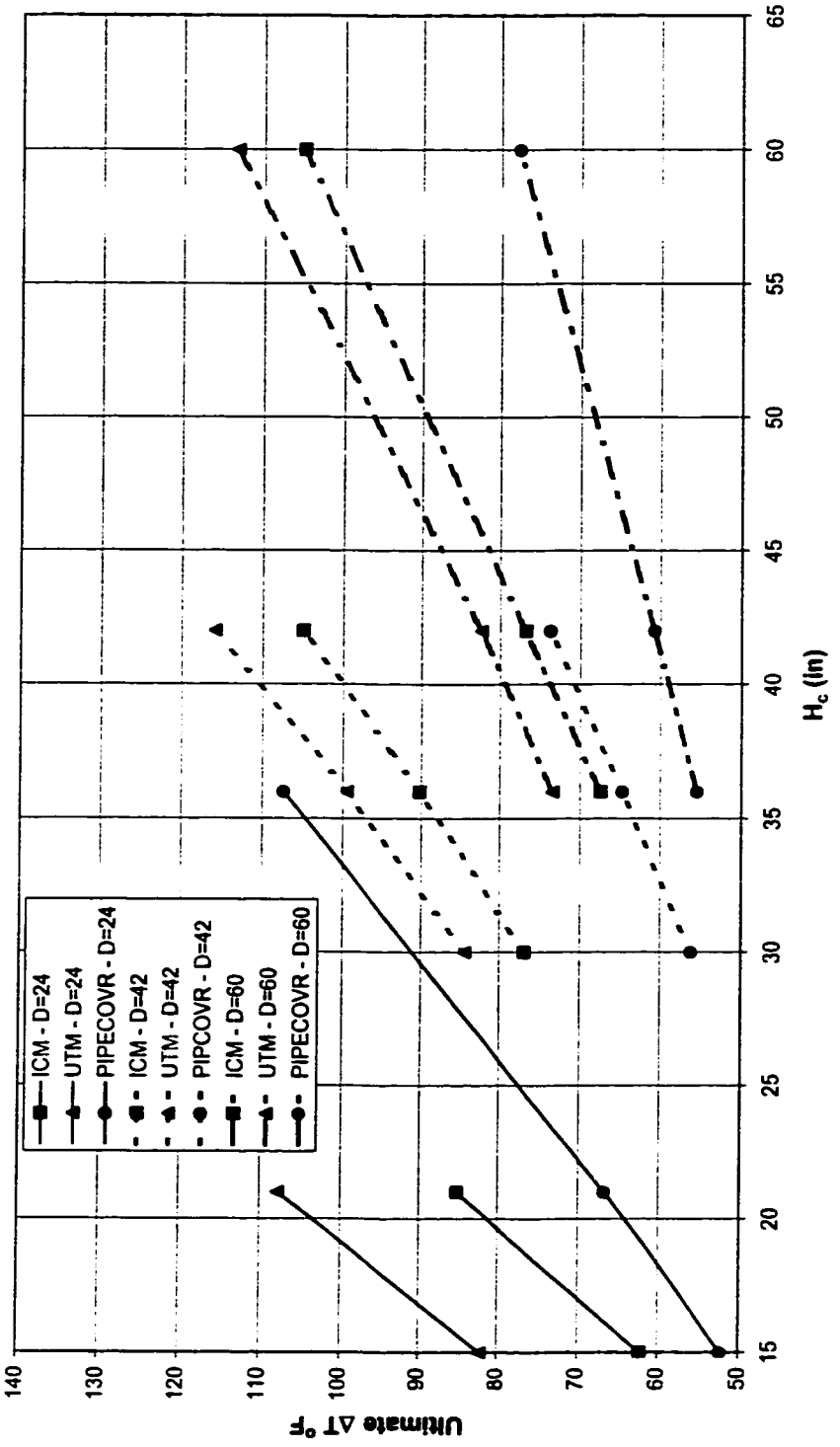

(f) R_b = 700 ft, θ = 15°

Figure 5-4 (Contd.)

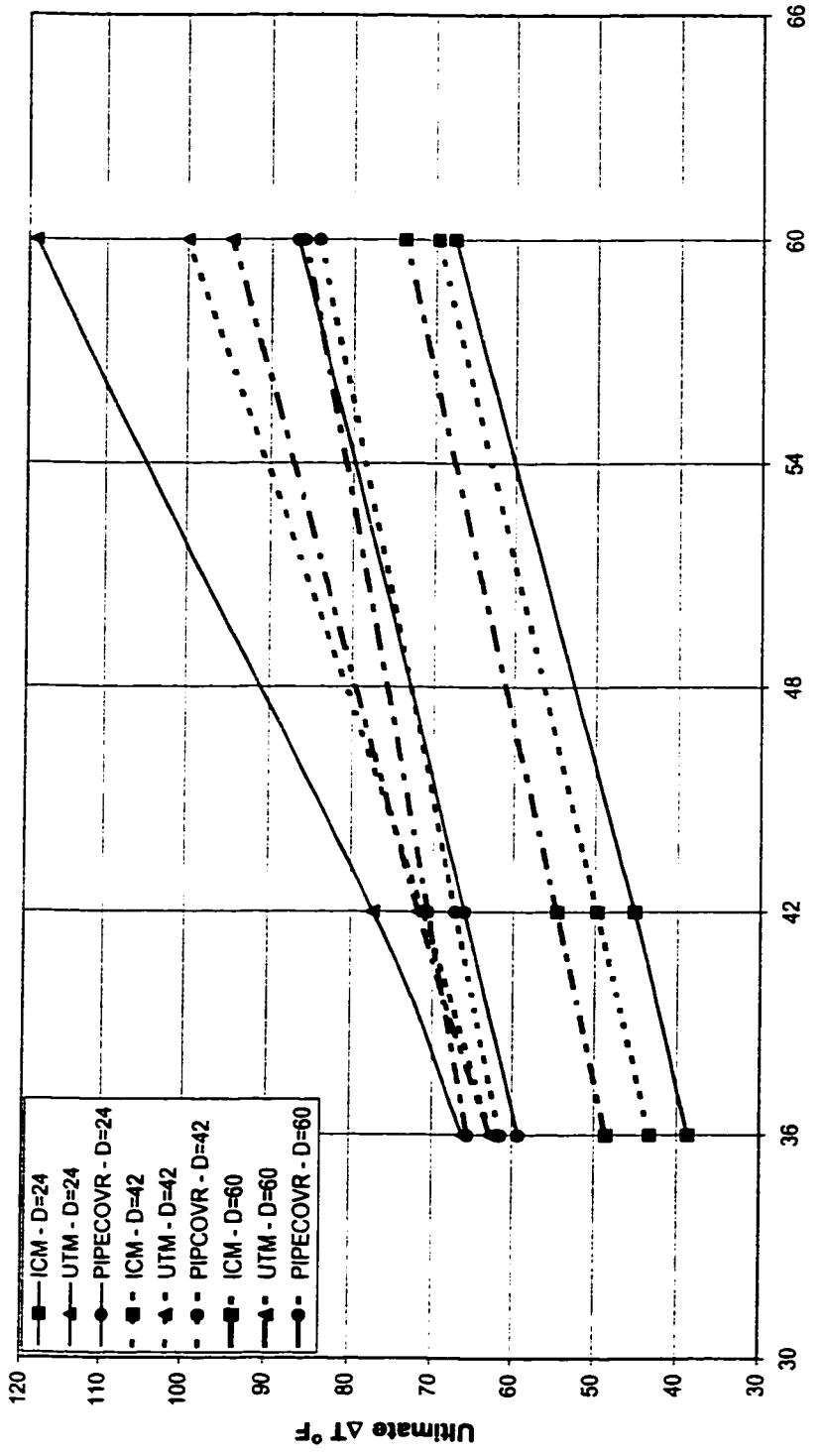

(g) R_b = 50 ft, $\theta = 8°$

Figure 5-4 (Contd.)

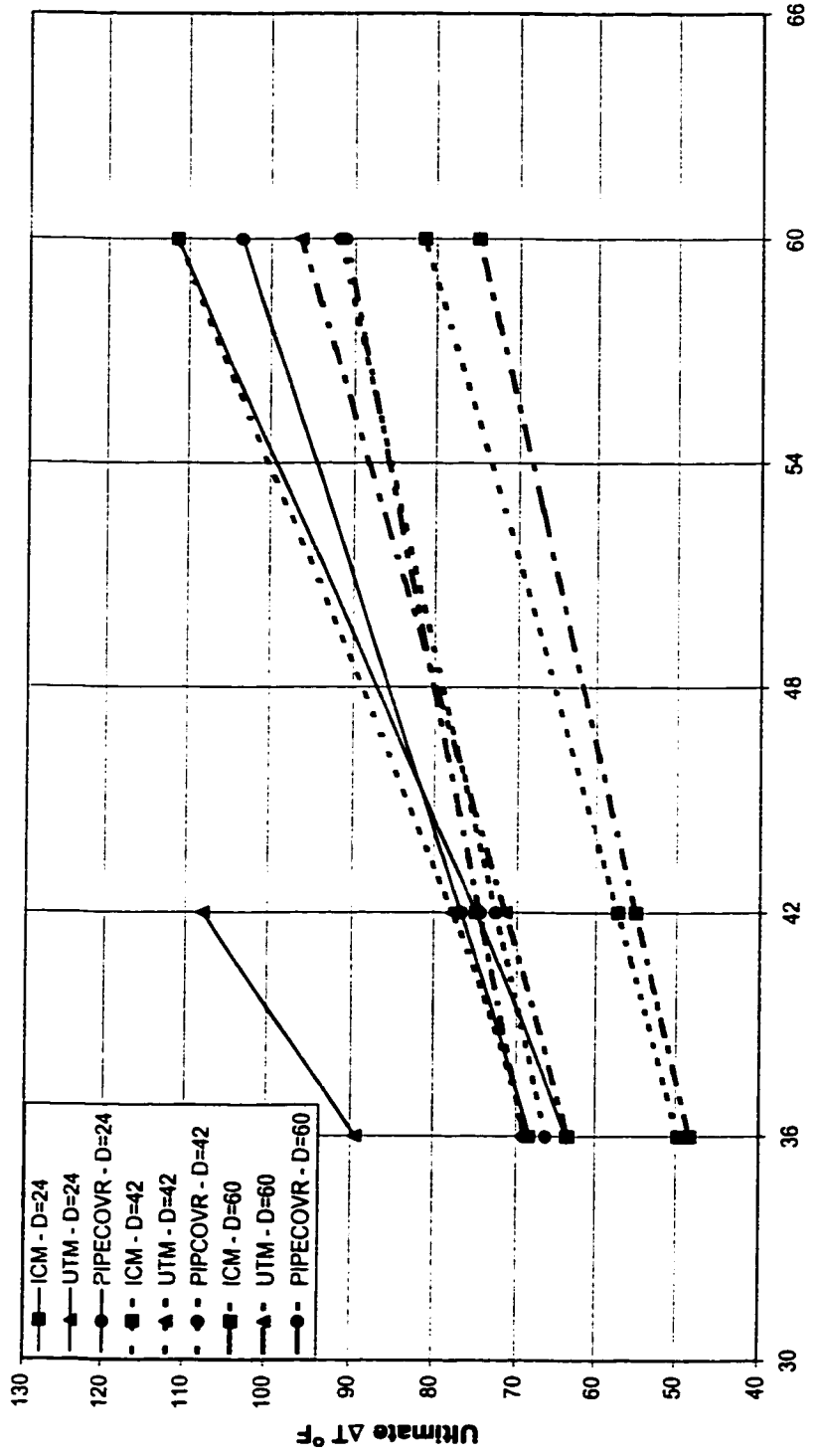

(h) R_b = 300 ft, $\theta = 8°$

Figure 5-4 (Contd.)

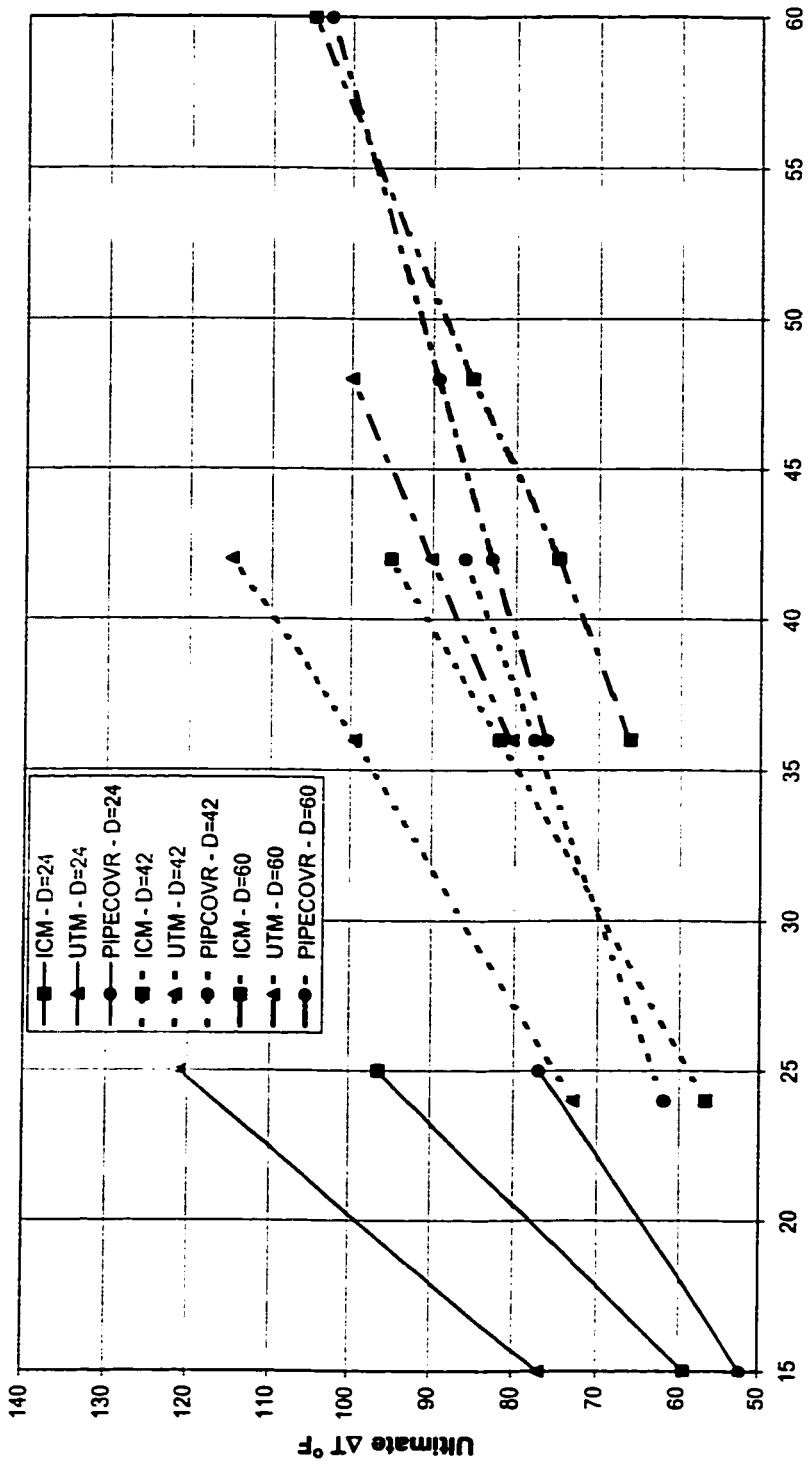

(i) R_b = 700 ft, $\theta = 8°$

Figure 5-4 (Contd.)

location of maximum stress shown in the Tables is specified according to the method as shown in Figure A-1, where Figure A-1(a) is assumed to be the elevation of a vertical bend. This method uses two parameters. The first parameter gives the longitudinal location. If the point of maximum stress lies within straight segment, then the location (x) is measured from the virtual anchor. However, if the point lies within the bend then the location is measured as an angle (θ_x) from the radial line passing through the bend apex. The second parameter (α) gives the location on the circumference of the pipe cross-section.

These stress values are also plotted in Figures A-2 to A-4. All stresses found are less than the allowable stress value of 0.72 SMYS = 43,200 psi, except for a few points on the maximum principal stress curves of R_b = 700 ft and θ = 20° (Figure A-2 (c)). These points however correspond to small H_c values, which are not usually used in practice. The overall trend of these stress diagrams shows that higher stresses are developed at ultimate ΔT for higher cover depths, which is expected. In certain cases however, the curves attain a negative slope; this happens if the location of the absolute maximum stress is changed within the pipe.

The API-RP 1102 (1993) specifications give a method to calculate the *total effective stress* (S_{eff}) and requires it to be less than the allowable stress. The *total effective stress* corresponding to the parameter values as listed in Table A-1 are calculated and are included in the principal stress plots shown in Figure A-2. The stresses obtained by the FEM analysis are mostly larger in value than that calculated as S_{eff}. However, in

most of the cases this difference is not large, and in some of the cases the stresses obtained by the two methods match closely with each other, which can be seen in Figure A-2 (a, b, j, k, and y).

5.2.2 The required cover for $\Delta T = 90°F$

The temperature change of $\Delta T = 90°F$ is selected as a reference temperature change for further interpretation of the obtained results. The value of ΔT is selected to be 90°F because this is the usual temperature differential of the fluid, transported in the local cross-country pipelines administered by Saudi Aramco.

The value of H_c corresponding to a ΔT of 90°F is found from the curves of Figure 5-4 for all the combinations of R_b, θ and D. These values are listed in Table 5-3 and plotted versus the pipe diameter in Figure 5-5. It can be observed from the curves that the required cover height increases as the diameter of the pipe increases in most of the cases. It can also be noticed that the curves are almost linear within the studied pipe diameter range of 24 in to 60 in, especially for UTM.

The PIPECOVR program curves stay close to the results of this study for bends having smaller bend circumferential length ($R_b.\theta$). In some of these cases of small circumferential length bends, the PIPECOVR curves lie between the ICM and the UTM curves, showing a close agreement with the results of this study. There is however an appreciable difference between the PIPECOVR values and the results of

Table 5-3 The cover height required for the vertical bends at 90°F

S. No.	D (in)	R_b (ft)	θ (Degrees)	Required Cover for 90°F (in)		
				Installation Condition Method	Ultimate Temperature Method	PIPECOVR* program
1	24	50	20	159.29	92.65	123.2
2	42	50	20	169.63	118.05	145.4
3	60	50	20	153.65	127.81	156.4
4	24	300	20	46.18	38.78	67
5	42	300	20	79.32	68.84	107
6	60	300	20	105.93	85.14	126.5
7	24	700	20	22.07	16.64	36*
8	42	700	20	34.24	30.69	52.3
9	60	700	20	47.15	42.79	74
10	24	50	15	128.66	75.76	101.6
11	42	50	15	131.71	96.98	116.2
12	60	50	15	137.20	112.84	122.1
13	24	300	15	48.33	42.92	66.7
14	42	300	15	80.69	67.11	92.8
15	60	300	15	101.95	85.11	103.9
16	24	700	15	22.27	16.97	36*
17	42	700	15	35.83	32.31	52.3
18	60	700	15	50.49	46.47	72.4
[illegible]	24	50	8	80.04	47.73	62.8
[illegible]	42	50	8	78.96	54.15	66.2
21	60	50	8	75.74	55.61	64.8
22	24	300	8	49.56	36.21	51
23	42	300	8	66.90	48.86	58.2
24	60	300	8	73.36	55.56	58.7
25	24	700	8	23.28	17.98	36*
[illegible]	42	700	8	39.78	31.80	44.8
27	60	700	8	51.44	41.92	48.6

* The PIPECOVR program specifies the minimum 36 in. cover if calculated cover comes out to be less than 36 in.

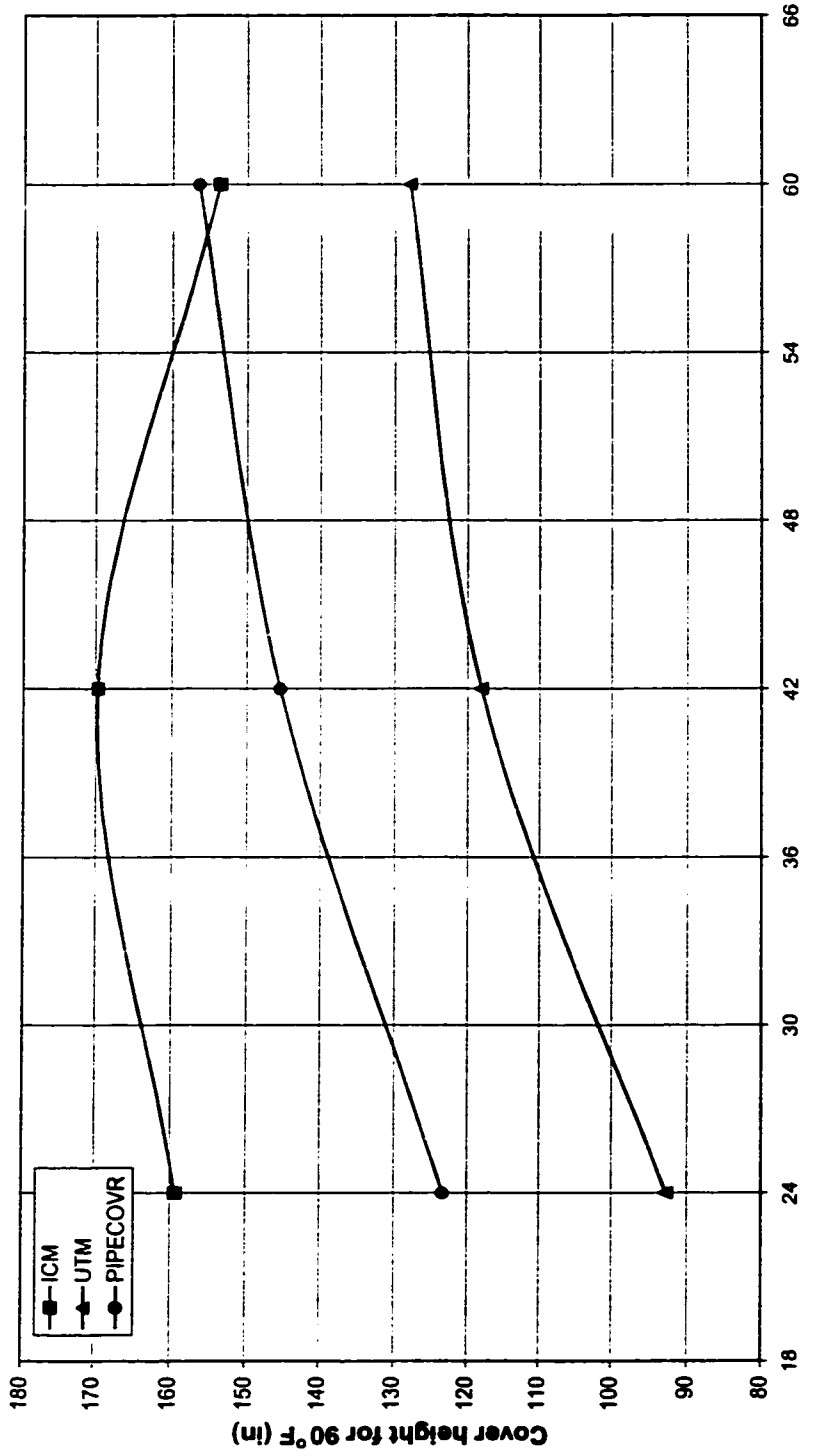

(a) R_b = 50 ft, θ = 20°

Figure 5-5 The effect of pipe diameter on cover height requirement of vertical bends

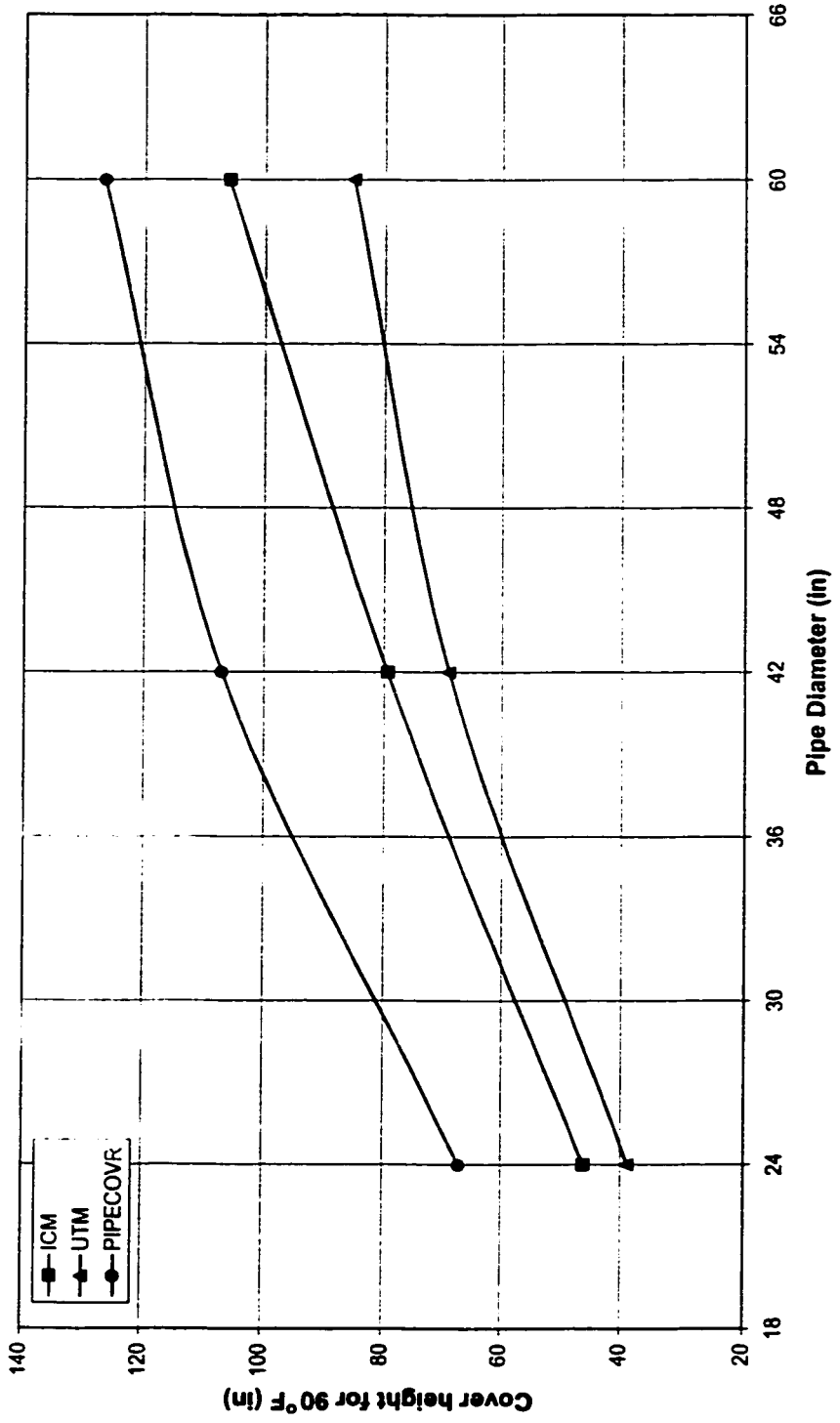

(b) R_b = 300 ft, θ = 20°

Figure 5-5 (Contd.)

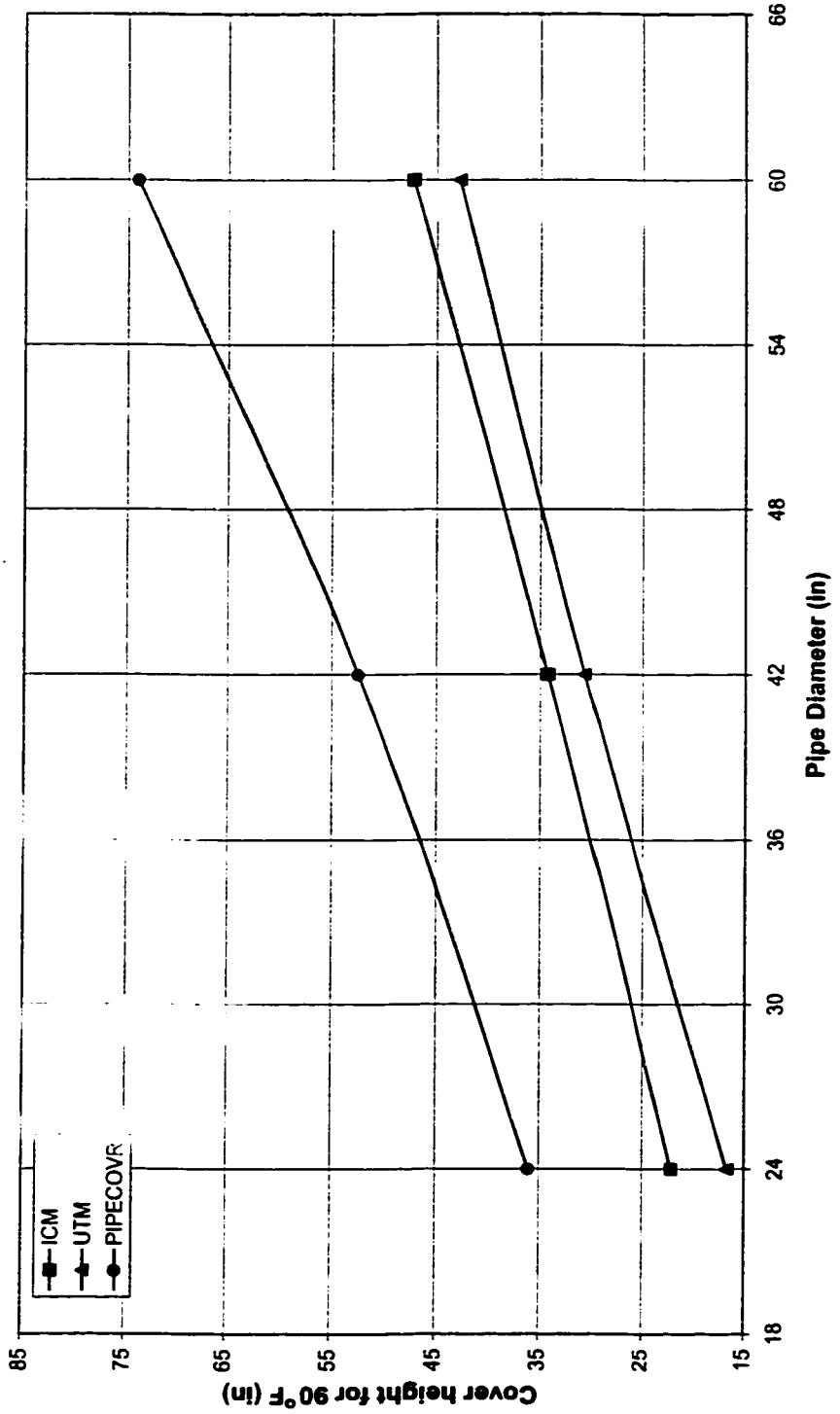

(c) R_b = 700 ft, θ = 20°

Figure 5-5 (Contd.)

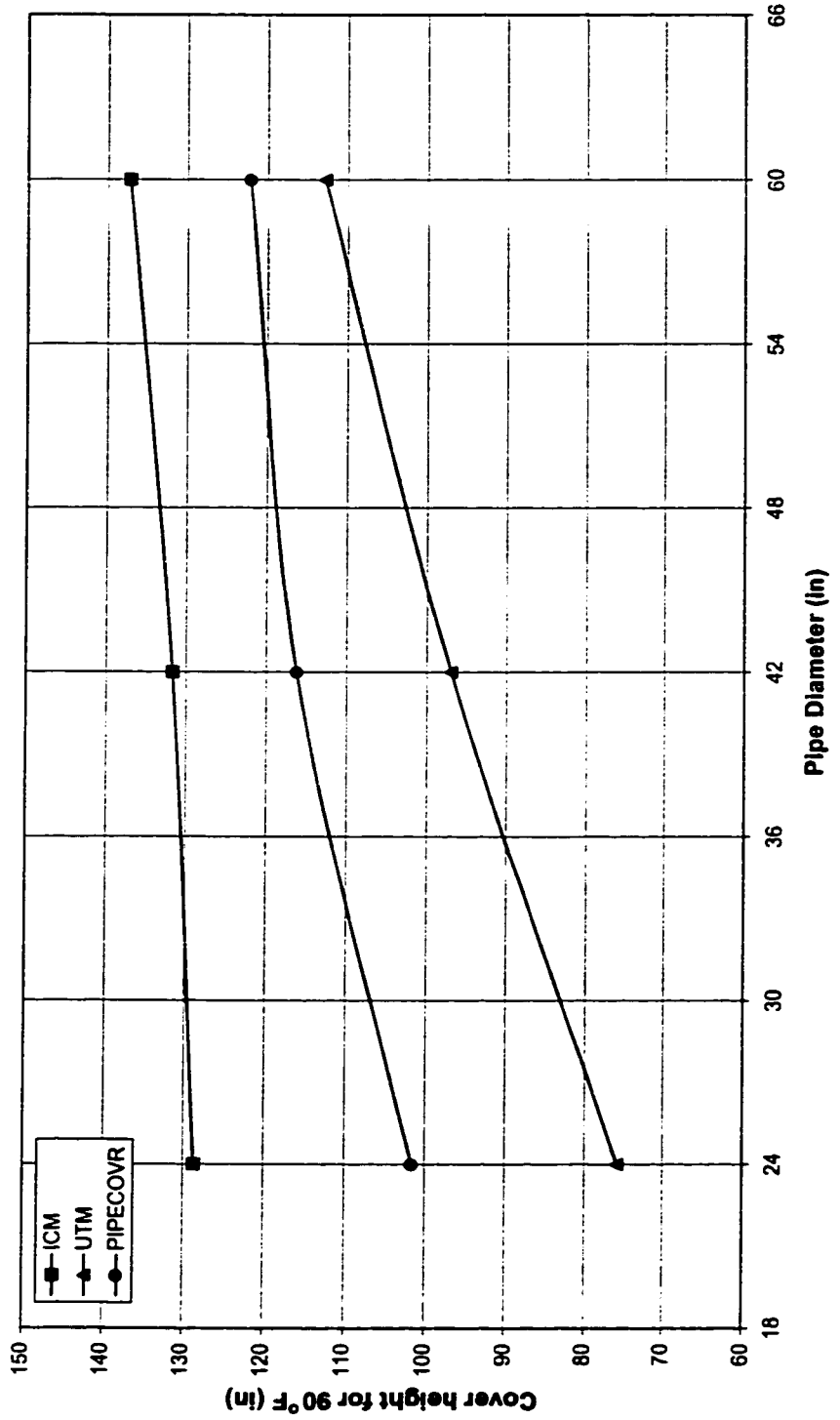

(d) R_b = 50 ft, θ = 15°

Figure 5-5 (Contd.)

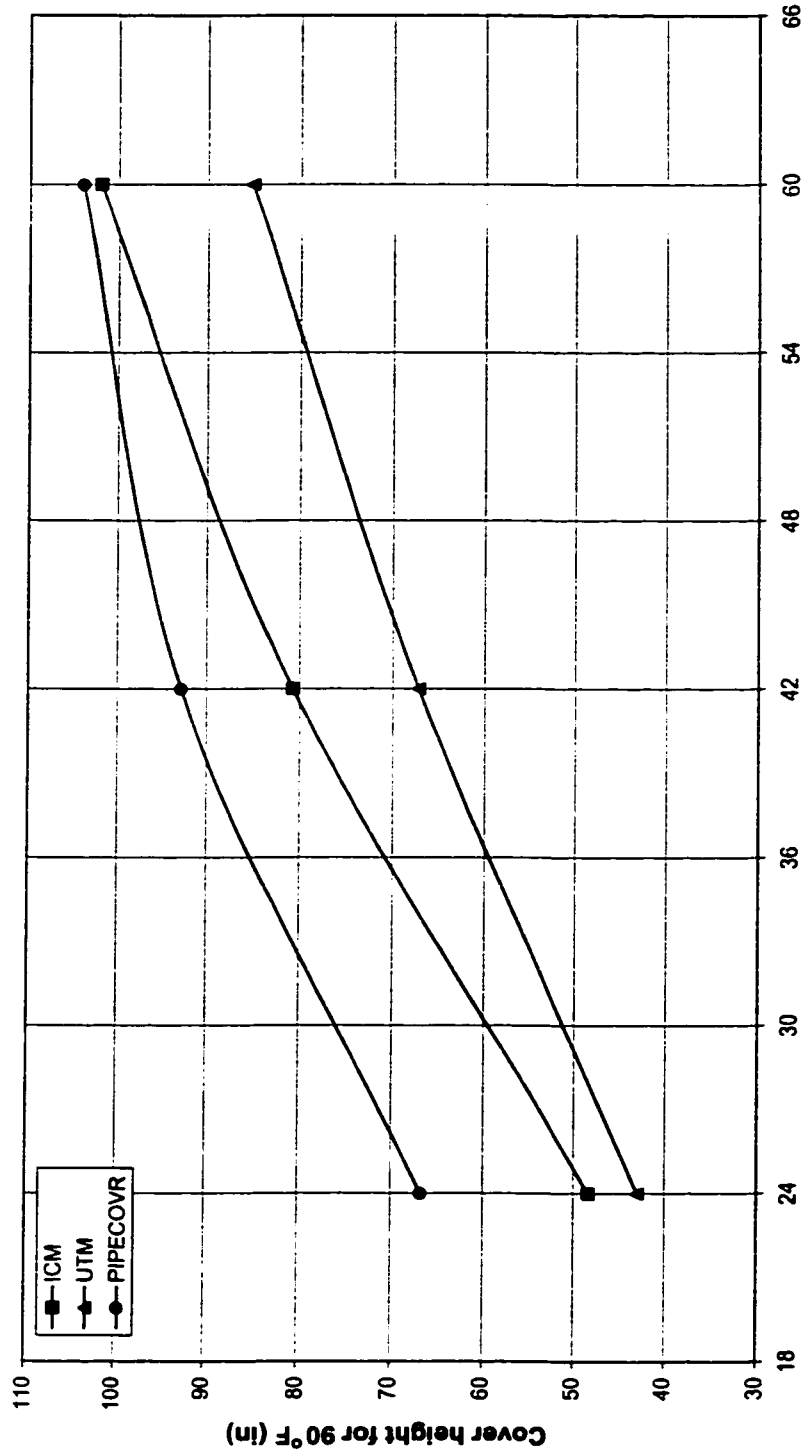

(e) R_b = 300 ft, θ = 15°

Figure 5-5 (Contd.)

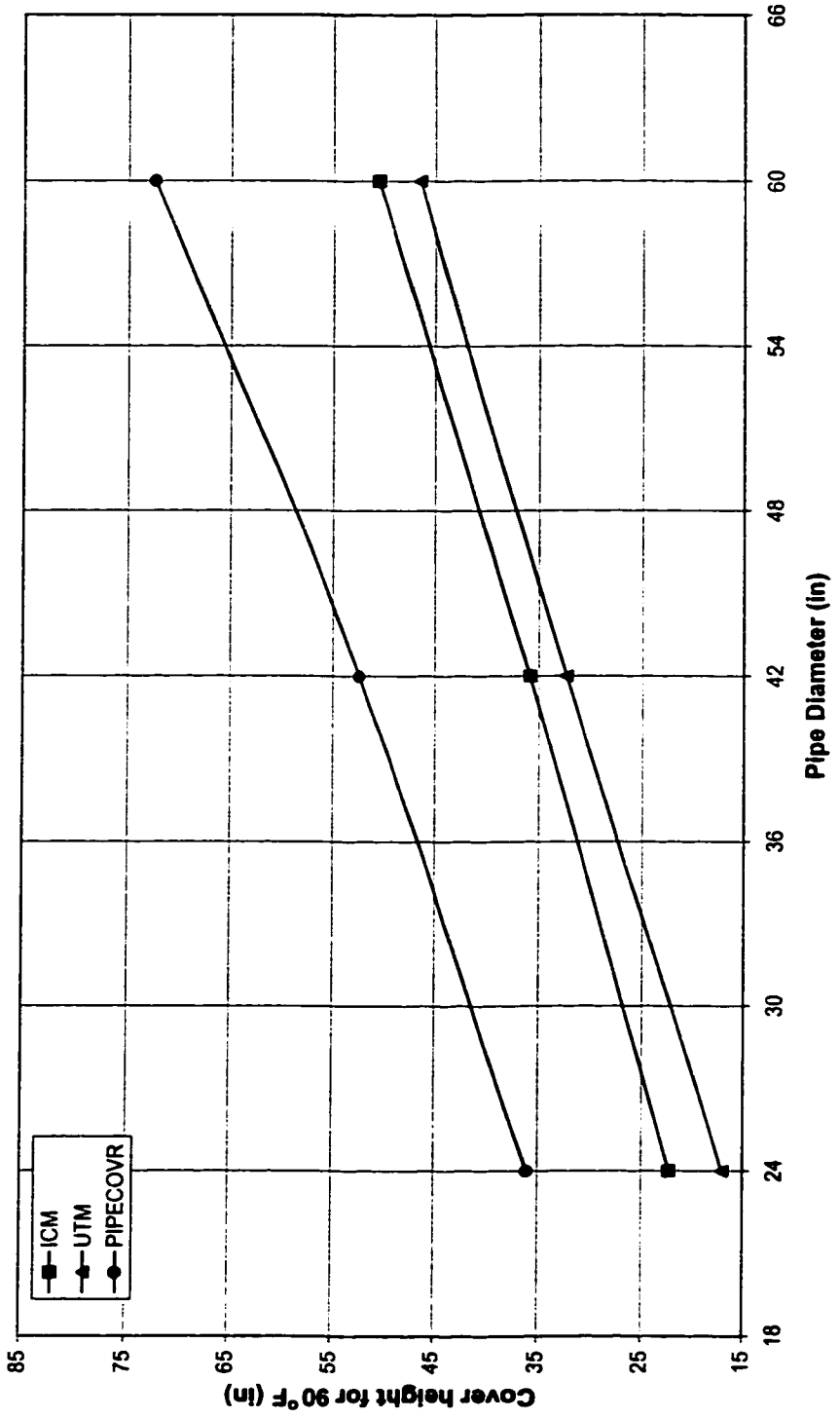

(f) R_b = 700 ft, θ = 15°

Figure 5-5 (Contd.)

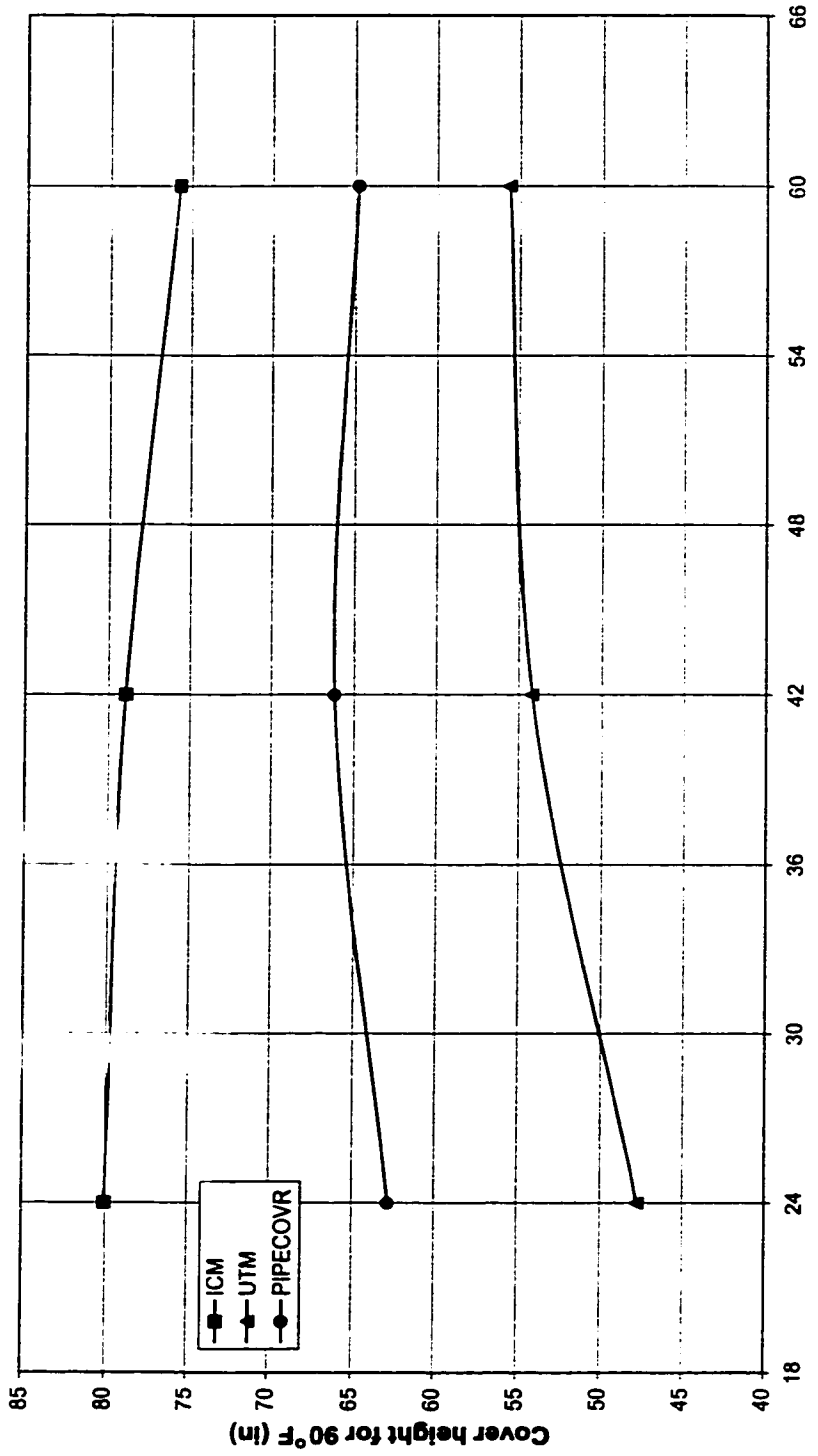

(g) R_b = 50 ft, $\theta = 8^\circ$

Figure 5-5 (Contd.)

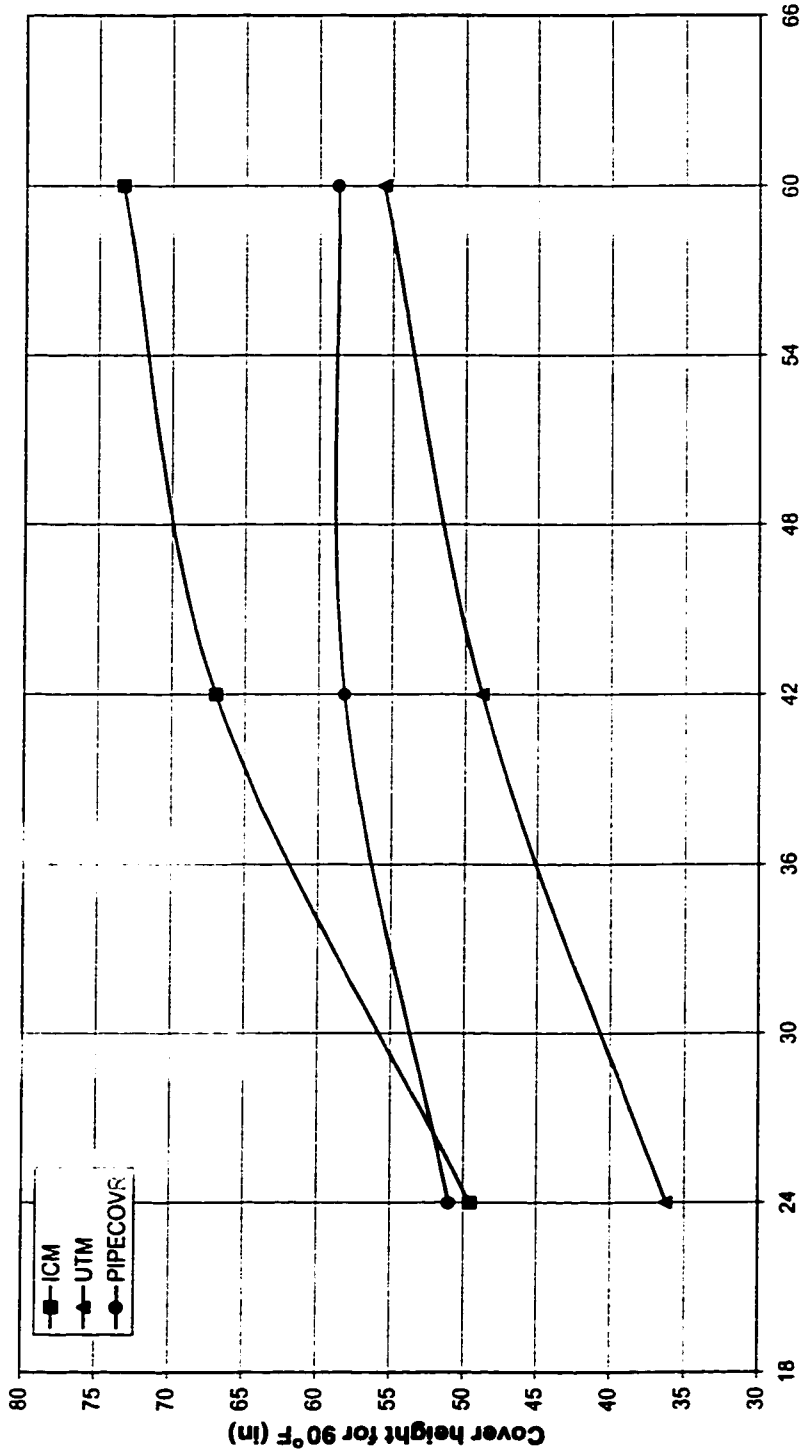

(h) R_b = 300 ft, θ = 8°

Figure 5-5 (Contd.)

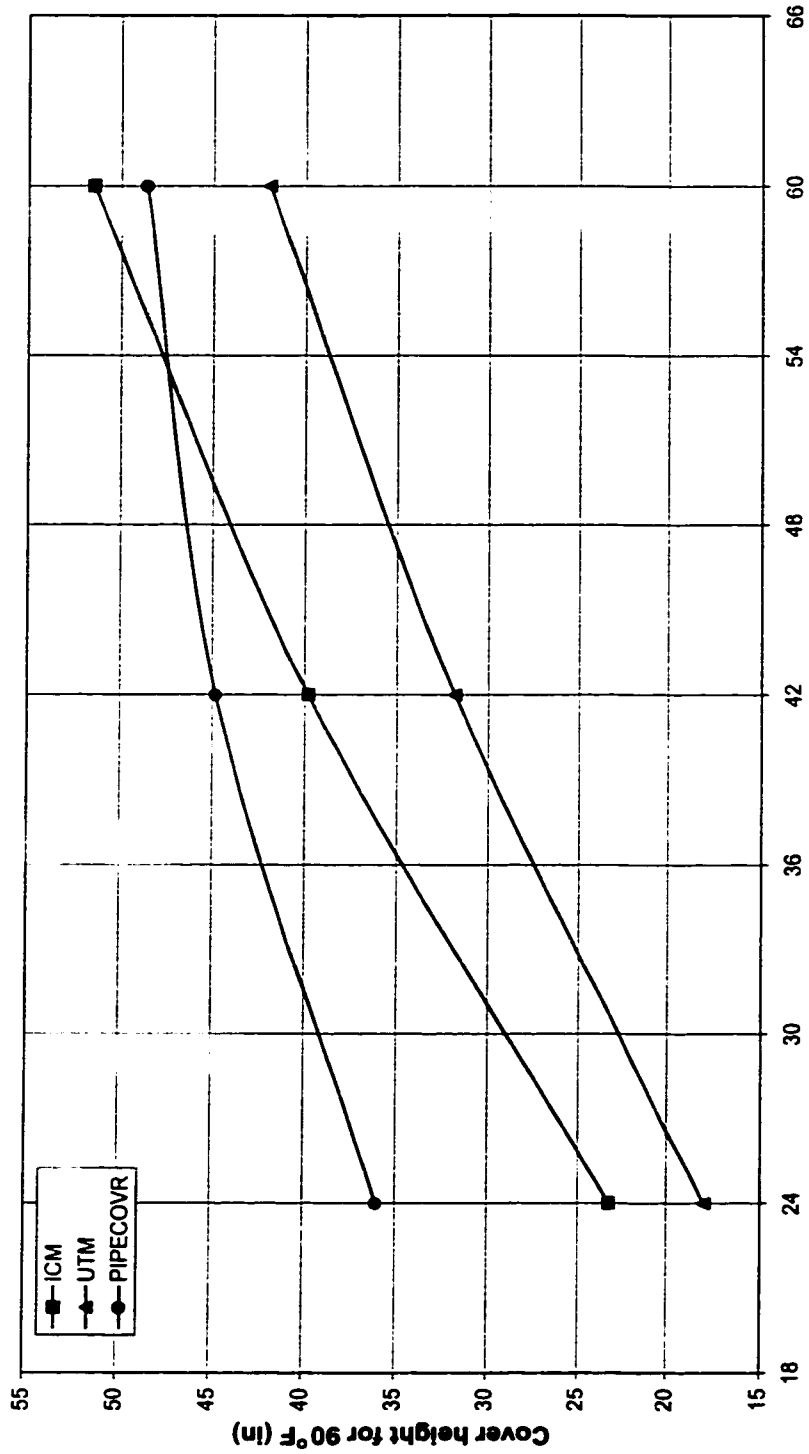

(i) R_b = 700 ft, θ = 8°

Figure 5-5 (Contd.)

this study for the case of R_b = 700 ft and $\theta \geq 15°$ (Figure 5-5(c & f)) and R_b = 300 ft and θ = 20° (Figure 5-5(b)). This shows that PIPECOVR program gives conservative results for the bends with long bend circumferential length.

The values of the minimum cover height are re-plotted against the bend angle, θ, in Figure 5-6. Similar observations can be made from these curves. The results obtained by ICM and UTM are closest for the largest D. The PIPECOVR results of the smaller radius bend agree closely with the results of this study. The value of the required cover height is not significantly influenced by the bend angle in the case of larger radius bends.

5.2.3 Effect of D/t

The results discussed above are obtained for a constant D/t ratio of 50. Additional runs are made with a D/t value of 100 to see the effect of the ratio on the capacity of the buried pipe vertical bend against temperature change. These runs and their results are listed in Table 5-4. The cover height values for these runs are chosen based on the previous runs of D/t = 50. The ultimate ΔT value corresponding to each run is also calculated by the PIPECOVR program and is included in Table 5-4.

The results given in Table 5-4 are plotted in Figure 5-7. The corresponding results of D/t = 50 given in Table 5-2 are included in these plots for comparison purposes. The graphs show that the values of D/t do not affect the slope of the curve much.

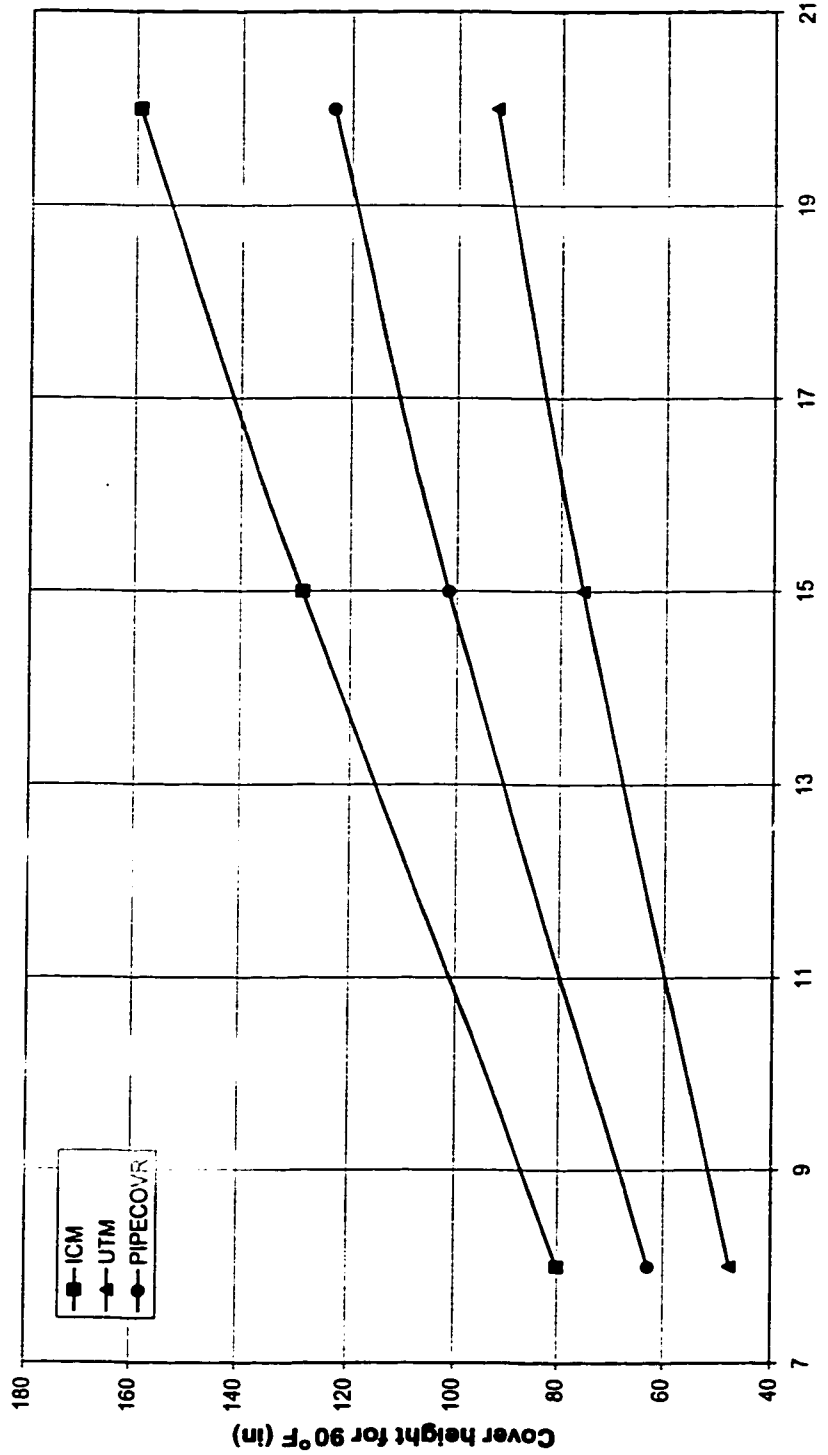

(a) R_b = 50 ft, D = 24 in

Figure 5-6 The effect of bend angle on cover height requirement of vertical bends

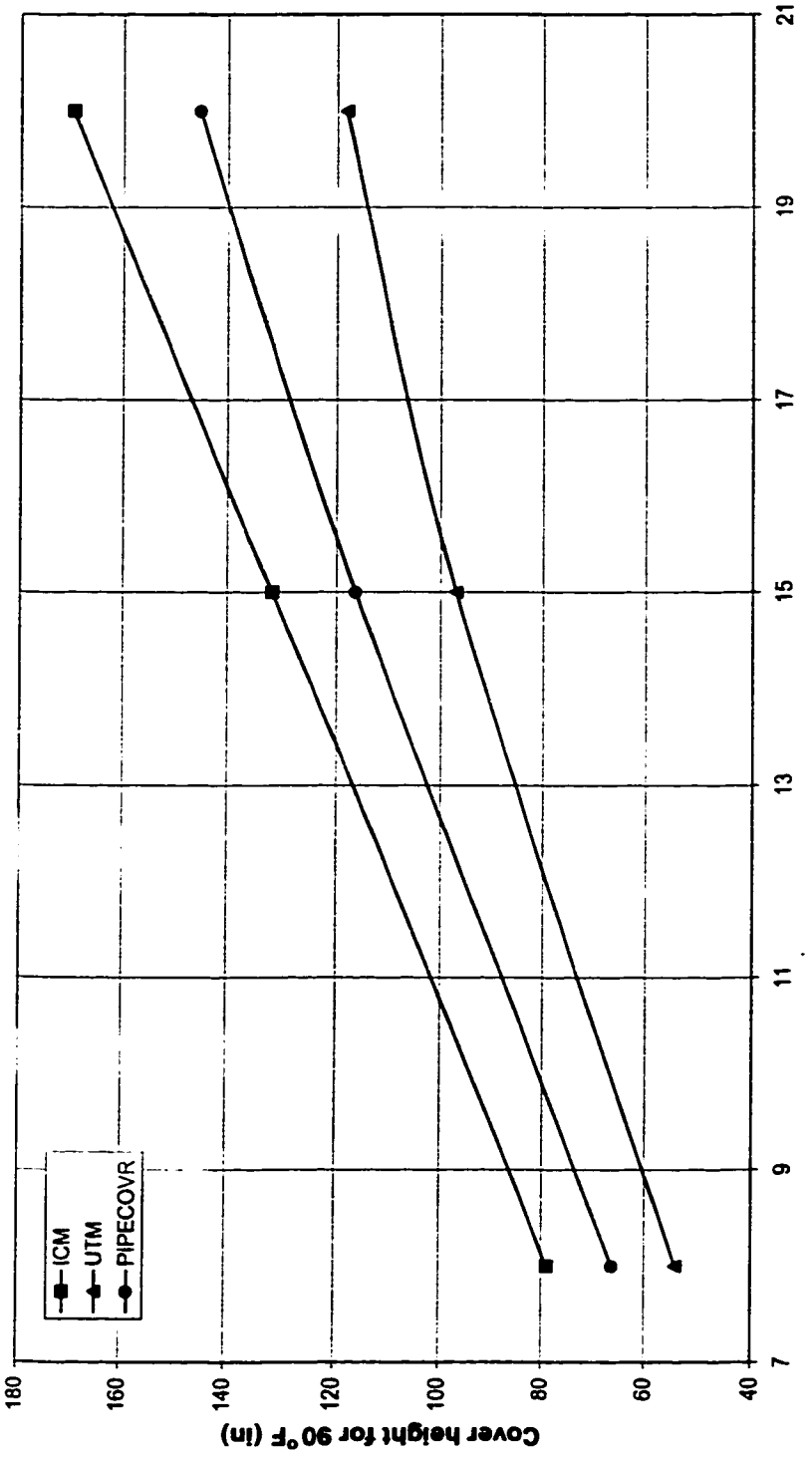

(b) R_b = 50 ft, D = 42 in

Figure 5-6 (Contd.)

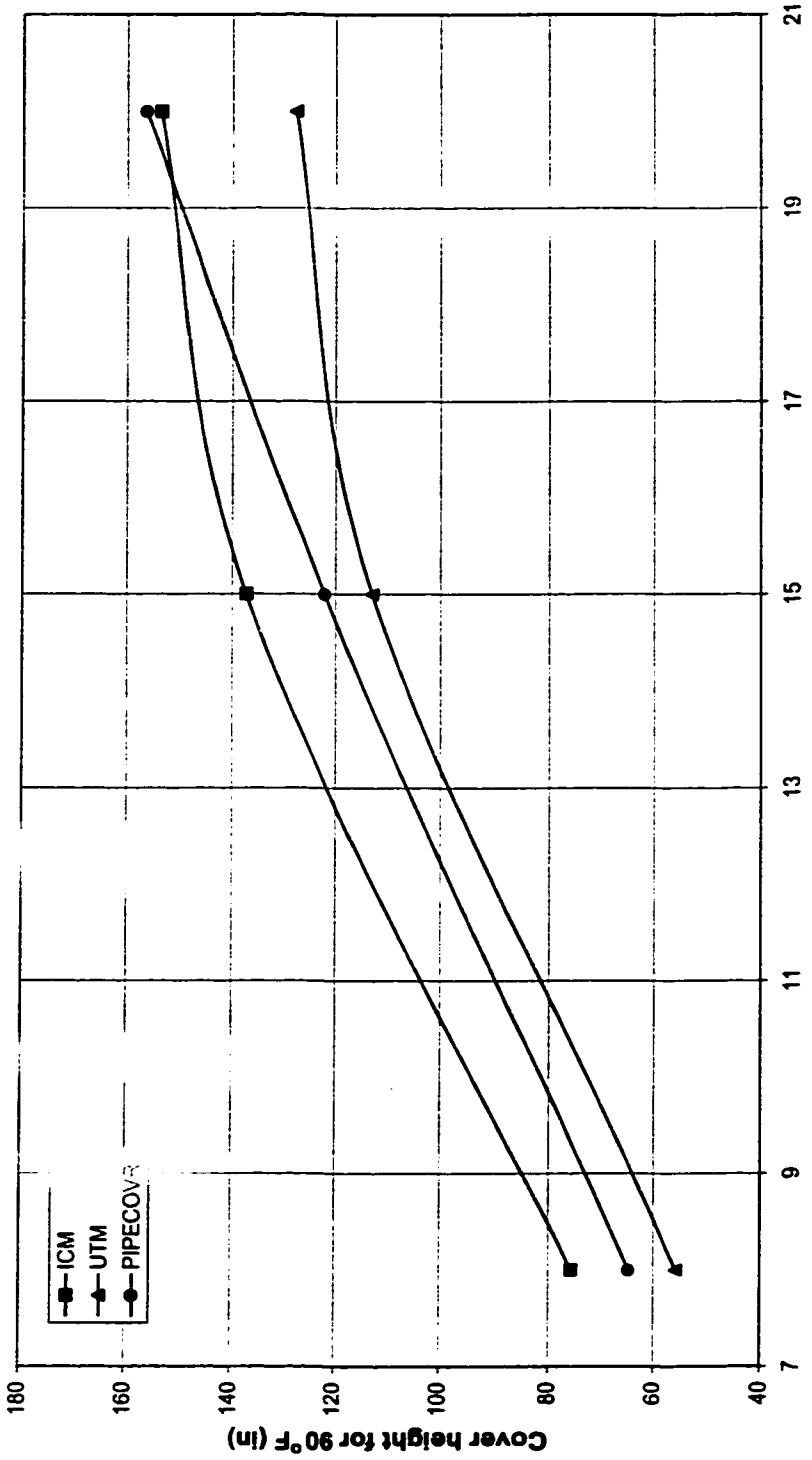

(c) R_b = 50 ft, D = 60 in

Figure 5-6 (Contd.)

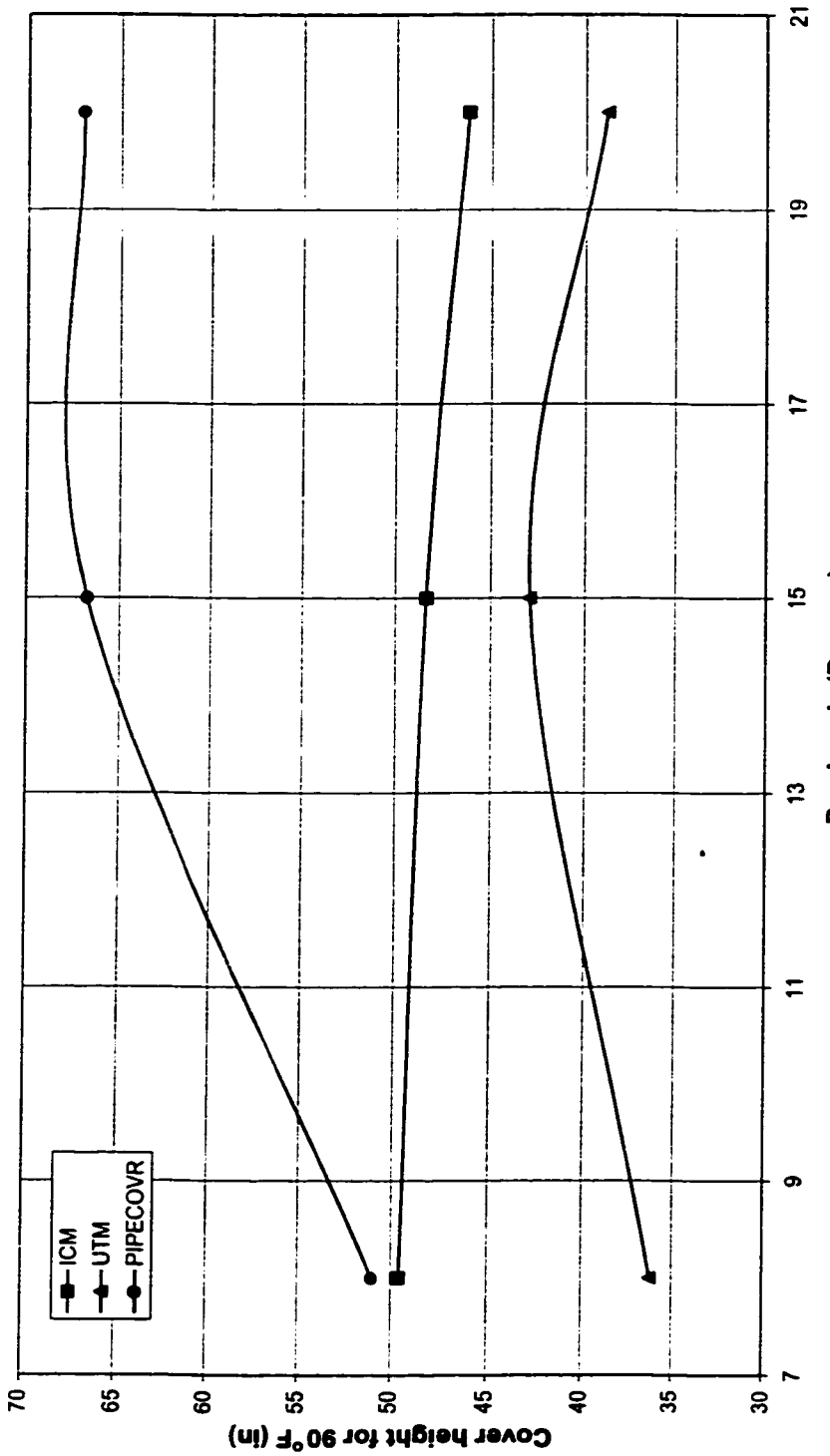

(d) R_b = 300 ft, D = 24 in

Figure 5-6 (Contd.)

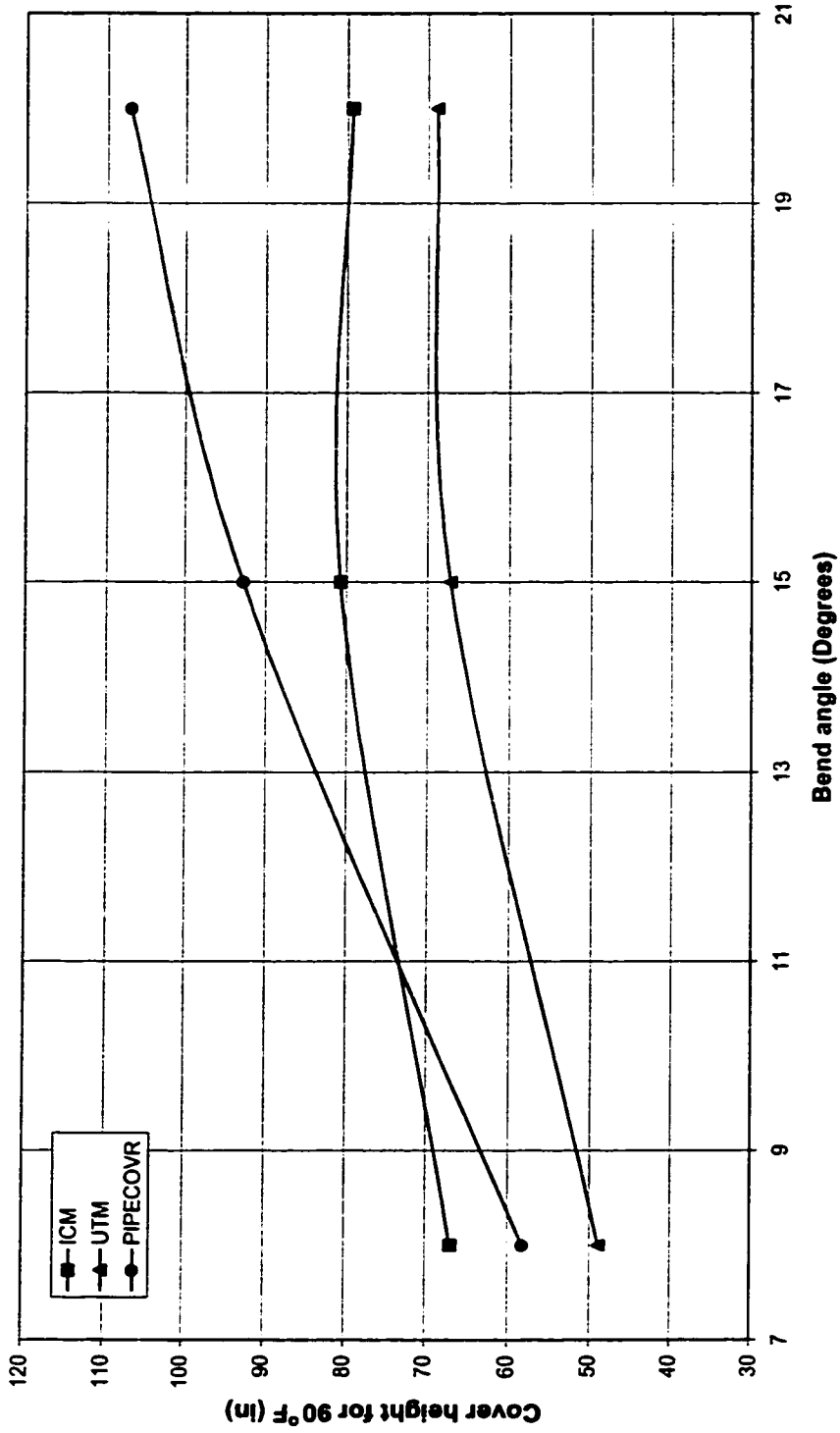

(e) R_b = 300 ft, D = 42 in

Figure 5-6 (Contd.)

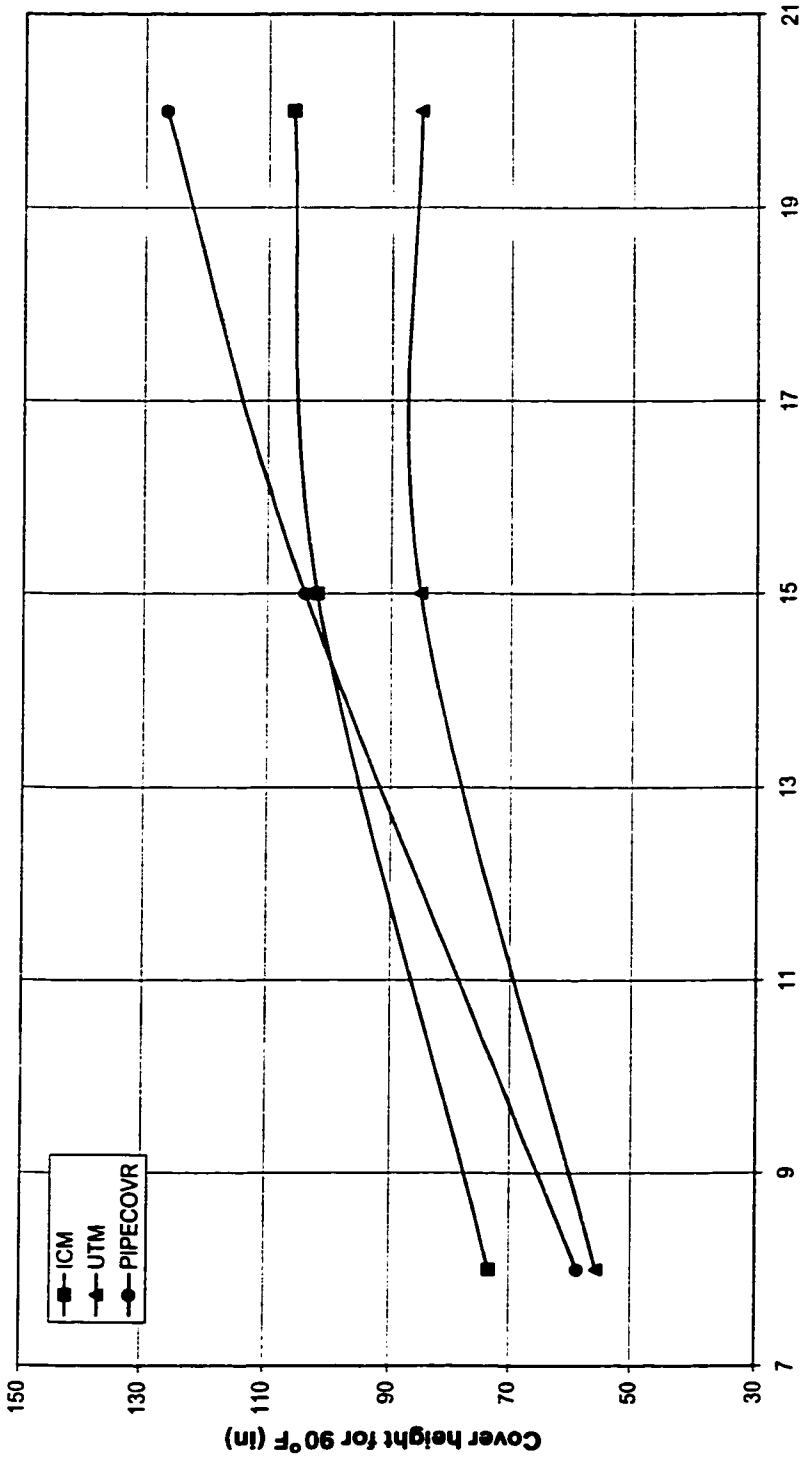

(f) R_b = 300 ft, D = 60 in

Figure 5-6 (Contd.)

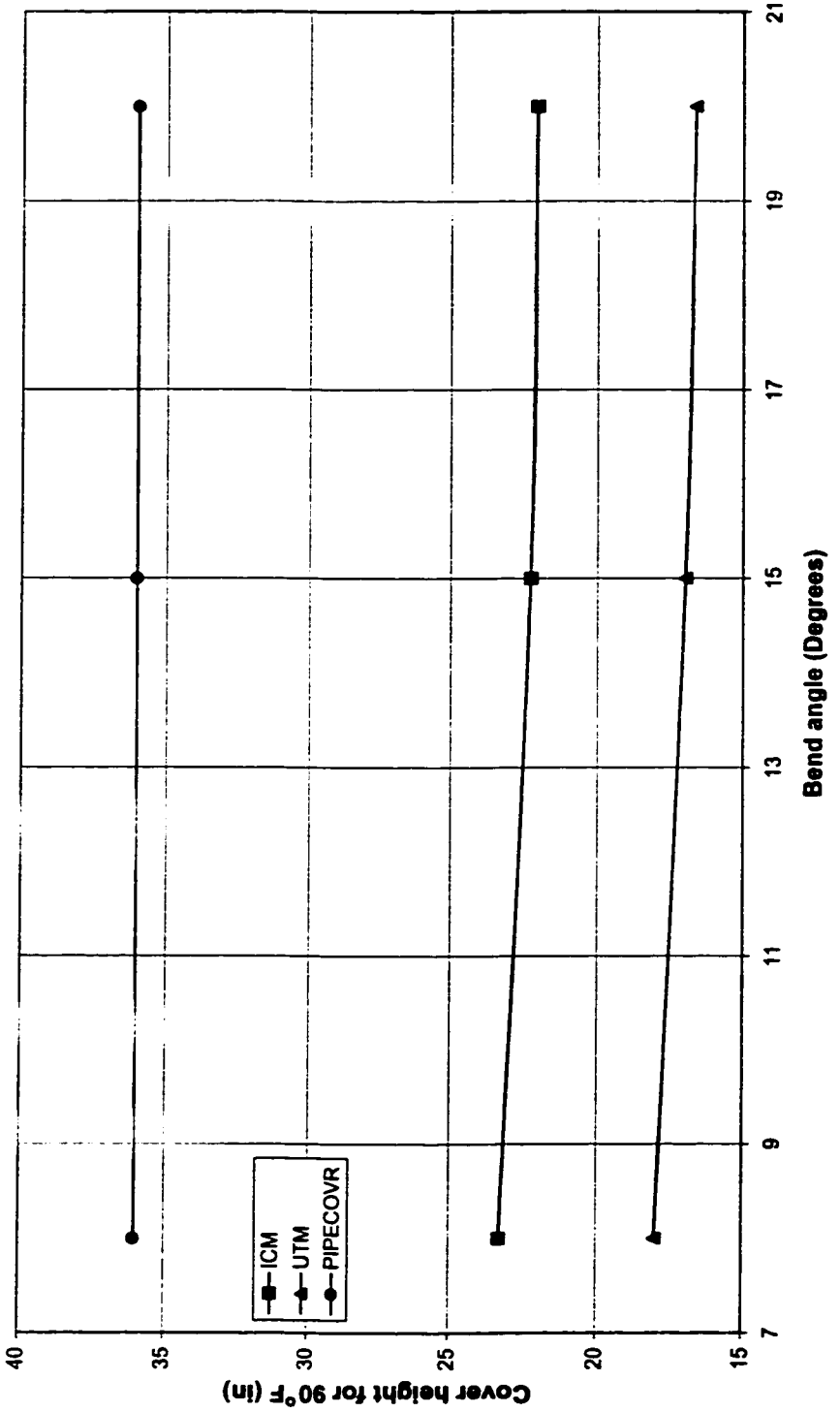

(g) R_b = 700 ft, D = 24 in

Figure 5-6 (Contd.)

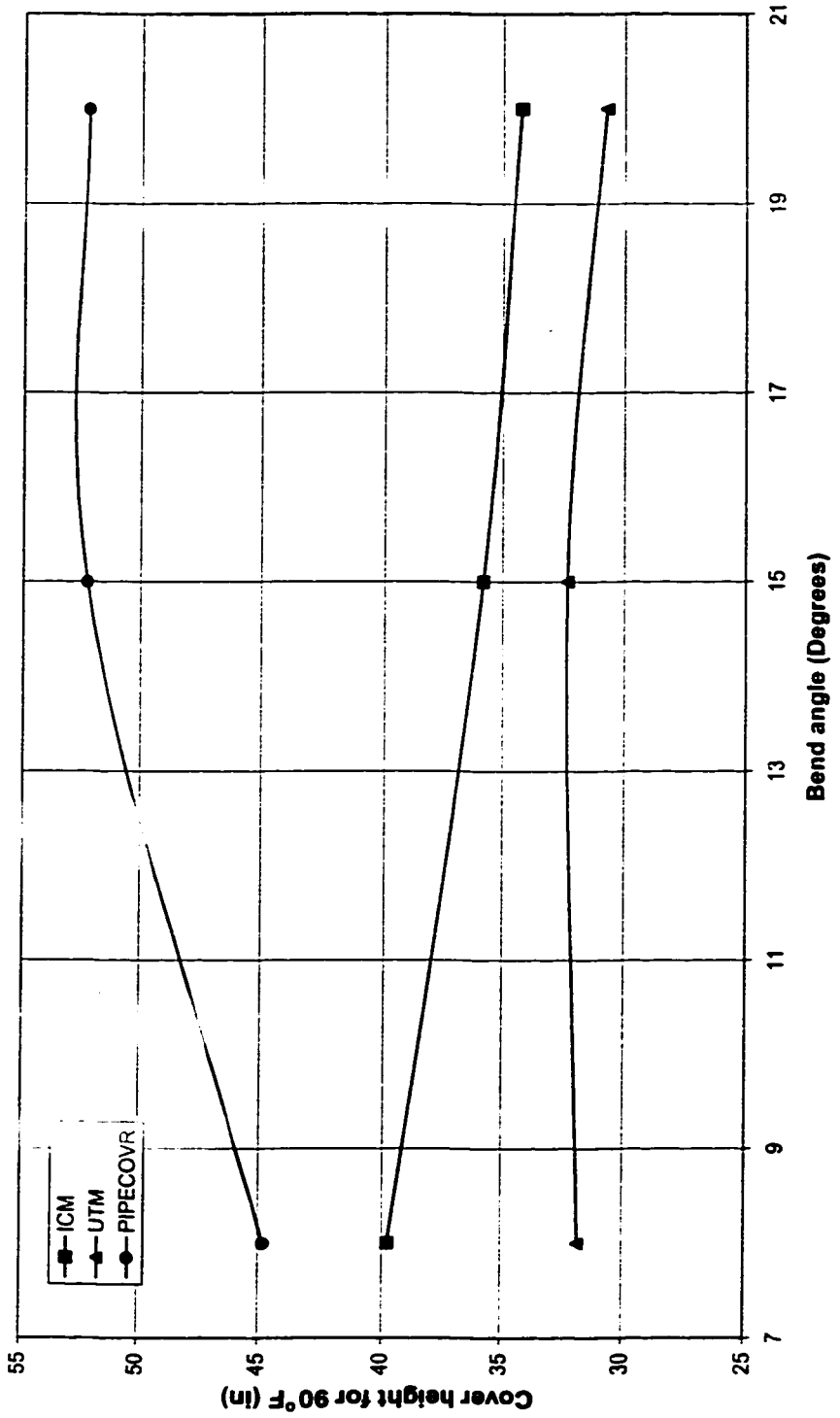

(h) R_b = 700 ft, D = 42 in

Figure 5-6 (Contd.)

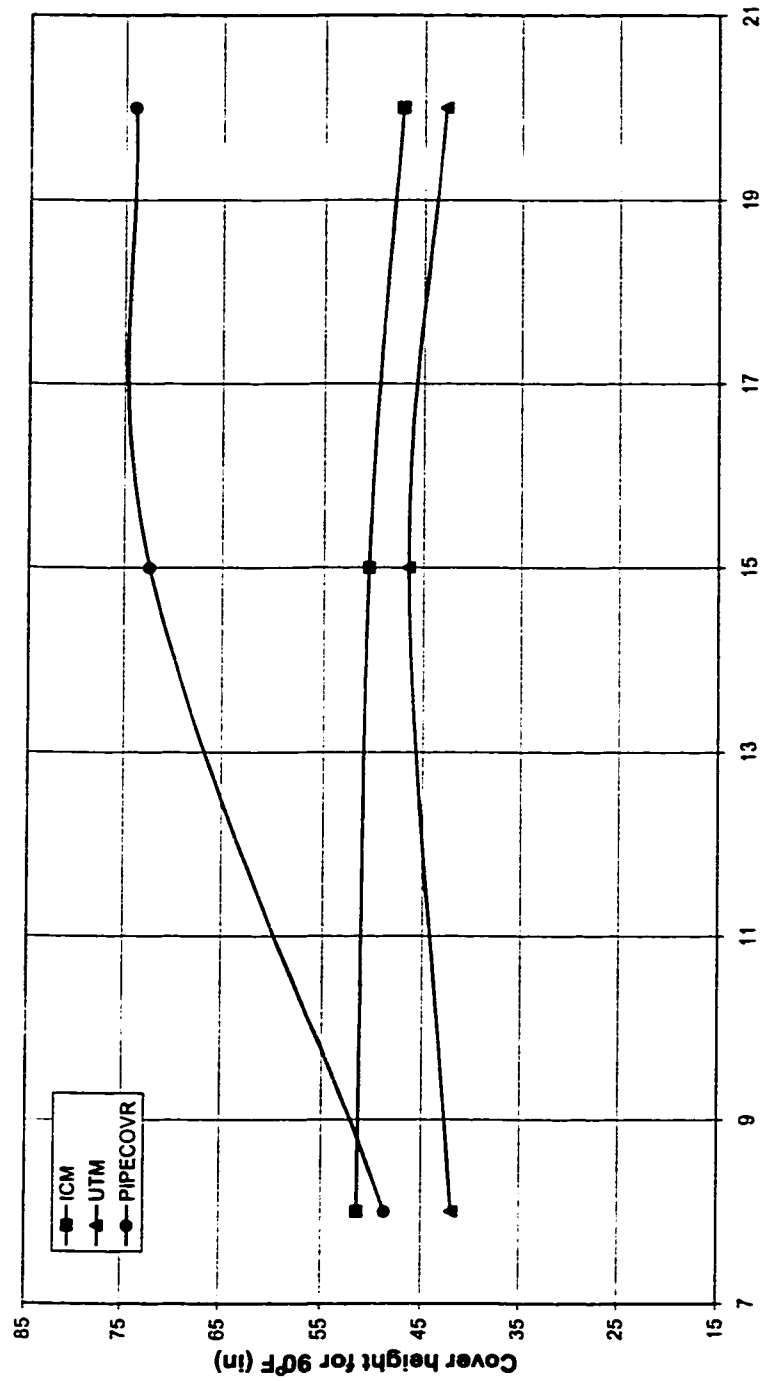

(i) R_b = 700 ft, D = 60 in

Figure 5-6 (Contd.)

Table 5-4 Vertical bend runs to study the effects of D, H_c, R_b and θ with D/t = 100

S. No.	D (in)	H_c (in)	R_b (ft)	θ (Degrees)	Ultimate Temperature °F		
					Installation Condition Method	Ultimate Temperature Method	PIPECOVR*
1	24	36	50	20	34.8	50.98	46.112
2	24	60	50	20	59.97	93.2	71.529
3	42	36	50	20	36.18	45.54	45.814
4	42	60	50	20	56.91	72.98	66.543
5	60	36	50	20	40.14	45.25	47.63
6	60	60	50	20	59.39	68.71	66.333
7	24	15	300	20	55.45	64.97	35.657
8	24	24	300	20	83.77	97.58	54.346
9	42	24	300	20	52.02	56.71	43.451
10	42	36	300	20	73.82	80.45	57.365
11	60	36	300	20	59.27	64.27	55.016
12	60	60	300	20	92.85	98.93	78.339
13	24	10	700	20	60.93	102.79	68.316
14	24	12	700	20	73.29	110.37	77.021
15	42	10	700	20	54.67	65.42	46.219
16	42	15	700	20	72.58	90.54	58.278
17	60	12	700	20	52.32	72.74	41.838
18	60	18	700	20	70.35	80.76	51.907
19	24	30	50	8	52.2	88.1	77.937
20	24	36	50	8	64.35	111.49	88.872
21	42	30	50	8	56.12	77.01	80.122
22	42	36	50	8	69.19	106.52	89.438
23	60	30	50	8	63.03	77.8	84.599
24	60	36	50	8	74.71	94.03	93.147
25	24	15	300	8	43.21	64.35	59.439
26	24	24	300	8	72.86	102.89	79.21
27	42	24	300	8	54.17	71.58	77.154
28	42	36	300	8	81.65	110.45	98.377
29	60	24	300	8	51.67	72.31	80.693
30	60	36	300	8	75.21	93.37	99.393
31	24	8	700	8	46.62	90.79	59.841
32	24	10	700	8	58.51	96.43	68.316
33	42	15	700	8	59.22	78.02	73.976
34	42	24	700	8	92.83	117.41	93.613
35	60	24	700	8	72.16	89	90.639
36	60	36	700	8	106.2	119.78	113.201

* The temperatures are obtained by iterating the PIPECOVR program to get the desired value of H_c. The PIPECOVR program does not give the calculated value of H_c if $H_c < 36$. In the case of $H_c < 36$ the temperature was found by the quadratic extrapolation.

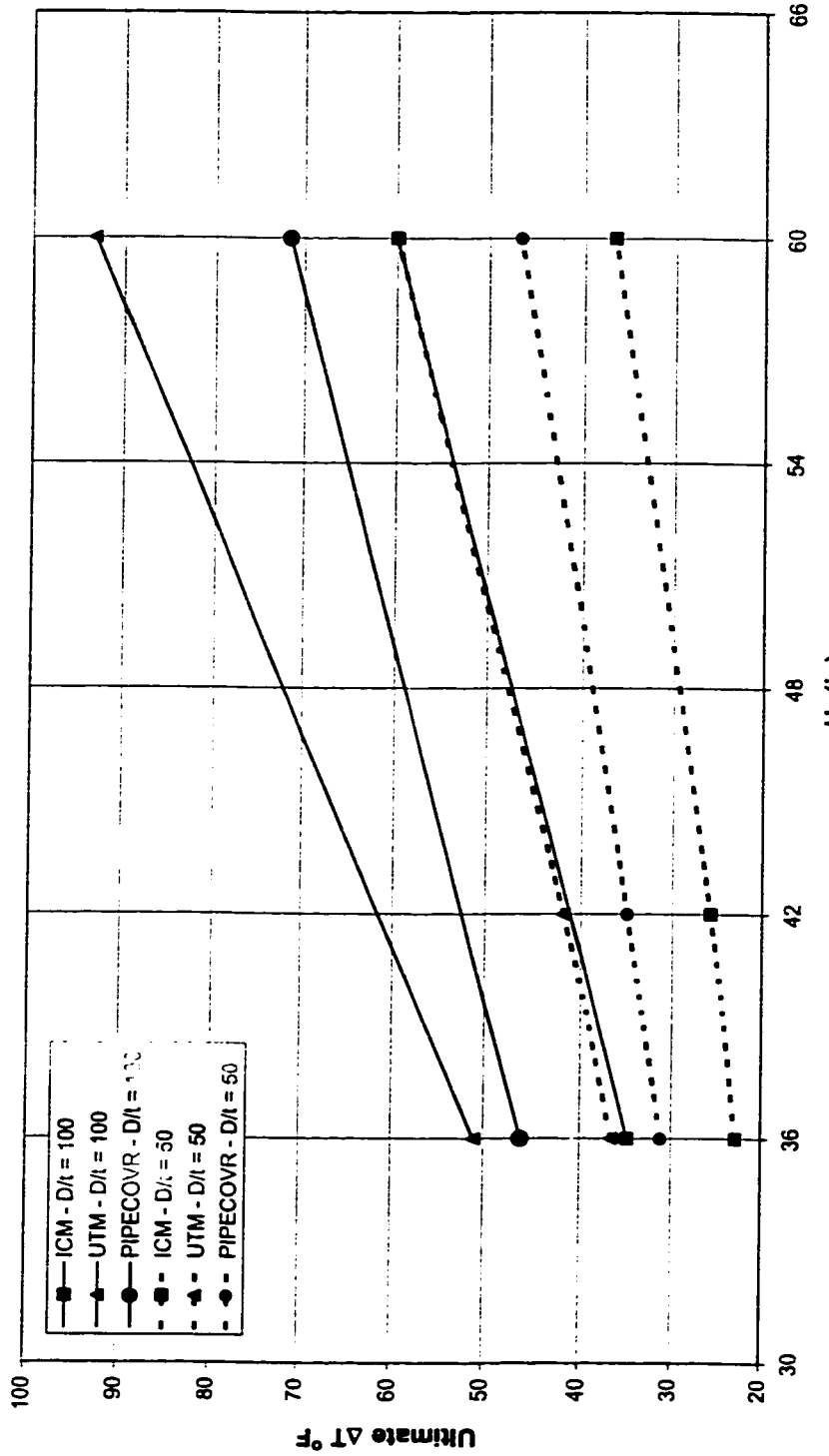

(a) R_b = 50 ft, θ = 20°, D = 24 in

Figure 5-7 Comparison of the results of vertical bend analysis for D/t = 50 and D/t = 100

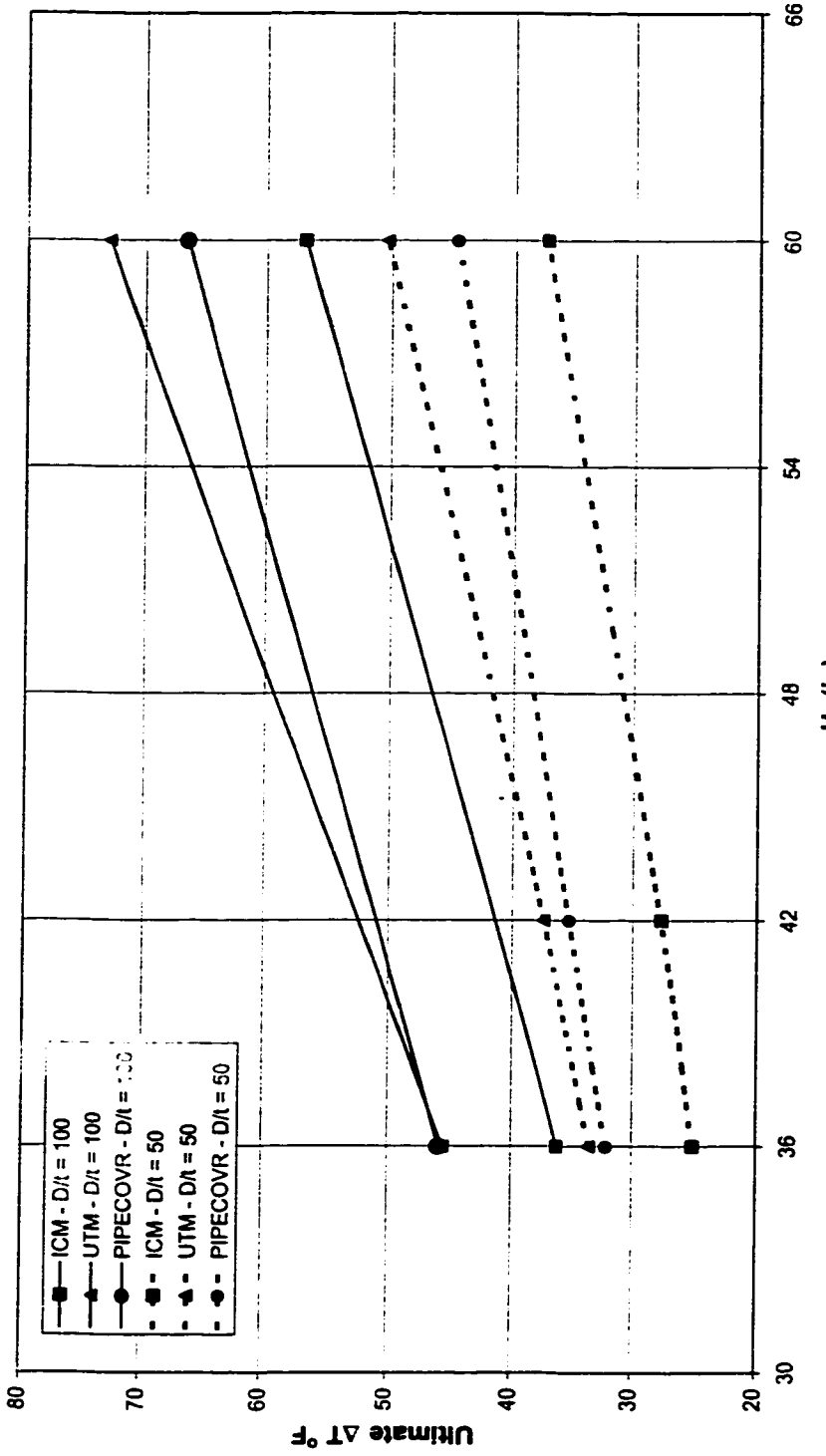

(b) R_b = 50 ft, θ = 20°, D = 42 in

Figure 5-7 (Contd.)

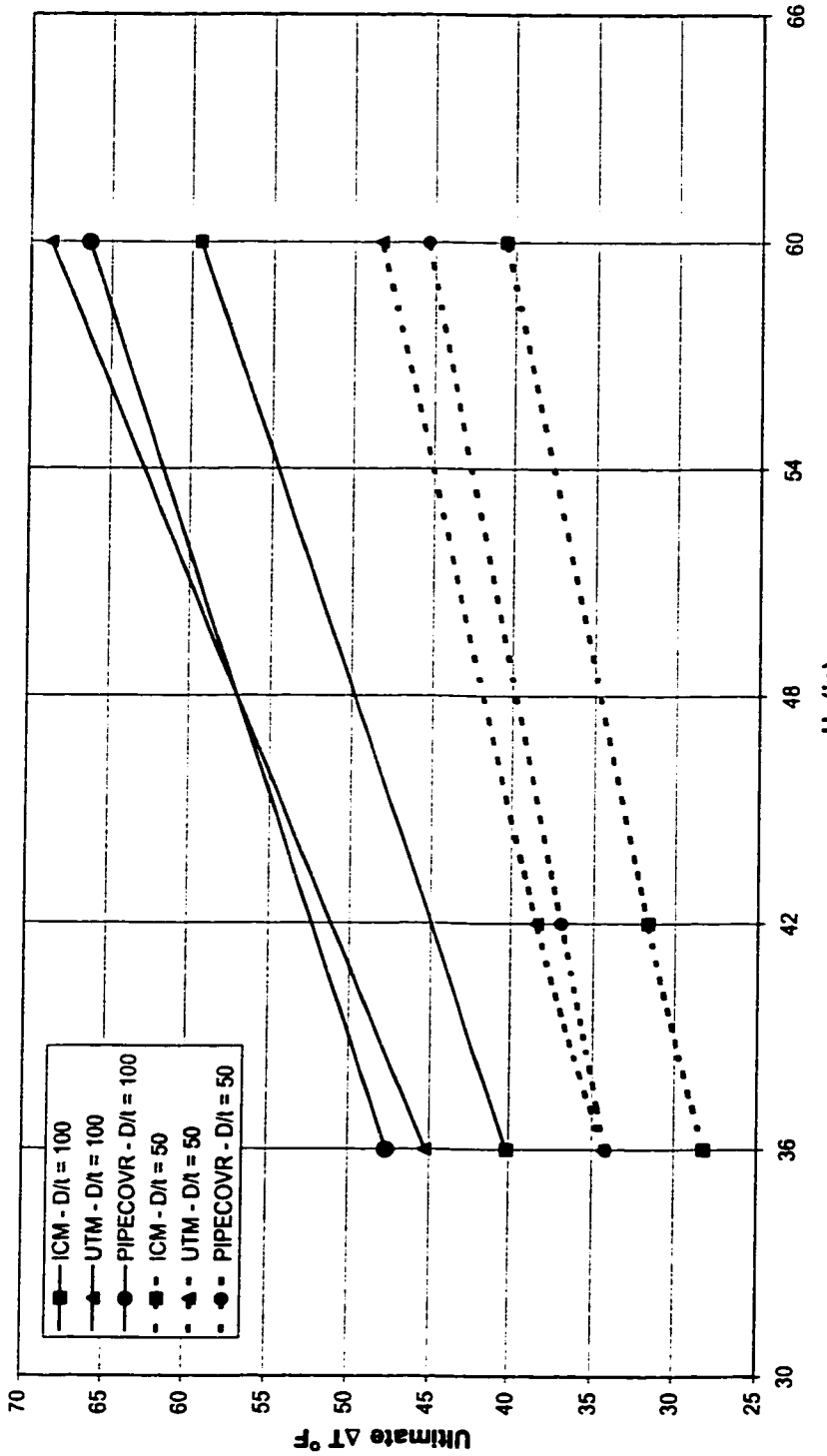

(c) R_b = 50 ft, θ = 20°, D = 60 in

Figure 5-7 (Contd.)

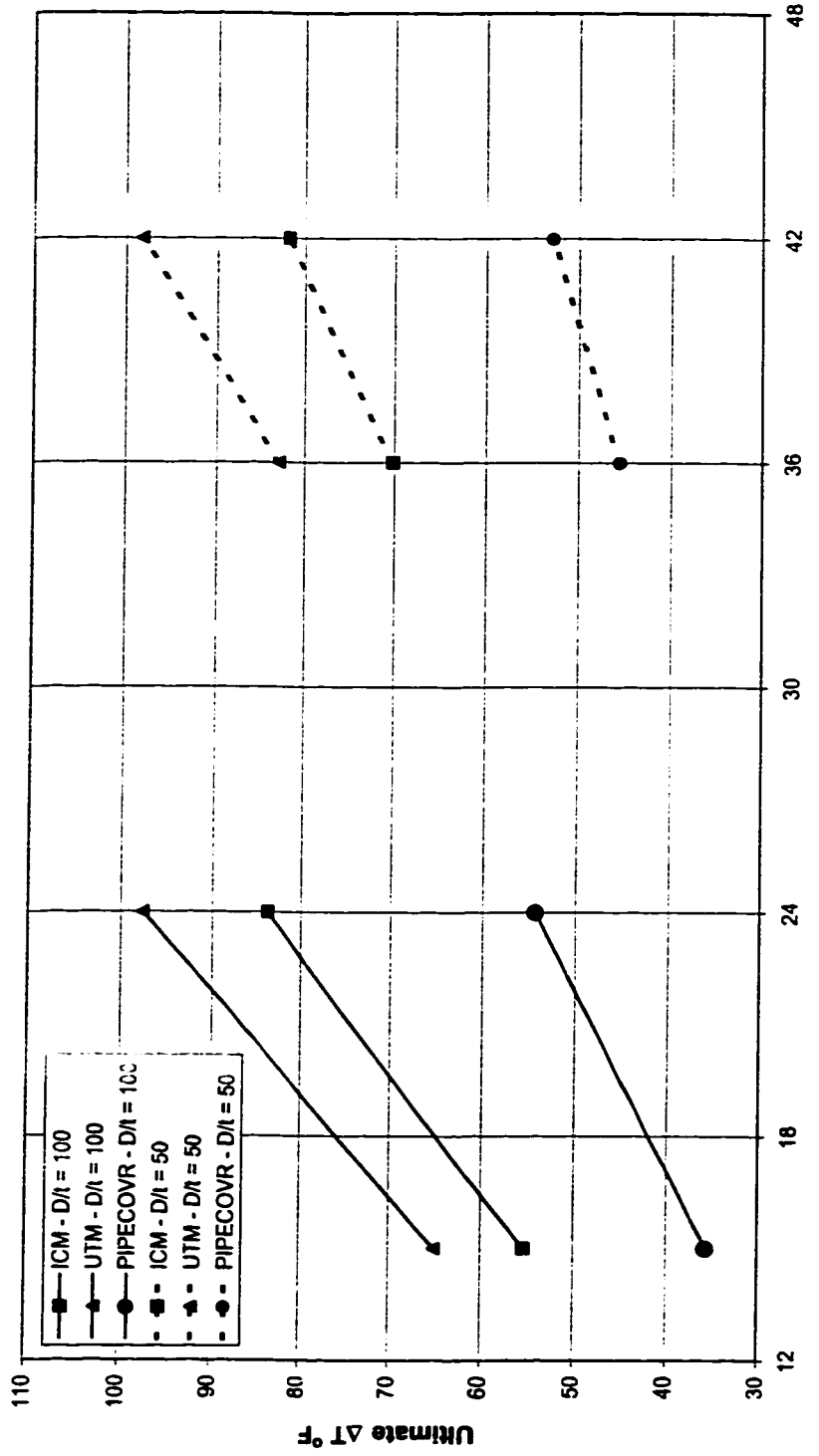

(d) R_b = 300 ft, θ = 20°, D = 24 in

Figure 5-7 (Contd.)

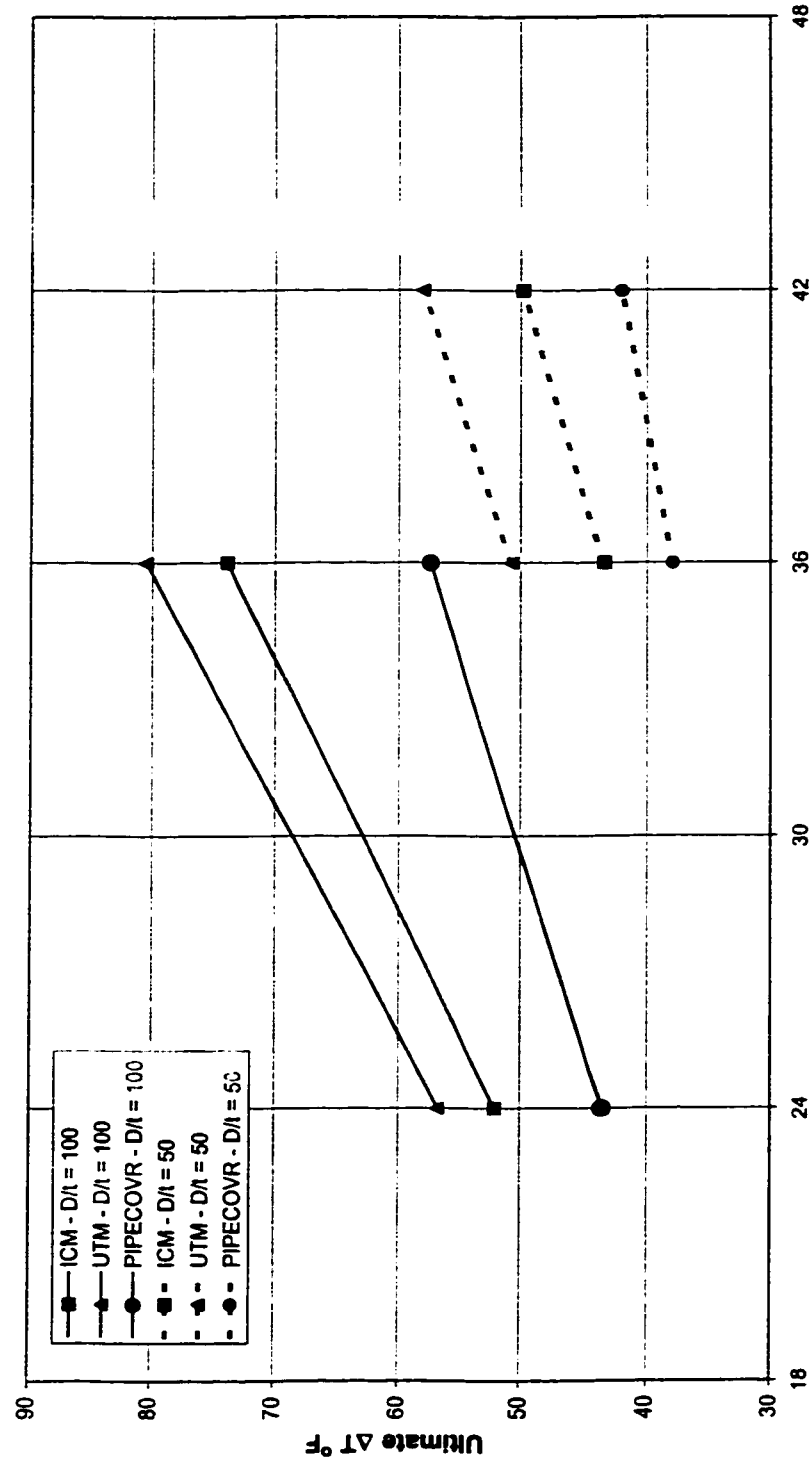

(e) R_b = 300 ft, θ = 20°, D = 42 in

Figure 5-7 (Contd.)

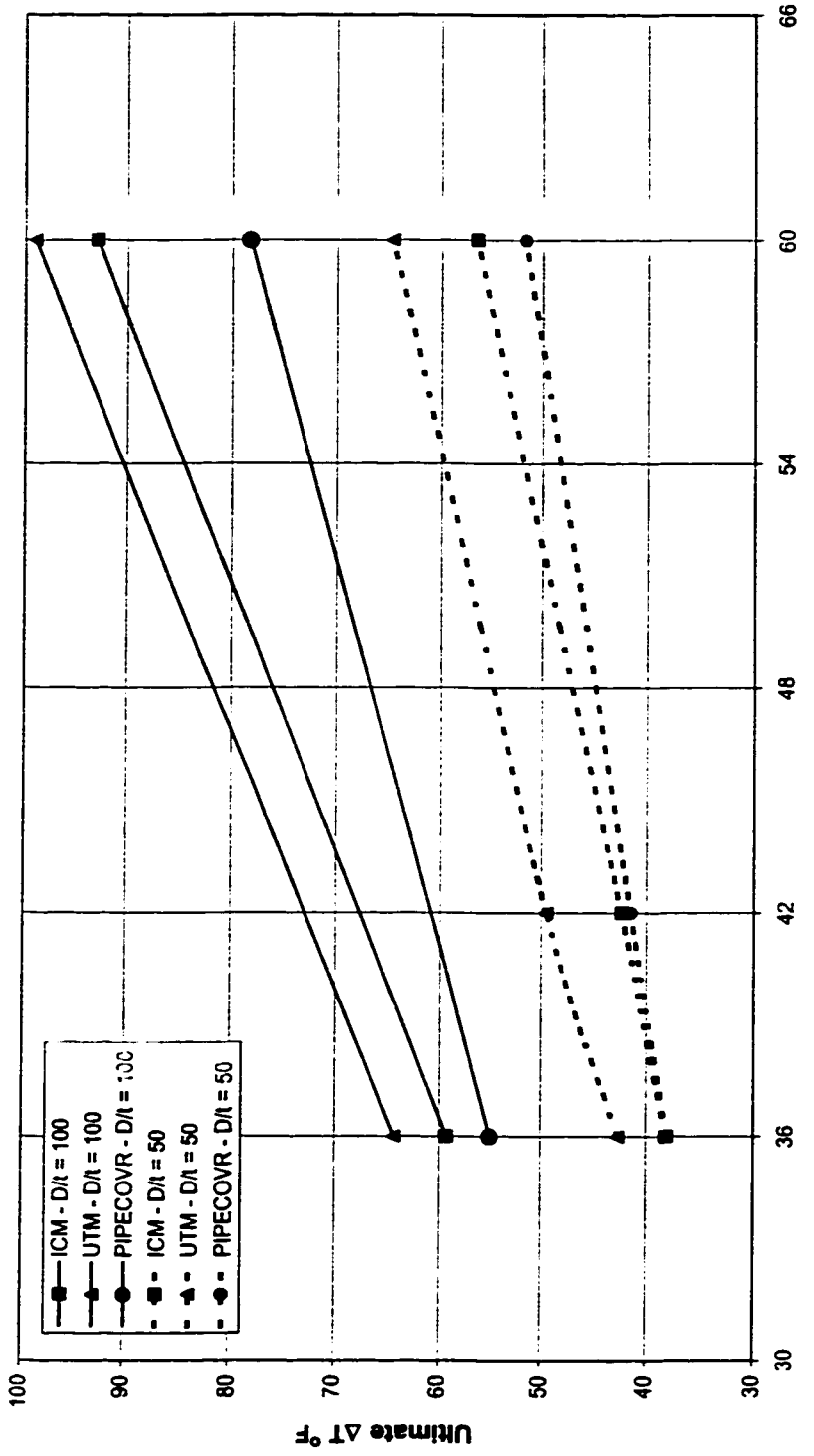

(f) R_b = 300 ft, θ = 20°, D = 60 in

Figure 5-7 (Contd.)

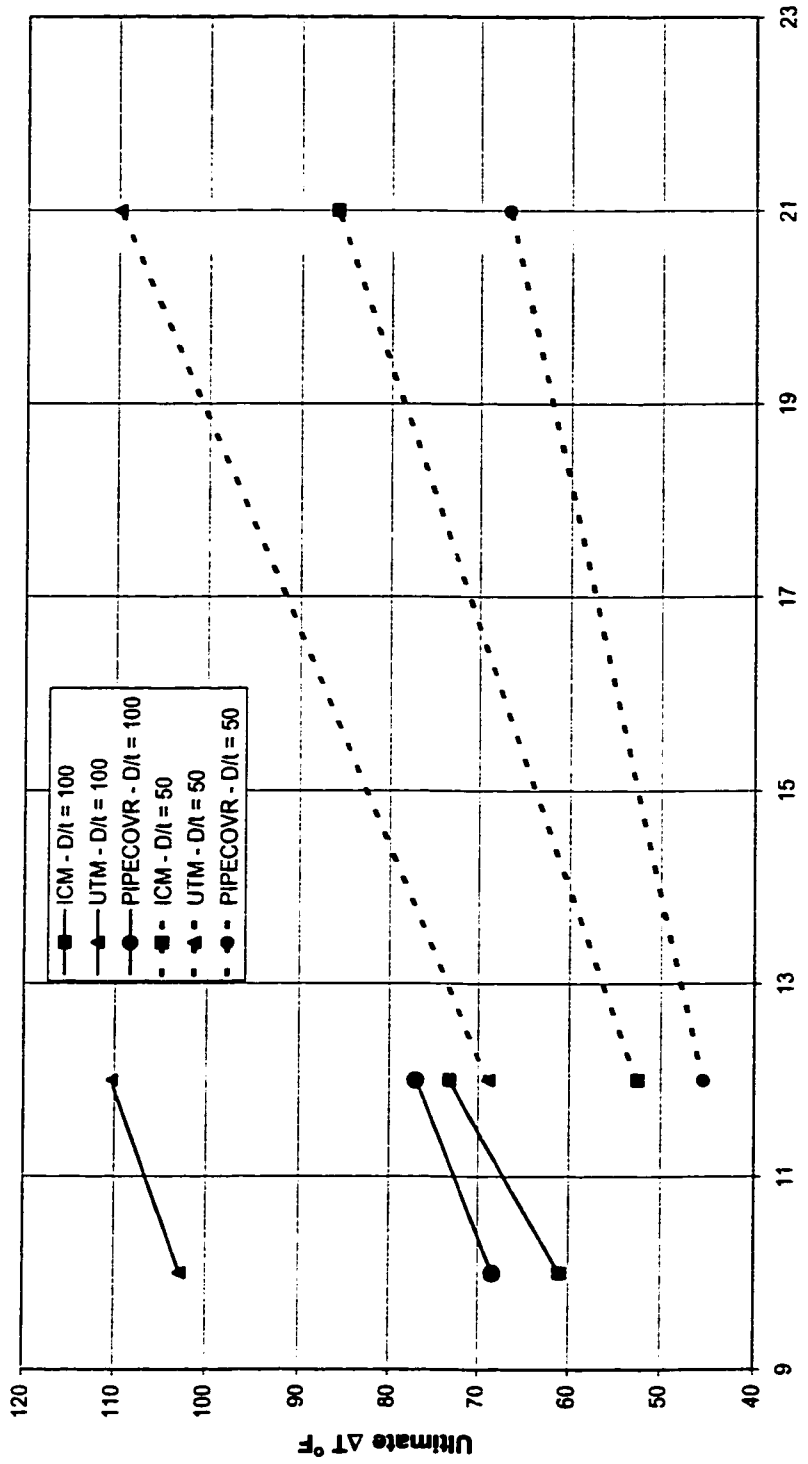

(g) R_b = 700 ft, θ = 20°, D = 24 in

Figure 5-7 (Contd.)

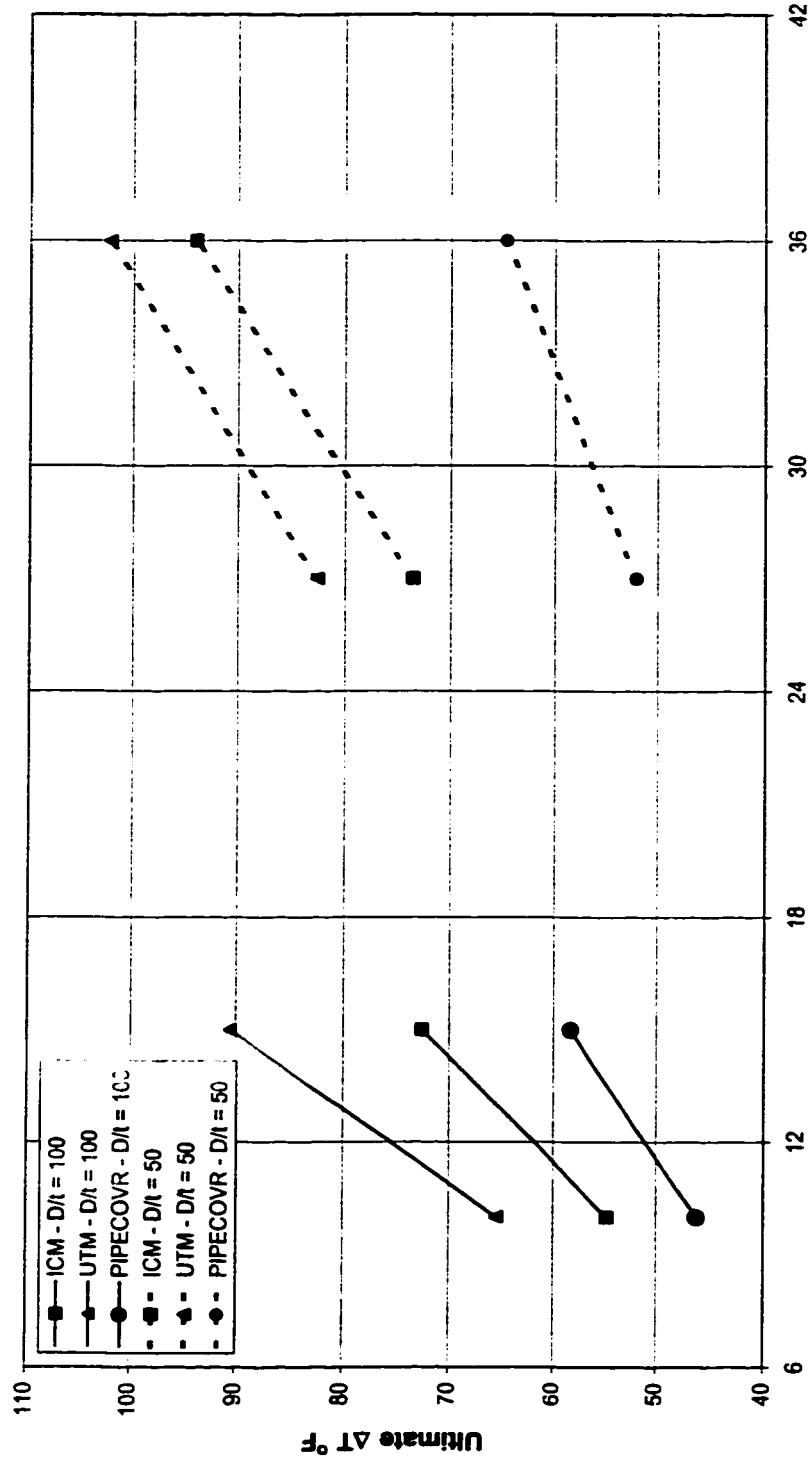

(h) R_b = 700 ft, θ = 20°, D = 42 in

Figure 5-7 (Contd.)

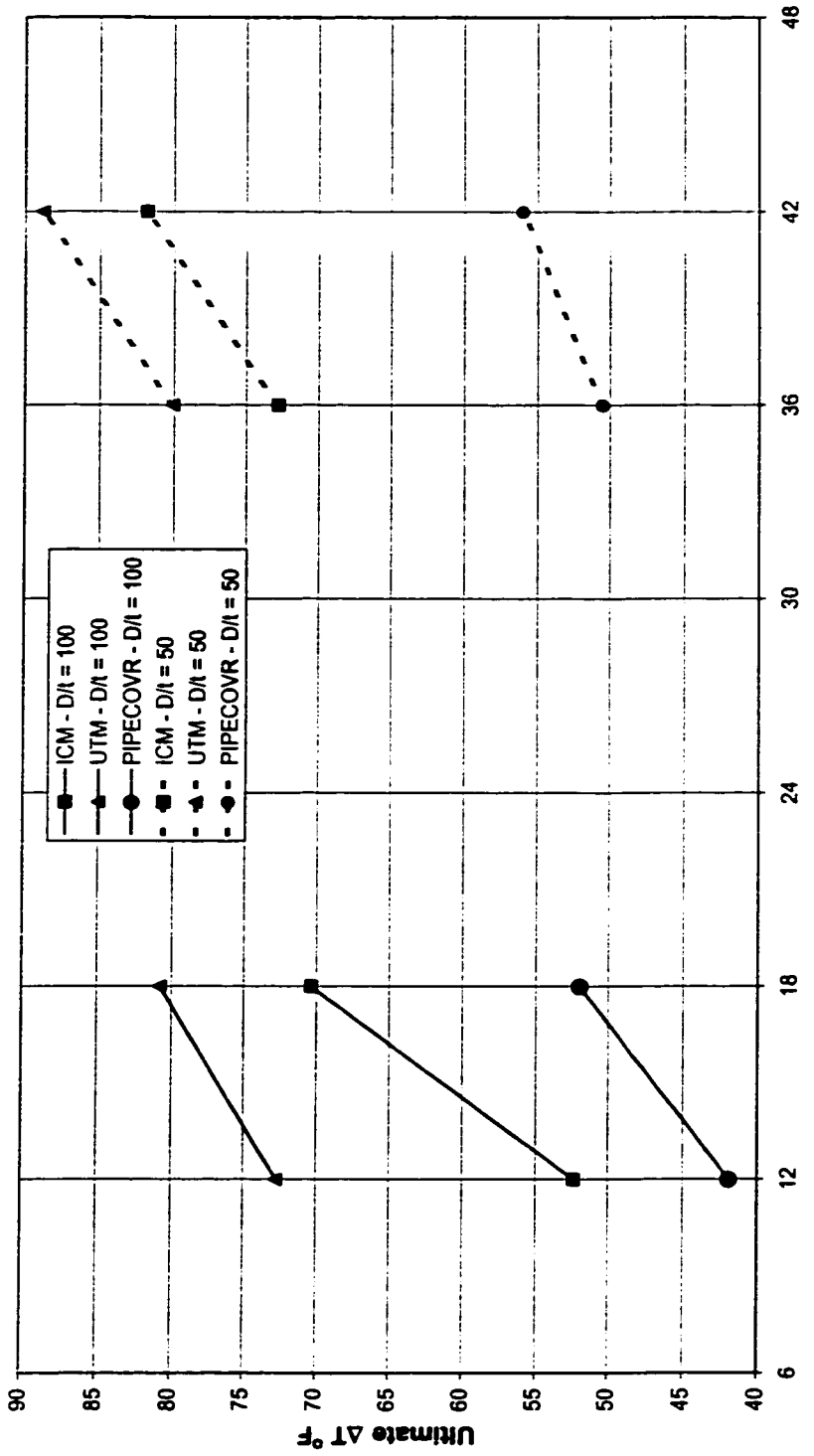

(i) R_b = 700 ft, θ = 20°, D = 60 in

Figure 5-7 (Contd.)

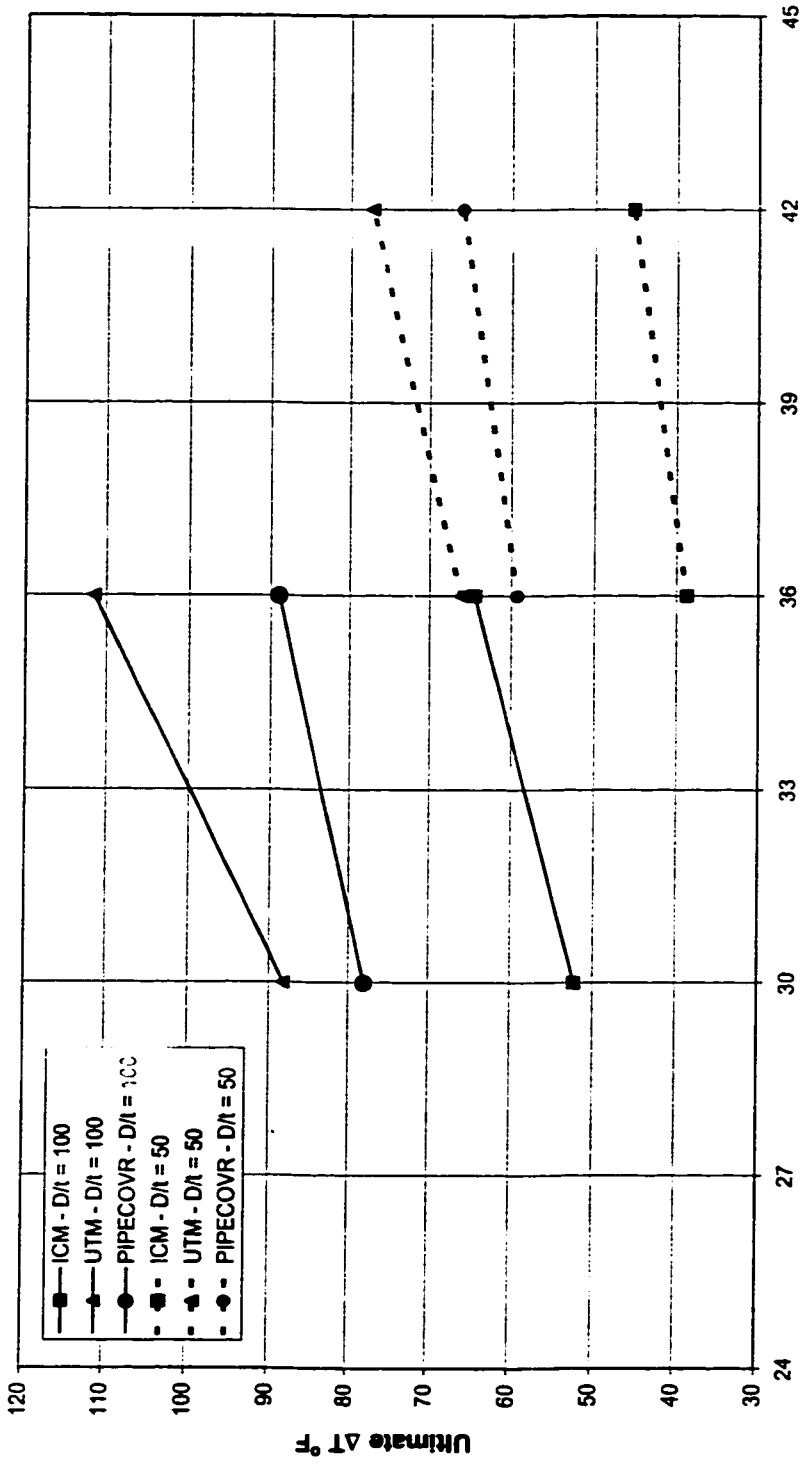

(j) R_b = 50 ft, θ = 8°, D = 24 in

Figure 5-7 (Contd.)

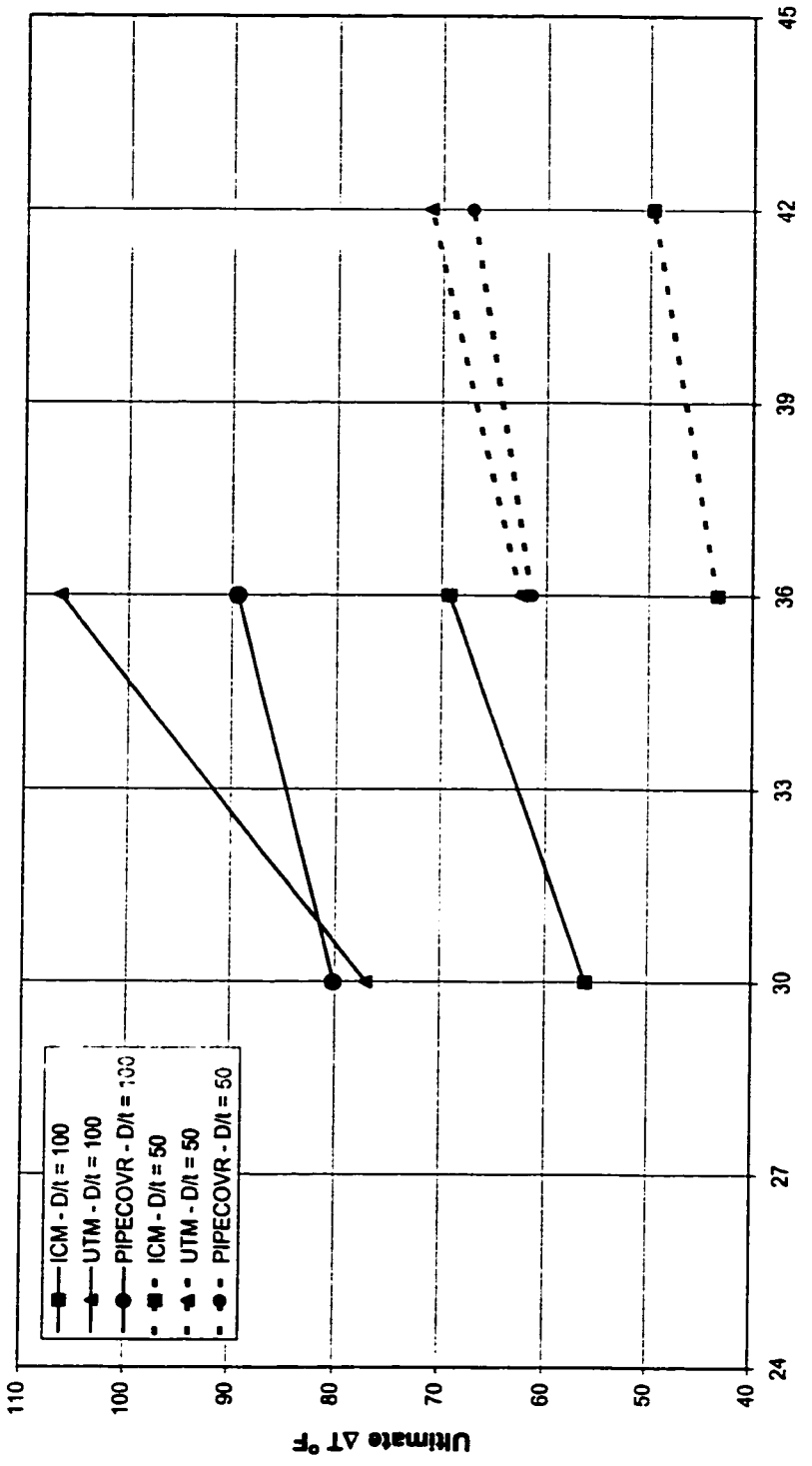

(k) R_b = 50 ft, θ = 8°, D = 42 in

Figure 5-7 (Contd.)

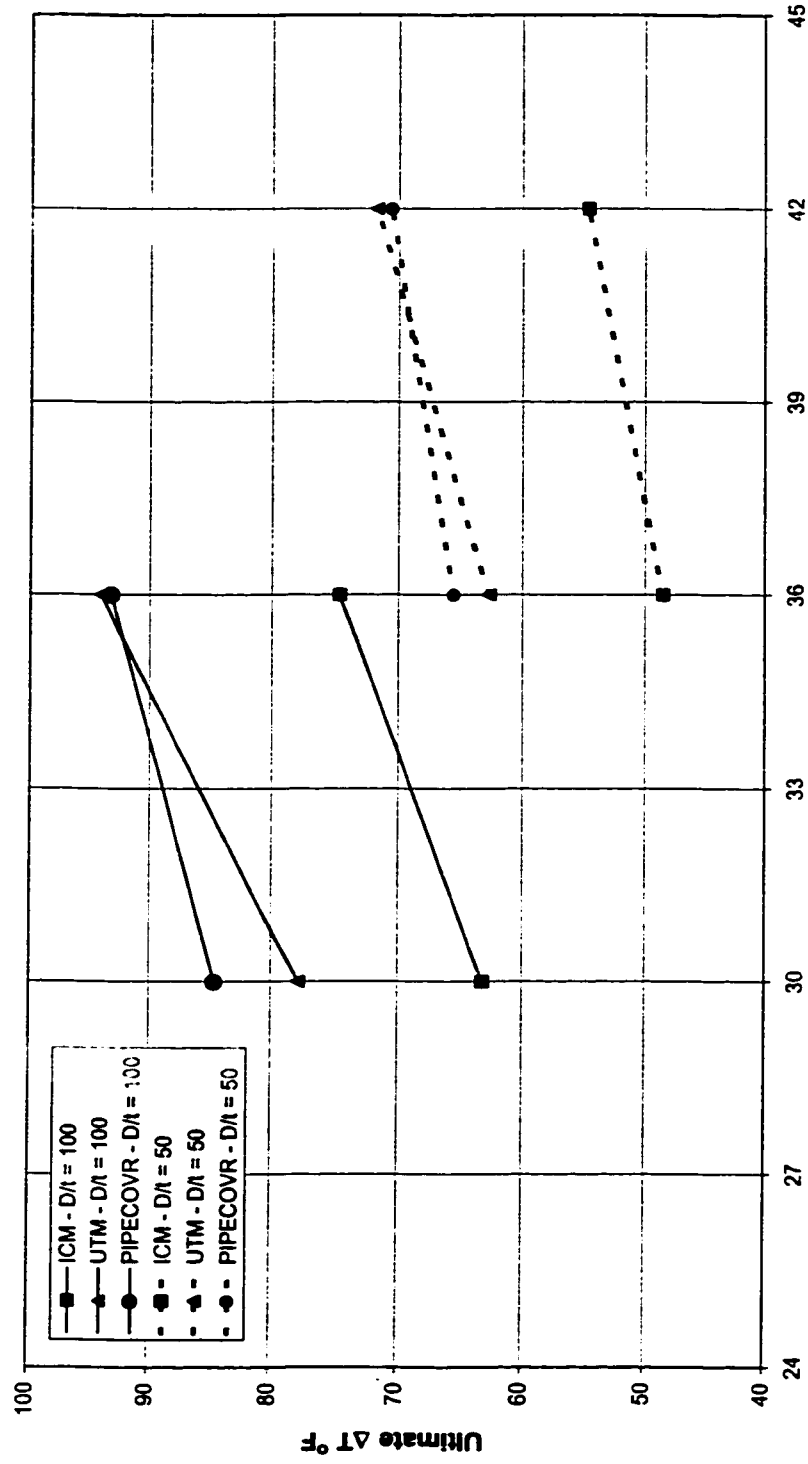

(l) R_b = 50 ft, θ = 8°, D = 60 in

Figure 5-7 (Contd.)

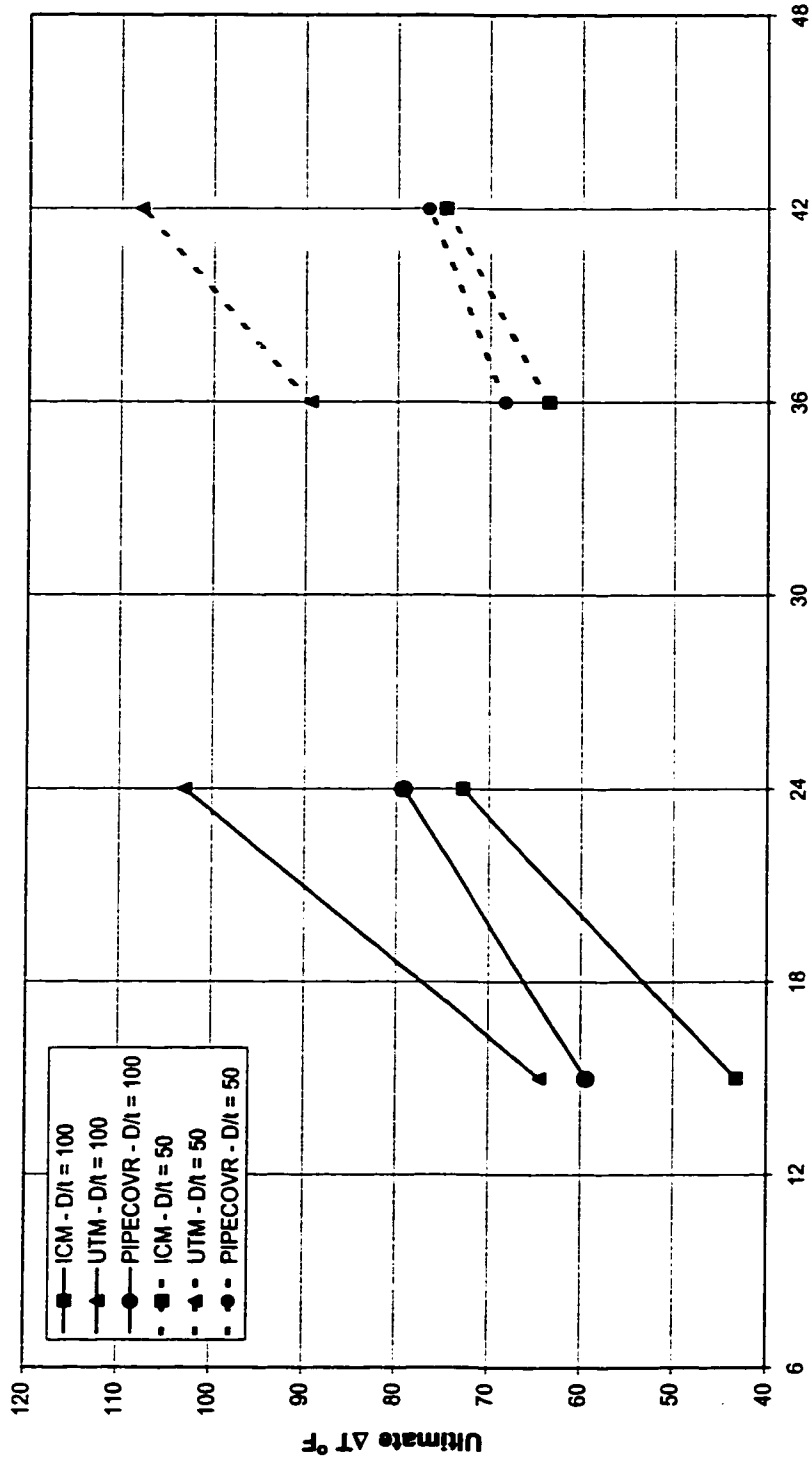

(m) R_h = 300 ft, θ = 8°, D = 24 in

Figure 5-7 (Contd.)

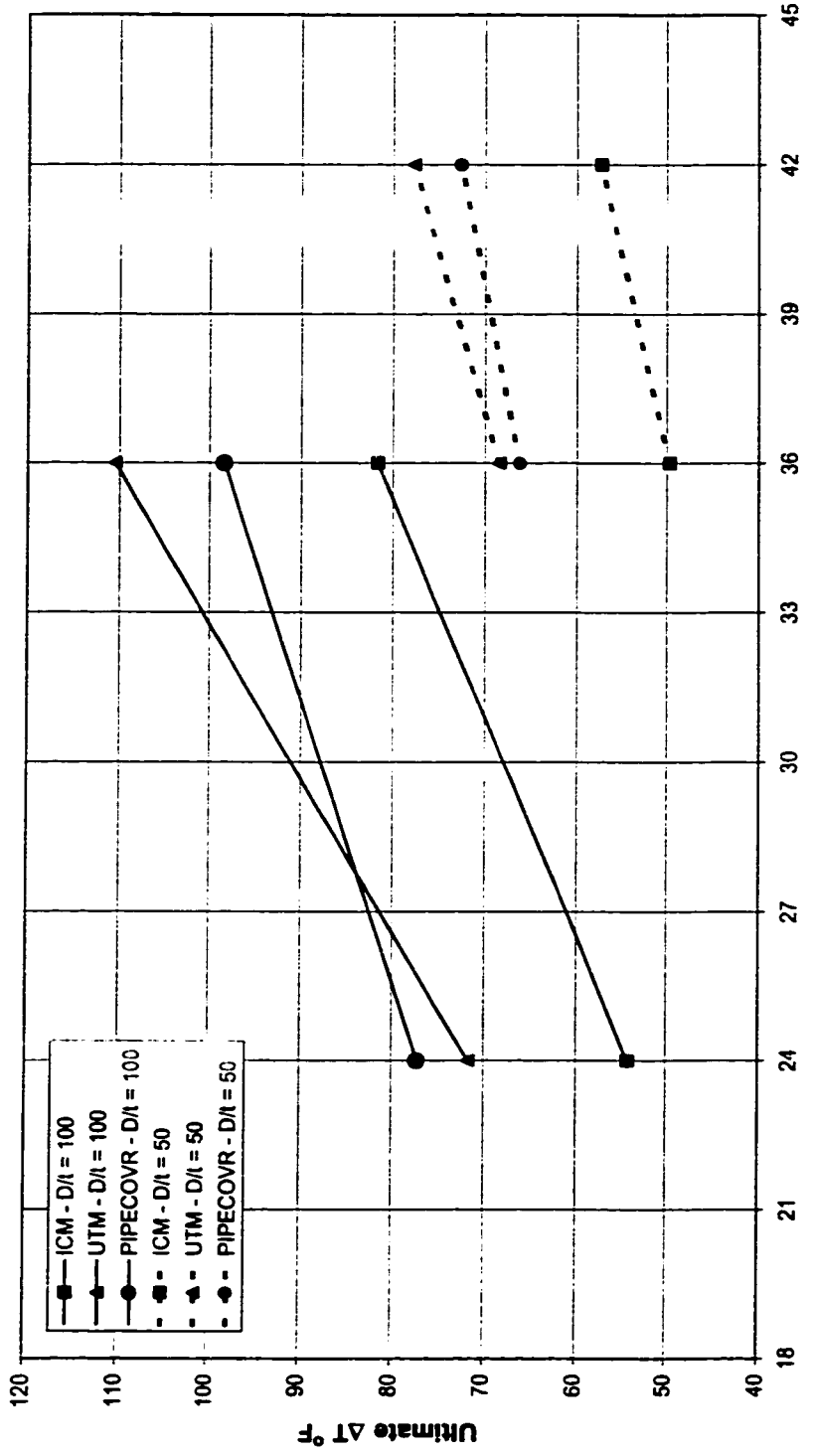

(ii) R_b = 300 ft, $\theta = 8^\circ$, D = 42 in

Figure 5-7 (Contd.)

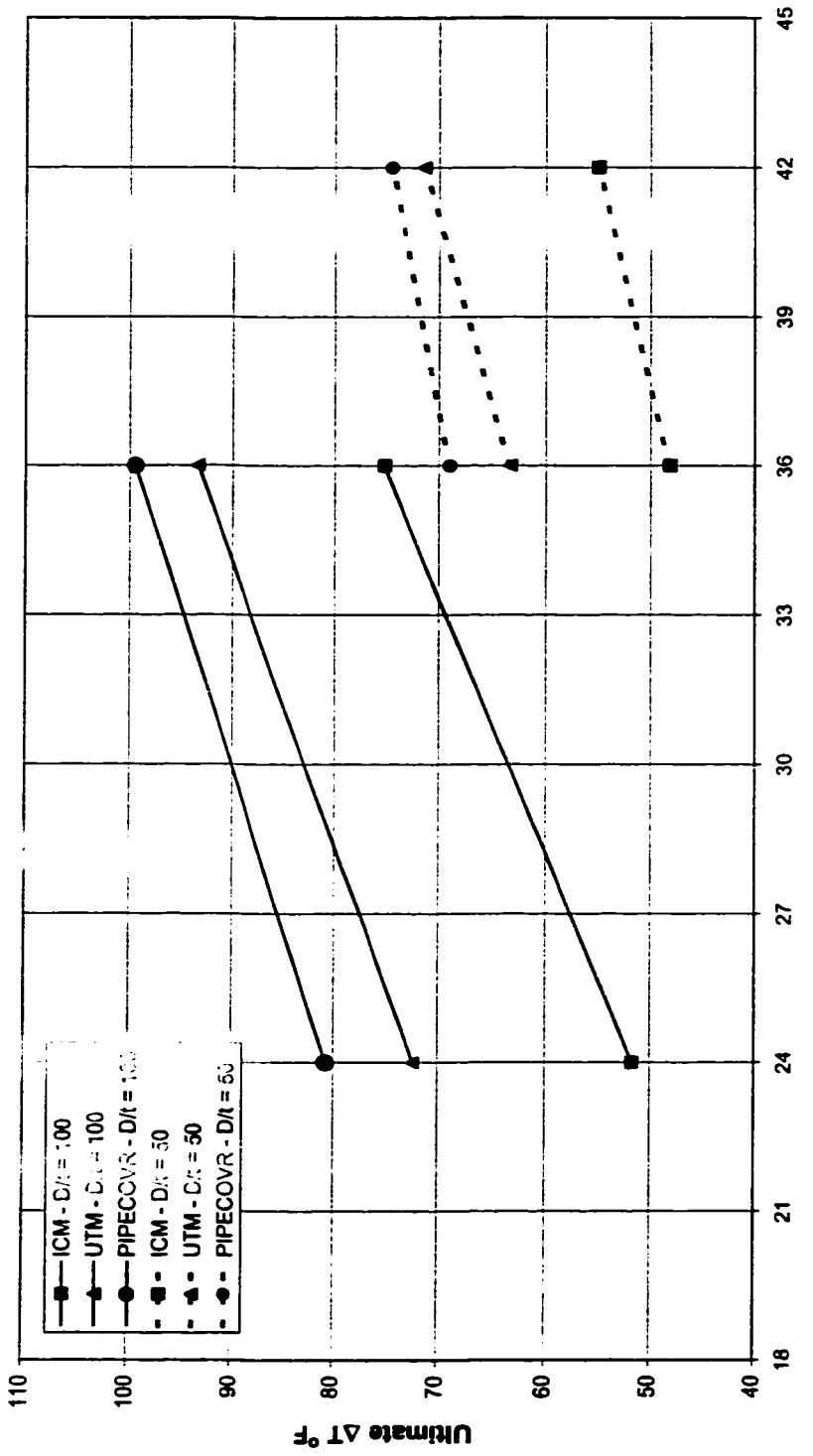

(o) R_b = 300 ft, θ = 8°, D = 60 in

Figure 5-7 (Contd.)

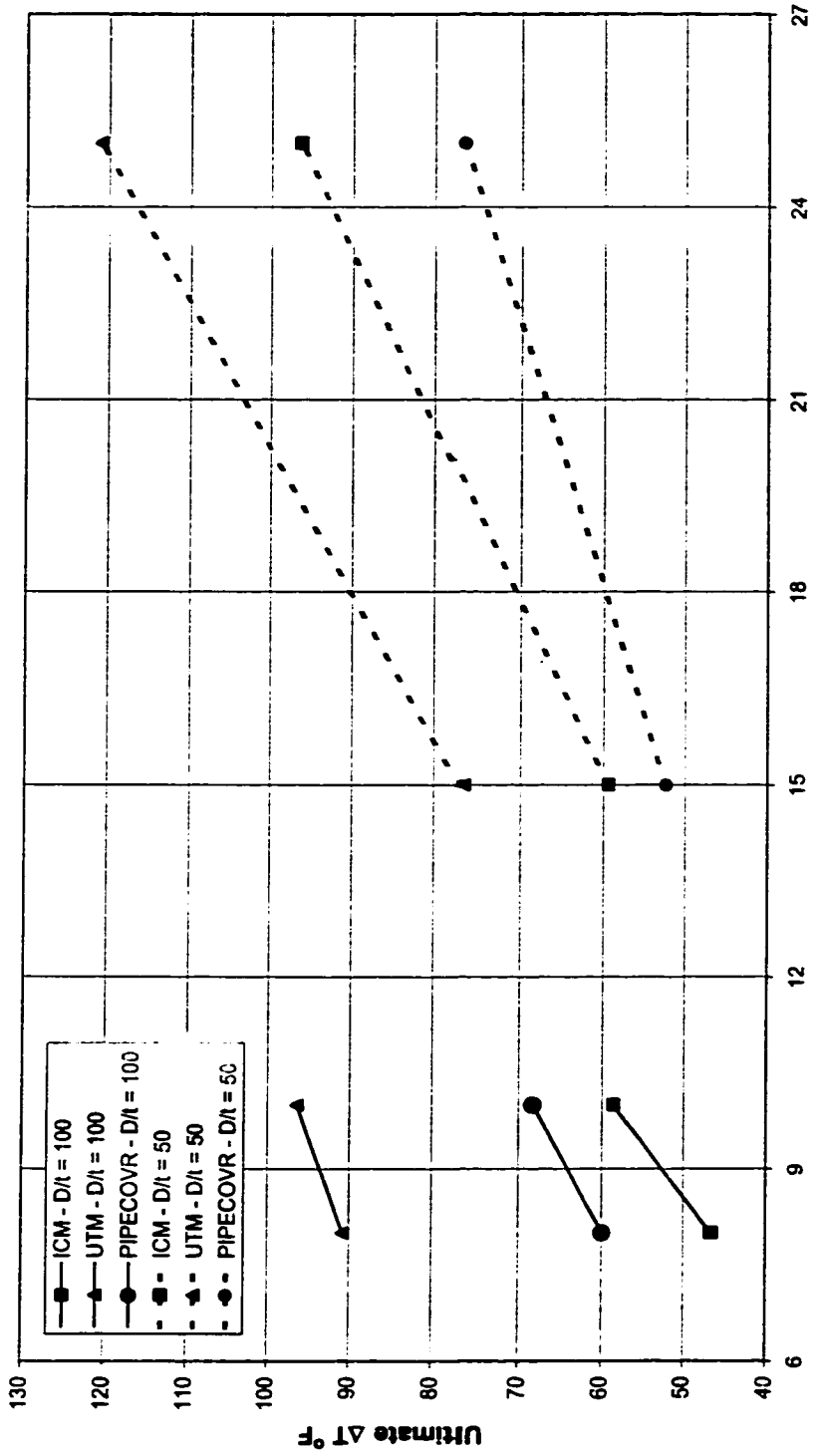

(p) R_b = 700 ft, θ = 8°, D = 24 in

Figure 5-7 (Contd.)

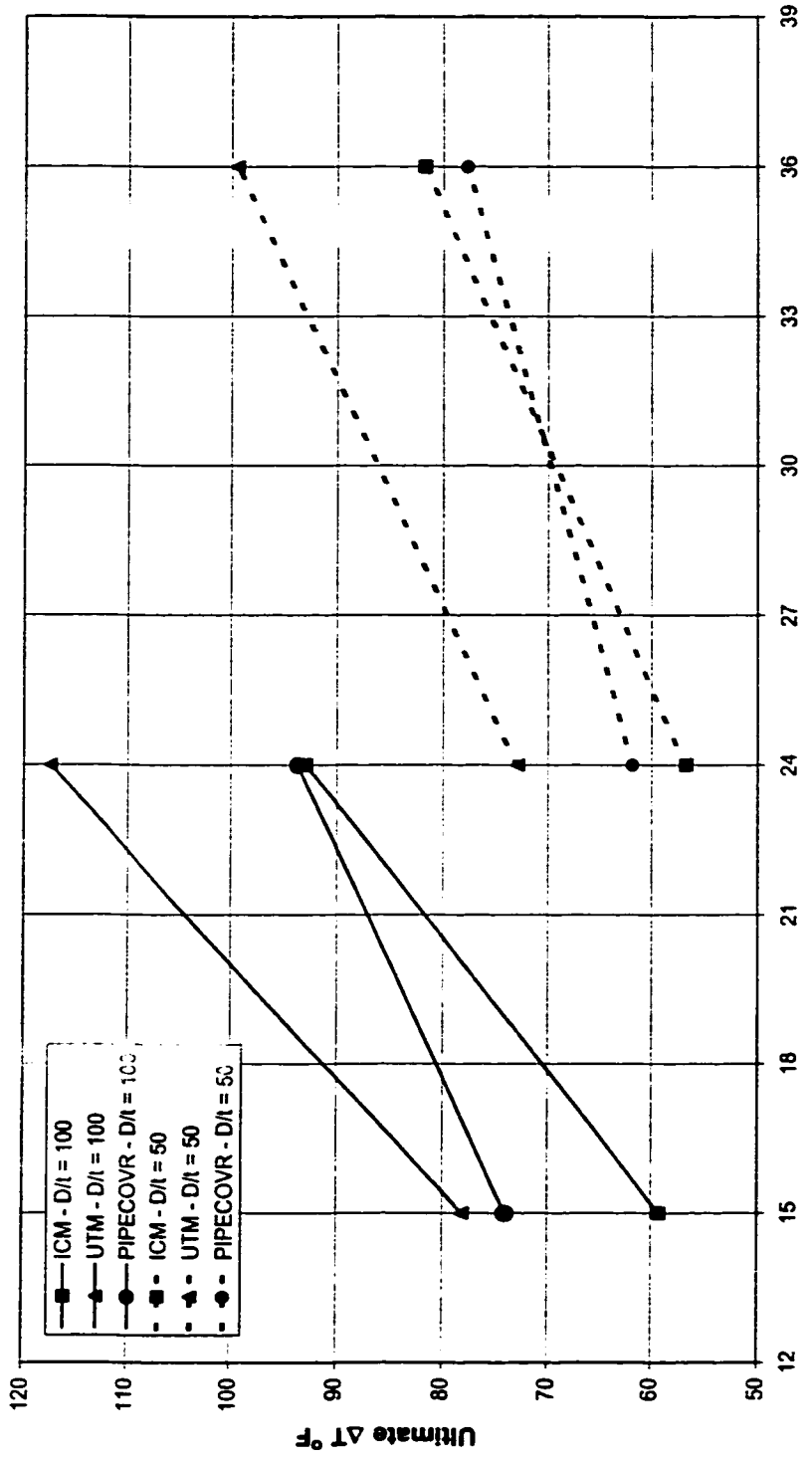

(q) R_b = 700 ft, θ = 8°, D = 42 in

Figure 5-7 (Contd.)

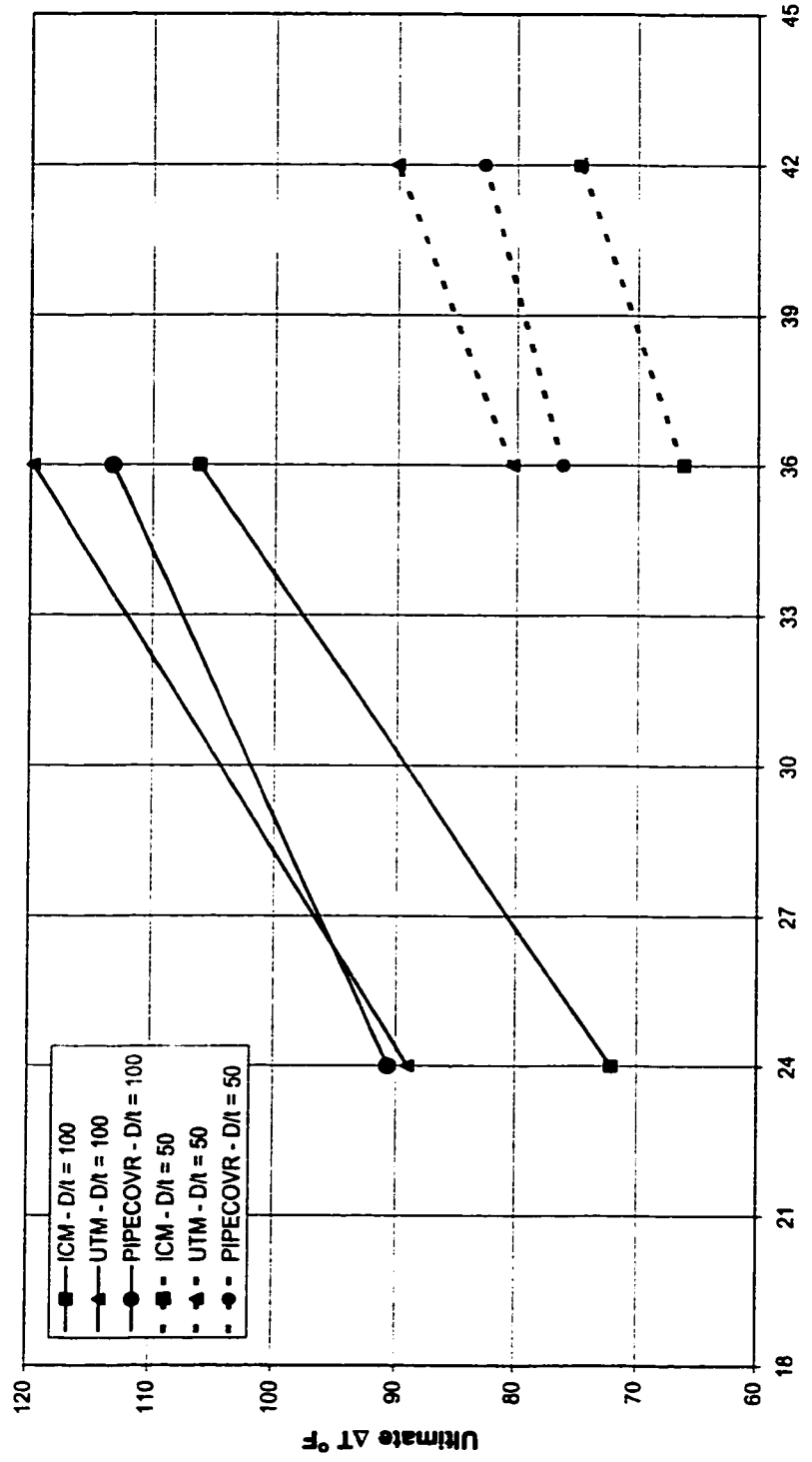

(r) R_b = 700 ft, θ = 8°, D = 60 in

Figure 5-7 (Contd.)

However, the values of the ultimate ΔT are higher for the smaller D/t ratios, showing that the reduction in the wall thickness of the buried pipe vertical bend increases its capacity against the temperature increase. The axial force induced in a pipe due to a temperature change is proportional to its cross-sectional area. The cross-sectional area of the pipe is reduced with the reduction in its thickness, which results in the reduction of the pipeline longitudinal force to be resisted by the soil cover. This is the reason why the values of the ultimate ΔT are higher for the smaller D/t ratios. The PIPECOVR results agree well with the results of this study for the bends with the small bend circumferential length. A similar agreement is observed with the results of D/t = 50. In the case of large bend angle, the PIPECOVR results for D/t = 100 are slightly on the unconservative side, as compared to ICM and UTM, for bends with small radius and large pipe diameter. However, in the case of small angle bends, this phenomenon is apparent for the whole range of bend radius.

5.2.4 Effects of pipe internal pressure and weight of pipe contents

Some runs are performed to study the effect of the pipe internal pressure and the weight of the pipe contents on the capacity of buried pipe vertical bends against temperature change. The results of these runs are listed in Table 5-5, and are also plotted in Figures 5-8 and 5-9. The pressure thrust developed at the bend augments the uplift caused by the change of temperature. However the Poisson's effect of the internal pressure reduces the longitudinal force developed by the temperature increase. Figure 5-8 shows a reduction in the values of the ultimate ΔT with the

Table 5-5 Vertical bend runs to study the effects of p and G_f
(D = 60 in, D/t = 50, H_c = 36 in)

S. No.	Pressure (psi)	Fluid Sp. Gravity	R_b (ft)	θ (Degrees)	Ultimate Temperature °F		
					Installation Condition Method	Ultimate Temperature Method	PIPECOVR
1	1100	0	700	20	52.67	57.97	25.2
2	625	0	700	20	62.15	66.11	37.8
3	150	0	700	20	72.79	80.05	50.4
4	1100	0	50	8	22.83	43.97	40.2
5	625	0	50	8	35.64	54.05	52.8
6	150	0	50	8	48.5	62.57	65.4
7	150	0.56	700	20	83.25	89.05	60.8
8	150	1	700	20	92.37	97.45	69.3
9	150	1	50	8	61.13	77.6	81.8

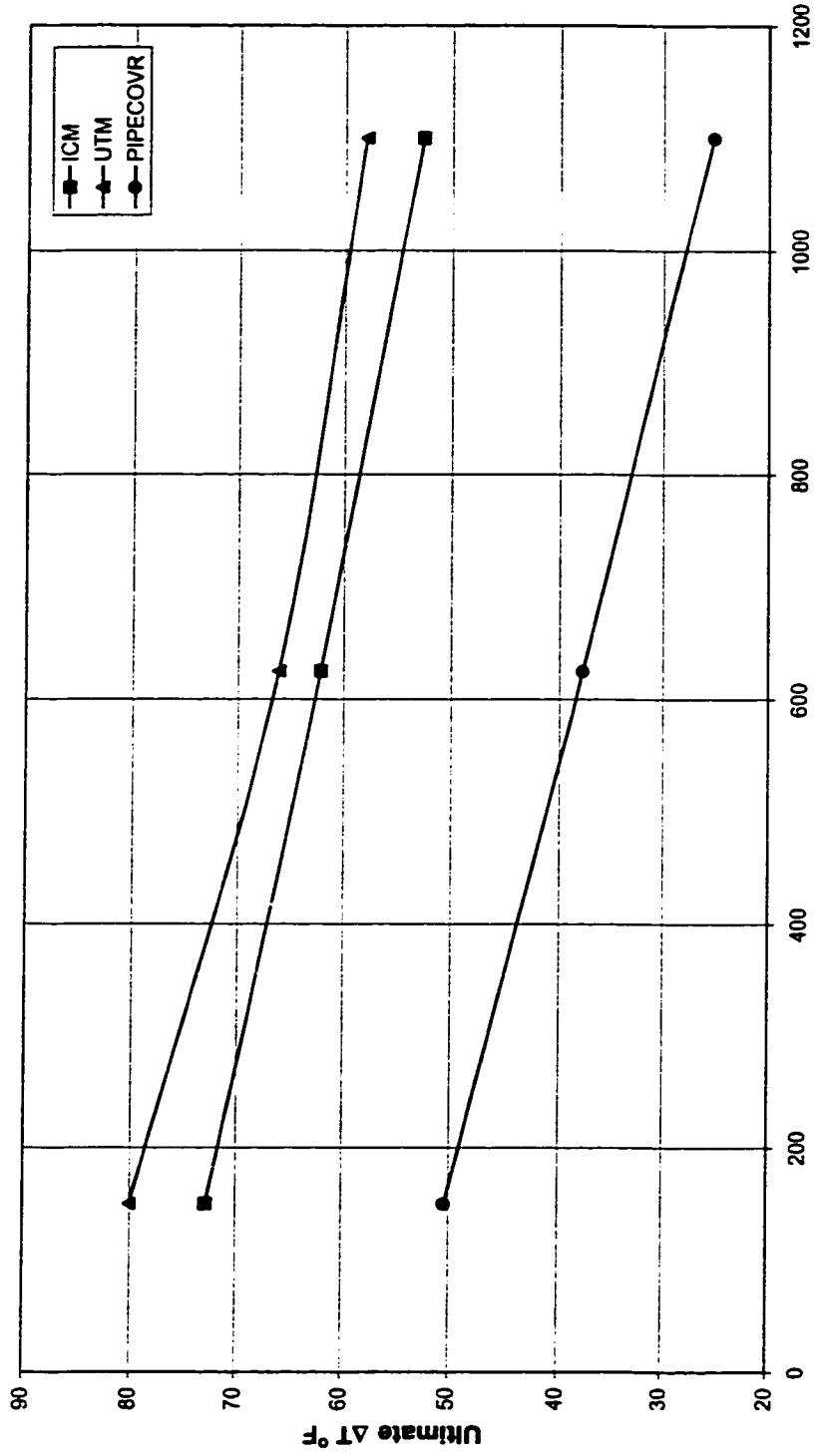

(a) R_b = 700 ft, θ = 20°, D = 60 in, H = 36 in, G_f=0

Figure 5-8 The effect of the pipe internal pressure on the value of the ultimate ΔT for the vertical bends

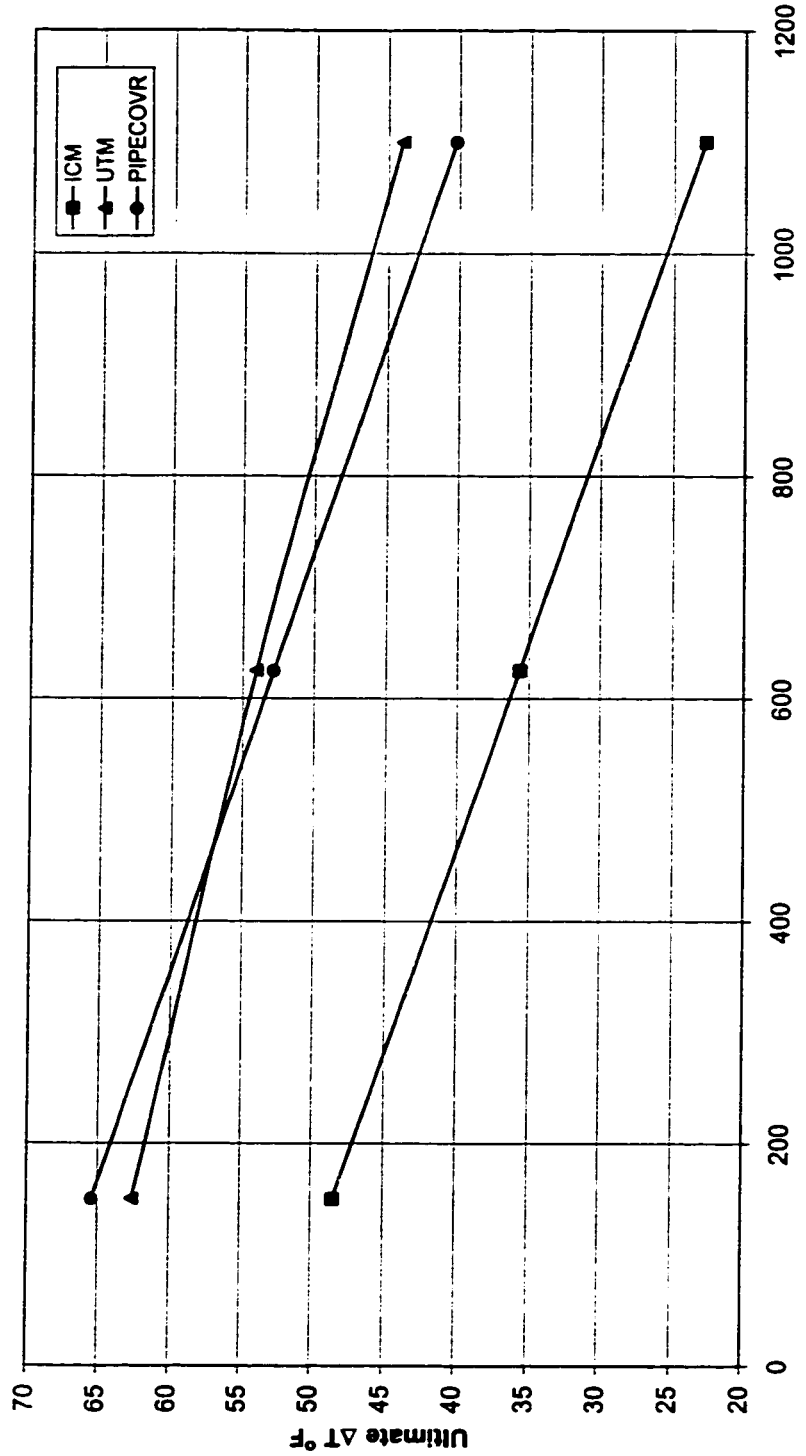

(b) R_b = 50 ft, θ = 8°, D = 60 in, H = 36 in, G_f=0

Figure 5-8 (Contd.)

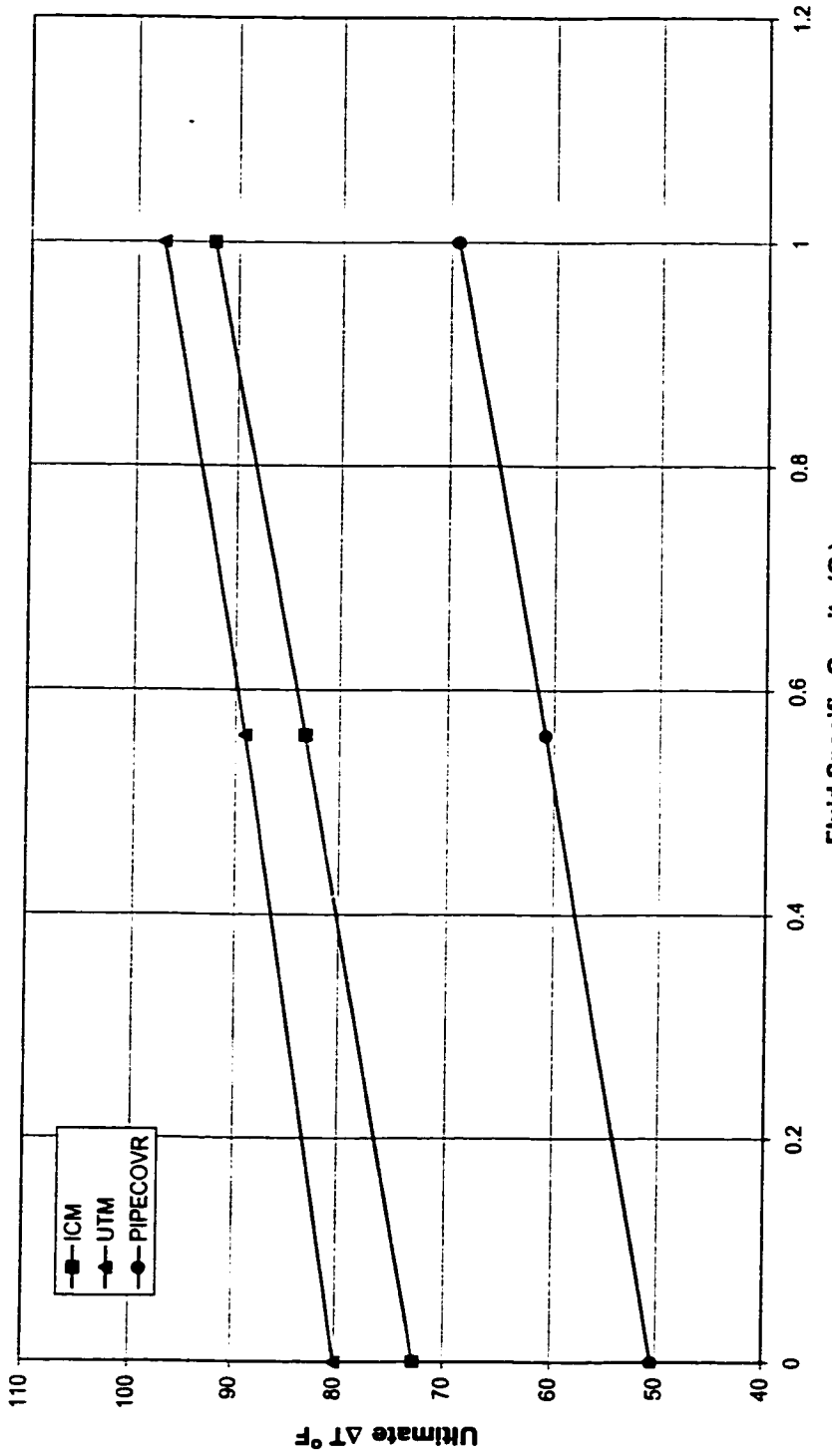

(a) R_b = 700 ft, θ = 20°, D = 60 in, H = 36 in, p = 150 psi

Figure 5-9 The effect of the pipe contents weight on the value of the ultimate ΔT for the vertical bends

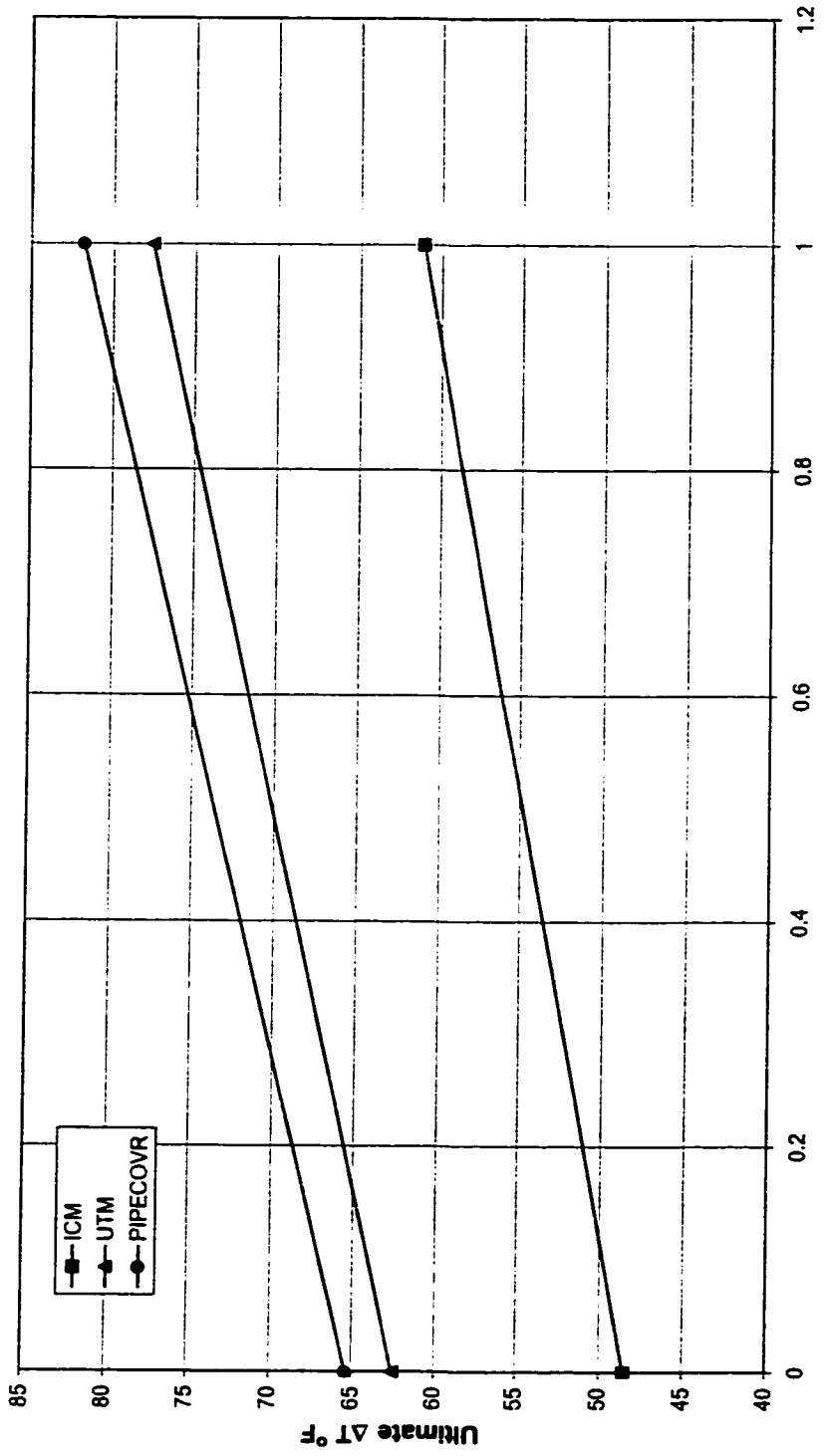

(b) R_b = 50 ft, θ = 8°, D = 60 in, H = 36 in, p = 150 psi

Figure 5-9 (Contd.)

increase in the pipe internal pressure, which demonstrates that the pressure thrust is more dominant as compared to the Poisson's effect of internal pressure. On the other hand, the weight of the pipe contents counteracts the uplift of the pipe bend and that is why Figure 5-9 shows an increase in the values of the ultimate ΔT with the increase in the fluid weight.

It can be observed that in both the cases of the pipe internal pressure and the weight of the pipe contents, the curves are almost linear. Once again, the results of the smaller radius bend as obtained by the PIPECOVR program lie closer to the FEM results as compared to the larger bend results. The PIPECOVR program results for the larger radius bend lie considerably lower than the FEM values showing that PIPECOVR produces conservative results for large radius vertical bends. In the case of small radius bends, the PIPECOVR results are quite close, however, they are on the unconservative side as compared to ICM and UTM.

5.3 Horizontal Bend Analysis

The SMAP-3D model for a buried pipe horizontal bend is loaded in a similar way as the vertical bend. The gravity load is applied in the first five load steps along with the pipe internal pressure. Then, the temperature increase in the shell elements takes place. The apex of the pipe bend extradose is the location where the effect of the temperature is most prominent. The apex moves along an oblique path as shown in

Figure 5-10(a). Typical plots of the horizontal and vertical components of the apex movement obtained by the FEM analysis are shown in Figure 5-10(b & c).

As the gravity load acts, the pipe deforms into an elliptical shape such that the pipe dimension between the springlines increases. The pressure further increases the horizontal diameter of the pipe. The horizontal movement curve in Figure 5-10 thus shows a relatively small displacement within the gravity load steps. The horizontal movement starts to increase rapidly when the temperature load begins to be applied. The horizontal curve within temperature load steps has initially a steep slope, which decreases slowly as the temperature load is increased. The curve loses the slope rapidly when the soil reaches its passive strength. The extradose apex of the bend moves at a higher rate on further increase of the temperature. The vertical movement curve, on the other hand, shows an appreciable downward movement in the gravity load steps as the pipe settles down under the soil and its own weight. The curve changes the slope as the pipe starts to move up, due to temperature increase. The vertical movement curve within the temperature load steps progresses in a similar way as the horizontal movement curve, except the magnitude of the vertical displacement is relatively small. The magnitude of the vertical movement at which the soil reaches its capacity is relatively larger for the case of horizontal bends as compared to the vertical bends. The reason is the higher confinement provided by the passive earth pressure at a horizontal bend.

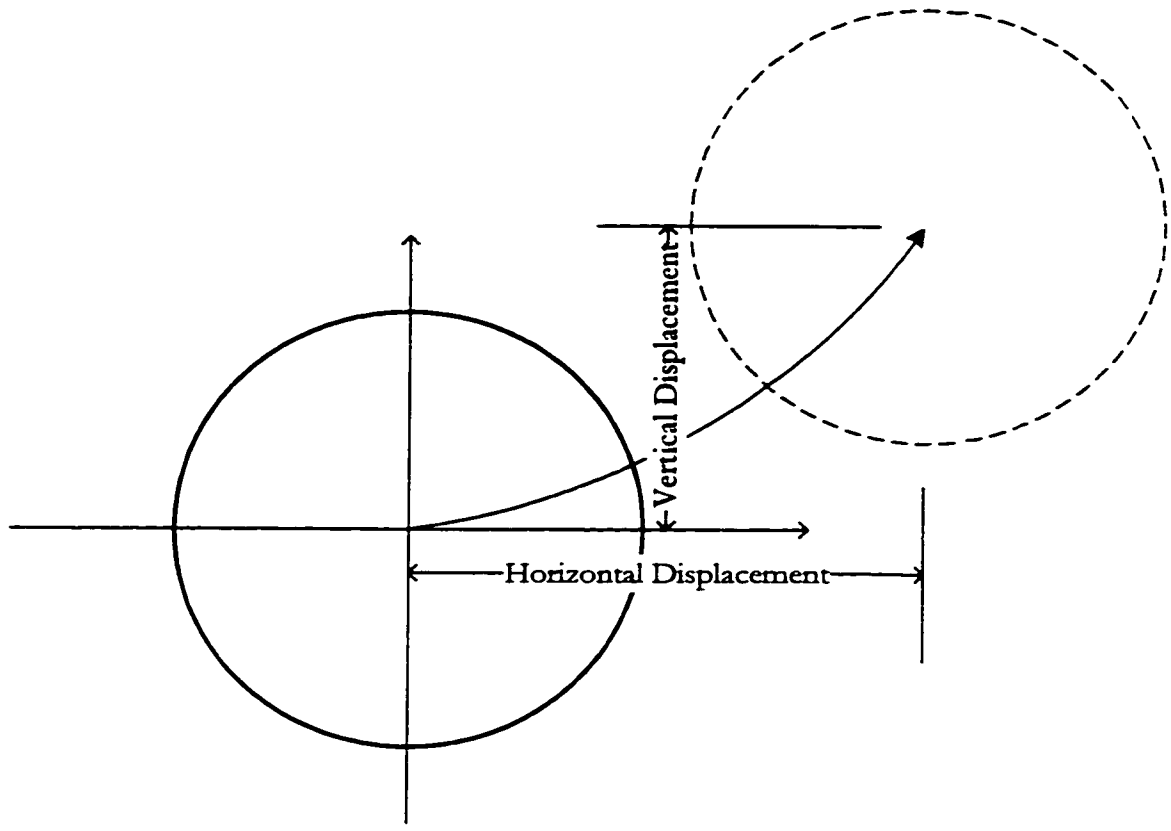

(a) The oblique movement can be resolved into vertical and horizontal components

Figure 5-10 The movement of a horizontal bend extradose apex obtained by the finite element analysis

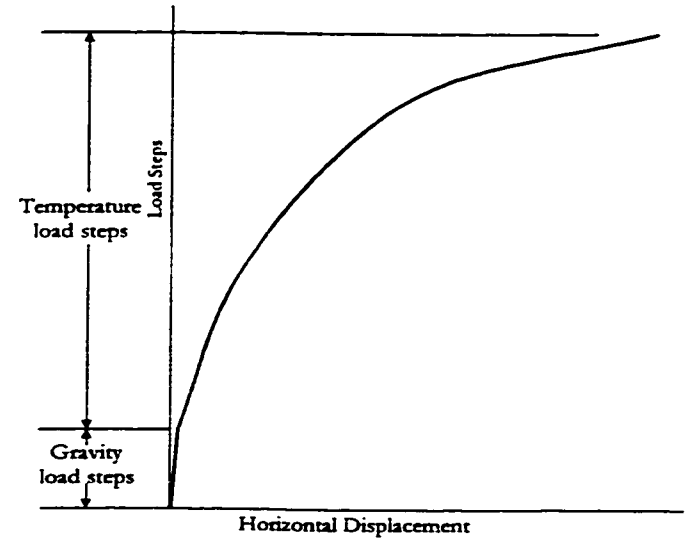

(b) Typical load-steps - horizontal displacement curve

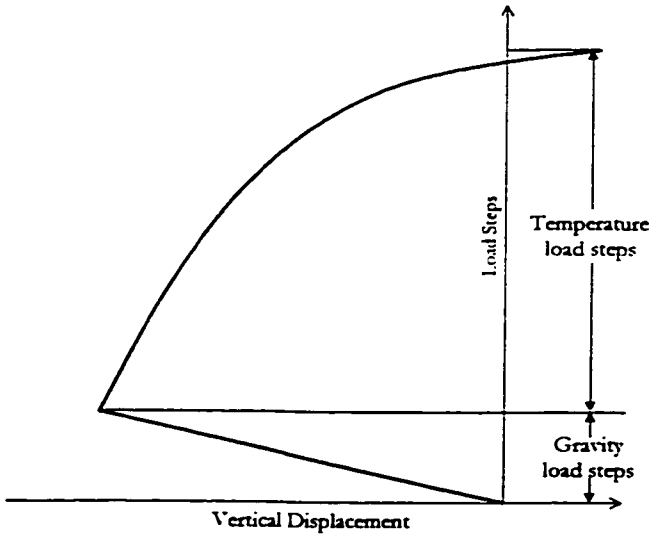

(c) Typical load-steps - vertical displacement curve

Figure 5-10 (Contd.)

Two criteria are considered for the buried pipe horizontal bend to define its capacity against the temperature change. The first method, which is based on the vertical movement of the bend apex and is called the *Installation Condition Method* (ICM), requires that the upward movement of the bend under the temperature change is restricted to the installation condition level, which is similar to how ICM was defined for the vertical bends. Therefore, according to the ICM, the allowed upward movement is equal to the settlement caused by the weight of the pipe and the soil cover. The capacity of the horizontal buried pipe bend against the temperature change can thus be calculated as shown in Figure 5-11. Note that the settlement of the mesh below the pipe under its own weight, calculated using Equation 5-1, is subtracted from the total settlement of the pipe bend extradose apex to get the allowed upward movement according to the method.

The other method is based on the horizontal movement of the bend apex and is called as the *Ultimate Temperature Method* (UTM). It defines the capacity as the point where the *temperature change – apex horizontal movement* curve attains a decreased slope, demonstrating that the soil has reached its passive strength due to the pipe horizontal movement. The change of the curve gradient from steep to flat is gradual and it is difficult to visually select a point at which the curve becomes flat. The procedure used to define a capacity point on the curve is shown in Figure 5-12. The displacement is plotted relative to the condition when the total gravity load is acting. A line is drawn parallel to the initial tangent modulus of the curve at an offset of 1.5% of H. The point at which this line intersects the curve is taken as the capacity.

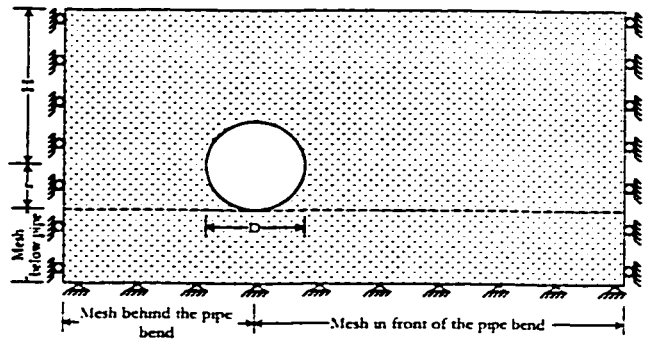

(a) The settlement of the mesh under its own weight below the pipe (dashed line) is subtracted from the total gravity load settlement

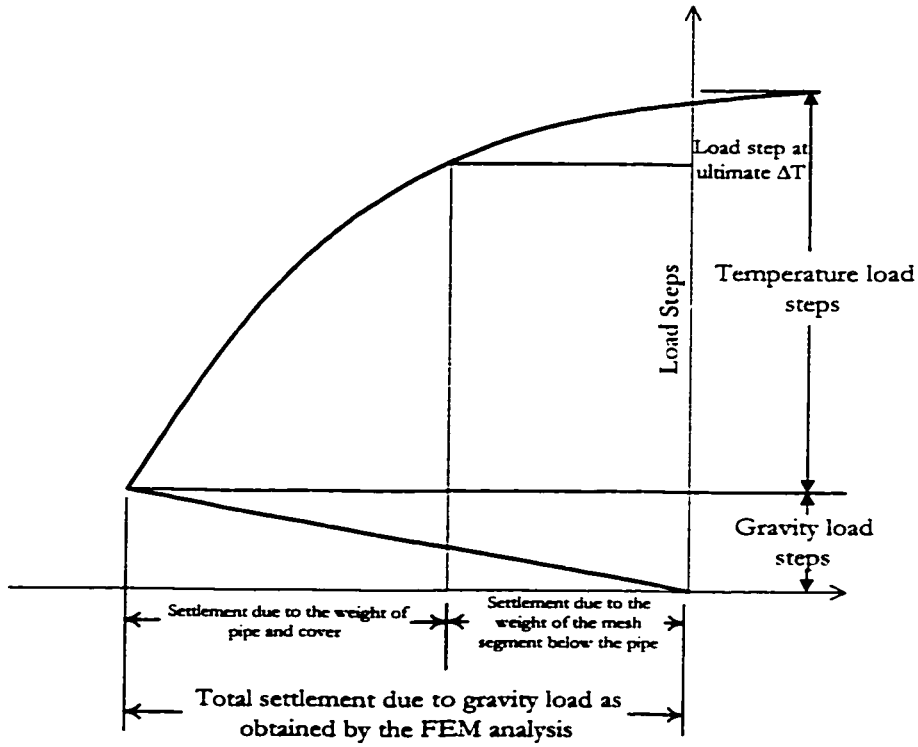

(b) Locating the capacity on the curve

Figure 5-11 Determination of the horizontal bend capacity against the temperature change using the Installation Condition Method

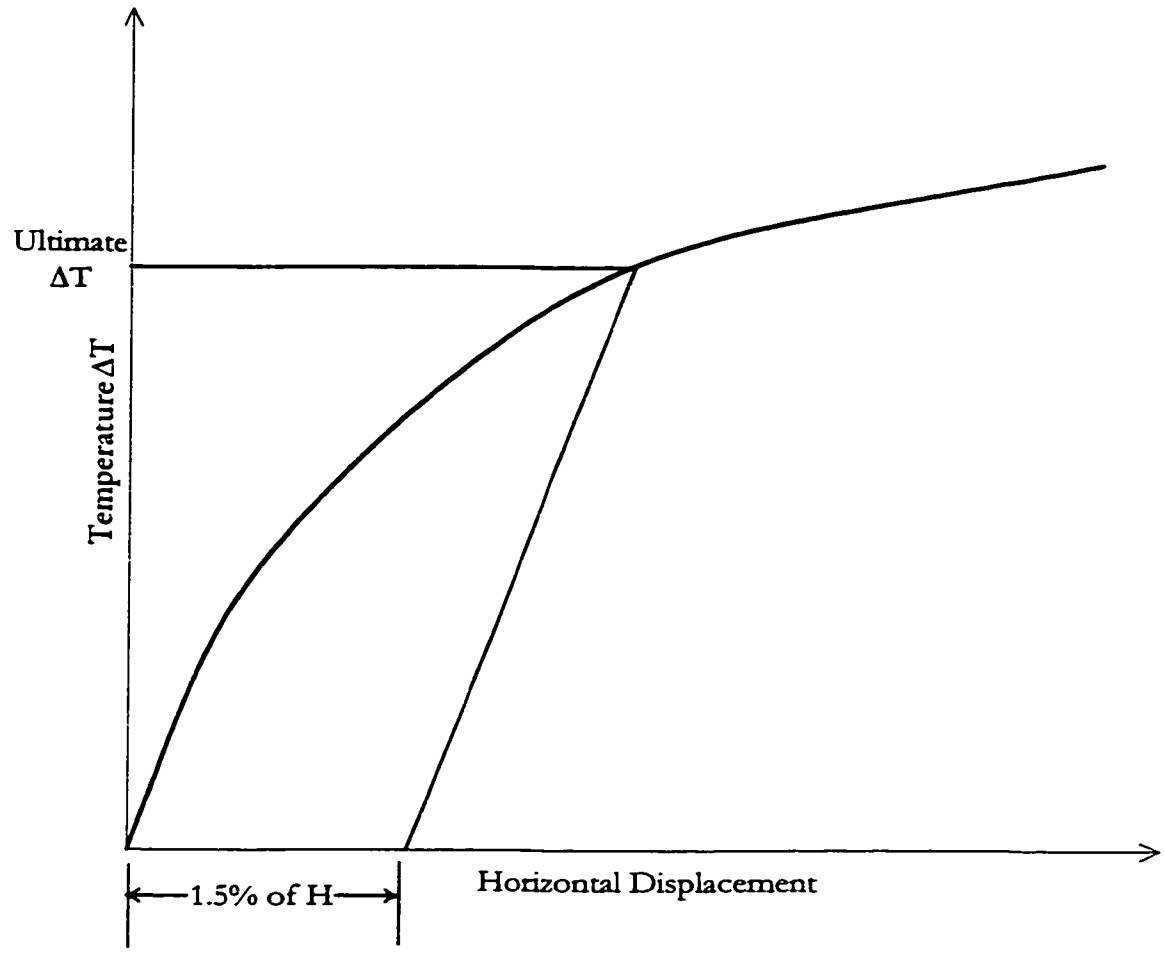

Figure 5-12 Determination of the horizontal bend capacity against the temperature change using the Ultimate Temperature Method

Note that the offset value used for the UTM in the case of the horizontal bend is much greater than that of the vertical bend. The vertical bend curve as obtained by the FEM analysis (Figure 5-3) stays almost linear before it changes the slope near the ultimate capacity point. The horizontal bend FEM analysis curve (Figure 5-12), on the other hand, changes its slope right from the beginning, requiring a larger value for the offset. The first method, i.e., ICM limits the vertical movement of the horizontal bend, while UTM is based on the passive strength of the surrounding soil at a horizontal bend.

5.3.1 Capacity against temperature change

A few runs were made to study the effect of the pipe diameter, cover height, bend radius and bend angle on the capacity of a buried pipe horizontal bend against temperature change. A summary of the results of these runs is shown in Table 5-6. SMAP-3D did not solve the problem of 90°-angle bend, giving a math overflow error during the solution of the third load step. SMAP-3D however solved problems with bend angles up to 89°, which shows that there is some singularity associated with the 90° problem. The cause of this problem could not be found.

The capacity is determined from the results of each run using each of the two methods, i.e., ICM and UTM. The maximum temperature increase specified in all the runs is 120°F. The bend system did not reach its capacity for some of the runs up to the specified maximum temperature increase, which shows that the specified cover is

Table 5-6 Horizontal bend runs to study the effects of D, H_c, R_b and θ

S. No.	Pipe Dia (in)	H (in)	R (ft)	θ (Degrees)	Ultimate Temperature °F		
					Installation Condition Method	Ultimate Temperature Method	PIPECOVR§ program
1	24	24	50	15	73.77	77.62	48.86
2	42	24	50	15	75.08	72.89	56.249
3	60	24	50	15	81.64	72.68	63.519
4	42	24	50	45	40.65	49.55	26.372
5	42	24	50	85	39.03	48.36	18.214
6	42	24	50	89	39.3	48.44	17.909
7	42	24	50	90	Not Solved	Not Solved	17.842
8	42	24	300	15	98.77	>120*	65.518
9	42	24	690	15	>120*	>120*	105.478
10	24	48	50	15	>120*	>120*	70.069
11	42	48	50	15	>120*	>120*	75.769
12	60	48	50	15	>120*	>120*	81.921

§ The temperatures are obtained by iterating PIPECOVR program to get the desired value of H_c. The PIPECOVR program does not give the calculated value of H_c if $H_c < 36$. In the case of $H_c < 36$ the temperature was found by the quadratic extrapolation.

* The bend system did not reach its capacity at the maximum specified temperature of 120°F

more than what is required for the temperature increase of 120°F. The ultimate ΔT value corresponding to each run is also calculated by the PIPECOVR program and is included in Table 5-6.

The runs, which yielded results, are plotted in Figures 5-13 to 5-15. The three plots show the effect of the pipe diameter, bend angle and bend radius, respectively. Among the results obtained by the two methods, ICM and UTM, some of the results of one method are larger and some are smaller than the results of the other one. The results of the two methods, however, happened to lie fairly close to each other. The curves of the bend angle and the bend radius corresponding to the PIPECOVR program follow a pattern similar to that of the FEM results. The pattern of the program curves for pipe diameter is, however, a little different. For the cases studied, the PIPECOVR curves lies fairly below the FEM curves, which illustrates that it is highly conservative in the case of horizontal pipe bends.

The FEM results show that the change in the pipe diameter does not have much effect on the bend capacity. The bend angle has an appreciable effect for values less than 45°. A larger radius of the bend results in an increase of the value of the temperature at which the bend reaches its capacity.

The maximum principle, longitudinal and hoop stresses corresponding to the ultimate ΔT, as given in Table 5-6, are listed in Tables B-1 to B-3. The values are the absolute maximum stresses that are developed anywhere in the modeled pipe. All

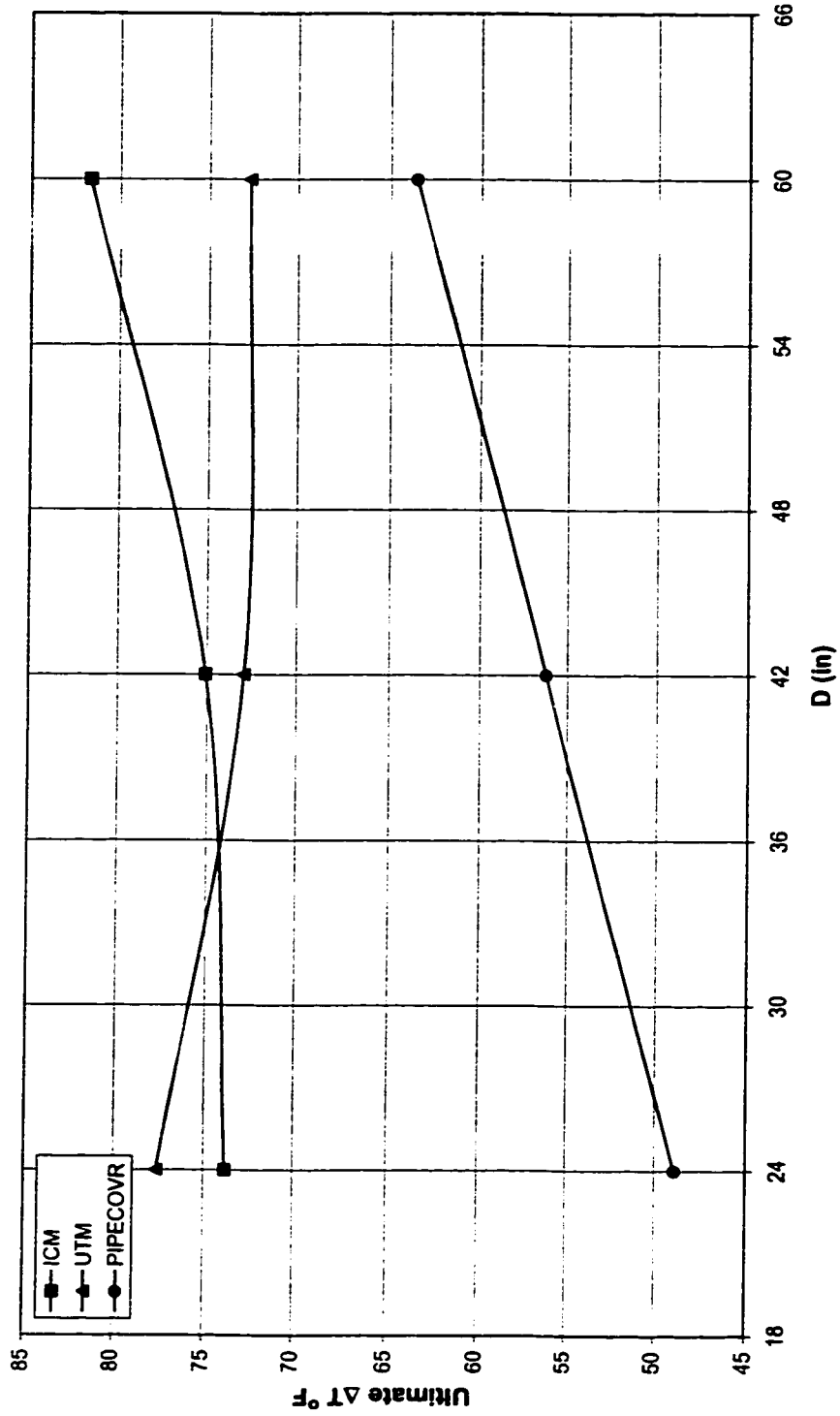

R_b = 50 ft, θ = 15°, H_c = 24 in

Figure 5-13 The effect of the pipe diameter on the value of the ultimate ΔT for the horizontal bends

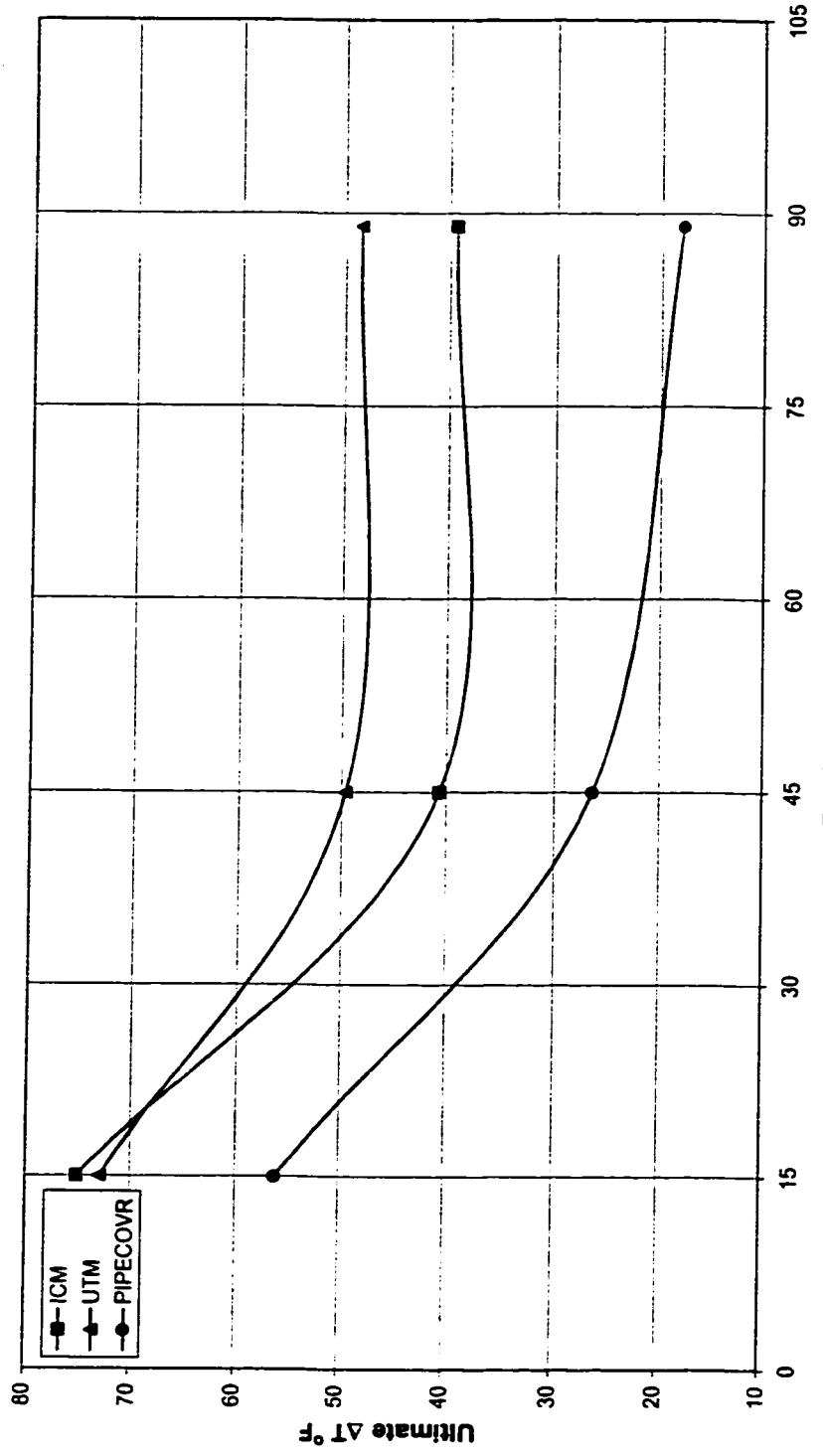

R_b = 50 ft, D = 42 in, H_c = 24 in

Figure 5-14 The effect of the bend angle on the value of the ultimate ΔT for the horizontal bends

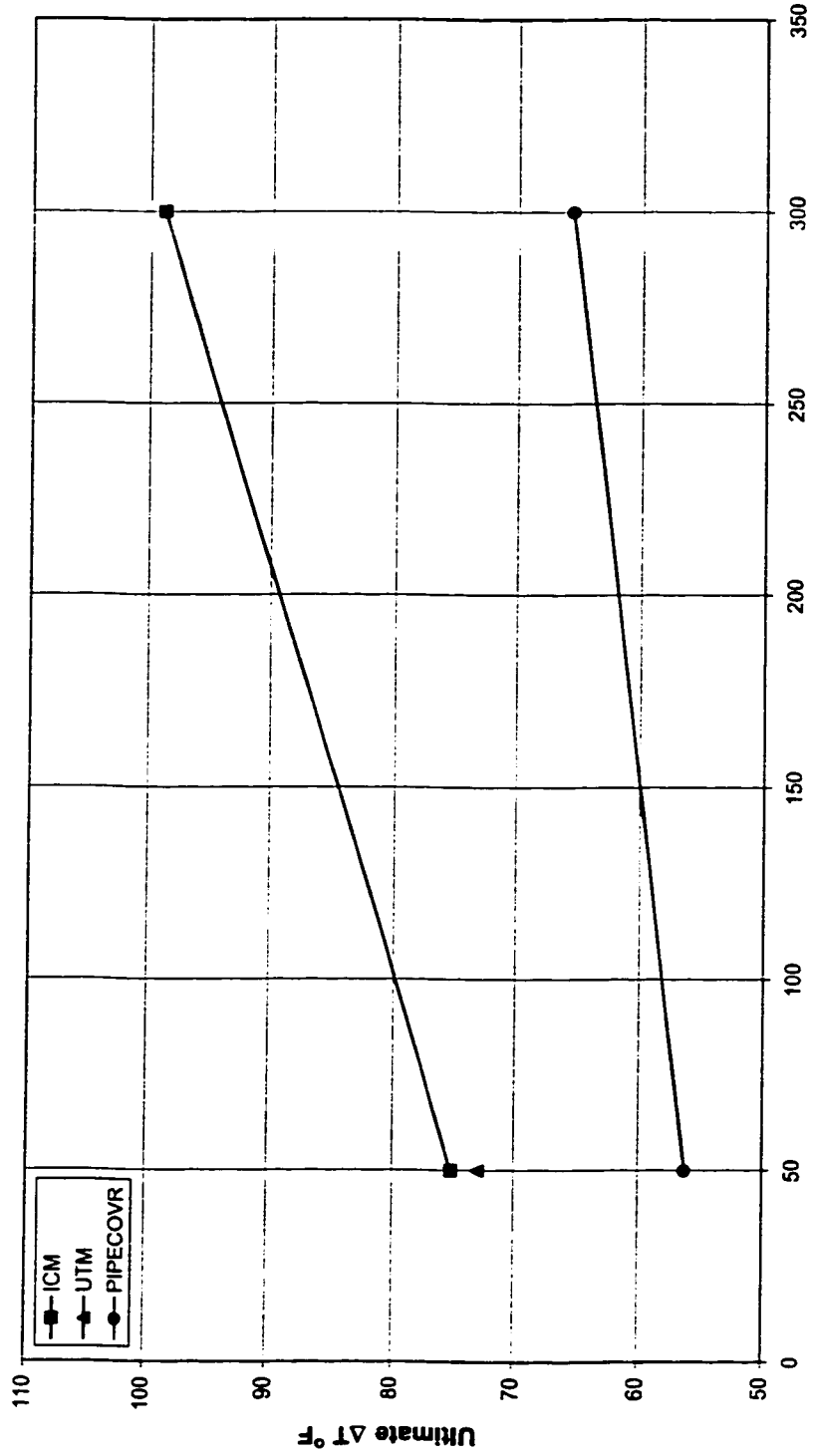

D = 42 in, θ = 15°, H_c = 24 in

Figure 5-15 The effect of the bend radius on the value of the ultimate ΔT for the horizontal bends

stresses found are less than the allowable stress value of 0.72 SMYS = 43,200 psi. The location of maximum stress shown in the Tables is specified according to the method as shown in Figure A-1, where Figure A-1(a) is assumed to be the plan view of the horizontal bend. This method uses two parameters. If the point of maximum stress lies within straight segment then the location (x) is measured from the virtual anchor. However if the point lies within the bend, then the location is measured as an angle (θ_x) from the radial line passing through the bend apex. The second parameter (α) gives the location on the circumference of the pipe cross-section.

CHAPTER 6
SUMMARY, CONCLUSIONS, AND RECOMMENDATIONS FOR FURTHER RESEARCH

6.1 Summary

The temperature change in a buried pipeline causes its bends to move in the transverse direction. This movement is resisted by the surrounding soil, and therefore a proper design of the soil cover is important for the integrity and serviceability of the pipelines.

The behavior of buried pipe bends under temperature change is investigated in this study. Three-dimensional continuum finite element analysis is carried out to study the behavior of buried pipe bends. The finite element program, SMAP-3D, is used for these analyses. The capability of SMAP-3D to model buried pipe bends could be validated for the isolated two-dimensional structural responses that exist along a buried pipe bend system. For this purpose SMAP-3D is compared with the data available in the well recognized published studies.

A number of finite element analyses are carried out to study the effects of various parameters on the buried pipe bends. The value of parameters is varied over a range

usually found in the cross-country buried pipelines. Two methods are considered to get the ultimate value of the temperature from the obtained FEM results. The installation condition method (ICM) requires the movement of the pipe to be restricted while the ultimate temperature method (UTM) is based on the strength of the soil. The results of a program named PIPECOVR are also compared with the results of this study. In addition, maximum pipe stresses and their locations are obtained.

6.2 Conclusions

The conclusions drawn related to the vertical bends are given below:

1) An increase in the cover height results in an increase in the capacity of the pipe bend against temperature change. The relation between the cover height and the ultimate ΔT is almost linear within the range of parameters investigated. The stresses developed at the ultimate ΔT increase with increasing cover height.

2) The cover height requirement increases as the diameter of the pipe increases in most of the cases. The bends with smaller diameter pipes, therefore, reach their capacity at a greater temperature change.

3) In the case of smaller radius bends, the required cover height increases with an increase in the bend angle. The effect of the bend angle is, however, not significant in the case of large radius bends.

4) The cover height requirement decreases as the radius of the bend increases. The larger bend radius provides a larger bearing area for the pipe bend against the soil. Therefore, the cover height requirement decreases as the radius of bend is increased, while the sharp bends require larger cover heights.

5) Buried pipe bends with larger D/t ratios have greater values for the ultimate ΔT. A larger value of D/t indicates a smaller pipe wall thickness and a smaller pipe cross-sectional area. The longitudinal force developed due to the temperature change is proportional to the pipe cross-sectional area. The cover height requirement therefore decreases as the value of D/t increases.

6) The internal pressure increases the uplift movement of the pipe bend caused by the temperature change. The value of the ultimate ΔT decreases as the pipe internal pressure increases.

7) The weight of the fluid inside the pipe acts against the uplift movement, and therefore increases the bend capacity against the temperature change.

8) In general, the results obtained by UTM are greater in values than those obtained by ICM. The difference in the results is the highest for smallest pipe diameters, and is also affected by the pipe bend radius.

9) The results of the program PIPECOVR agreed well for the bends with small radius. In some of these cases of small radius bends, the values given by the program are found to be in between the values obtained by ICM and UTM, which shows a close agreement. In some other cases of small radius bends with large pipe diameter the PIPECOVR program results are found to be slightly on the unconservative side as compared to ICM and UTM. The program should, therefore, be used cautiously for vertical bends having small radius bends and large pipe diameter. The program, however, gives conservative results for the bends having large radius and large bend angle. In such cases the difference between the program and FEM results increases as the pipe diameter decreases.

10) The pipe stresses do not exceed the value 0.72 SMYS = 43200 psi in most of the cases, except for a few ones of large radius bends with cover height less than 36 in. In such cases, pipe stresses controls and soil cover stability is not a problem. The stress criterion is usually checked during the normal pipe design procedure/practice, which is not part of this particular study. However this is worthwhile to mention that at least a minimum cover depth, H_c, of 36 in for gas and 24 in for oil and water pipelines is usually used in

practice. The cover depth was less than these minimum cover depths for the runs in which the stress is found to be greater than the allowable stress. Therefore, for normal buried pipe installations, stress criterion does not usually control.

11) The FEM analyses generally give a pipeline principal stress greater than the *total effective stress* (S_{eff}), calculated according to the method given in API-RP 1102 (1993). However, the difference is usually not large and in certain cases close agreement is also obtained.

The conclusions drawn related to the horizontal bends are given below:

1) The larger the cover height the more the capacity of the bend against the temperature change.

2) The finite element results show little effect of the change of the diameter on the capacity of the bend.

3) The bend angle has an appreciable effect on the capacity if it is less than 45°. For larger angles, the effect is much less.

4) The capacity of the bend increases as the radius of the bend increases.

5) The stresses in the pipe do not exceed 0.72 SMYS = 43200 psi for any of the runs carried out in this study.

6) The results of the two methods, ICM and UTM, were found to lie fairly close to each other.

7) The PIPECOVR program gives a noticeably increase in the value of ultimate ΔT as the pipe diameter increases and this pattern does not agree with the FEM results. This pattern is also opposite to what was observed in the case of vertical bends. The PIPECOVR program is considerably conservative in the case of horizontal buried pipe bends. Other more reliable methods should be considered for economical designing.

6.3 Recommendations

Although this research related to the buried pipe bends is extensive. There is still a lot of room to extend and improve the current study. Several options for further research are listed below.

1) No experimental study on the structural behavior of buried pipe bends is published to date. It is recommended that full scale or lab tests are carried out to study the structural behavior of buried pipe bends.

2) The significance of the two methods defined in this study, i.e., ICM and UTM requires further evaluation and more validation. Some tests can be performed for this purpose.

3) The large deformation and stability of the bend could not be modeled using the SMAP-3D program. It is advisable to check if the bend remains structurally stable before it reaches its capacity found by ICM or UTM.

4) This is only a guideline and foundation work on the subject. More runs are required to be performed, especially for the horizontal bends to further understand and quantify the capacity of buried pipe bends.

5) Investigating different soil types and trench conditions that generally exist in normal pipeline installation practice, can further increase the domain of the work.

6) In addition to circular vertical and horizontal bends, bends installed at an angle and compound bends can also be analyzed.

7) Regression models can be developed incorporating the effect of different parameters, which can be helpful in the analysis and design of buried pipe bends

8) This study assumes a uniform temperature through the wall of the pipe. The effects of variation of temperature through pipe wall thickness can be investigated in a similar way.

9) No previous significant work could be found on buried pipe bends. The comparison of this work with any other work can be helpful in further understanding the problem.

APPENDIX A

STRESSES IN THE VERTICAL BENDS

Table A-1 Maximum principal stresses corresponding to runs listed in Table 5-2

S. No.	D (in)	H_c (in)	R_b (ft)	θ (Degrees)	Maximum pipe principal stress (psi)					
					Installation Condition Method			Ultimate Temperature Method		
					Stress	x / θ_x	α	Stress	x / θ_x	α
1	24	36	50	20	6,470.65	10275 in	7.5°	11,277.32	124 in	-7.3°
2	24	42	50	20	7,774.68	123 in	-7.3°	13,810.26	123 in	-7.3°
3	24	60	50	20	10,671.61	122 in	-7.3°	17,641.44	122 in	-7.3°
4	42	36	50	20	7,021.97	5°	-8.1°	8,737.06	1.7°	-82.5°
5	42	42	50	20	7,883.88	5°	-8.1°	10,125.96	1.7°	-82.5°
6	42	60	50	20	12,189.12	215 in	-7.3°	16,275.45	215 in	-7.3°
7	60	36	50	20	8,782.35	5°	-7.9°	9,560.50	5°	-7.9°
8	60	42	50	20	9,943.34	5°	-7.9°	10,569.65	5°	-7.9°
9	60	60	50	20	12,443.01	5°	-7.9°	13,473.05	1.7°	-82.5°
10	24	36	300	20	26,168.20	124 in	-7.3°	31,389.67	124 in	-7.3°
11	24	42	300	20	30,967.46	123 in	-7.3°	37,220.68	123 in	-7.3°
12	24	60	300	20	Not Found			Not Found		
13	42	36	300	20	14,090.40	218 in	-7.3°	16,549.67	218 in	-7.3°
14	42	42	300	20	17,247.92	215 in	-7.3°	20,004.75	215 in	-7.3°
15	42	60	300	20	23,625.63	215 in	-7.3°	26,883.37	215 in	-7.3°
16	60	36	300	20	12,398.41	311 in	-7.3°	13,312.15	311 in	-7.3°
17	60	42	300	20	13,992.79	306 in	-7.3°	14,663.31	306 in	-7.3°
18	60	60	300	20	19,779.95	307 in	-7.3°	20,777.73	307 in	-7.3°
19	24	12	700	20	78,639.02	125 in	52.1°	81,006.13	7226 in	82.5°
20	24	21	700	20	28,200.89	122 in	-7.3°	40,917.00	122 in	-7.3°
21	24	36	700	20	Not Found			Not Found		
22	24	42	700	20	Not Found			Not Found		
23	24	60	700	20	Not Found			Not Found		
24	42	27	700	20	26,576.15	217 in	-7.3°	31,213.00	217 in	-7.3°
25	42	36	700	20	35,711.83	218 in	-7.3°	37,514.20	218 in	-7.3°
26	42	42	700	20	40,942.00	215 in	-7.3°	44,091.25	215 in	-7.3°
27	42	60	700	20	Not Found			Not Found		
28	60	36	700	20	26,067.81	311 in	-7.3°	26,822.31	311 in	-7.3°
29	60	42	700	20	29,309.71	306 in	-7.3°	30,175.00	306 in	-7.3°
30	60	60	700	20	40,953.15	307 in	-7.3°	41,978.20	307 in	-7.3°
31	24	36	50	15	6,988.68	1.9°	-68°	12,846.95	1.9°	-68°
32	24	42	50	15	8,446.31	1.9°	-68°	14,686.76	1.9°	-68°
33	24	60	50	15	12,560.30	1.9°	-68°	21,179.63	1.9°	-68°
34	42	36	50	15	7,479.43	1.3°	-82.4°	11,780.26	1.3°	-82.4°
35	42	42	50	15	9,255.18	1.3°	-82.4°	13,909.54	1.3°	-82.4°
36	42	60	50	15	13,770.63	3.8°	-82.4°	19,822.50	1.3°	-82.5°
37	60	36	50	15	9,960.65	1.2°	-82.4°	12,108.90	1.2°	-82.4°
38	60	42	50	15	11,230.90	1.2°	-82.4°	13,969.15	1.2°	-82.4°
39	60	60	50	15	15,472.90	1.2°	-82.4°	16,999.40	1.2°	-82.4°
40	24	36	300	15	15,882.57	123 in	-7.3°	20,292.81	123 in	-7.3°
41	24	42	300	15	18,703.69	122 in	-7.3°	24,023.50	122 in	-7.3°
42	24	60	300	15	30,109.44	121 in	-7.3°	Not Found		
43	42	36	300	15	11,533.89	649 in	-52.2°	12,950.45	649 in	-52.2°
44	42	42	300	15	13,205.59	639 in	-52.2°	14,059.38	213 in	-7.3°
45	42	60	300	15	17,233.07	213 in	-7.3°	20,696.17	213 in	-7.3°
46	60	36	300	15	11,836.76	924 in	-52.2°	12,852.05	924 in	-52.2°
47	60	42	300	15	13,168.95	909 in	-52.2°	14,338.88	909 in	-52.2°
48	60	60	300	15	14,791.32	304 in	-7.3°	17,325.97	304 in	-7.3°

Table A-1 (Contd.)

S. No.	D (in)	H_c (in)	R_b (ft)	θ (Degrees)	Maximum pipe principal stress (psi)					
					Installation Condition Method			Ultimate Temperature Method		
					Stress	x / θ_x	α	Stress	x / θ_x	α
49	24	15	700	15	17,597.16	124 in	67.3°	20,126.26	122 in	-7.3°
50	24	21	700	15	23,218.36	1335 in	22.4°	18,124.30	1334 in	-7.3°
51	24	36	700	15	Not Found			Not Found		
52	24	42	700	15	Not Found			Not Found		
53	24	60	700	15	Not Found			Not Found		
54	42	30	700	15	18,828.65	214 in	-7.3°	21,084.37	214 in	-7.3°
55	42	36	700	15	22,488.00	217 in	-7.3°	25,269.00	217 in	-7.3°
56	42	42	700	15	27,504.52	213 in	-7.3°	30,720.50	213 in	-7.3°
57	42	60	700	15	Not Found			Not Found		
58	60	36	700	15	16,640.35	309 in	-7.3°	18,363.17	309 in	-7.3°
59	60	42	700	15	20,142.51	304 in	-7.3°	21,812.85	304 in	-7.3°
60	60	60	700	15	28,269.15	304 in	-7.3°	30,782.46	304 in	-7.3°
61	24	36	50	8	10,793.71	2°	-82.4°	20,446.57	0.7°	-82.4°
62	24	42	50	8	12,564.55	2°	-82.4°	23,749.35	0.7°	-82.4°
63	24	60	50	8	18,692.29	2°	-82.4°	36,469.61	0.7°	-82.4°
64	42	36	50	8	13,455.15	0.7°	-82.4°	20,328.34	0.7°	-82.4°
65	42	42	50	8	15,335.46	0.7°	-82.4°	24,051.20	0.7°	-82.4°
66	42	60	50	8	21,530.89	0.7°	-82.4°	33,724.69	0.7°	-82.4°
67	60	36	50	8	15,660.70	2°	-82.4°	21,718.24	2°	-82.4°
68	60	42	50	8	17,487.74	2°	-82.4°	25,319.10	2°	-82.4°
69	60	60	50	8	24,233.44	2°	-82.4°	33,102.30	2°	-82.4°
70	24	36	300	8	16,213.63	365 in	-37.3°	20,508.50	365 in	-37.3°
71	24	42	300	8	18,743.04	364 in	-37.3°	24,303.28	364 in	-37.3°
72	24	60	300	8	26,346.90	121 in	37.4°	Not Found		
73	42	36	300	8	14,587.55	645 in	-52.3°	16,380.46	0.7°	-67.7°
74	42	42	300	8	16,282.20	635 in	-52.3°	19,448.85	635 in	-52.3°
75	42	60	300	8	21,446.54	634 in	-37.3°	26,267.57	0.7°	-67.7°
76	60	36	300	8	14,910.53	919 in	-52.3°	15,574.33	0.7°	-67.6°
77	60	42	300	8	16,473.57	904 in	-52.3°	17,805.81	0.7°	-67.6°
78	60	60	300	8	20,852.74	906 in	-52.3°	23,857.69	0.7°	-67.6°
79	24	15	700	8	12,959.60	363 in	-52.3°	15,981.38	363 in	-52.3°
80	24	25	700	8	20,637.28	366 in	-52.3°	Not Found		
81	24	36	700	8	Not Found			Not Found		
82	24	42	700	8	Not Solved			Not Solved		
83	24	60	700	8	Not Solved			Not Solved		
84	42	24	700	8	14,694.30	632 in	-52.3°	17,256.53	632 in	-52.3°
85	42	36	700	8	19,738.38	645 in	-52.3°	22,643.30	645 in	-52.3°
86	42	42	700	8	22,499.08	635 in	-52.3°	25,788.48	635 in	-37.3°
87	42	60	700	8	Not Found			Not Found		
88	60	36	700	8	17,773.96	919 in	-52.3°	19,893.49	919 in	-52.3°
89	60	42	700	8	19,683.89	904 in	-52.3°	22,165.42	904 in	-52.3°
90	60	48	700	8	21,690.11	917 in	-52.3°	24,033.60	917 in	-52.3°
91	60	60	700	8	25,733.95	906 in	-37.3°	Not Found		

Table A-2 Maximum longitudinal stresses corresponding to runs listed in Table 5-2

S. No.	D (in)	H_c (in)	R_b (ft)	θ (Degrees)	Maximum pipe longitudinal stress (psi)					
					Installation Condition Method			Ultimate Temperature Method		
					Stress	x / θ_x	α	Stress	x / θ_x	α
1	24	36	50	20	5,471.97	124 in	-7.3°	9,414.15	1.7°	-67.9°
2	24	42	50	20	5,635.59	1.7°	-67.9°	11,199.31	1.7°	-67.9°
3	24	60	50	20	9,138.82	1.7°	-67.9°	15,731.06	1.7°	-67.9°
4	42	36	50	20	5,440.20	1.7°	-82.5°	8,722.62	1.7°	-82.5°
5	42	42	50	20	6,513.32	1.7°	-82.5°	10,108.70	1.7°	-82.5°
6	42	60	50	20	10,105.92	1.7°	-82.5°	15,358.92	1.7°	-82.5°
7	60	36	50	20	7,343.08	1.7°	-82.5°	8,773.70	1.7°	-82.5°
8	60	42	50	20	8,867.41	1.7°	-82.5°	10,034.22	1.7°	-82.5°
9	60	60	50	20	12,247.54	1.7°	-82.5°	13,467.34	1.7°	-82.5°
10	24	36	300	20	18,860.77	124 in	-7.3°	22,201.73	124 in	-7.3°
11	24	42	300	20	22,080.60	123 in	-7.3°	26,295.82	123 in	-7.3°
12	24	60	300	20	Not Found			Not Found		
13	42	36	300	20	11,401.39	218 in	-7.3°	13,126.74	218 in	-7.3°
14	42	42	300	20	13,443.99	215 in	-7.3°	15,392.04	215 in	-7.3°
15	42	60	300	20	17,988.68	215 in	-7.3°	20,281.82	215 in	-7.3°
16	60	36	300	20	10,626.78	311 in	-7.3°	11,290.60	311 in	-7.3°
17	60	42	300	20	11,791.66	306 in	-7.3°	12,288.09	306 in	-7.3°
18	60	60	300	20	15,322.87	307 in	-7.3°	16,027.00	307 in	-7.3°
19	24	12	700	20	25,076.18	3324 in	22.3°	39,797.68	3815 in	67.3°
20	24	21	700	20	22,361.01	122 in	-7.3°	30,121.75	122 in	-7.3°
21	24	36	700	20	Not Found			Not Found		
22	24	42	700	20	Not Found			Not Found		
23	24	60	700	20	Not Found			Not Found		
24	42	27	700	20	20,199.75	217 in	-7.3°	23,045.77	217 in	-7.3°
25	42	36	700	20	25,821.40	218 in	-7.3°	27,114.37	218 in	-7.3°
26	42	42	700	20	29,527.60	215 in	-7.3°	31,607.03	215 in	-7.3°
27	42	60	700	20	Not Found			Not Found		
28	60	36	700	20	20,172.19	311 in	-7.3°	20,678.44	311 in	-7.3°
29	60	42	700	20	22,551.72	306 in	-7.3°	23,146.67	306 in	-7.3°
30	60	60	700	20	30,058.41	307 in	-7.3°	30,745.38	307 in	-7.3°
31	24	36	50	15	6,297.13	1.9°	-68°	12,098.58	1.9°	-68°
32	24	42	50	15	7,667.15	1.9°	-68°	13,907.01	1.9°	-68°
33	24	60	50	15	11,582.38	1.9°	-68°	20,217.06	1.9°	-68°
34	42	36	50	15	7,475.84	1.3°	-82.4°	11,777.68	1.3°	-82.4°
35	42	42	50	15	9,250.57	1.3°	-82.4°	13,906.70	1.3°	-82.4°
36	42	60	50	15	13,401.55	1.3°	-82.5°	19,822.50	1.3°	-82.5°
37	60	36	50	15	9,956.05	1.2°	-82.4°	12,105.01	1.2°	-82.4°
38	60	42	50	15	11,225.56	1.2°	-82.4°	13,965.08	1.2°	-82.4°
39	60	60	50	15	15,461.95	1.2°	-82.4°	16,988.75	1.2°	-82.4°
40	24	36	300	15	13,656.78	123 in	-7.3°	17,111.94	123 in	-7.3°
41	24	42	300	15	16,002.44	122 in	-7.3°	20,149.94	122 in	-7.3°
42	24	60	300	15	24,421.90	121 in	-7.3°	Not Found		
43	42	36	300	15	9,318.65	649 in	-37.2°	11,149.84	649 in	-37.2°
44	42	42	300	15	10,738.44	639 in	-37.2°	11,292.38	0.6°	-67.6°
45	42	60	300	15	14,917.33	638 in	-37.2°	17,262.00	213 in	-7.3°
46	60	36	300	15	9,037.84	925 in	-37.2°	10,388.08	925 in	-37.2°
47	60	42	300	15	10,128.81	910 in	-37.2°	11,720.01	910 in	-37.2°
48	60	60	300	15	11,429.55	0.9°	-67.8°	14,232.44	0.9°	-67.8°

Table A-2 (Contd.)

S. No.	D (in)	H_c (in)	R_b (ft)	θ (Degrees)	Maximum pipe longitudinal stress (psi)					
					Installation Condition Method			Ultimate Temperature Method		
					Stress	x / θ_x	α	Stress	x / θ_x	α
49	24	15	700	15	12,923.65	122 in	-7.3°	17,780.69	122 in	-7.3°
50	24	21	700	15	19,671.74	1335 in	22.4°	9,359.42	1577 in	-7.3°
51	24	36	700	15	Not Found			Not Found		
52	24	42	700	15	Not Found			Not Found		
53	24	60	700	15	Not Found			Not Found		
54	42	30	700	15	16,504.03	214 in	-7.3°	18,258.25	214 in	-7.3°
55	42	36	700	15	19,362.20	217 in	-7.3°	21,517.47	217 in	-7.3°
56	42	42	700	15	22,888.32	213 in	-7.3°	25,381.38	213 in	-7.3°
57	42	60	700	15	Not Found			Not Found		
58	60	36	700	15	14,639.91	309 in	-7.3°	16,011.79	309 in	-7.3°
59	60	42	700	15	17,020.08	304 in	-7.3°	18,345.27	304 in	-7.3°
60	60	60	700	15	23,411.80	304 in	-7.3°	25,315.98	304 in	-7.3°
61	24	36	50	8	10,592.22	0.7°	-82.4°	20,446.57	0.7°	-82.4°
62	24	42	50	8	12,378.33	0.7°	-82.4°	23,748.21	0.7°	-82.4°
63	24	60	50	8	18,431.67	0.7°	-82.4°	36,468.98	0.7°	-82.4°
64	42	36	50	8	13,454.36	0.7°	-82.4°	20,328.34	0.7°	-82.4°
65	42	42	50	8	15,335.07	0.7°	-82.4°	24,051.20	0.7°	-82.4°
66	42	60	50	8	21,530.89	0.7°	-82.4°	33,724.69	0.7°	-82.4°
67	60	36	50	8	15,660.23	2°	-82.4°	21,718.24	2°	-82.4°
68	60	42	50	8	17,478.09	2°	-82.4°	25,315.66	2°	-82.4°
69	60	60	50	8	24,226.01	2°	-82.4°	33,098.40	2°	-82.4°
70	24	36	300	8	12,448.36	0.3°	-67.5°	18,314.90	0.3°	-67.5°
71	24	42	300	8	14,876.33	364 in	-37.3°	22,206.41	0.3°	-67.5°
72	24	60	300	8	22,279.60	0.3°	-67.5°	Not Found		
73	42	36	300	8	10,947.83	0.7°	-67.7°	15,711.76	0.7°	-67.7°
74	42	42	300	8	12,665.17	0.7°	-67.7°	17,857.79	0.7°	-67.7°
75	42	60	300	8	18,003.93	0.7°	-67.7°	25,548.25	0.7°	-67.7°
76	60	36	300	8	11,068.55	0.7°	-67.6°	15,246.57	0.7°	-67.6°
77	60	42	300	8	12,565.21	0.7°	-67.6°	17,430.58	0.7°	-67.6°
78	60	60	300	8	17,568.41	0.7°	-67.6°	23,481.39	0.7°	-67.6°
79	24	15	700	8	11,309.93	364 in	-37.3°	14,704.87	364 in	-37.3°
80	24	25	700	8	18,745.56	366 in	-37.3°	Not Found		
81	24	36	700	8	Not Found			Not Found		
82	24	42	700	8	Not Solved			Not Solved		
83	24	60	700	8	Not Solved			Not Solved		
84	42	24	700	8	10,421.00	0.3°	-67.5°	14,254.25	0.3°	-67.5°
85	42	36	700	8	16,337.96	645 in	-37.3°	19,760.30	645 in	-37.3°
86	42	42	700	8	19,022.90	635 in	-37.3°	22,838.31	635 in	-37.3°
87	42	60	700	8	Not Found			Not Found		
88	60	36	700	8	13,142.50	0.4°	-67.6°	16,361.52	0.4°	-67.6°
89	60	42	700	8	15,319.08	904 in	-37.3°	18,431.92	0.4°	-67.6°
90	60	48	700	8	17,042.88	0.4°	-67.6°	20,320.04	0.4°	-67.6°
91	60	60	700	8	20,970.20	0.4°	-67.6°	Not Found		

Table A-3 Maximum hoop stresses corresponding to runs listed in Table 5-2

S. No.	D (in)	H_c (in)	R_b (ft)	θ (Degrees)	Maximum pipe hoop stress (psi)					
					Installation Condition Method			Ultimate Temperature Method		
					Stress	x / θ_x	α	Stress	x / θ_x	α
1	24	36	50	20	5,616.48	5°	82.3°	7,326.19	5°	-8.6°
2	24	42	50	20	6,062.39	5°	-8.6°	8,232.64	5°	-8.6°
3	24	60	50	20	7,871.03	5°	-8.6°	10,141.81	5°	-8.6°
4	42	36	50	20	6,895.52	5°	-8.1°	8,485.17	5°	-8.1°
5	42	42	50	20	7,788.56	5°	-8.1°	9,466.15	5°	-8.1°
6	42	60	50	20	10,249.36	5°	-8.1°	12,566.31	5°	-8.1°
7	60	36	50	20	8,686.75	5°	-7.9°	9,467.89	5°	-7.9°
8	60	42	50	20	9,875.92	5°	-7.9°	10,504.48	5°	-7.9°
9	60	60	50	20	12,418.18	5°	-7.9°	13,032.05	5°	-7.9°
10	24	36	300	20	8,722.26	371 in	-7.3°	9,727.27	371 in	-7.3°
11	24	42	300	20	9,488.96	370 in	-7.3°	10,545.29	370 in	-7.3°
12	24	60	300	20	Not Found			Not Found		
13	42	36	300	20	6,464.19	219 in	7.4°	6,753.07	219 in	7.4°
14	42	42	300	20	6,715.44	646 in	-7.3°	7,191.75	646 in	-7.3°
15	42	60	300	20	7,309.08	644 in	-7.3°	7,843.32	644 in	-7.3°
16	60	36	300	20	7,145.51	317 in	82.4°	7,200.16	317 in	82.4°
17	60	42	300	20	6,700.95	312 in	82.4°	6,744.31	312 in	82.4°
18	60	60	300	20	6,568.92	921 in	-7.3°	6,730.59	921 in	-7.3°
19	24	12	700	20	22,987.01	125 in	52.1°	41,431.74	3815 in	82.4°
20	24	21	700	20	8,499.10	612 in	-7.3°	11,311.10	367 in	-7.3°
21	24	36	700	20	Not Found			Not Found		
22	24	42	700	20	Not Found			Not Found		
23	24	60	700	20	Not Found			Not Found		
24	42	27	700	20	8,284.55	1087 in	-7.3°	9,218.43	652 in	-7.3°
25	42	36	700	20	10,071.42	656 in	-7.3°	10,335.34	656 in	-7.3°
26	42	42	700	20	10,726.00	646 in	-7.3°	11,258.59	646 in	-7.3°
27	42	60	700	20	Not Found			Not Found		
28	60	36	700	20	8,014.36	934 in	-7.3°	8,147.34	934 in	-7.3°
29	60	42	700	20	8,436.04	919 in	-7.3°	8,576.00	919 in	-7.3°
30	60	60	700	20	9,973.85	921 in	-7.3°	10,143.82	921 in	-7.3°
31	24	36	50	15	5,472.45	1.9°	-9°	7,610.91	1.9°	-9°
32	24	42	50	15	6,141.13	1.9°	-9°	8,425.02	1.9°	-9°
33	24	60	50	15	7,521.26	1.9°	-9°	10,383.34	1.9°	-9°
34	42	36	50	15	7,399.58	3.8°	-7.8°	9,079.87	3.8°	-7.8°
35	42	42	50	15	8,456.03	3.7°	-7.8°	10,266.44	3.7°	-7.8°
36	42	60	50	15	10,610.35	3.8°	-7.8°	12,914.38	3.8°	-7.8°
37	60	36	50	15	9,141.69	3.8°	-7.7°	10,087.56	3.8°	-7.7°
38	60	42	50	15	10,041.71	3.7°	-7.7°	11,235.24	3.7°	-7.7°
39	60	60	50	15	12,352.06	3.8°	-7.7°	12,947.86	3.8°	-7.7°
40	24	36	300	15	6,610.72	123 in	7.4°	7,270.48	123 in	7.4°
41	24	42	300	15	6,696.34	123 in	7.4°	7,495.76	123 in	7.4°
42	24	60	300	15	7,619.50	122 in	7.4°	Not Found		
43	42	36	300	15	6,103.52	217 in	7.4°	6,429.45	217 in	7.4°
44	42	42	300	15	6,126.93	214 in	7.4°	6,510.16	214 in	7.4°
45	42	60	300	15	6,794.73	212 in	-37.2°	6,754.38	214 in	7.4°
46	60	36	300	15	6,357.97	310 in	7.4°	6,597.87	310 in	7.4°
47	60	42	300	15	6,339.53	305 in	7.4°	6,600.71	305 in	7.4°
48	60	60	300	15	5,815.52	2.8°	-8.3°	6,387.37	2.8°	-8.3°

Table A-3 (Contd.)

S. No.	D (in)	H_c (in)	R_b (ft)	θ (Degrees)	Maximum pipe hoop stress (psi)					
					Installation Condition Method			Ultimate Temperature Method		
					Stress	x / θ_x	α	Stress	x / θ_x	α
49	24	15	700	15	7,175.97	123 in	7.4°	9,314.95	123 in	7.4°
50	24	21	700	15	8,847.74	1335 in	22.4°	13,339.85	1334 in	-7.3°
51	24	36	700	15	Not Found			Not Found		
52	24	42	700	15	Not Found			Not Found		
53	24	60	700	15	Not Found			Not Found		
54	42	30	700	15	7,886.85	214 in	7.4°	8,218.28	214 in	7.4°
55	42	36	700	15	7,857.02	217 in	7.4°	8,234.77	217 in	7.4°
56	42	42	700	15	8,259.82	214 in	7.4°	8,727.35	214 in	7.4°
57	42	60	700	15	Not Found			Not Found		
58	60	36	700	15	7,143.31	310 in	7.4°	7,287.37	310 in	7.4°
59	60	42	700	15	7,420.46	305 in	7.4°	7,622.33	305 in	7.4°
60	60	60	700	15	7,739.23	305 in	7.4°	8,079.62	305 in	7.4°
61	24	36	50	8	6,633.59	2°	-7.6°	8,379.05	2°	-7.6°
62	24	42	50	8	6,998.48	2°	-7.6°	9,194.20	2°	-7.6°
63	24	60	50	8	8,169.38	2°	-7.6°	12,313.30	2°	-7.6°
64	42	36	50	8	7,747.61	2°	-7.5°	9,139.89	2°	-7.5°
65	42	42	50	8	8,080.93	2°	-7.5°	10,071.33	2°	-7.5°
66	42	60	50	8	9,490.96	2°	-7.5°	12,737.21	2°	-7.5°
67	60	36	50	8	8,345.02	2°	-7.5°	9,697.00	2°	-7.5°
68	60	42	50	8	8,711.55	2°	-7.5°	10,783.39	2°	-7.5°
69	60	60	50	8	10,621.66	2°	-7.5°	13,151.00	2°	-7.5°
70	24	36	300	8	5,110.46	122 in	7.5°	5,652.57	122 in	7.5°
71	24	42	300	8	5,449.53	121 in	-37.3°	5,915.11	122 in	7.5°
72	24	60	300	8	5,767.25	121 in	22.5°	Not Found		
73	42	36	300	8	5,331.60	214 in	-37.3°	5,435.90	215 in	7.5°
74	42	42	300	8	5,183.66	2°	-8.1°	5,672.27	2°	-8.1°
75	42	60	300	8	5,713.44	2°	-8.1°	6,557.47	2°	-8.1°
76	60	36	300	8	5,388.20	306 in	-37.3°	5,464.87	2°	-7.9°
77	60	42	300	8	5,537.06	301 in	-37.3°	5,960.84	2°	-7.9°
78	60	60	300	8	6,270.04	2°	-7.9°	6,920.03	2°	-7.9°
79	24	15	700	8	5,526.47	121 in	7.5°	5,985.23	121 in	7.5°
80	24	25	700	8	6,095.43	122 in	7.5°	Not Found		
81	24	36	700	8	Not Found			Not Found		
82	24	42	700	8	Not Solved			Not Solved		
83	24	60	700	8	Not Solved			Not Solved		
84	42	24	700	8	5,417.68	211 in	7.5°	5,791.59	211 in	7.5°
85	42	36	700	8	5,706.67	215 in	7.5°	6,110.26	215 in	7.5°
86	42	42	700	8	5,878.22	212 in	7.5°	6,338.72	212 in	7.5°
87	42	60	700	8	Not Found			Not Found		
88	60	36	700	8	5,436.38	307 in	7.5°	5,705.17	307 in	7.5°
89	60	42	700	8	5,563.34	302 in	7.5°	5,883.78	302 in	7.5°
90	60	48	700	8	5,718.60	306 in	7.5°	6,015.40	306 in	7.5°
91	60	60	700	8	6,062.77	303 in	7.5°	Not Found		

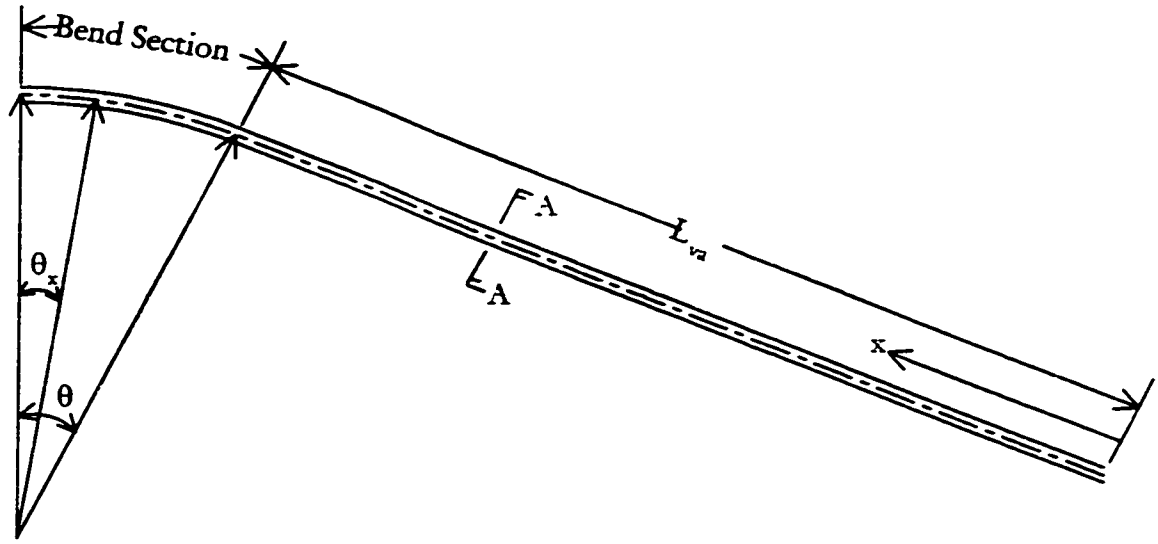

(a) Location defined using x/θ_x in the longitudinal direction

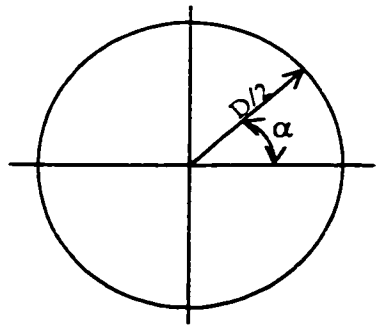

(b) Location defined using the angle α in the circumferential direction (Section-AA)

Figure A-1 Method used to locate the point of maximum stress along a pipeline

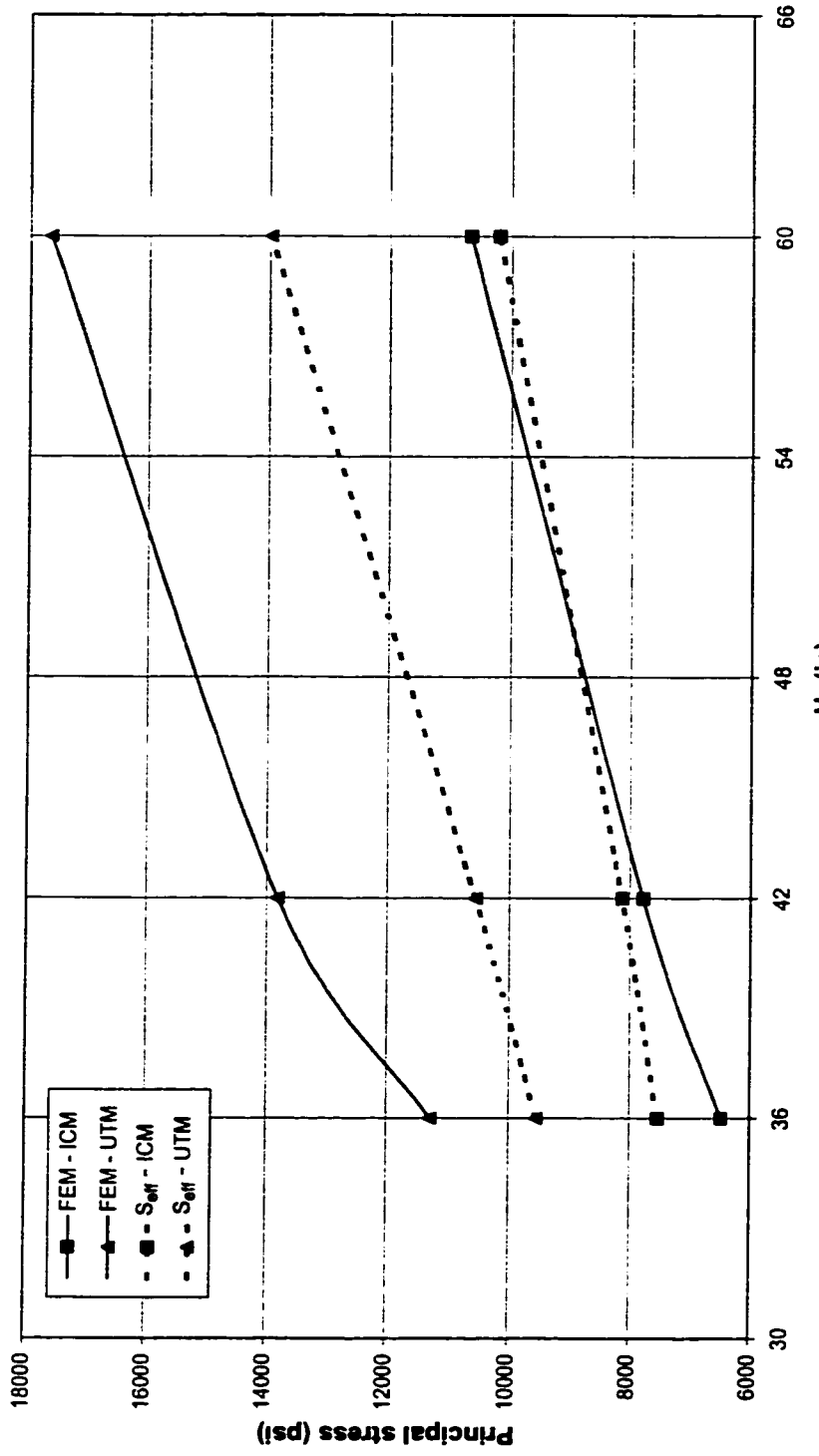

(a) D = 24 in, R_b = 50 ft, θ = 20°

Figure A-2 The effect of cover height on the principal stresses

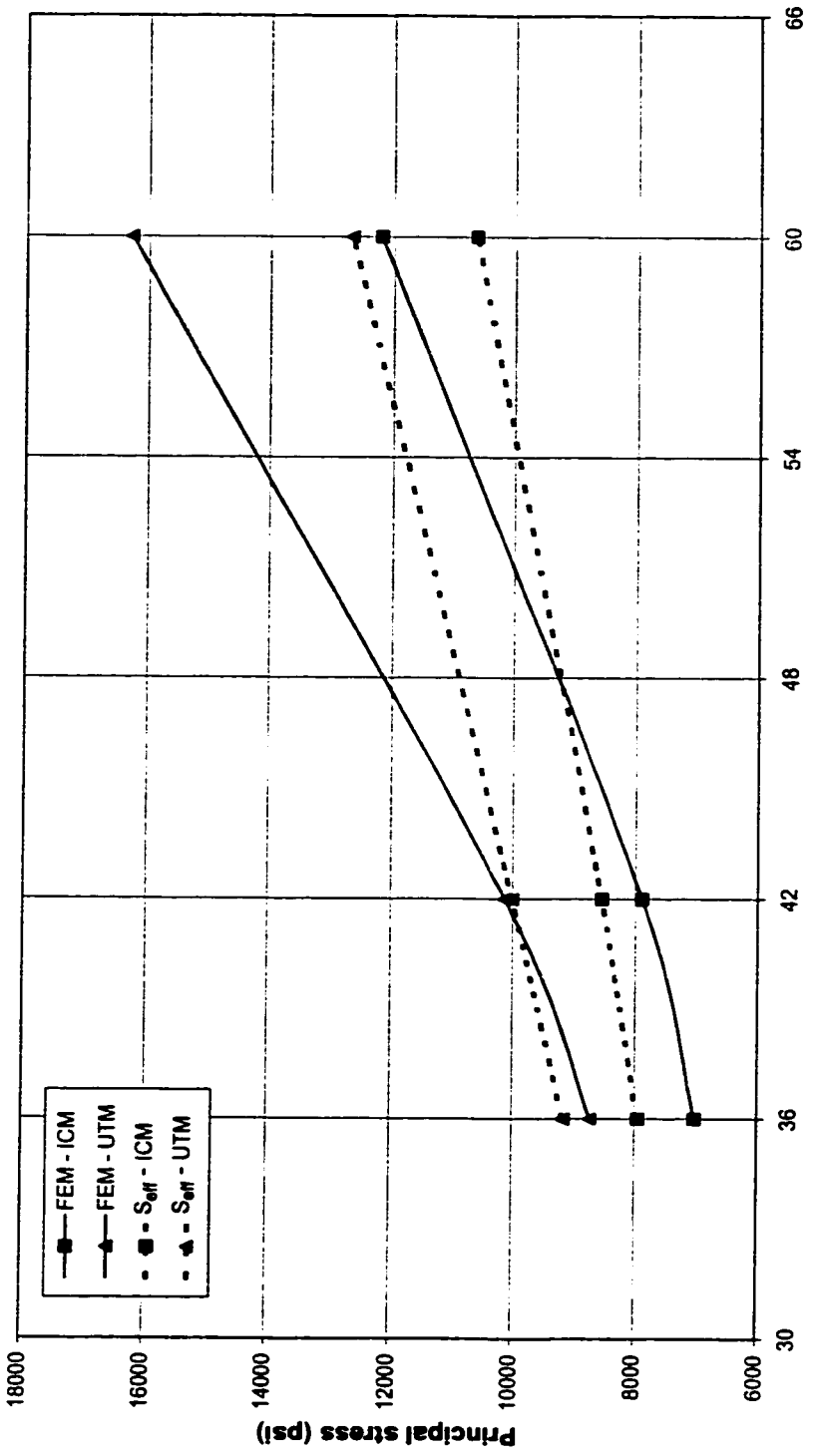

(b) D = 42 in, R_b = 50 ft, $\theta = 20^\circ$

Figure A-2 (Contd.)

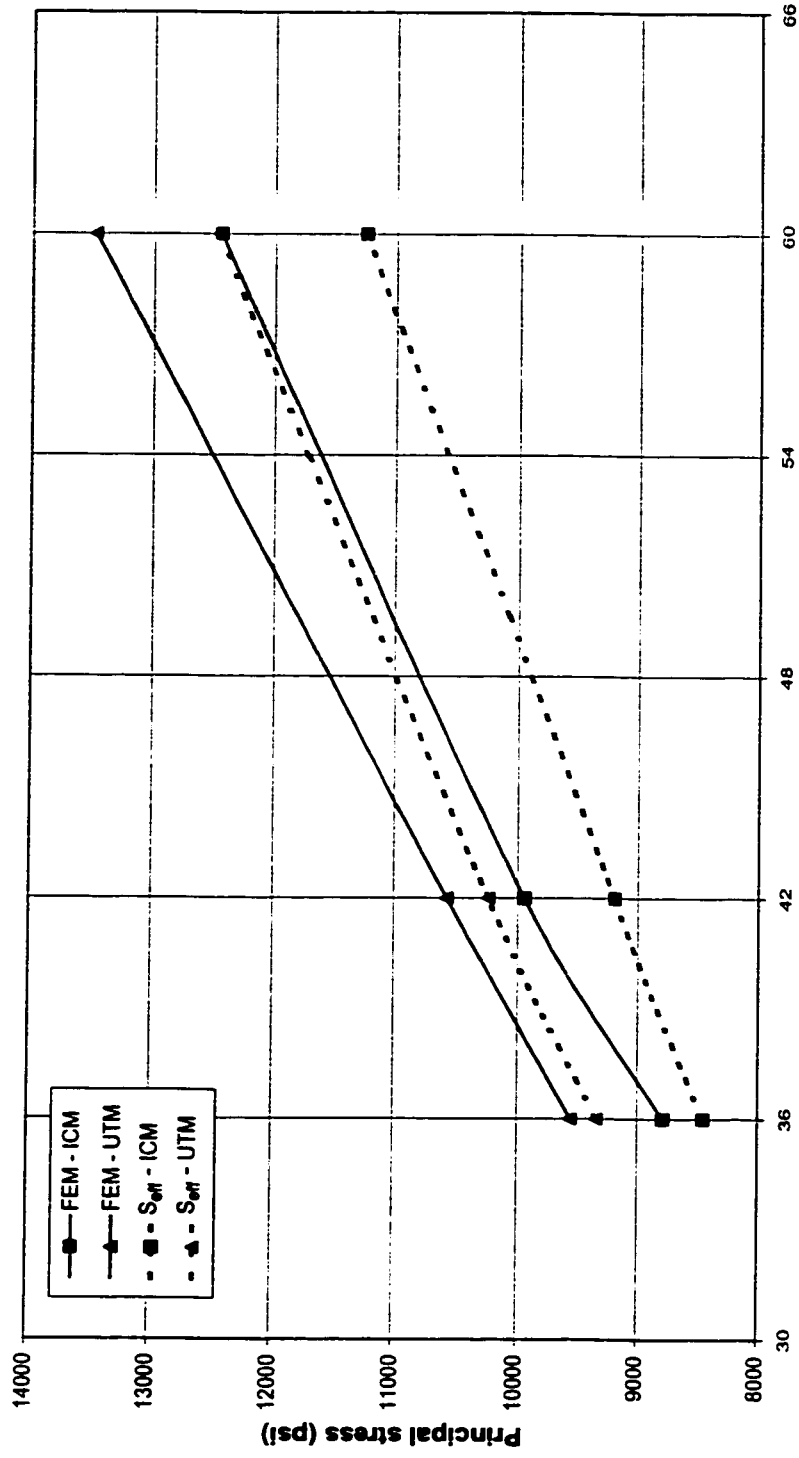

(c) D = 60 in, R_b = 50 ft, θ = 20°

Figure A-2 (Contd.)

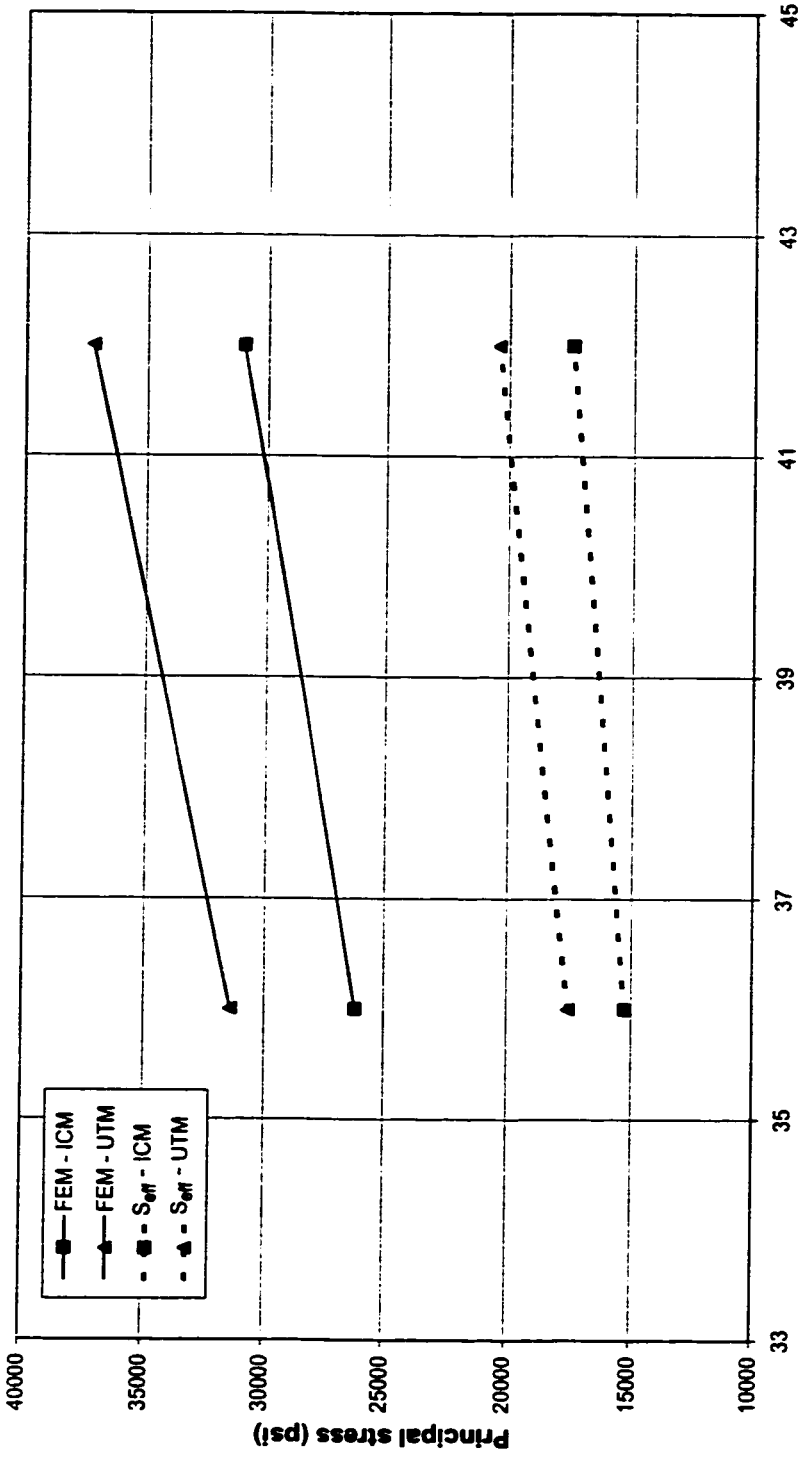

(d) D = 24 in, R_b = 300 ft, $\theta = 20^\circ$

Figure A-2 (Contd.)

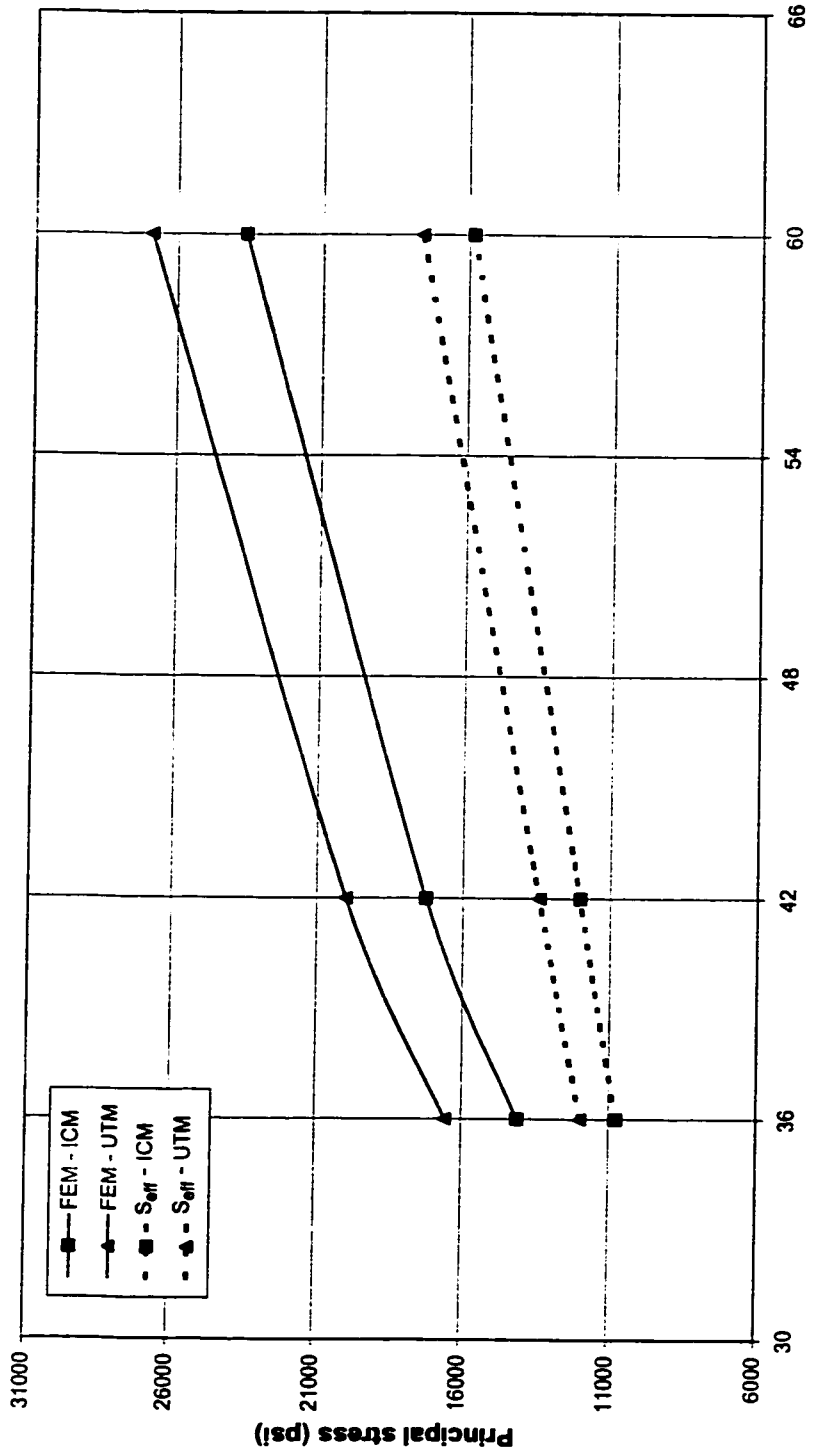

(e) D = 42 in, R_b = 300 ft, θ = 20°

Figure A-2 (Contd.)

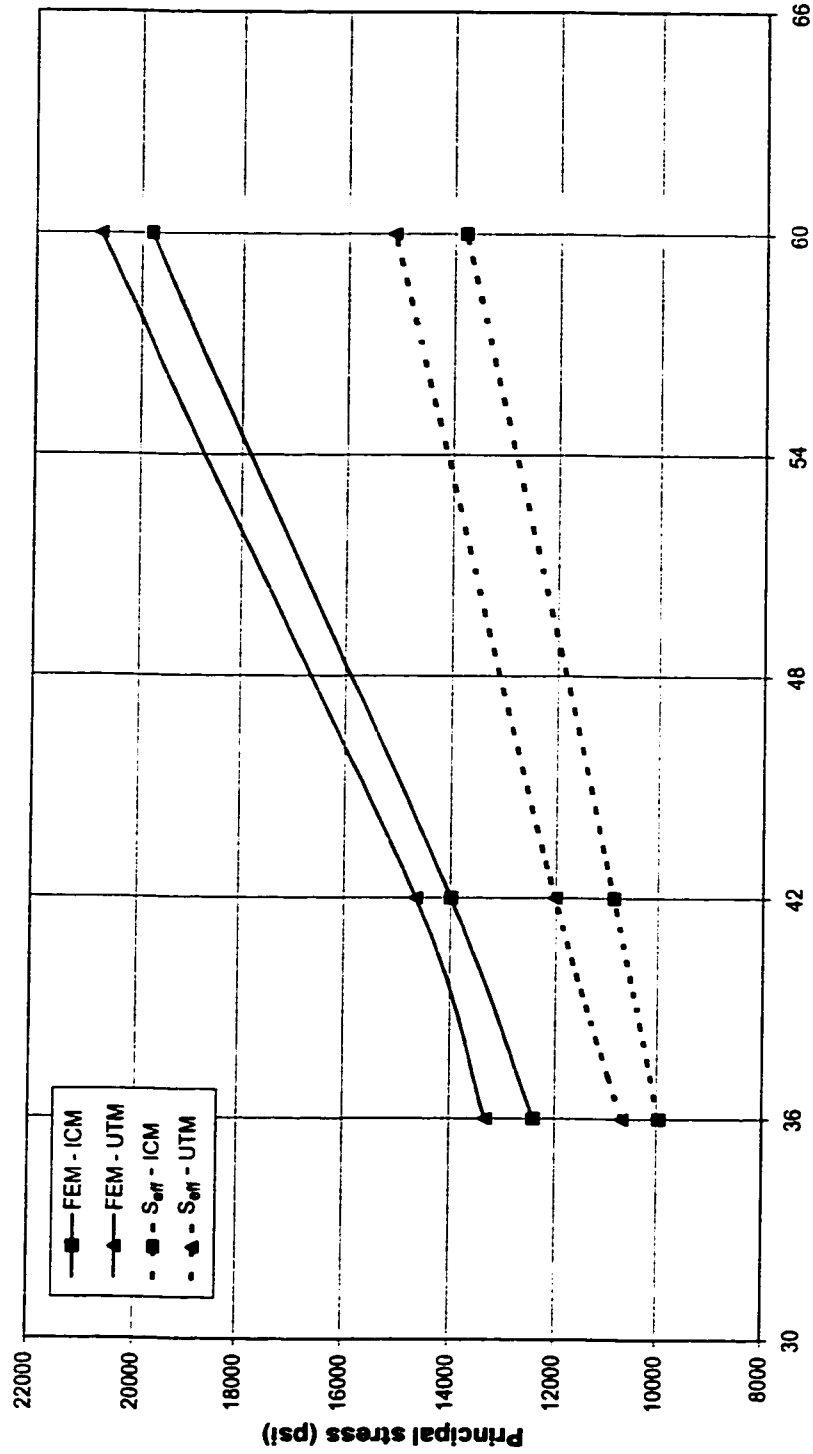

(f) D = 60 in, R_b = 300 ft, θ = 20°

Figure A-2 (Contd.)

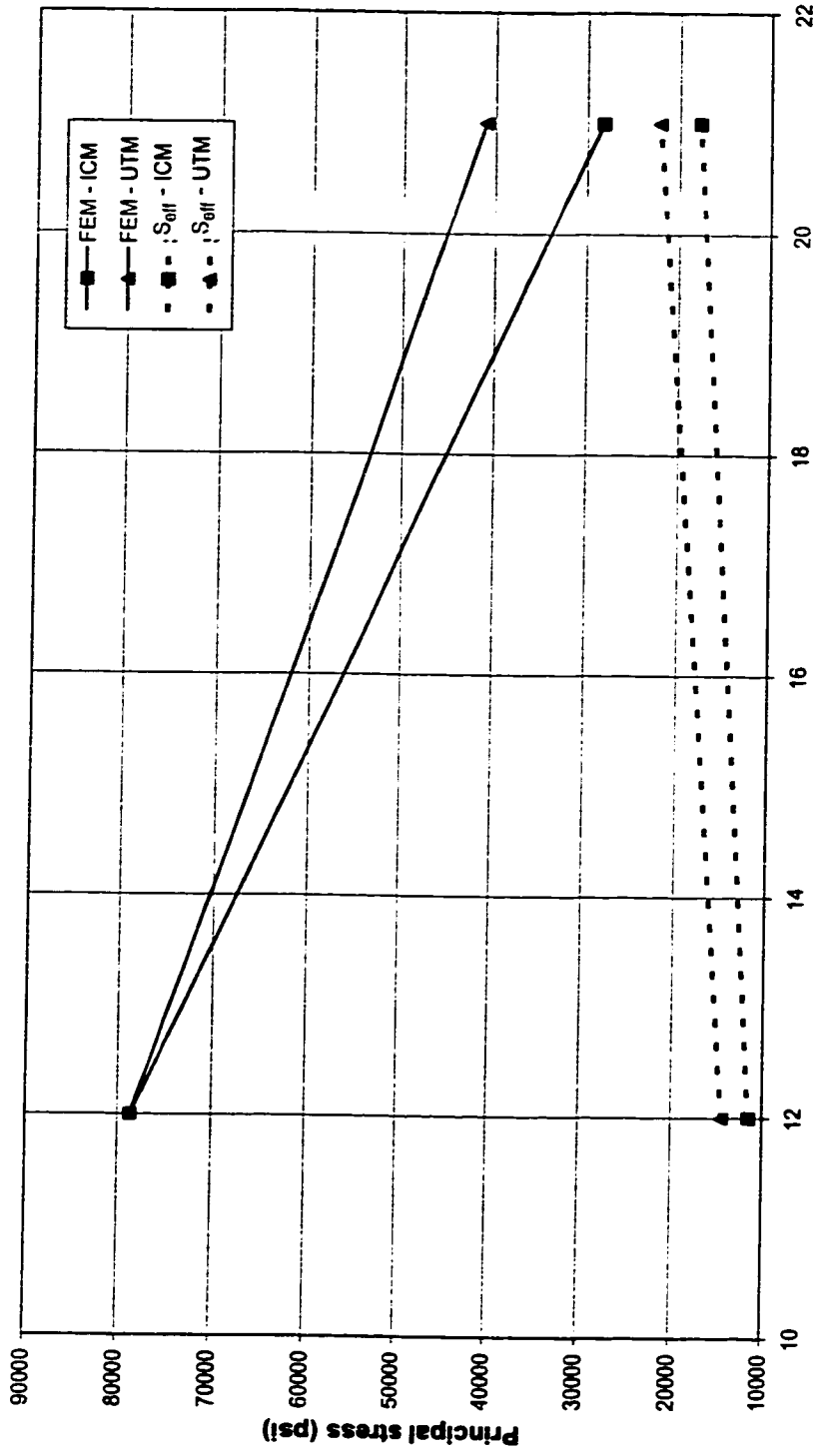

(g) D = 24 in, R_b = 700 ft, θ = 20°

Figure A-2 (Contd.)

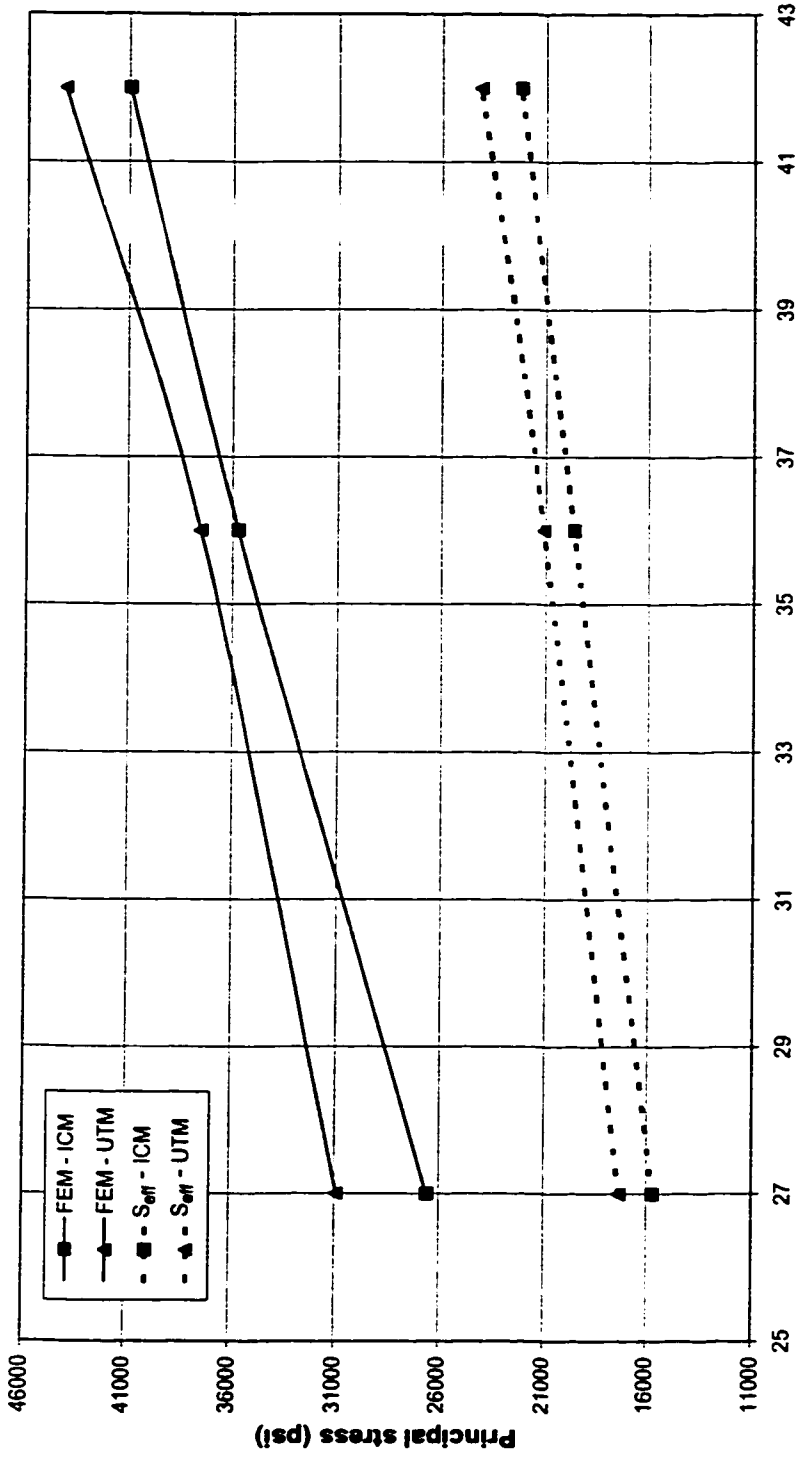

(h) D = 42 in, R_b = 700 ft, θ = 20°

Figure A-2 (Contd.)

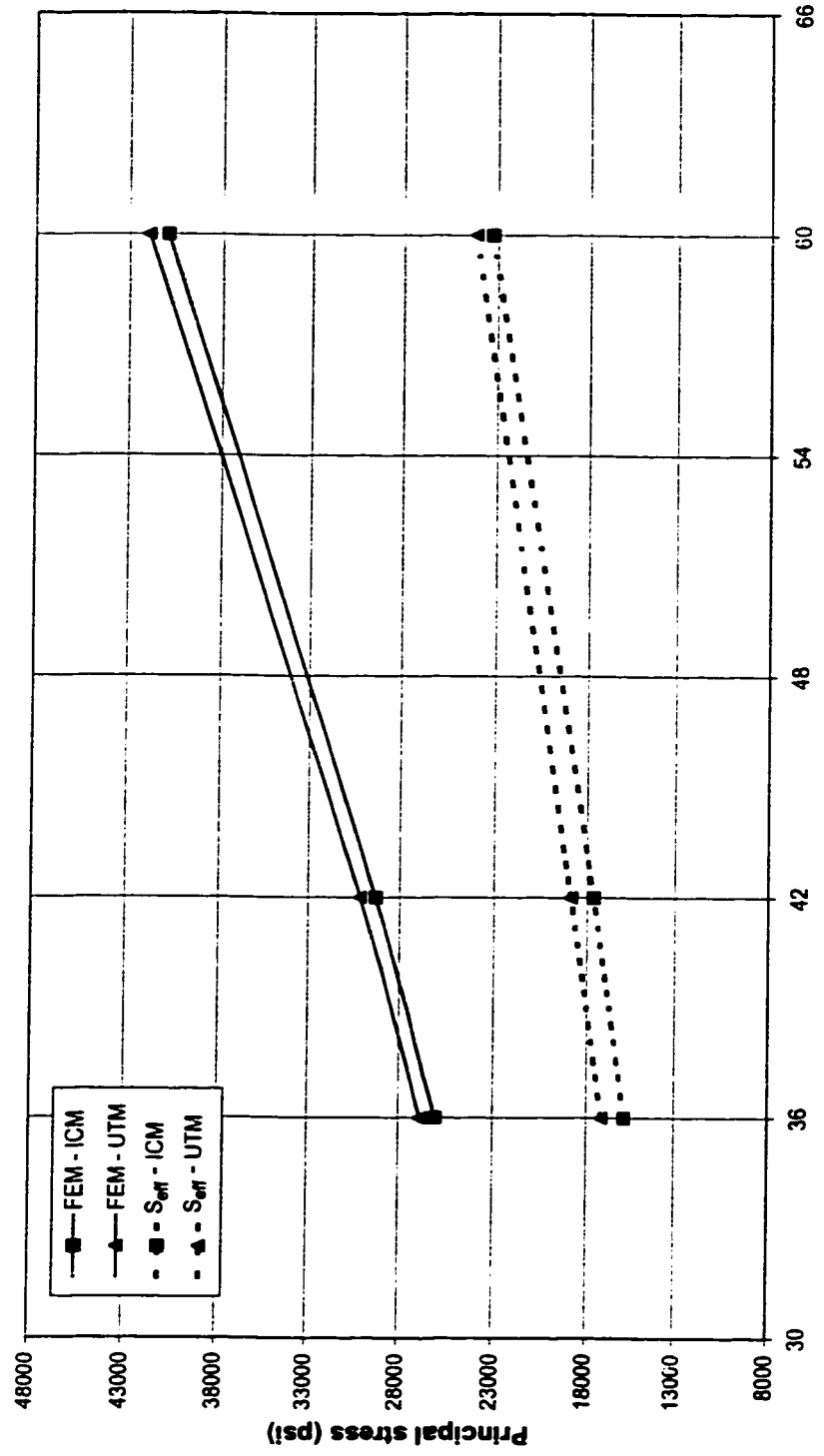

(i) D = 60 in, R_b = 700 ft, θ = 20°

Figure A-2 (Contd.)

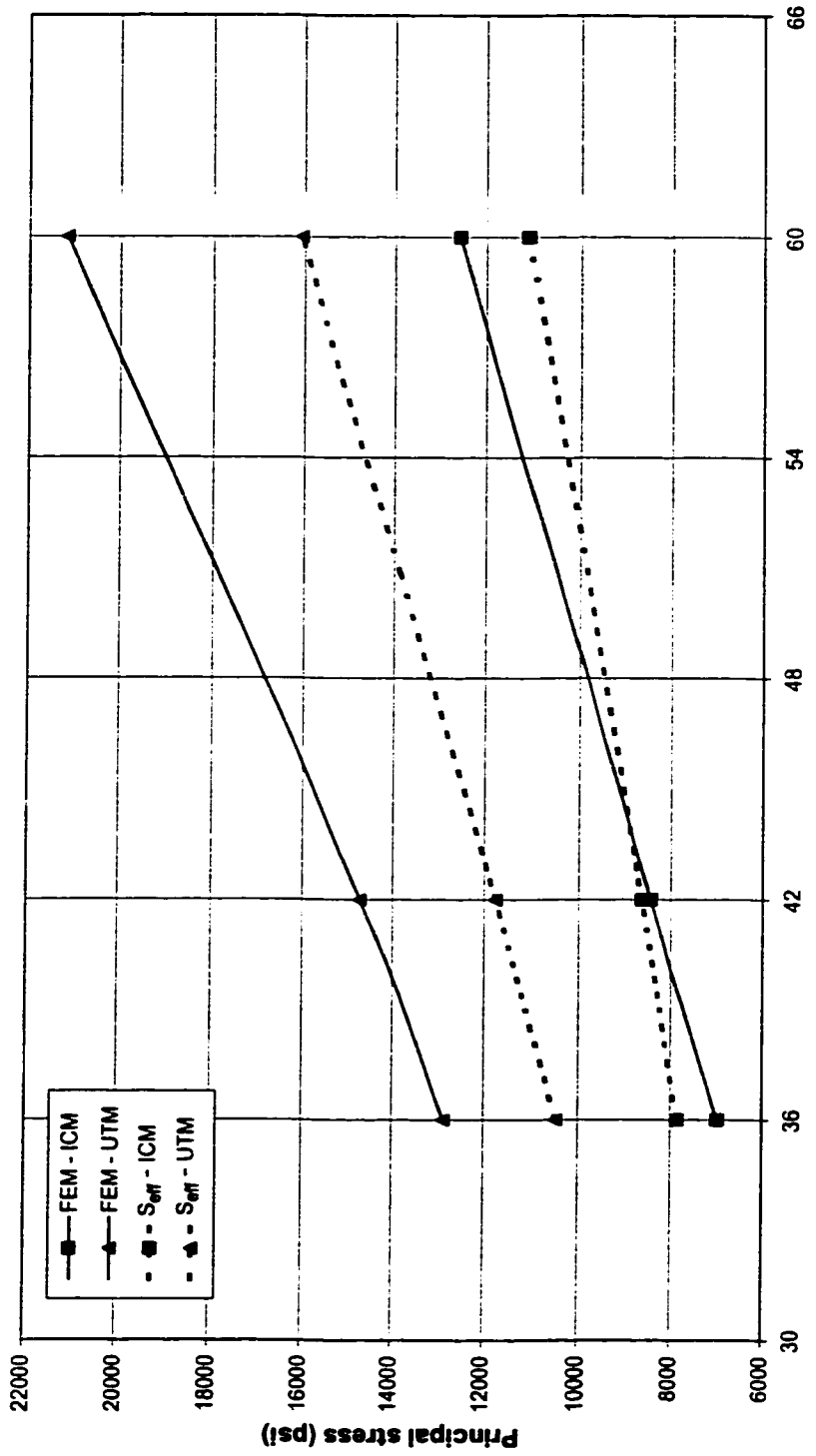

(j) D = 24 in, R_b = 50 ft, θ = 15°

Figure A-2 (Contd.)

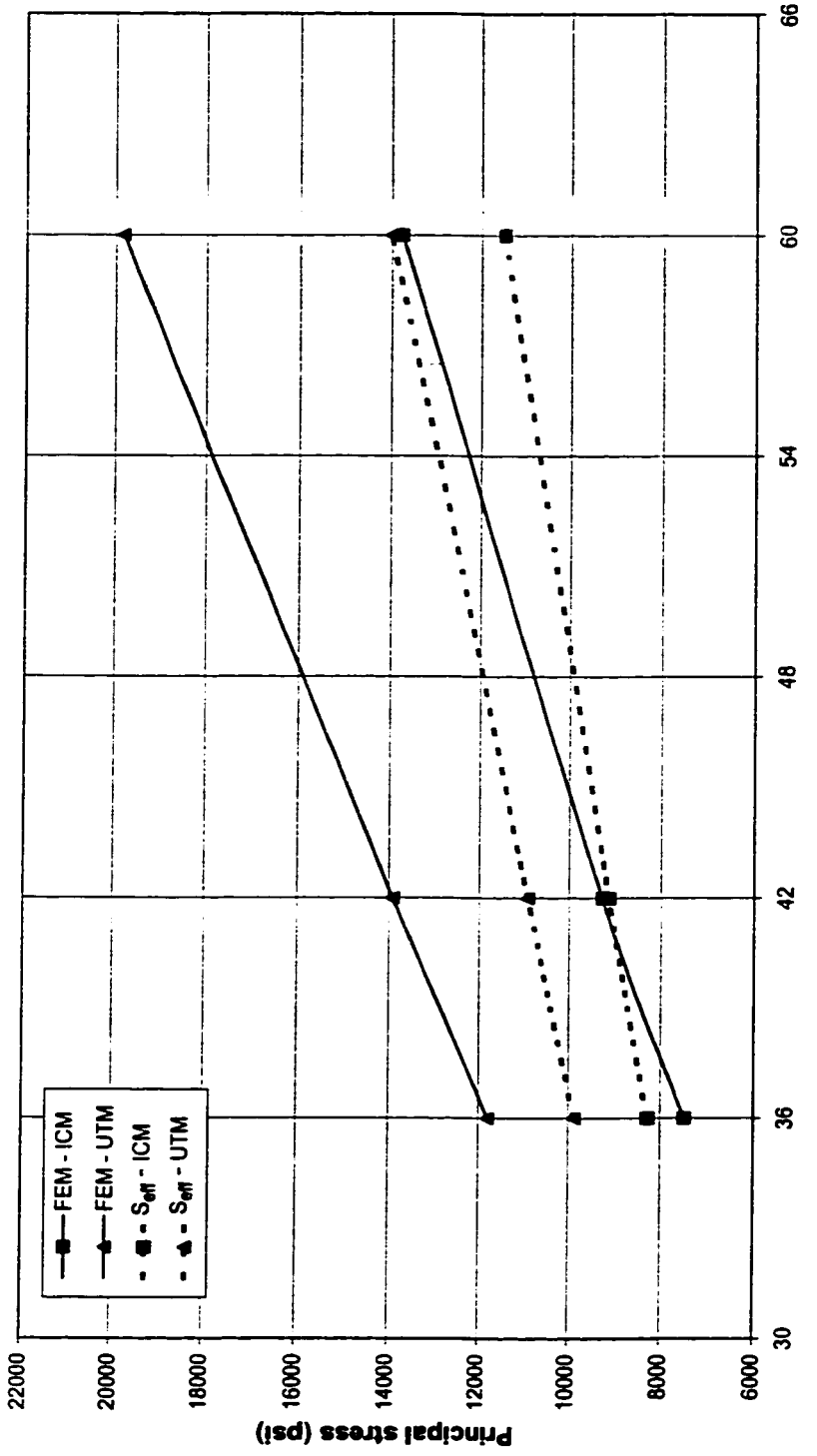

(k) D = 42 in, R_b = 50 ft, θ = 15°

Figure A-2 (Contd.)

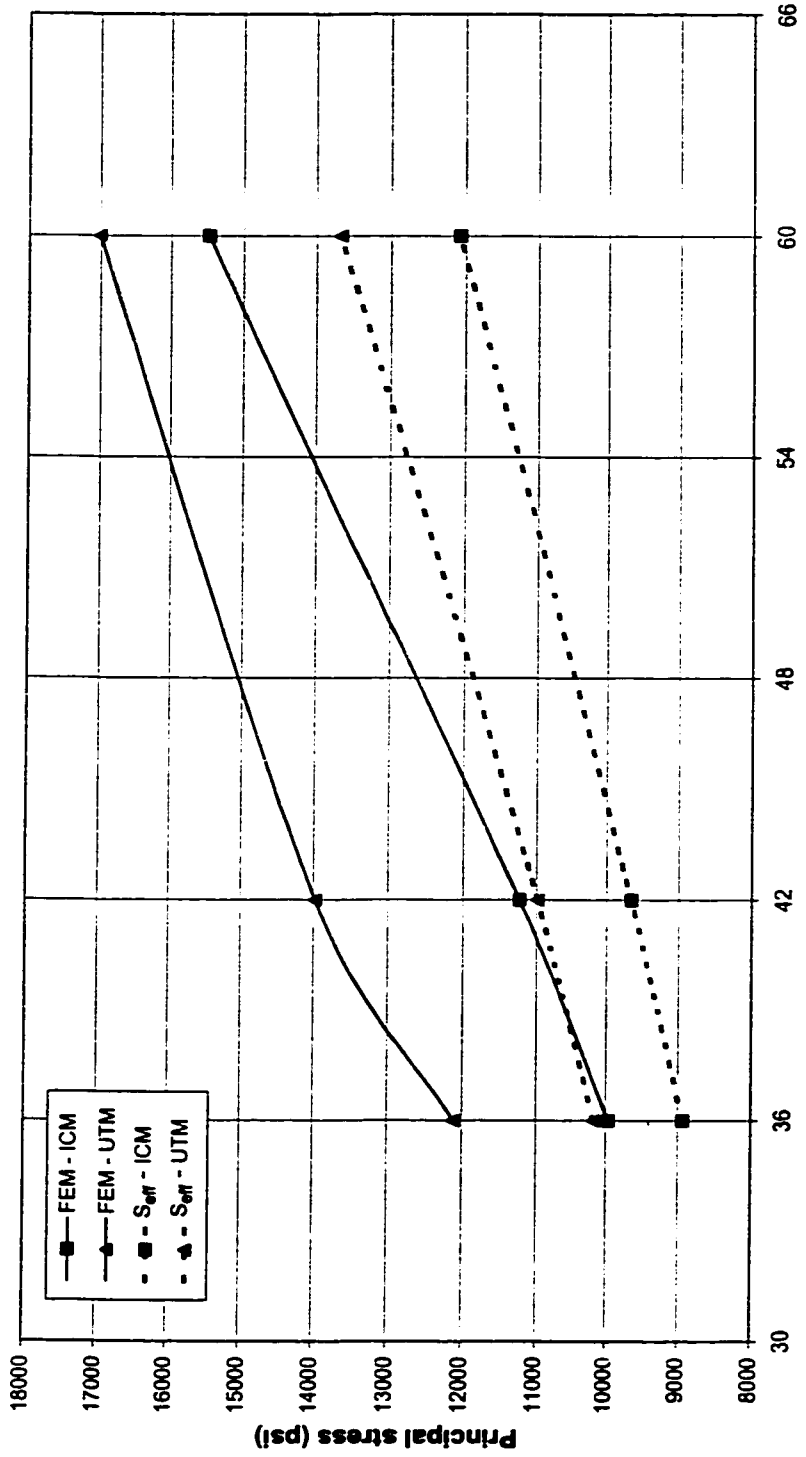

(l) D = 60 in, R_b = 50 ft, θ = 15°

Figure A-2 (Contd.)

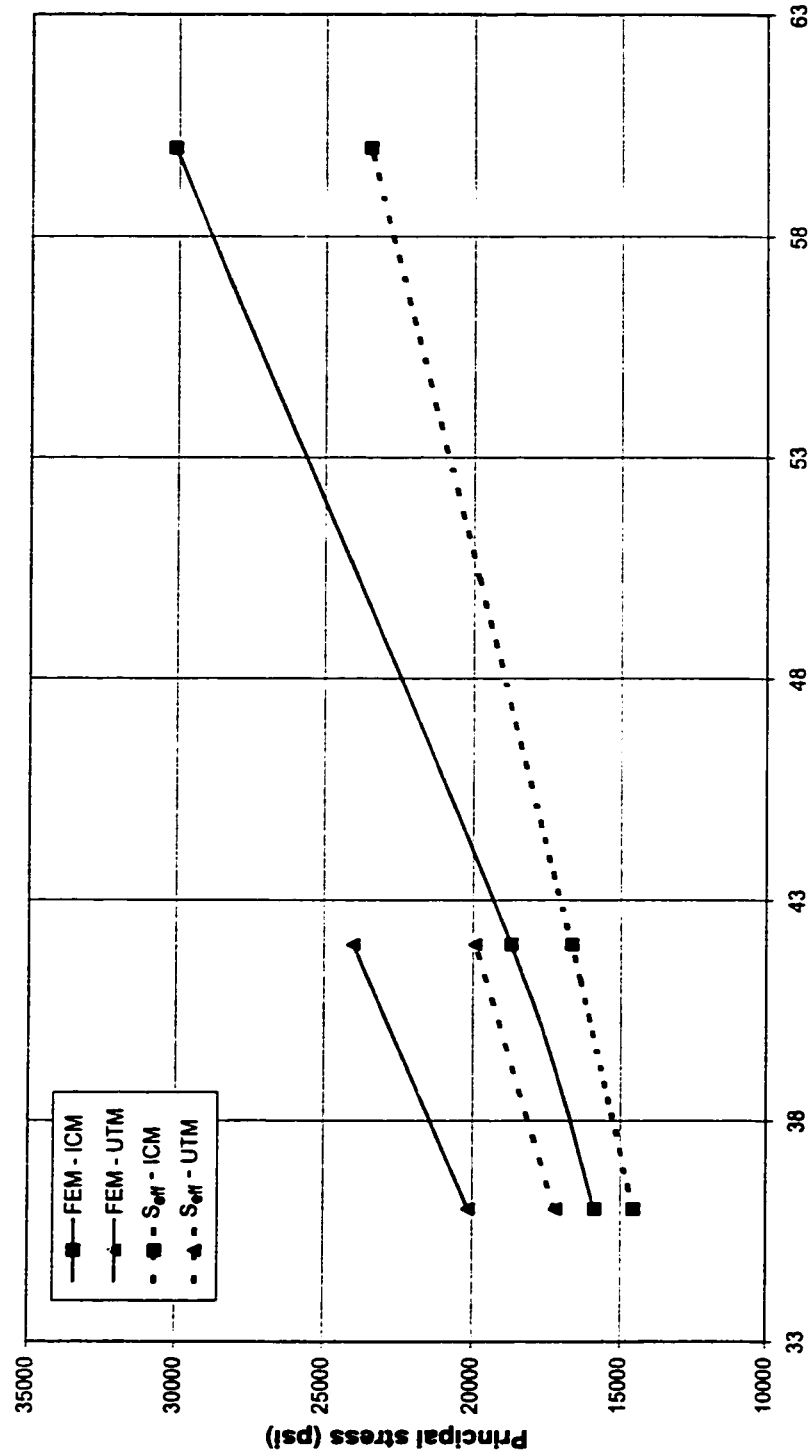

(m) D = 24 in, R_b = 300 ft, θ = 15°

Figure A-2 (Contd.)

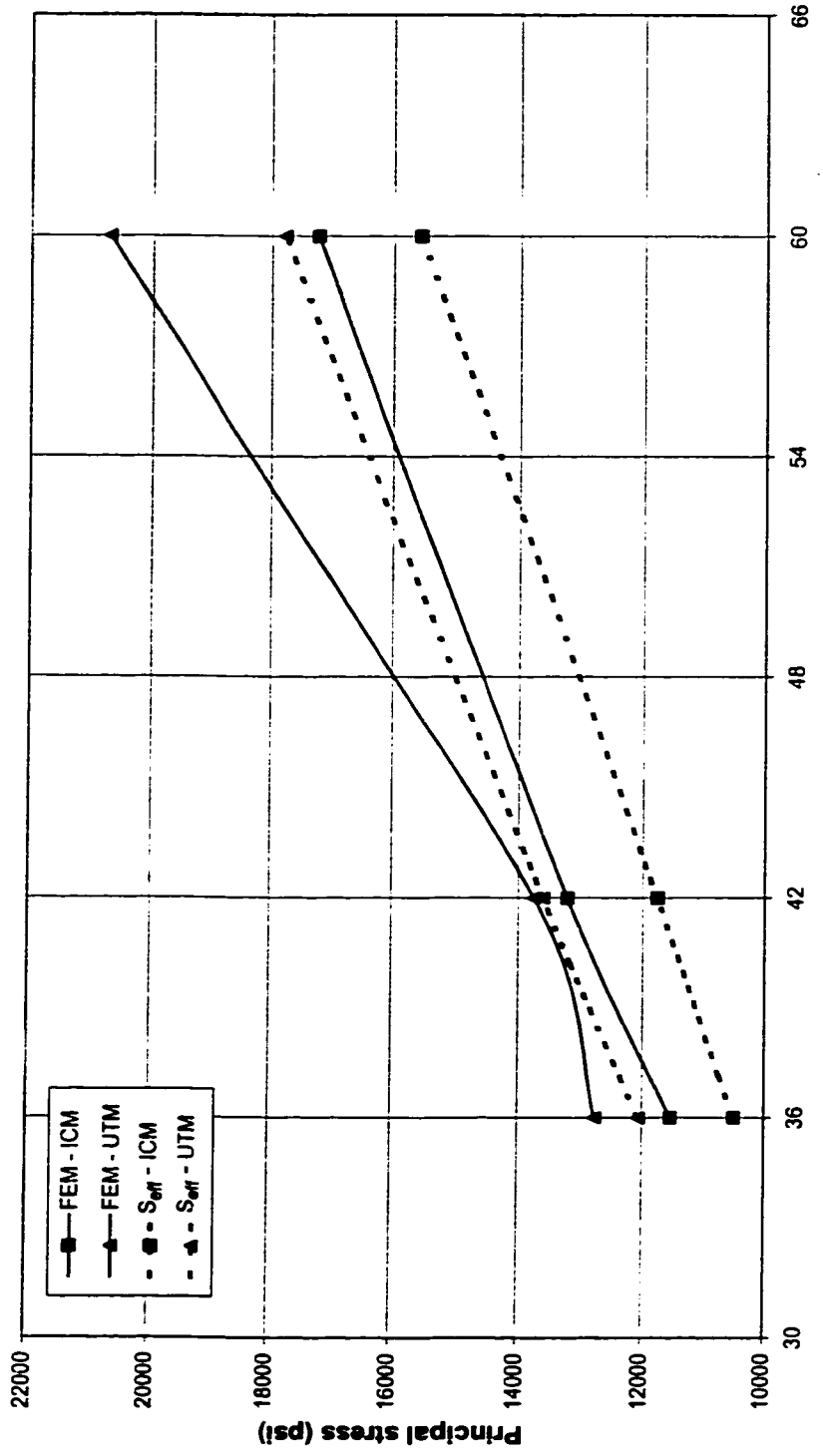

(n) D = 42 in, R_b = 300 ft, $\theta = 15^\circ$

Figure A-2 (Contd.)

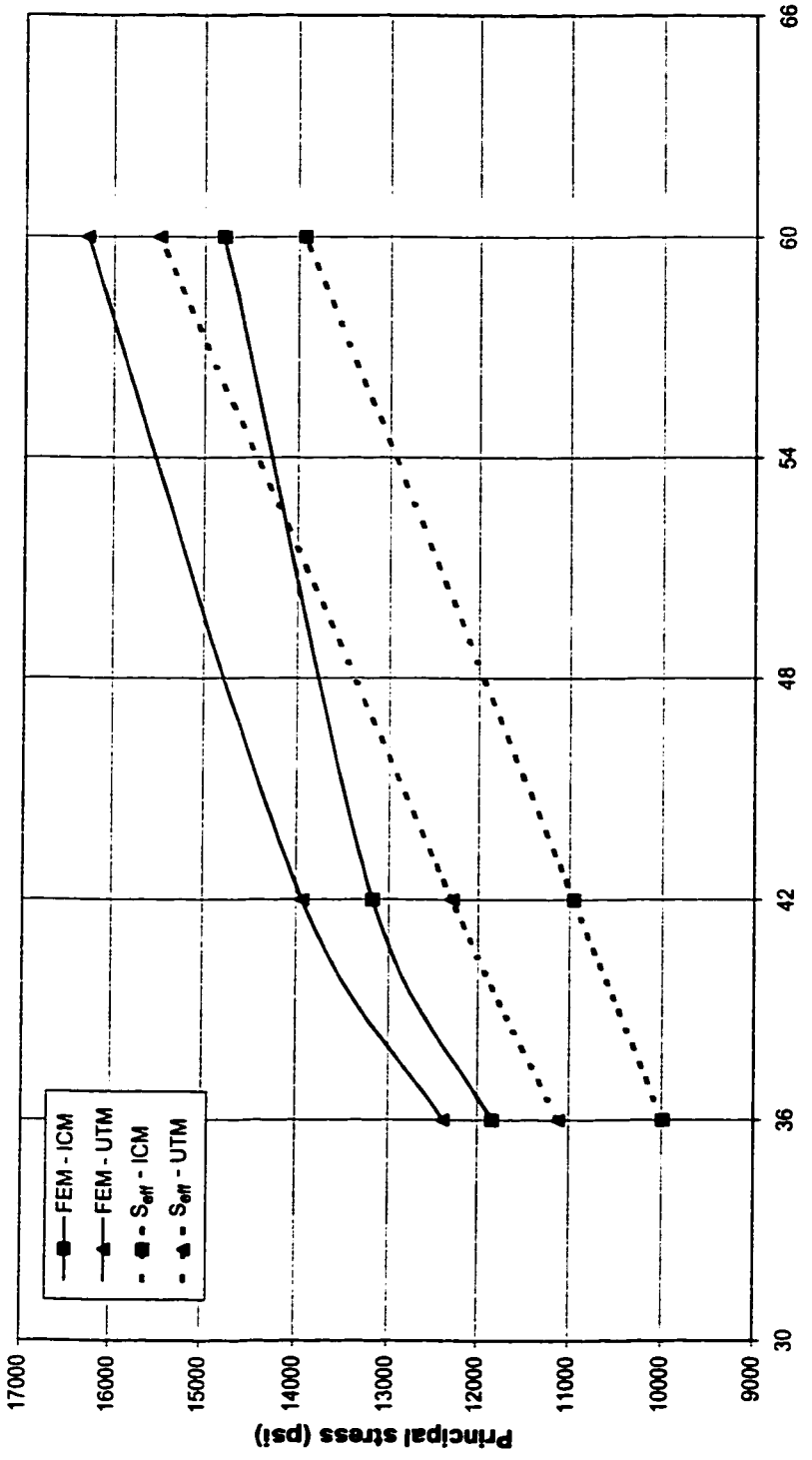

(o) D = 60 in, R_b = 300 ft, θ = 15°

Figure A-2 (Contd.)

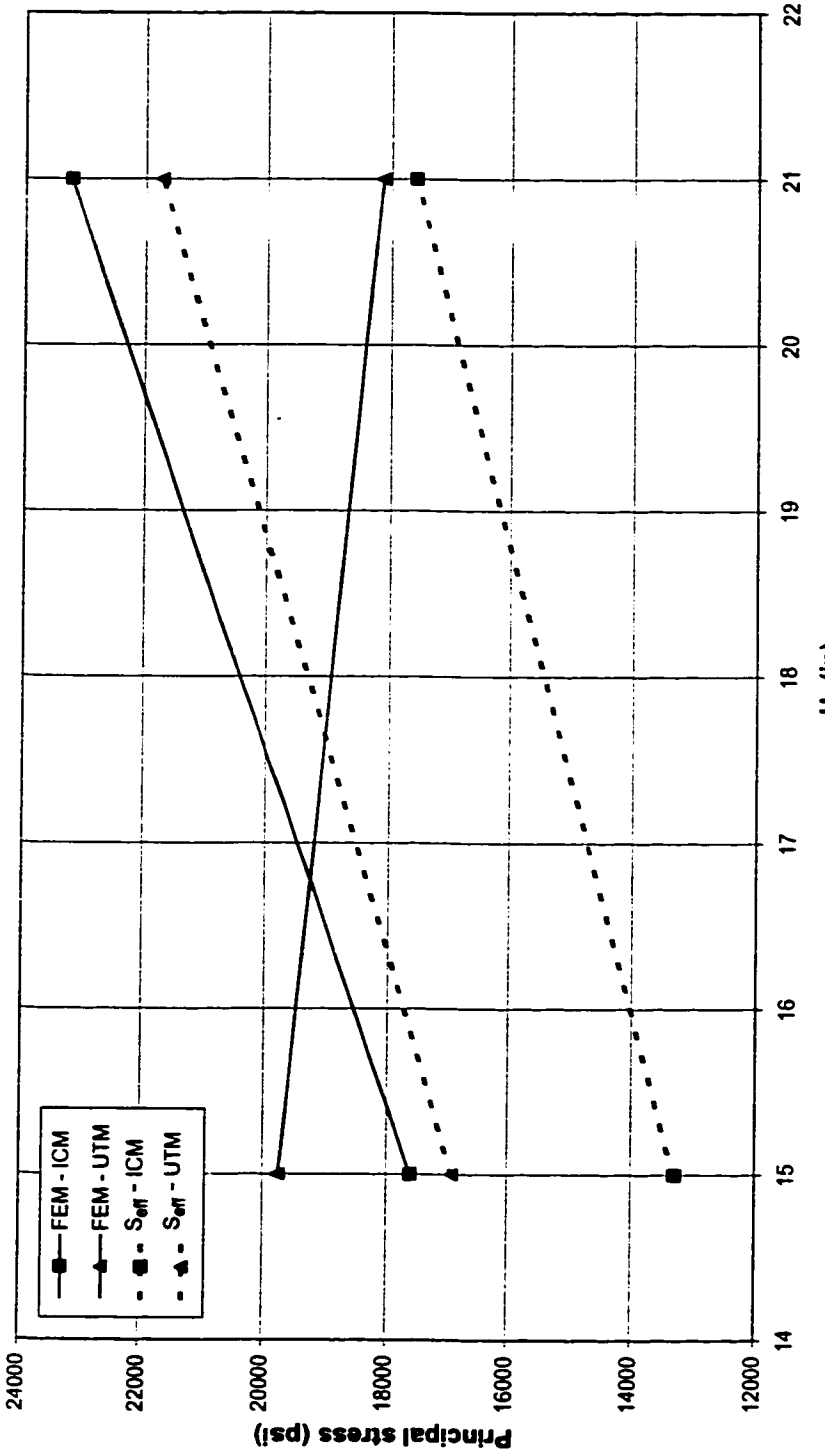

(p) D = 24 in, R_b = 700 ft, θ = 15°

Figure A-2 (Contd.)

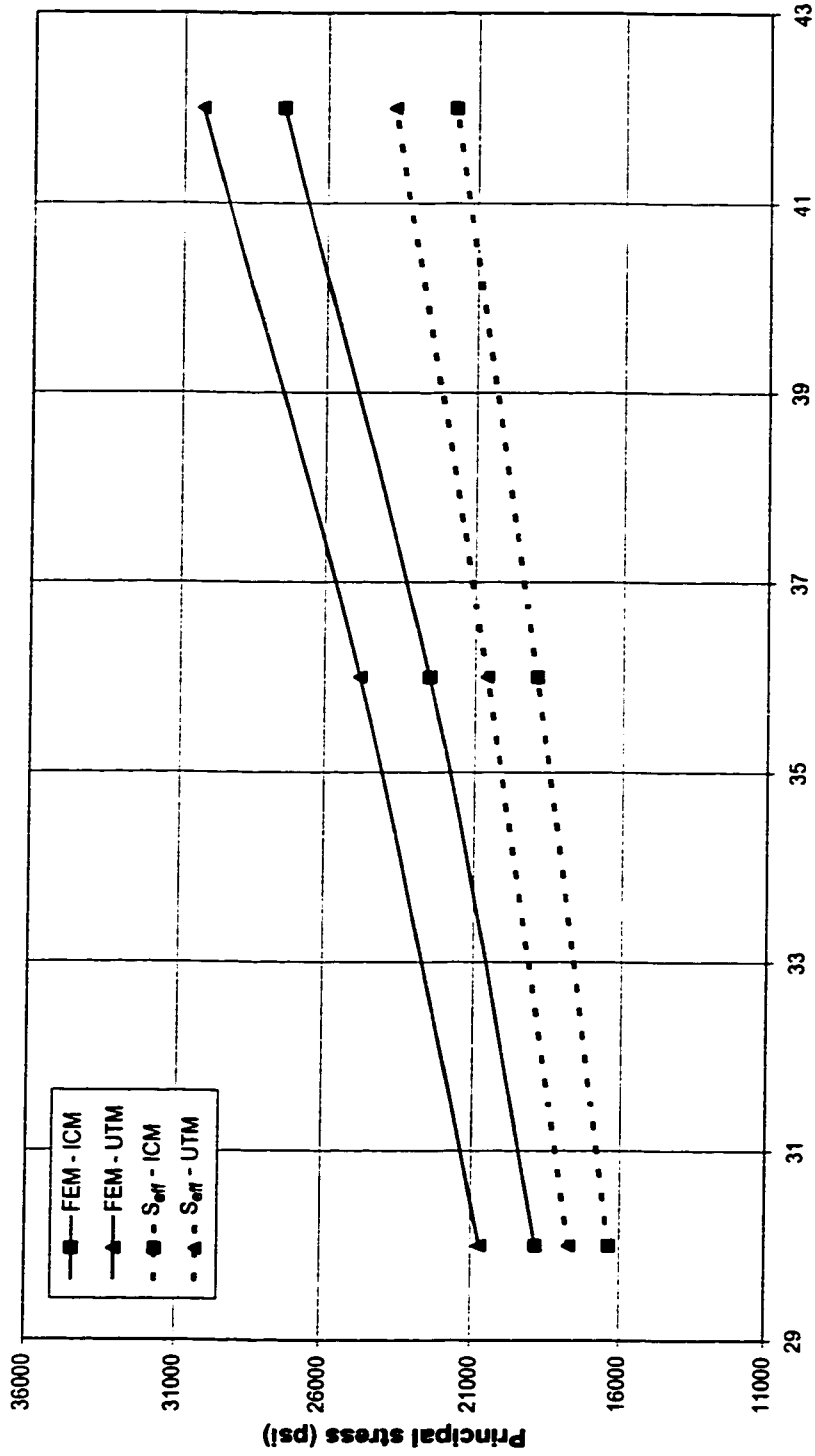

(q) D = 42 in, R_b = 700 ft, θ = 15°

Figure A-2 (Contd.)

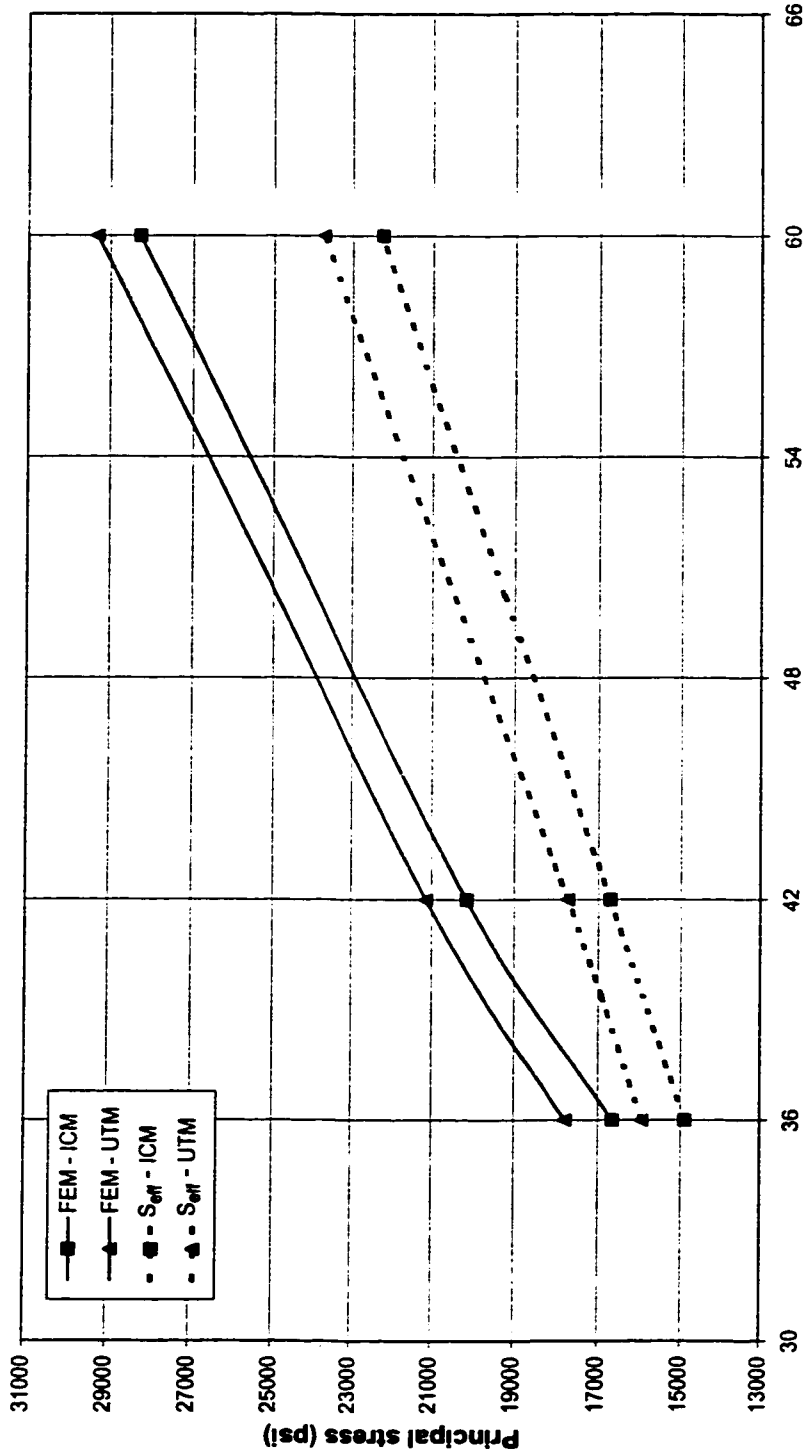

(r) D = 60 in, R_b = 700 ft, θ = 15°

Figure A-2 (Contd.)

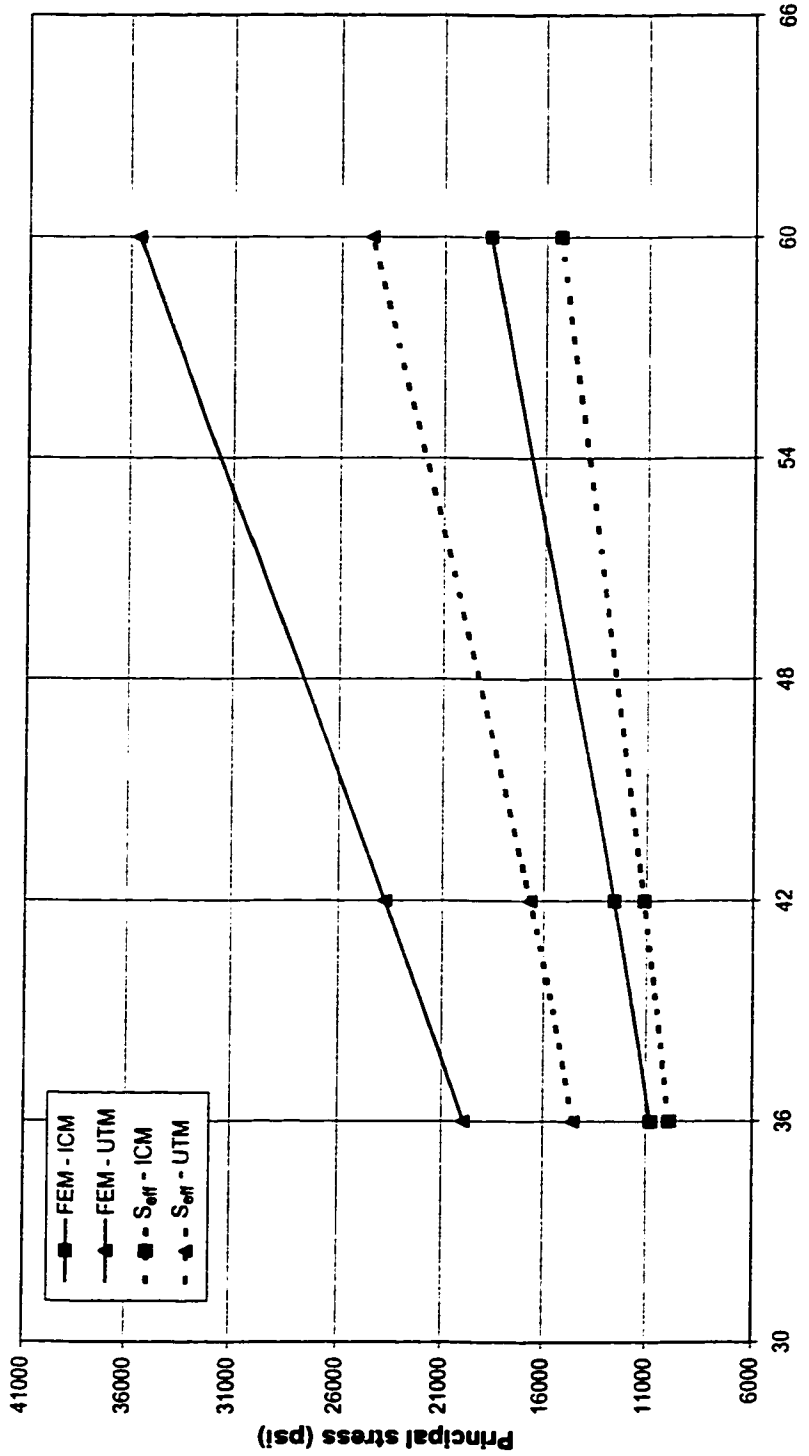

(s) D = 24 in, R_b = 50 ft, $\theta = 8^\circ$

Figure A-2 (Contd.)

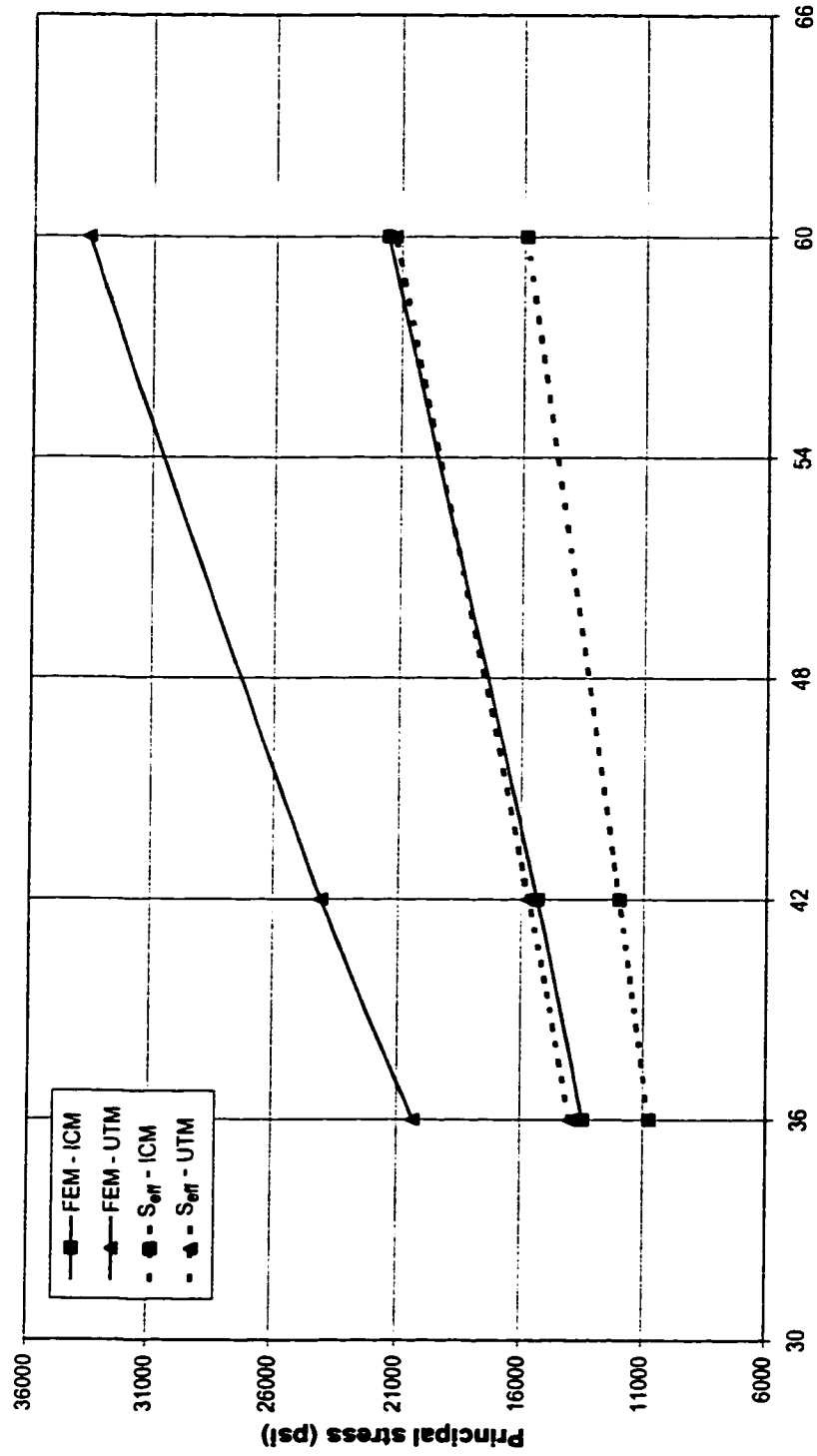

(t) D = 42 in, R_b = 50 ft, $\theta = 8^\circ$

Figure A-2 (Contd.)

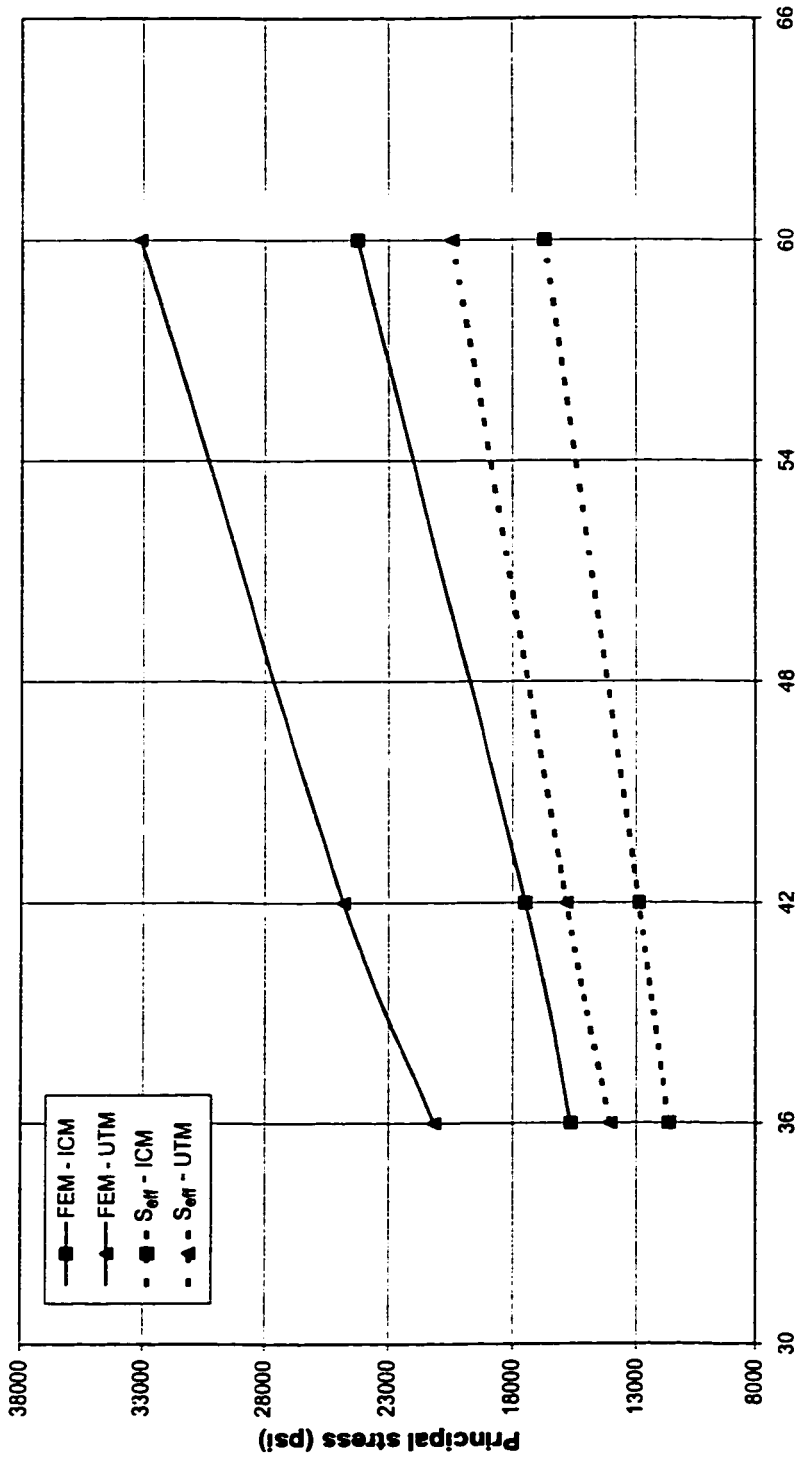

(u) D = 60 in, R_b = 50 ft, θ = 8°

Figure A-2 (Contd.)

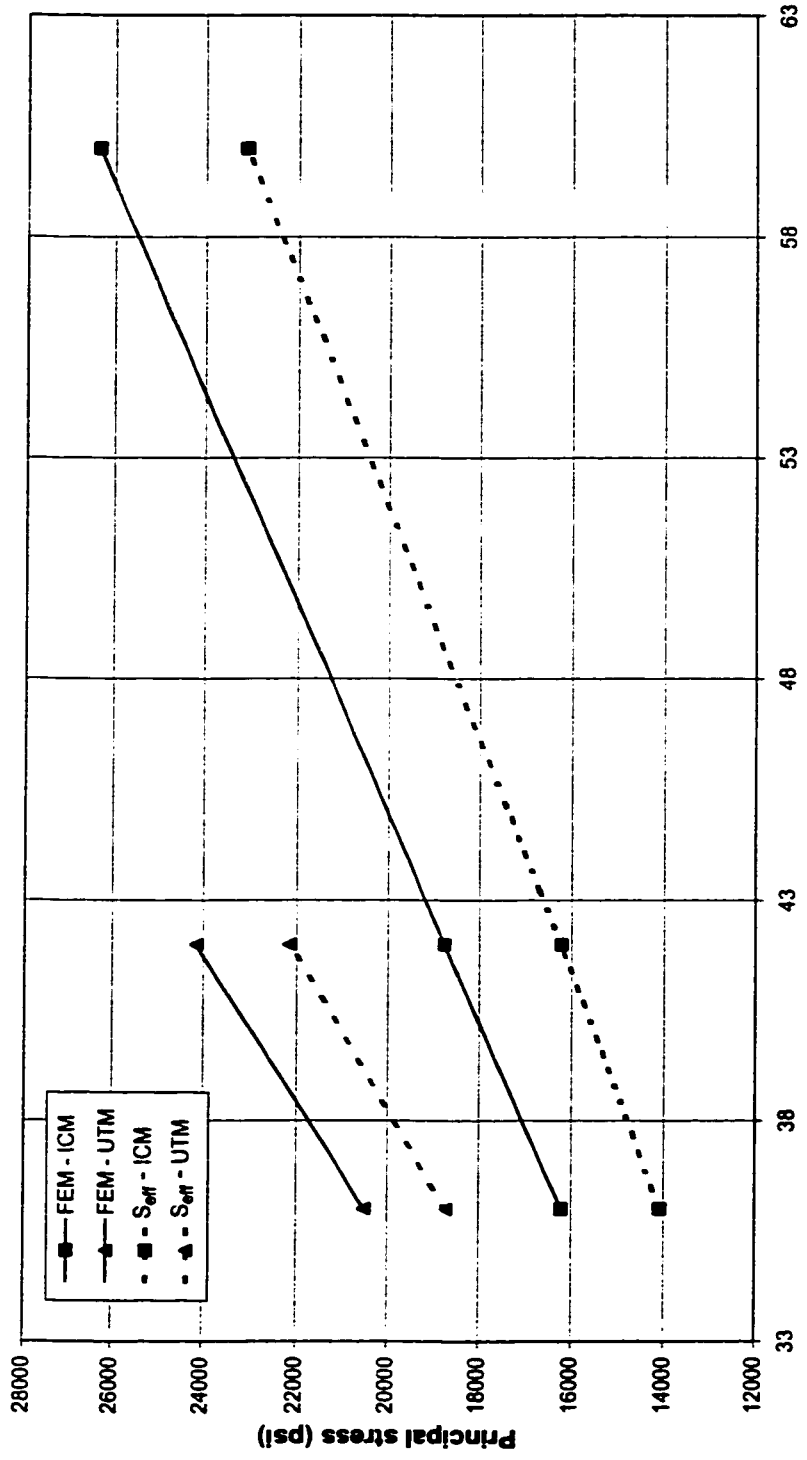

(v) D = 24 in, R_b = 300 ft, $\theta = 8^\circ$

Figure A-2 (Contd.)

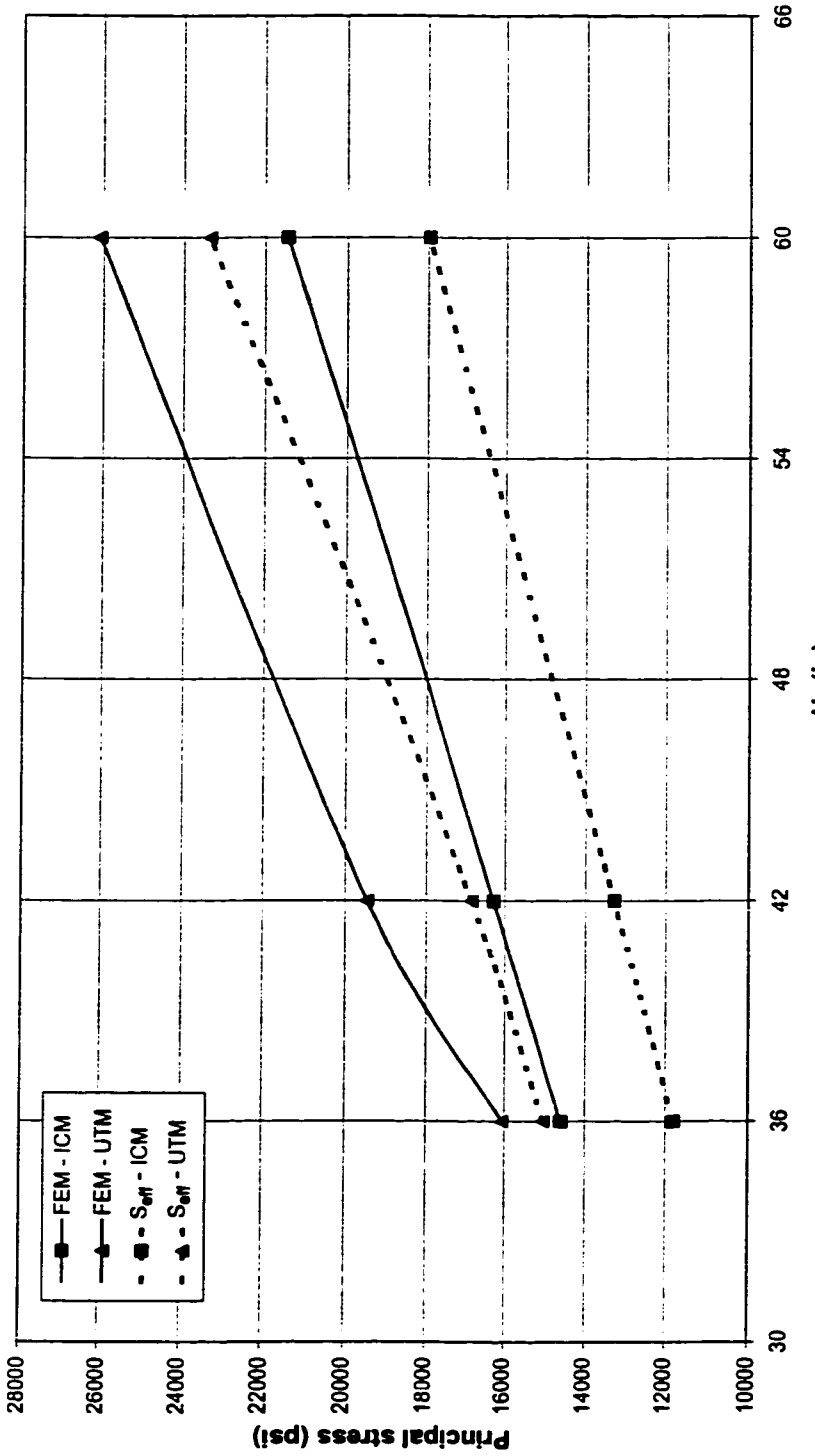

(w) D = 42 in, R_b = 300 ft, $\theta = 8^\circ$

Figure A-2 (Contd.)

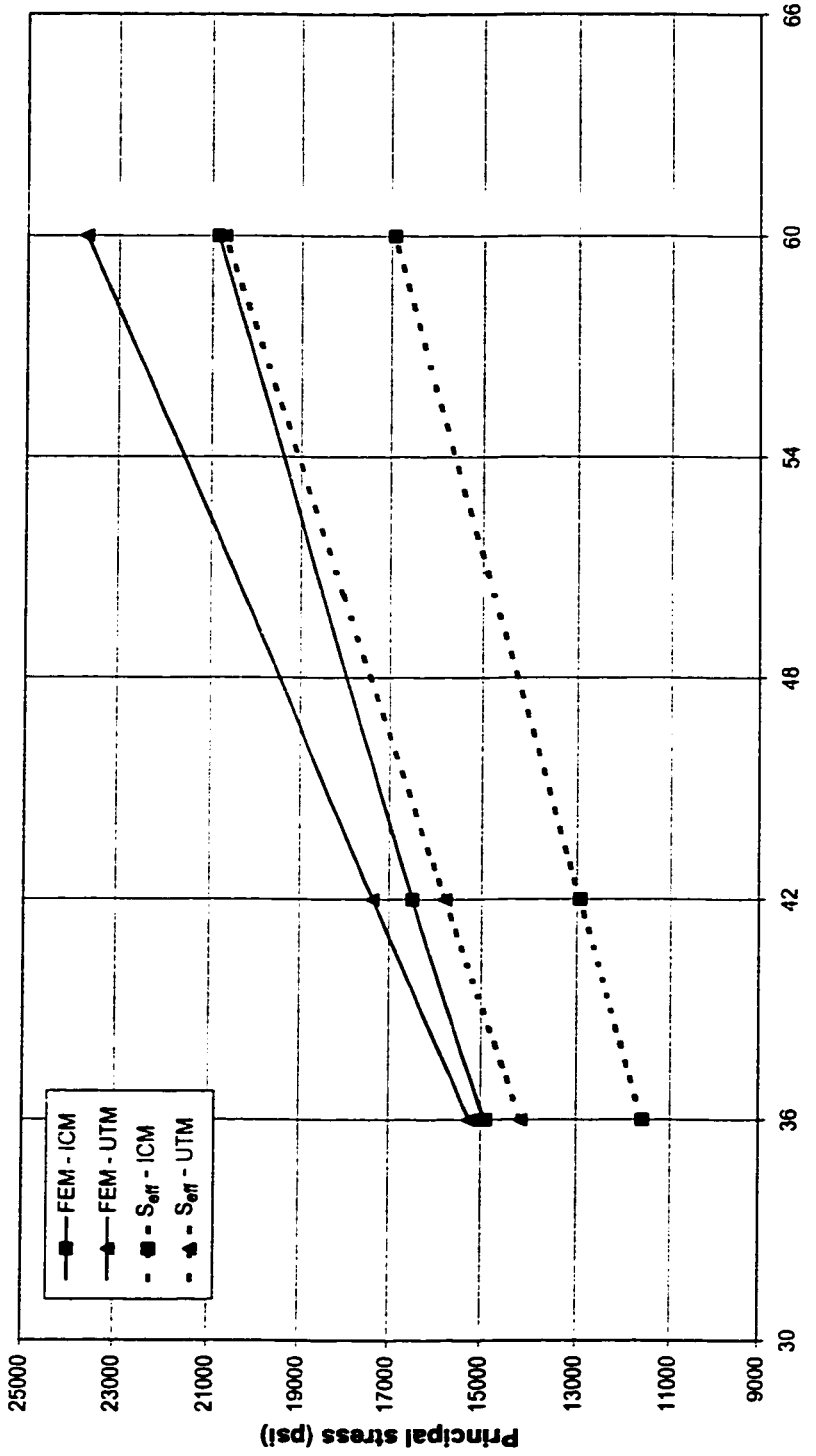

(x) D = 60 in, R_b = 300 ft, $\theta = 8^\circ$

Figure A-2 (Contd.)

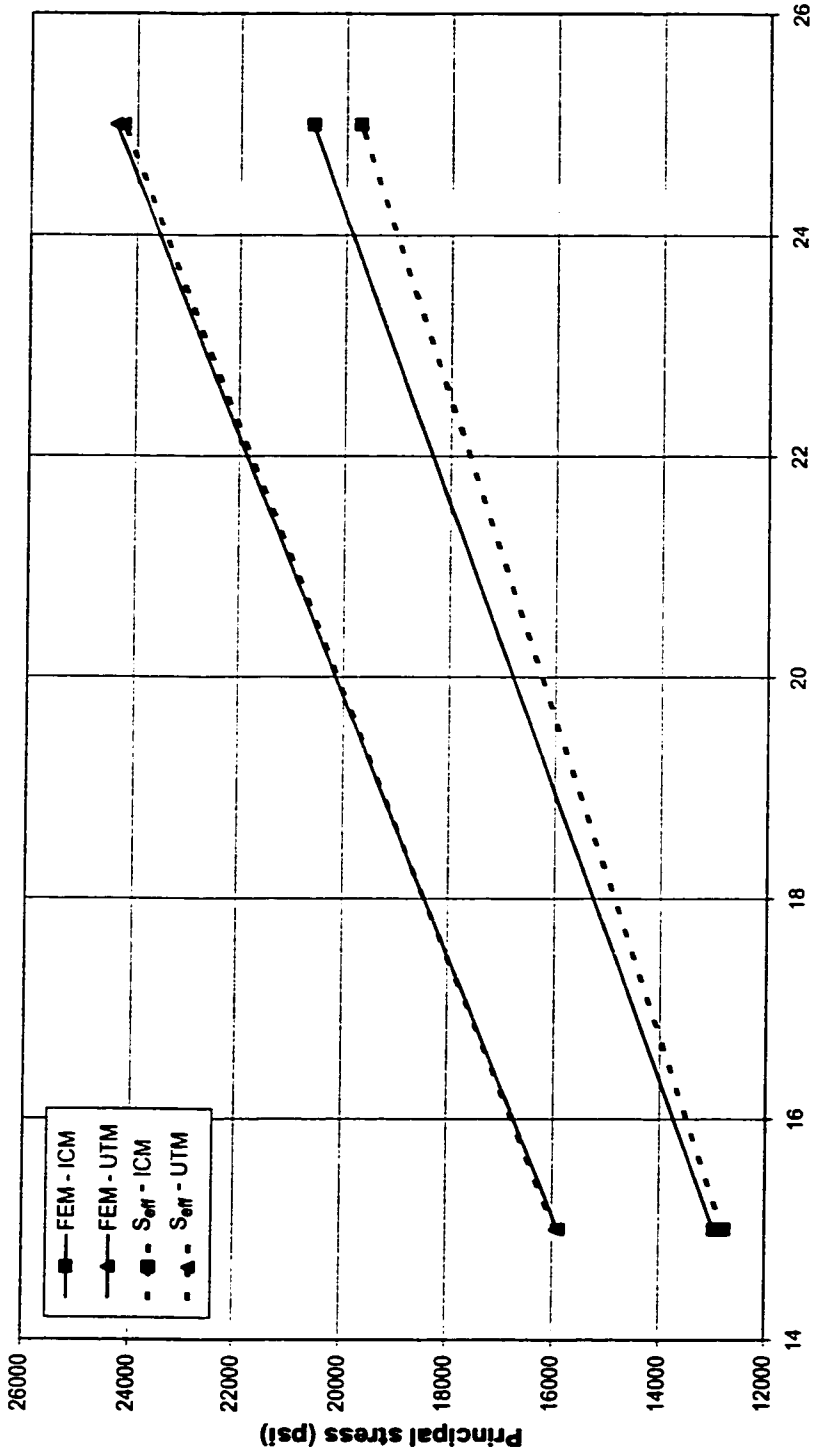

(y) D = 24 in, R_b = 700 ft, $\theta = 8^\circ$

Figure A-2 (Contd.)

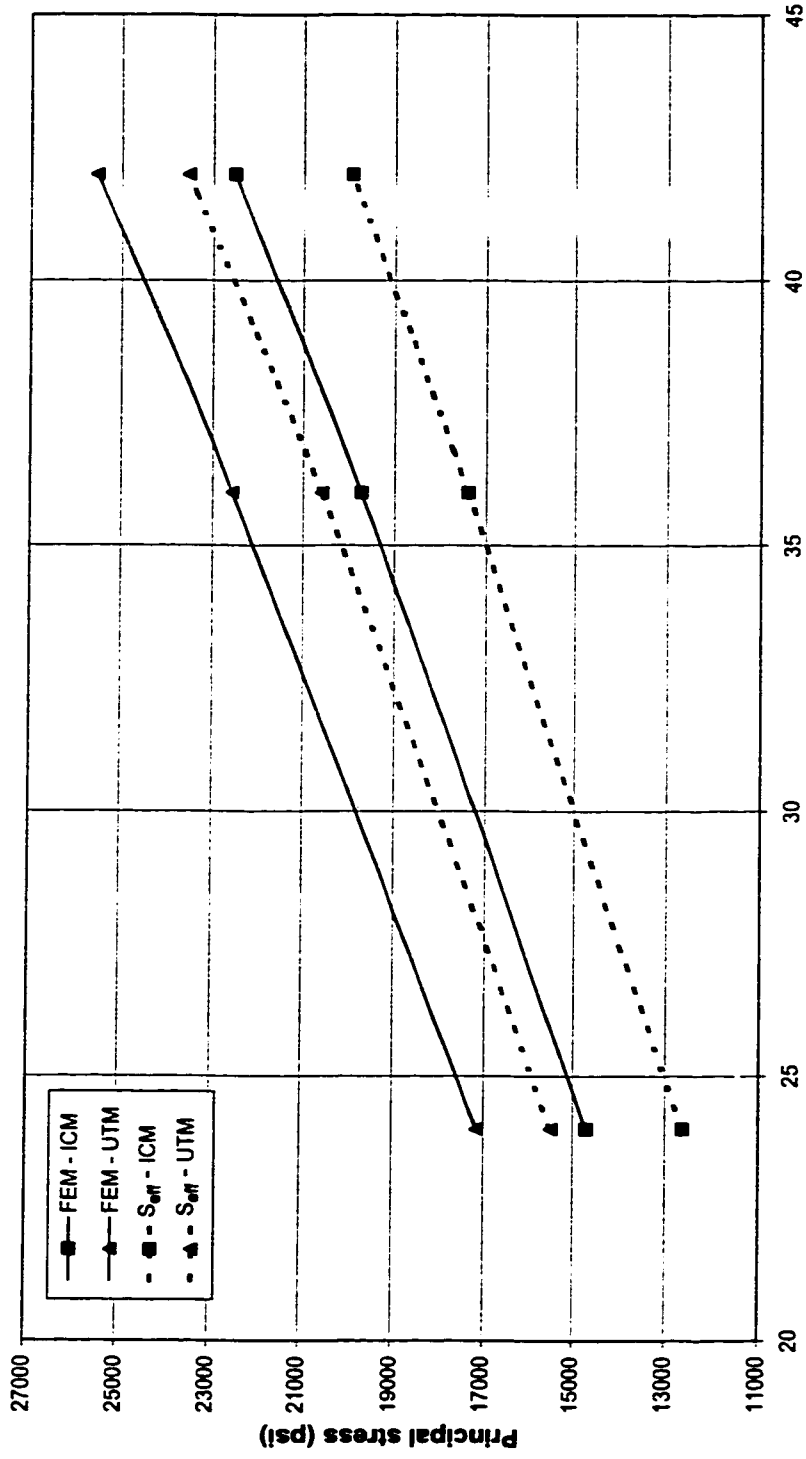

(z) D = 42 in, R_b = 700 ft, $\theta = 8^\circ$

Figure A-2 (Contd.)

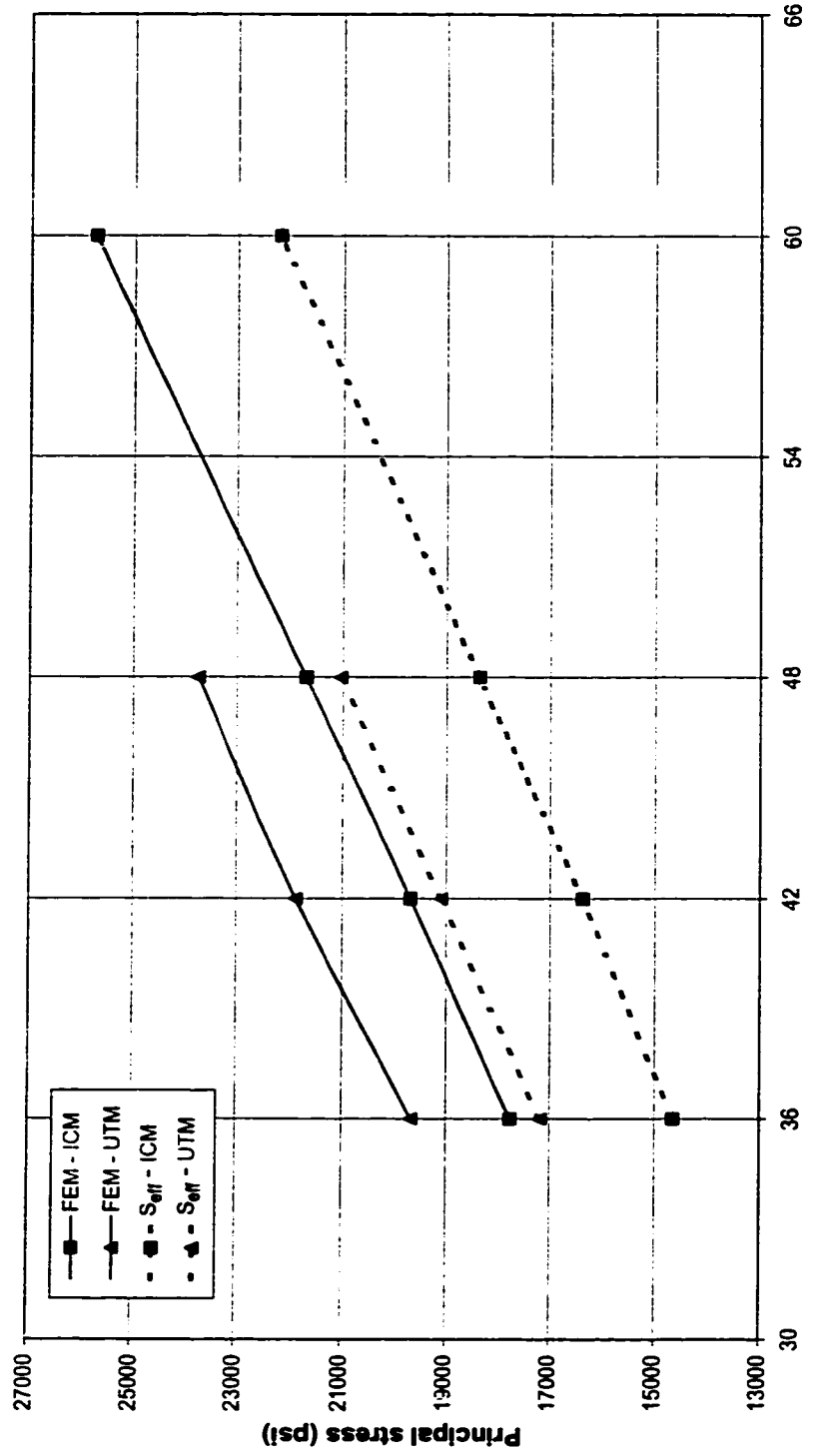

(aa) D = 60 in, R_b = 700 ft, $\theta = 8^\circ$

Figure A-2 (Contd.)

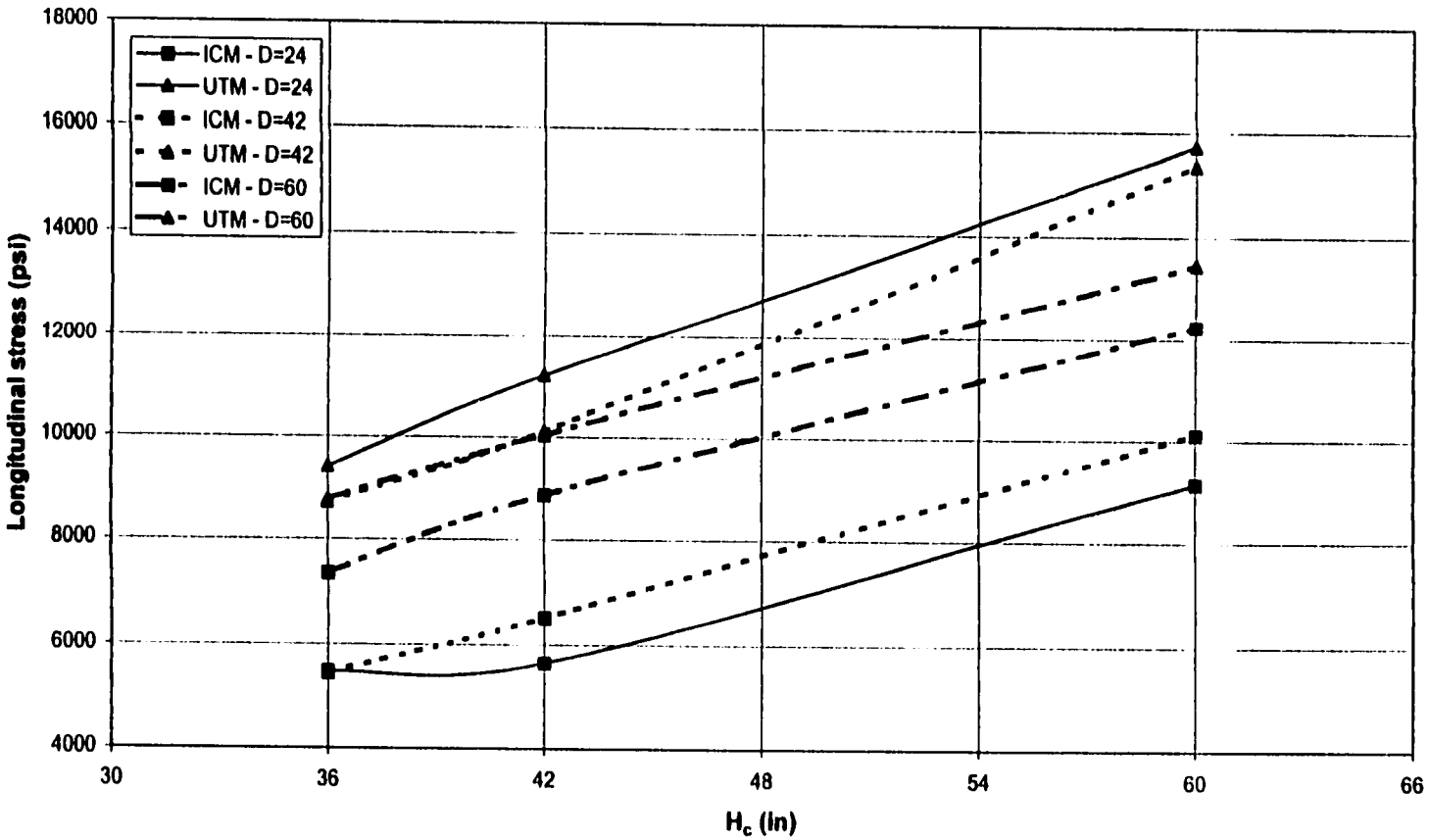

(a) R_b = 50 ft, θ = 20°

Figure A-3 The effect of cover height on the longitudinal stresses

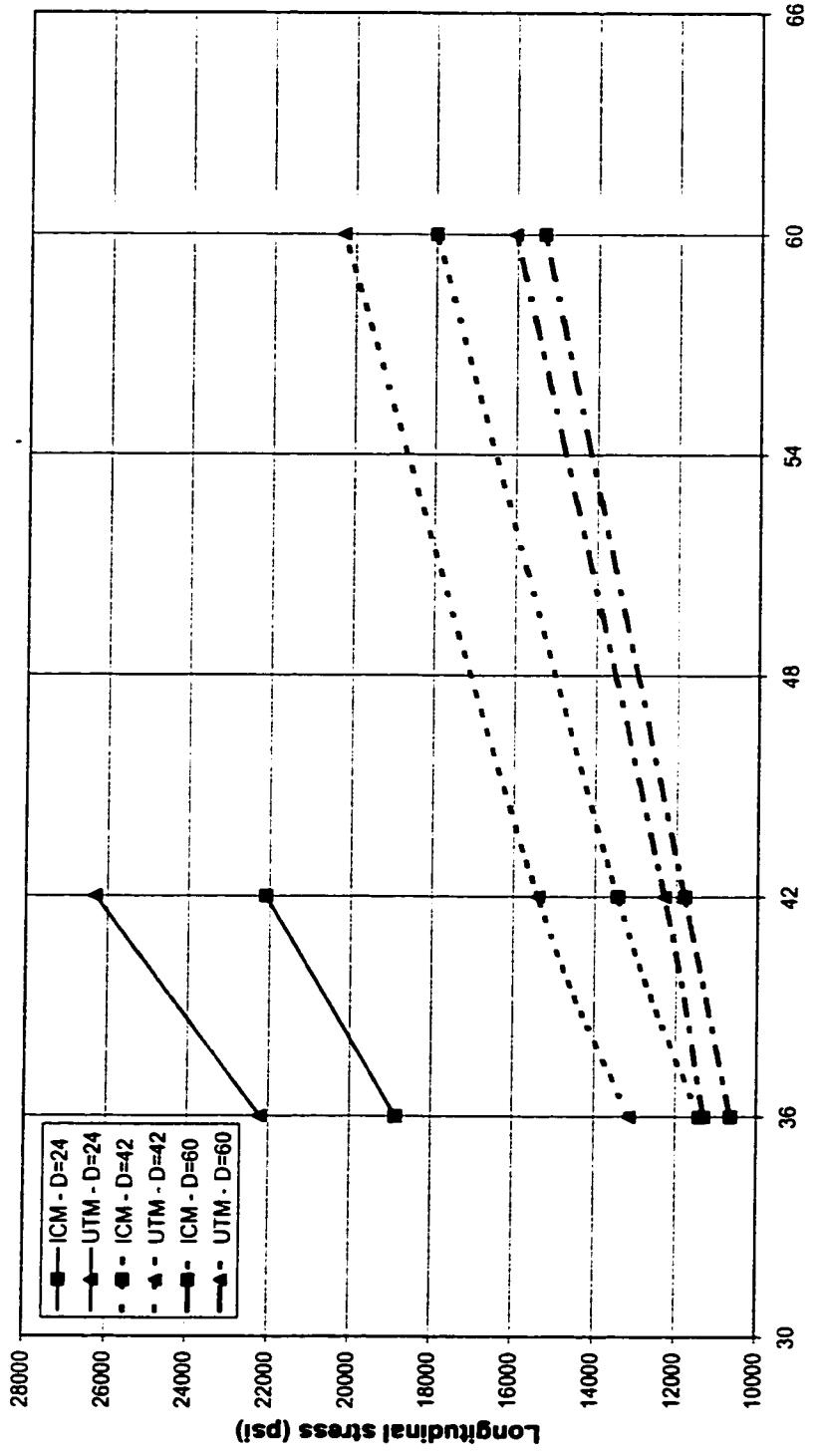

(b) R_b = 300 ft, $\theta = 20^\circ$

Figure A-3 (Contd.)

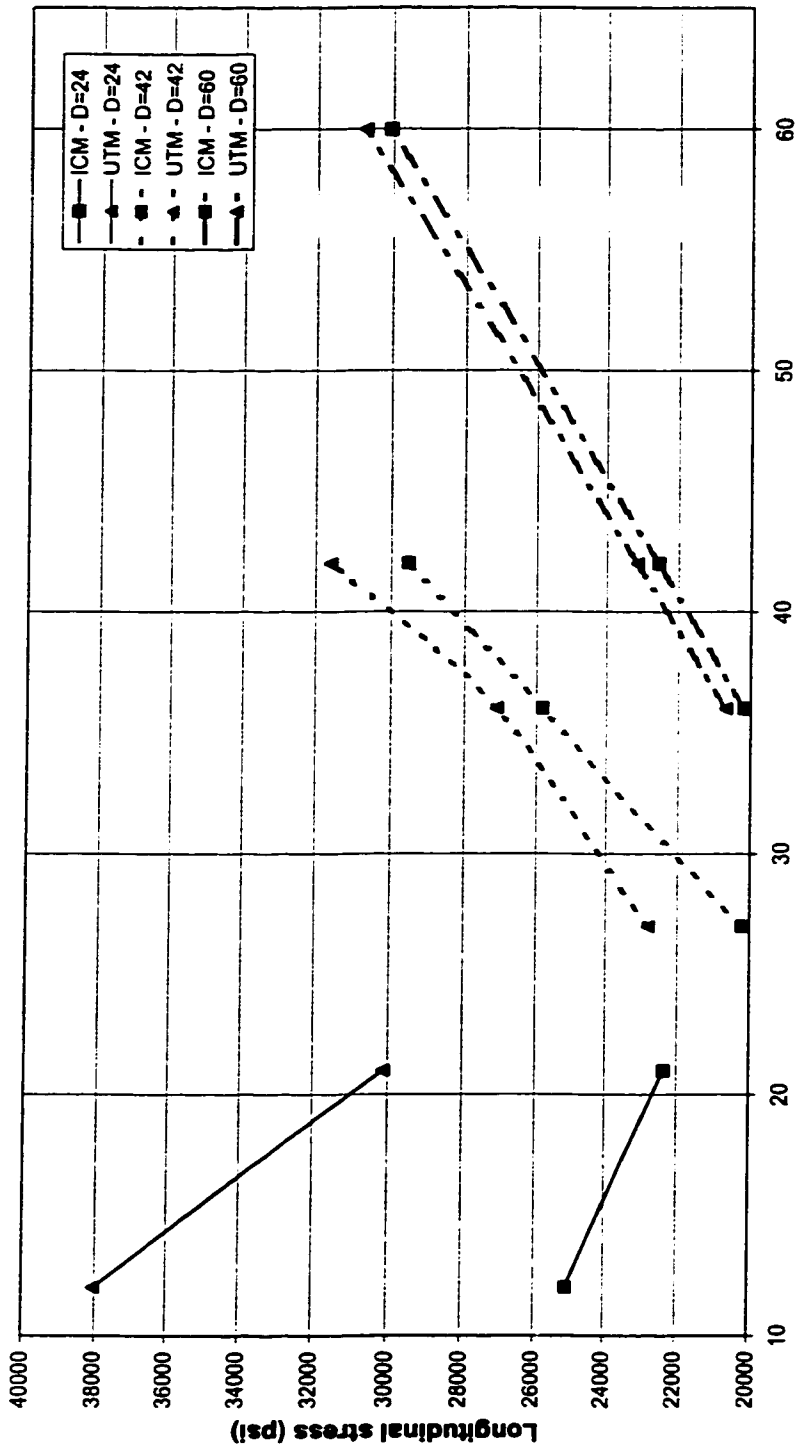

(c) R_b = 700 ft, θ = 20°

Figure A-3 (Contd.)

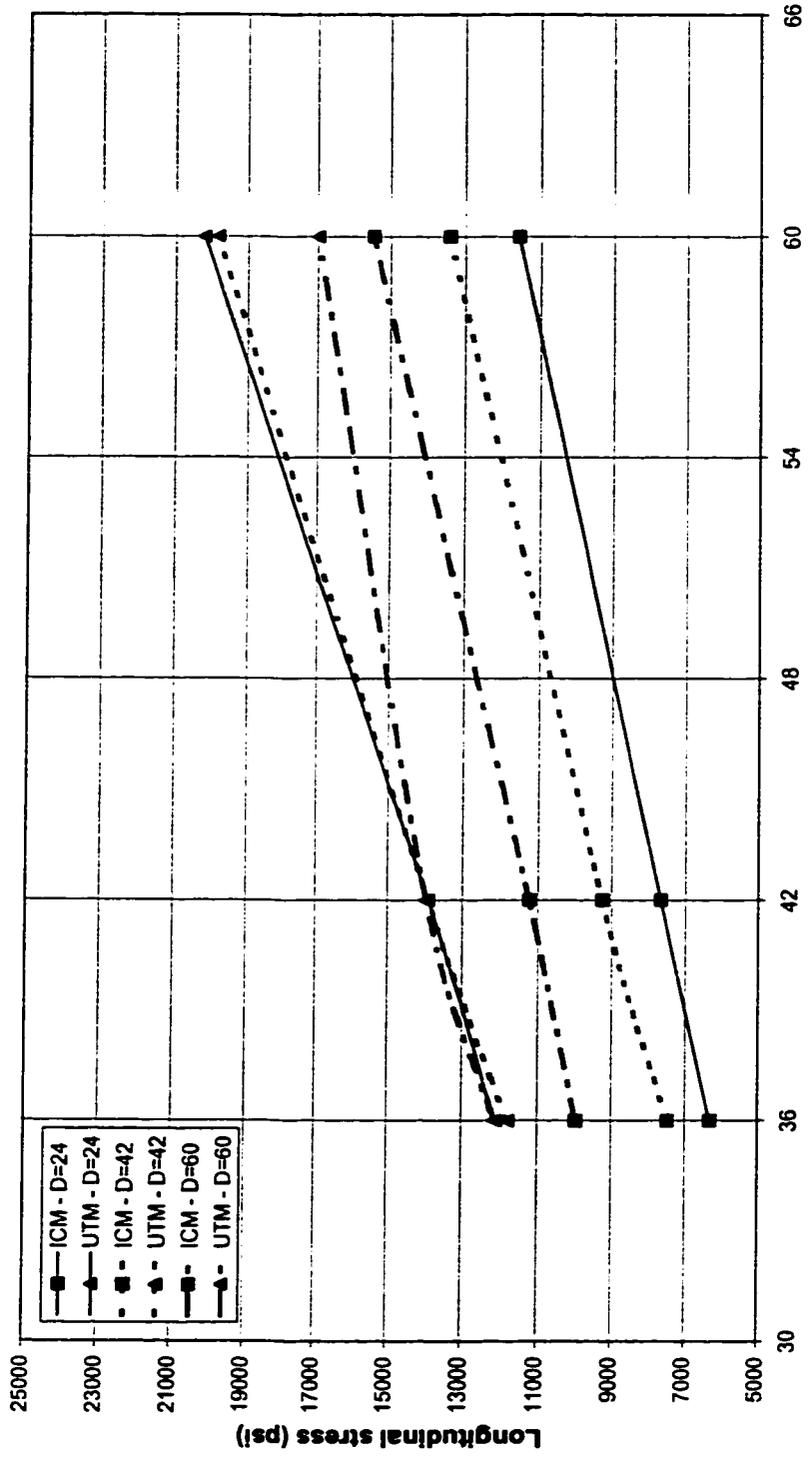

(d) R_b = 50 ft, θ = 15°

Figure A-3 (Contd.)

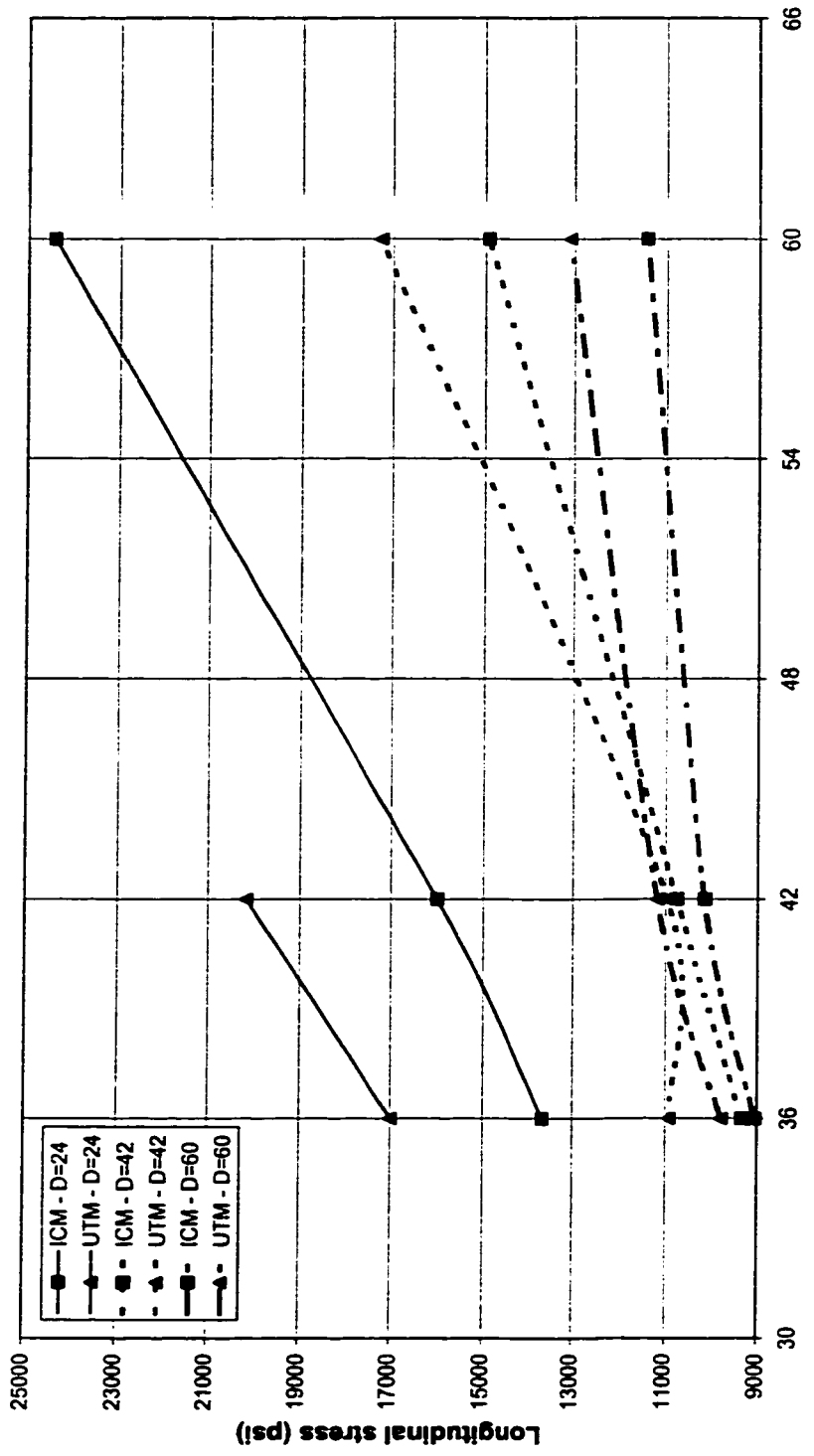

(e) R_b = 300 ft, θ = 15°

Figure A-3 (Contd.)

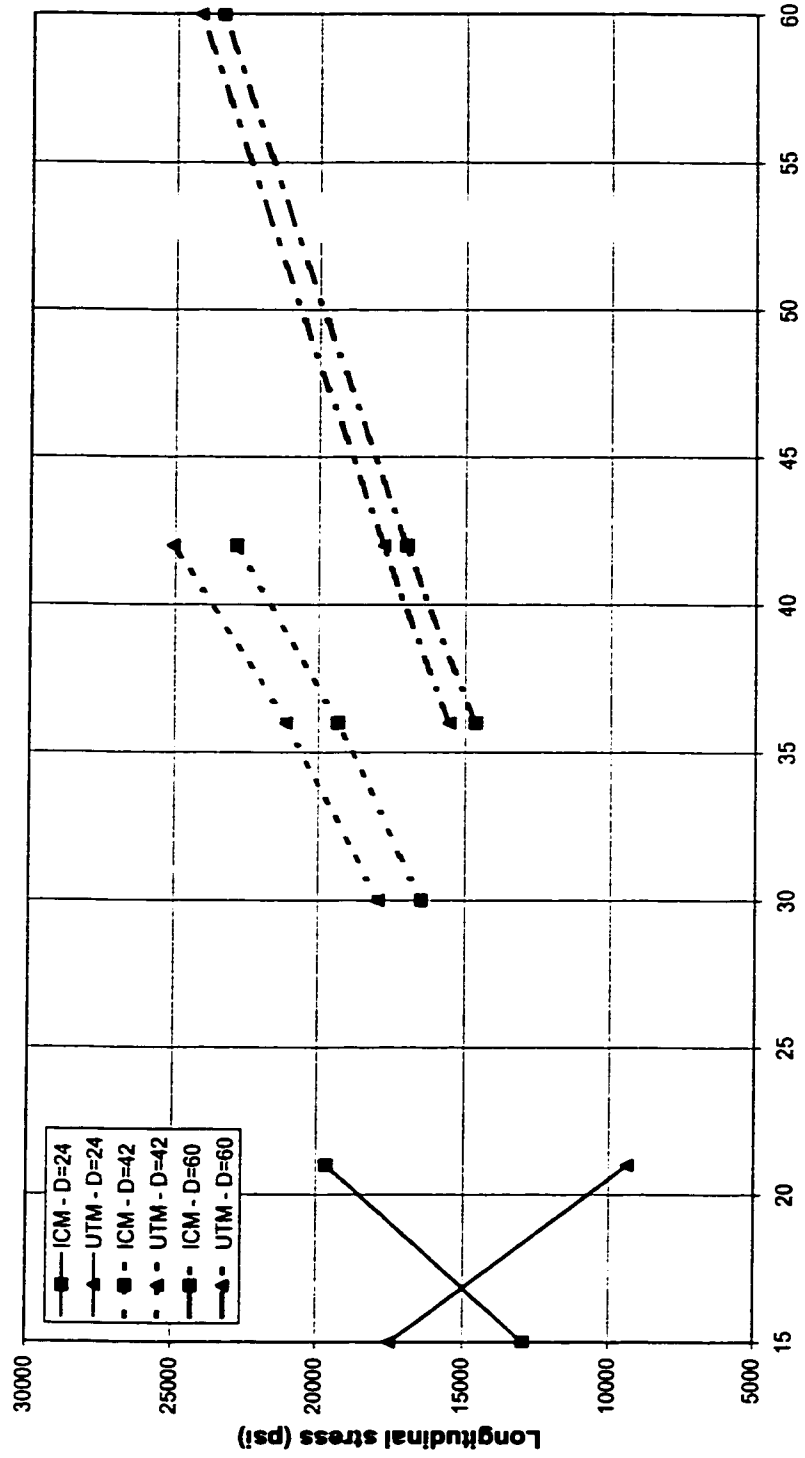

(f) R_b = 700 ft, θ = 15°

Figure A-3 (Contd.)

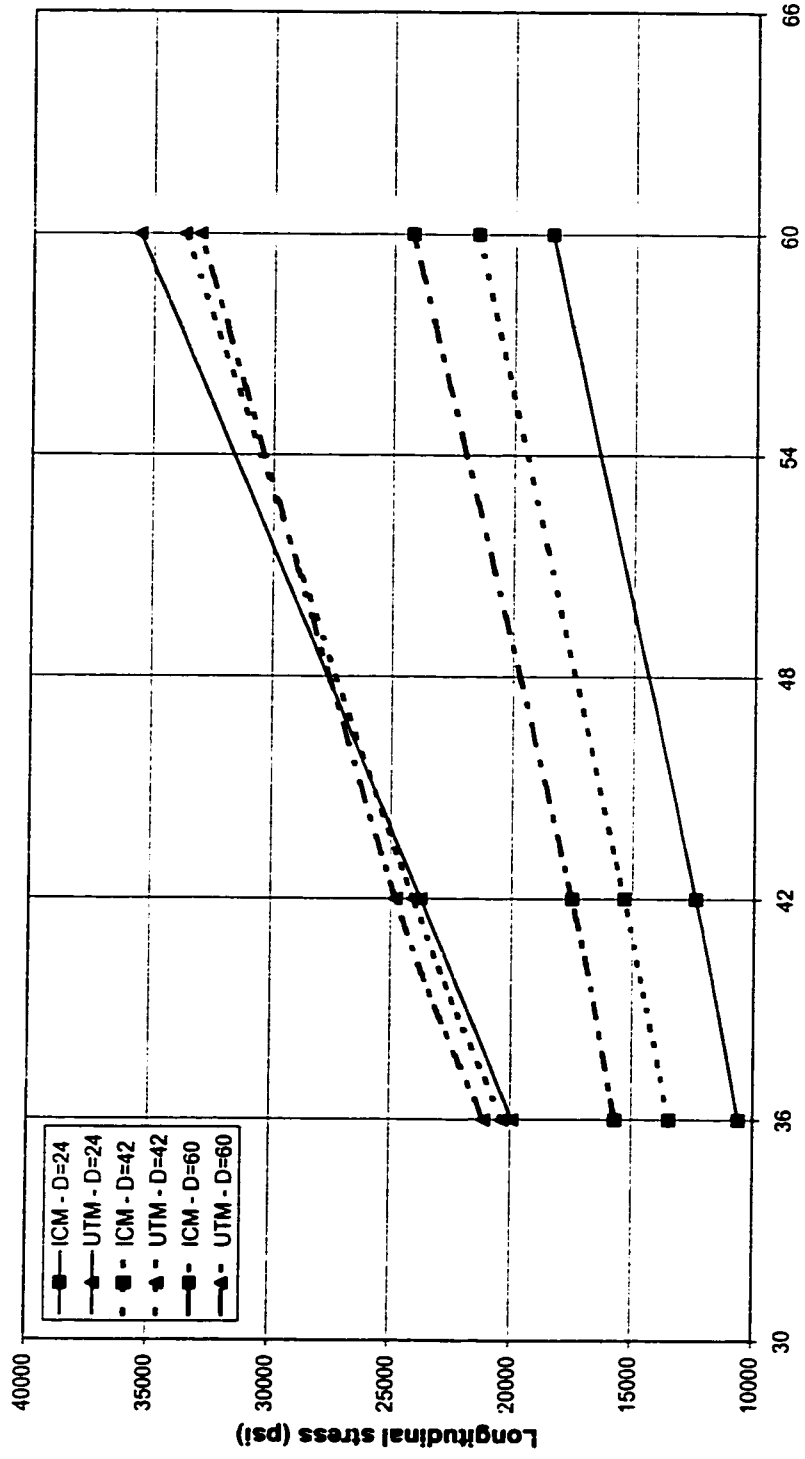

(g) R_b = 50 ft, θ = 8°

Figure A-3 (Contd.)

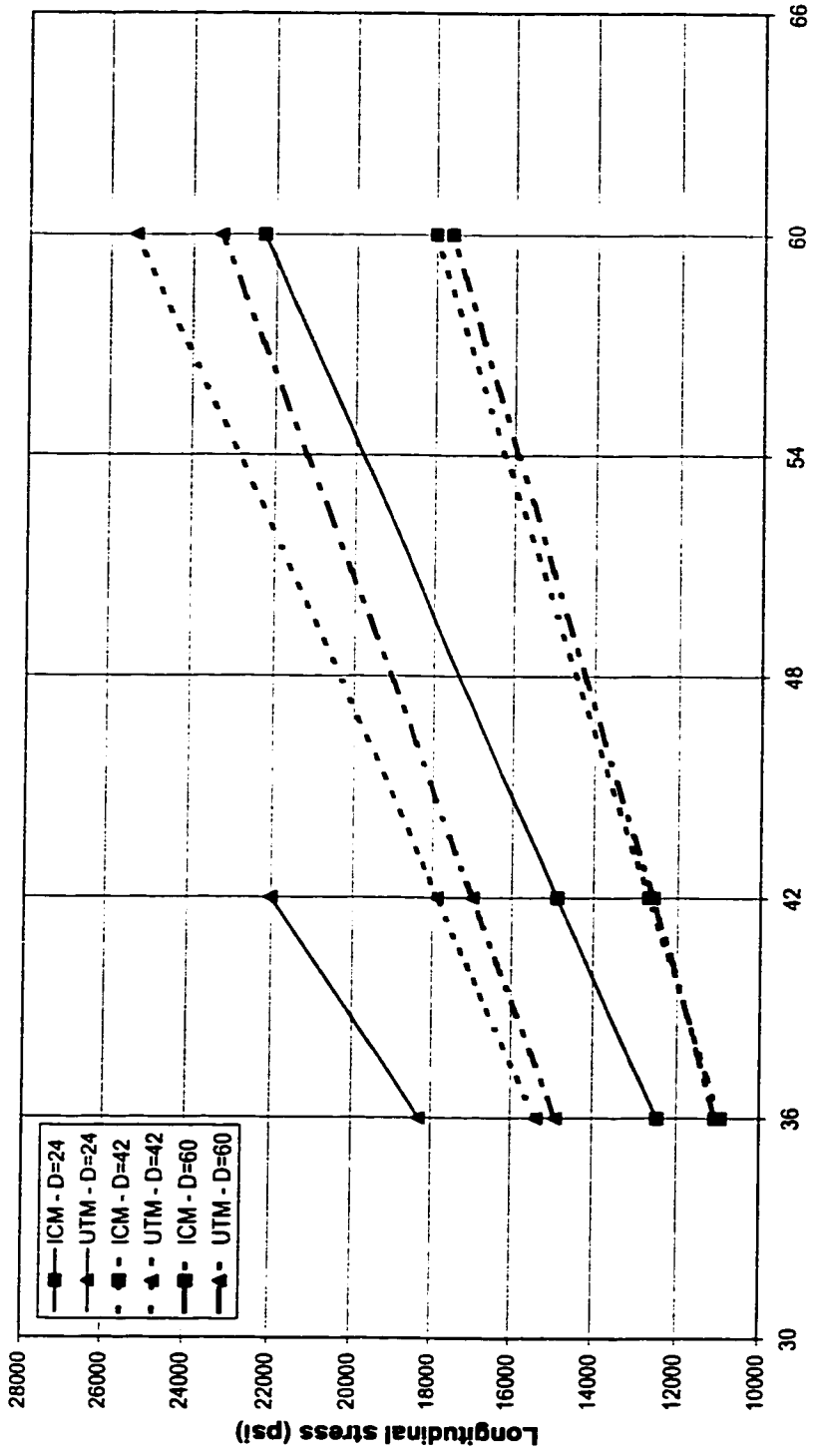

(h) R_b = 300 ft, θ = 8°

Figure A-3 (Contd.)

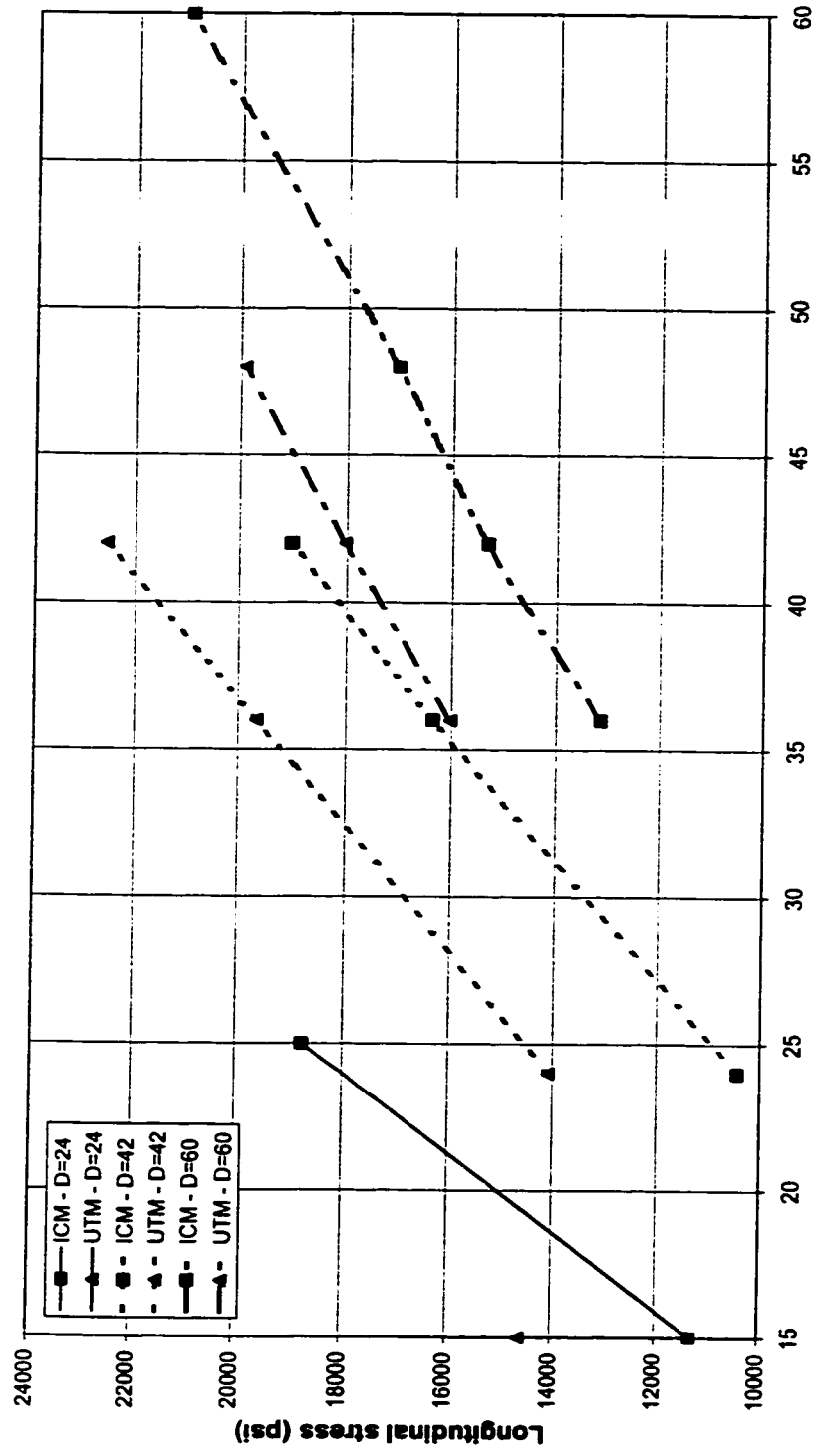

(i) R_b = 700 ft, $\theta = 8°$

Figure A-3 (Contd.)

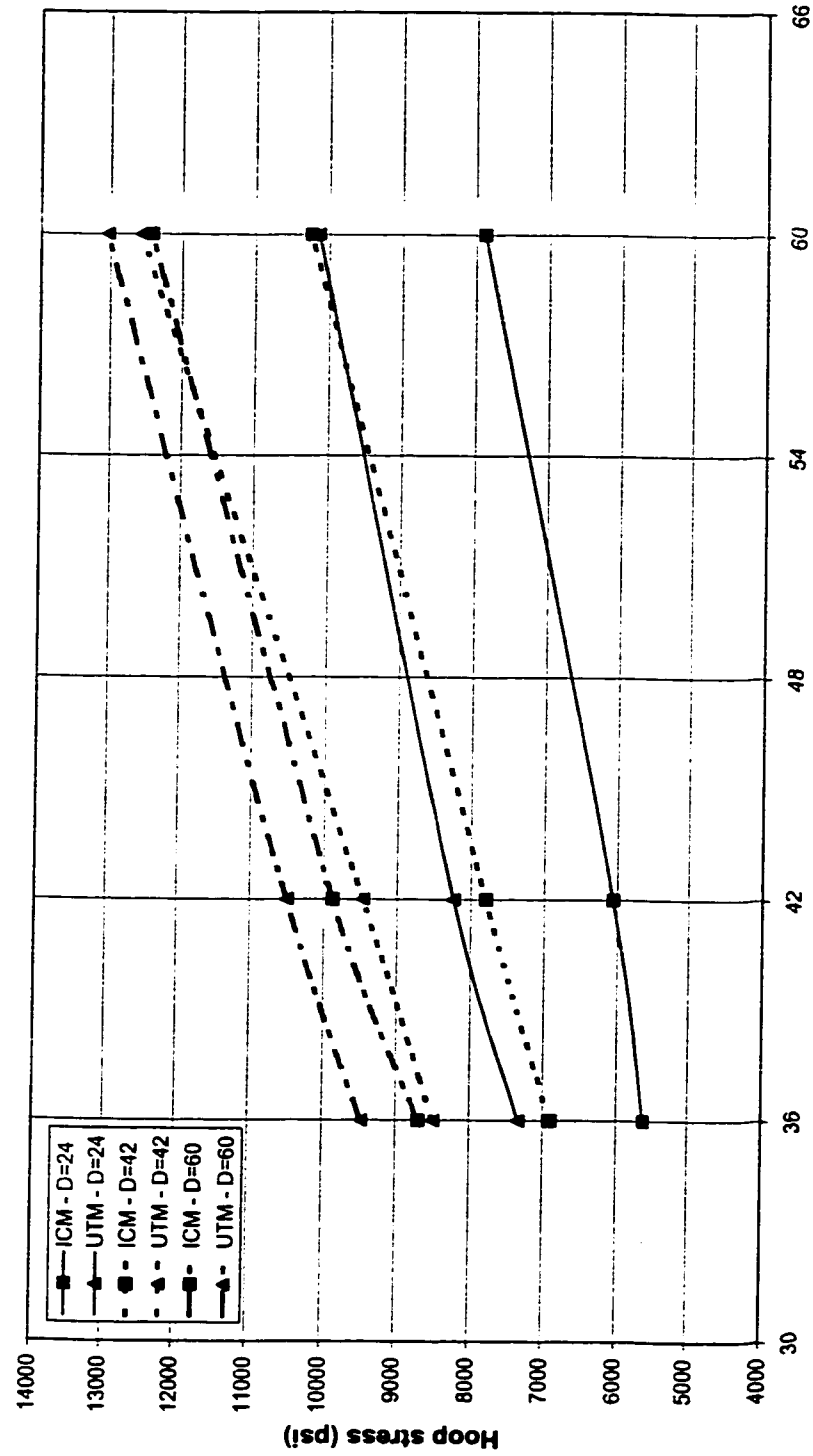

(a) R_b = 50 ft, θ = 20°

Figure A-4 The effect of cover height on the hoop stresses

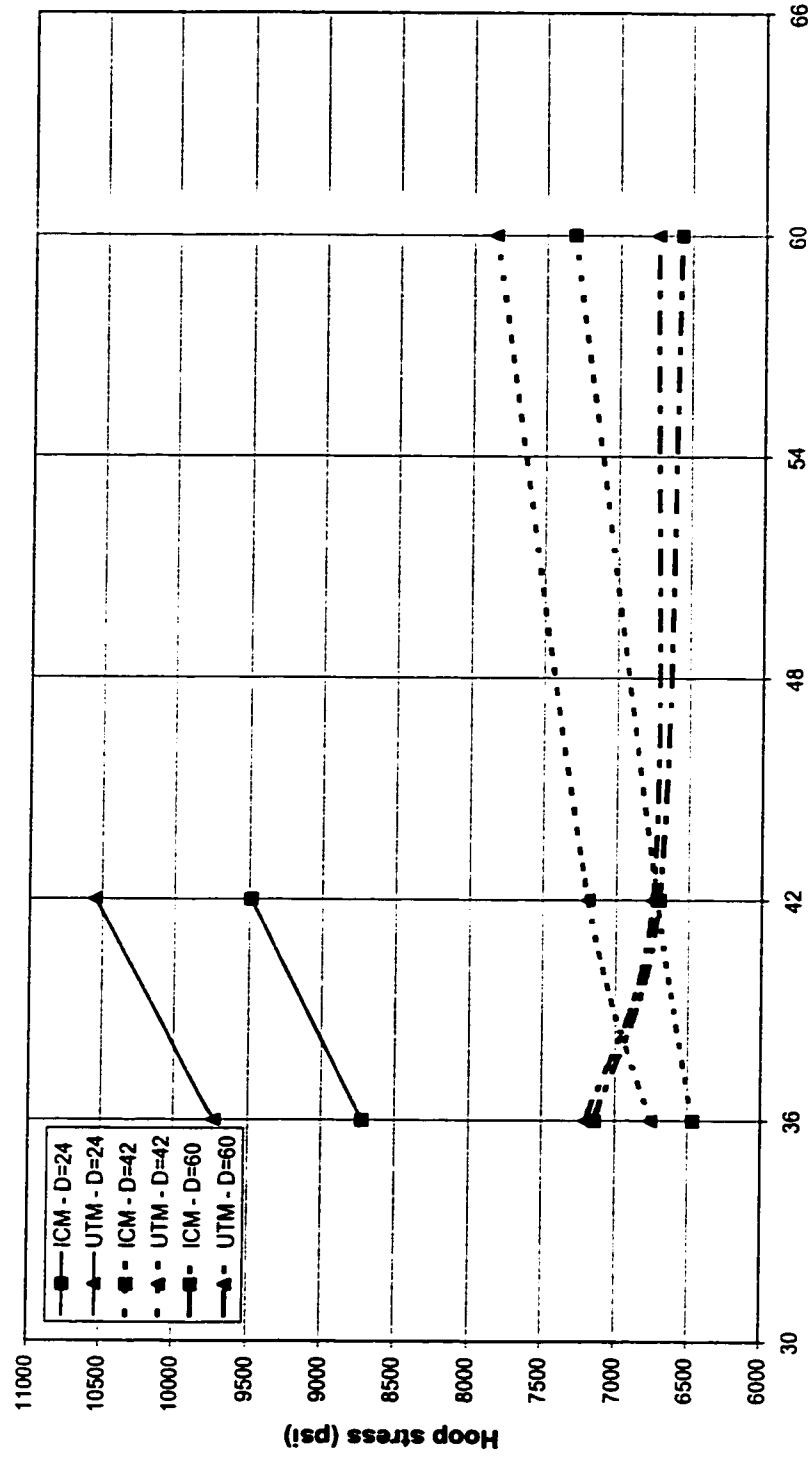

(b) R_b = 300 ft, θ = 20°

Figure A-4 (Contd.)

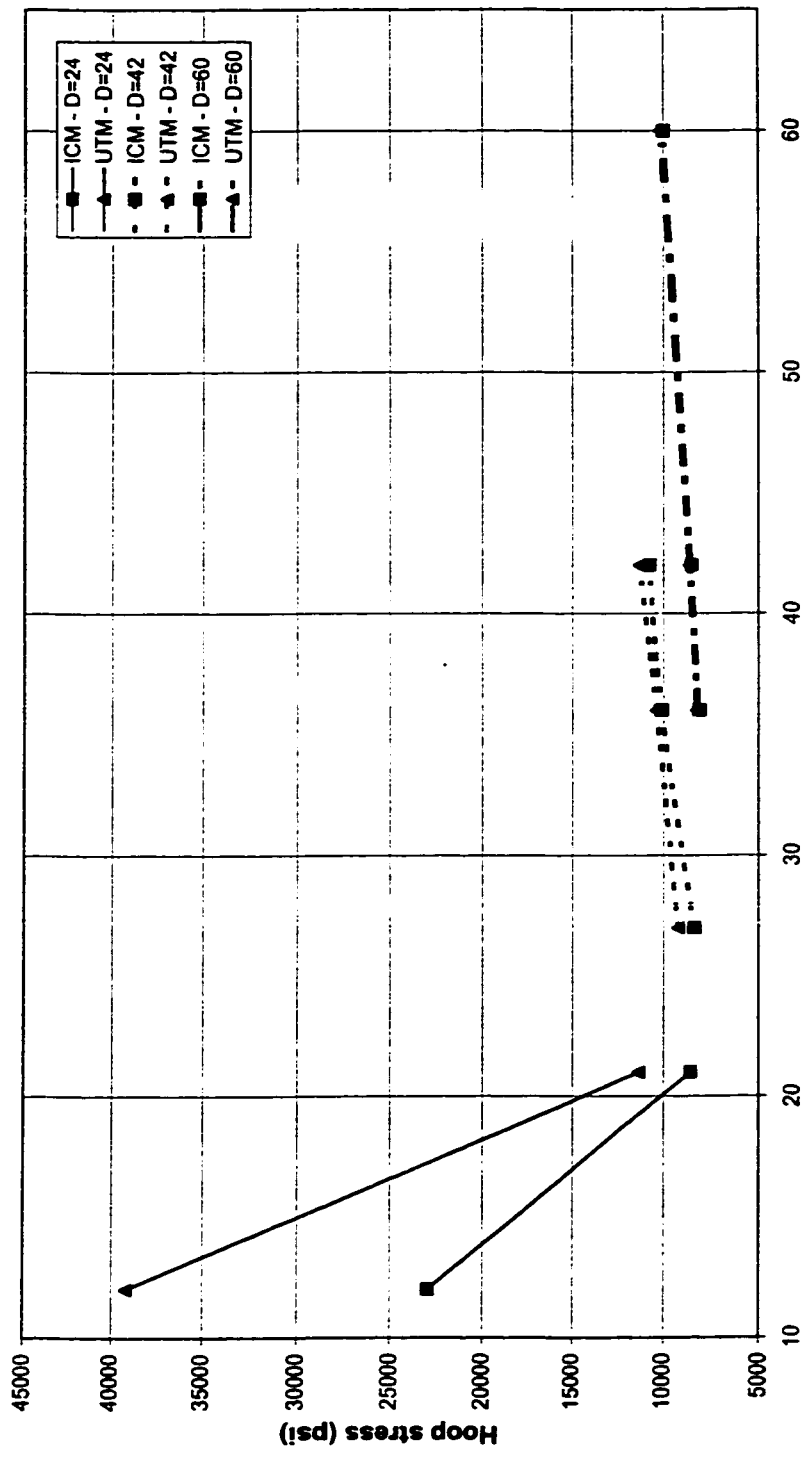

(c) R_b = 700 ft, θ = 20°

Figure A-4 (Contd.)

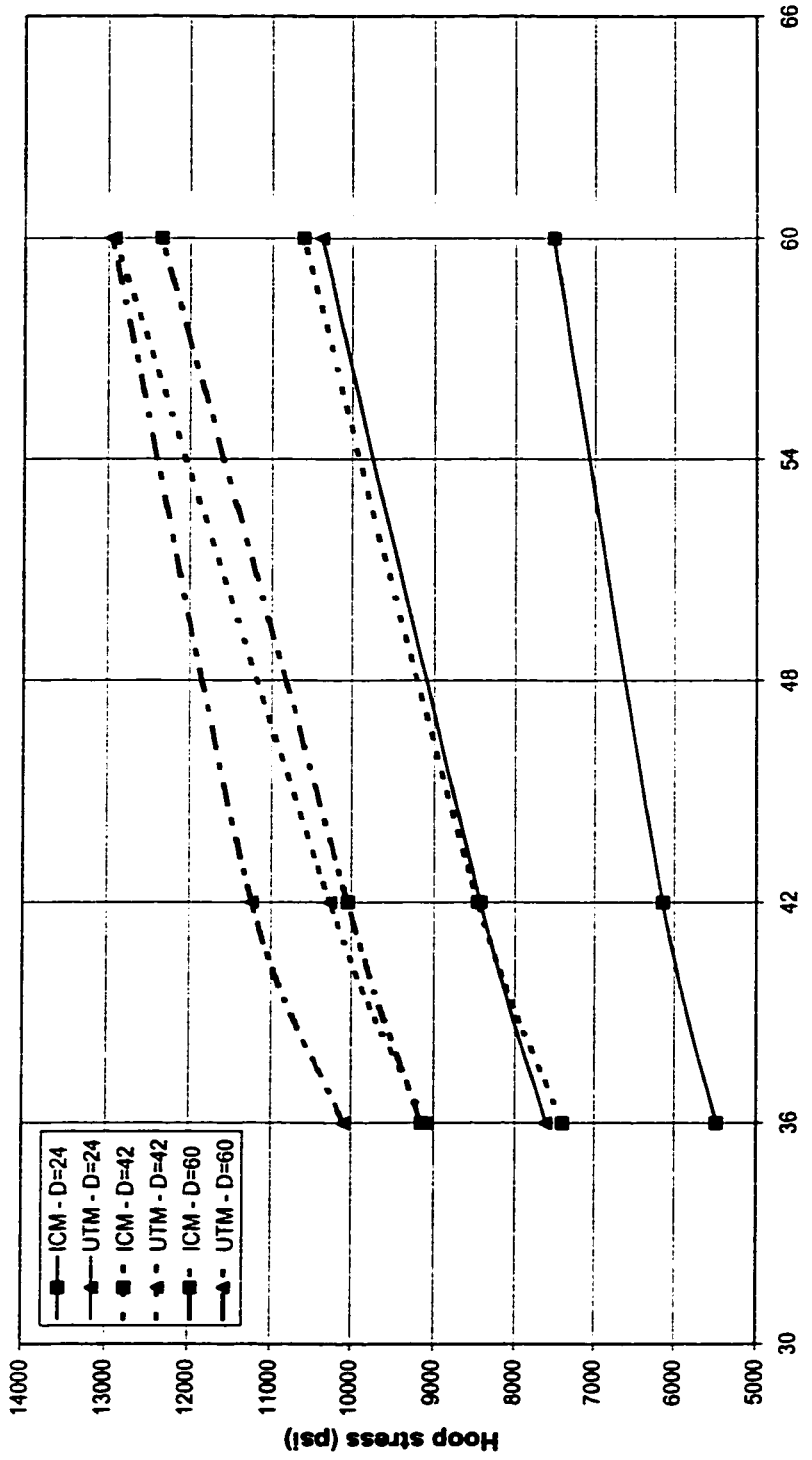

(d) R_b = 50 ft, θ = 15°

Figure A-4 (Contd.)

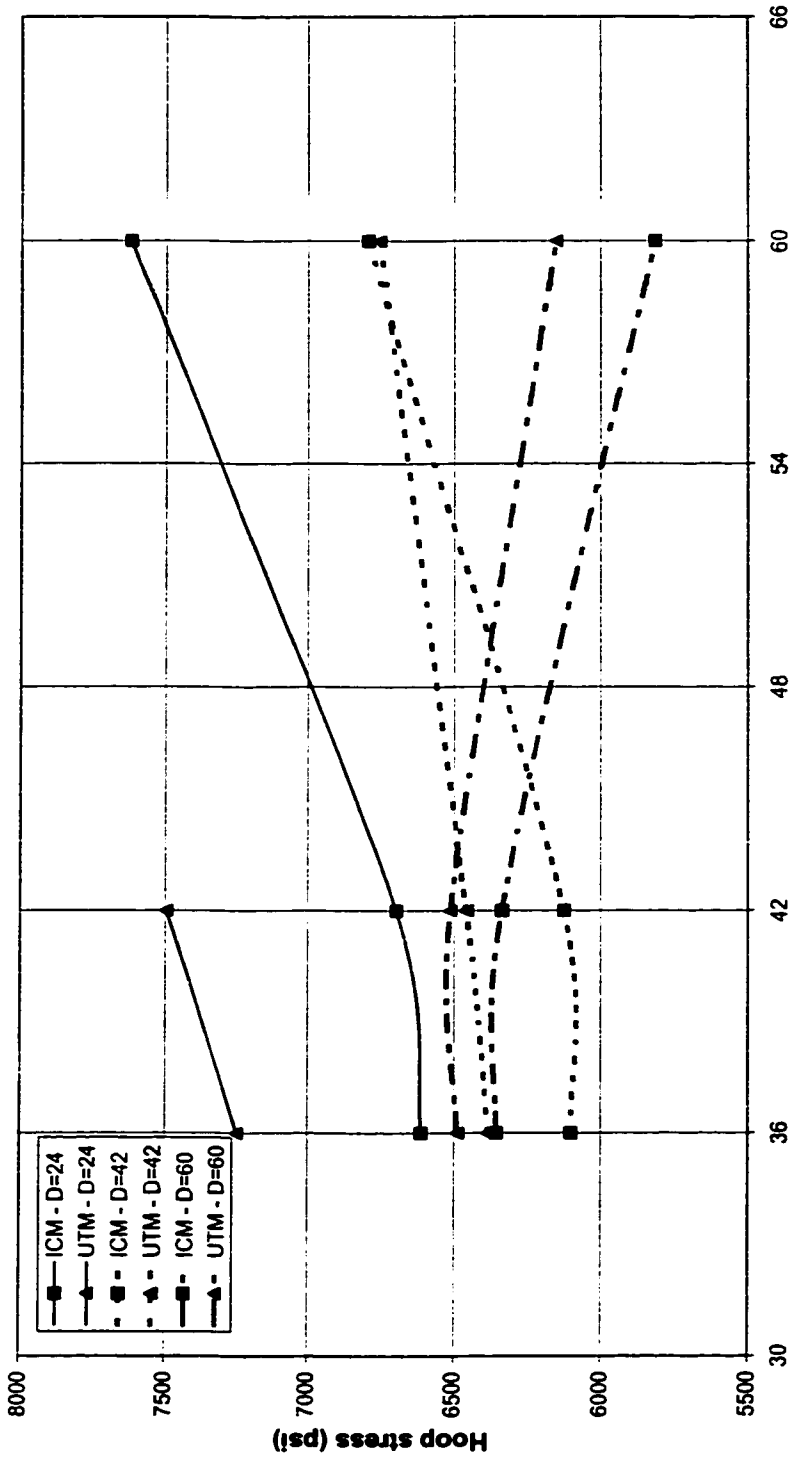

(e) R_b = 300 ft, θ = 15°

Figure A-4 (Contd.)

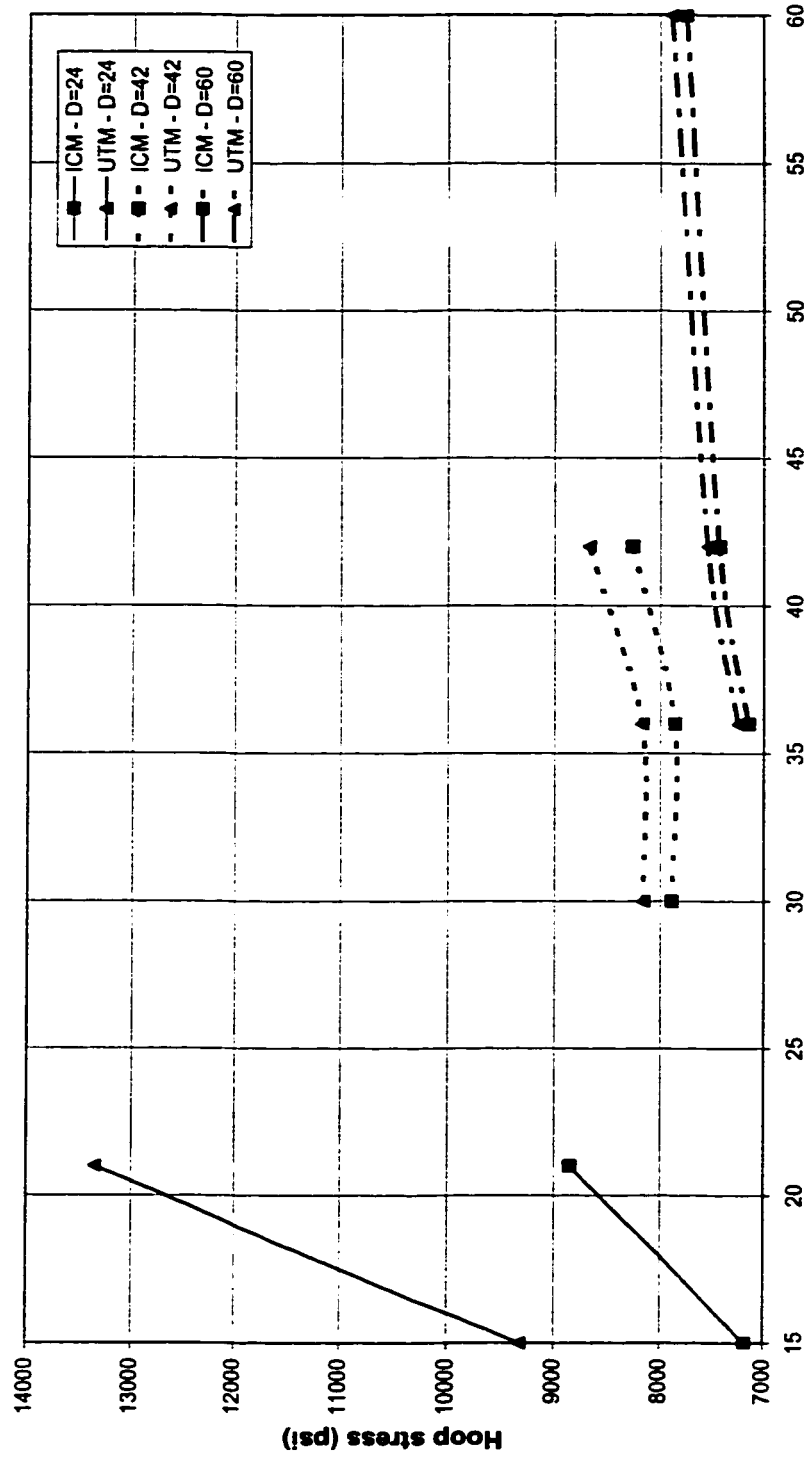

(f) R_b = 700 ft, θ = 15°

Figure A-4 (Contd.)

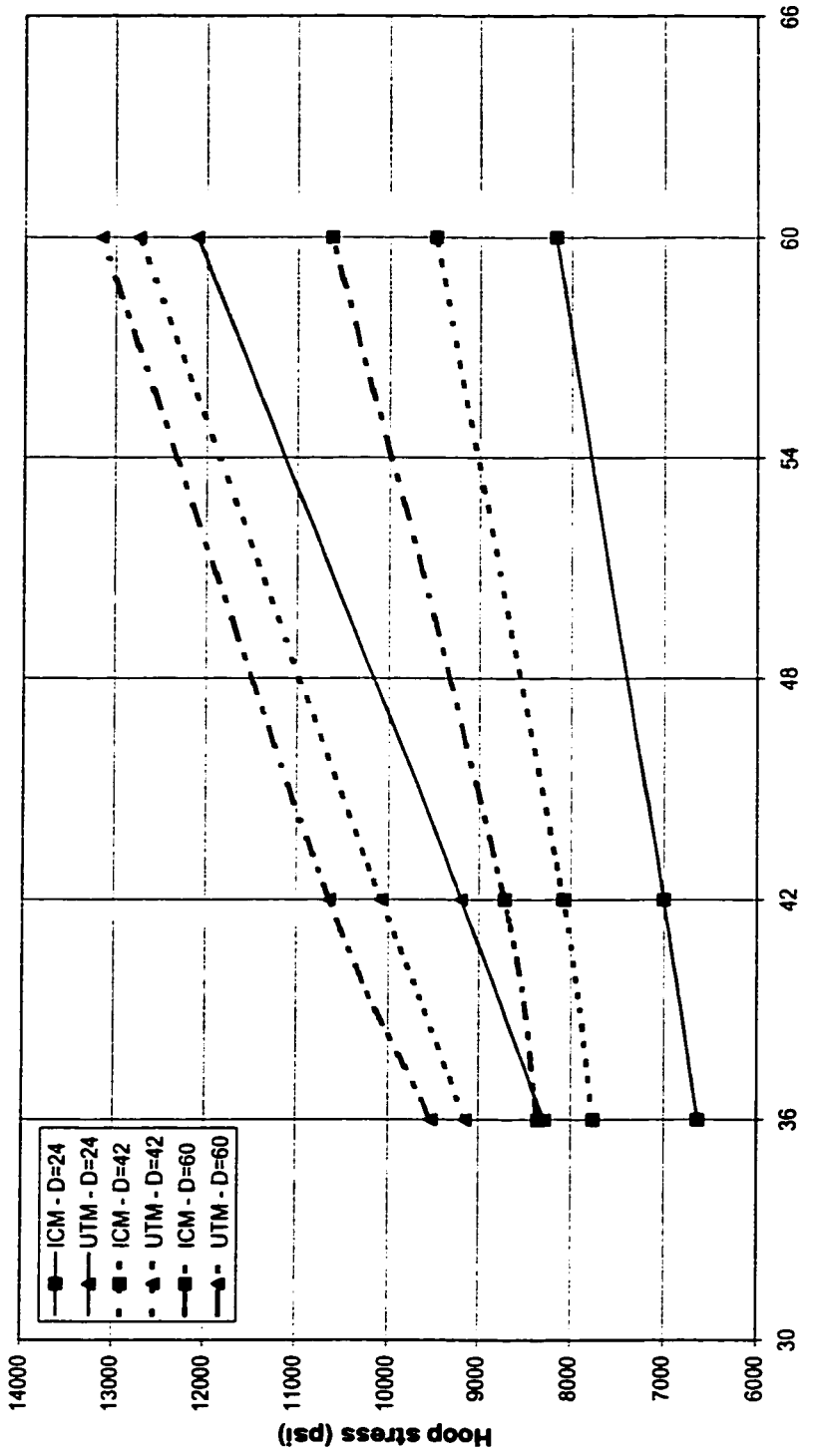

(g) R_b = 50 ft, $\theta = 8^\circ$

Figure A-4 (Contd.)

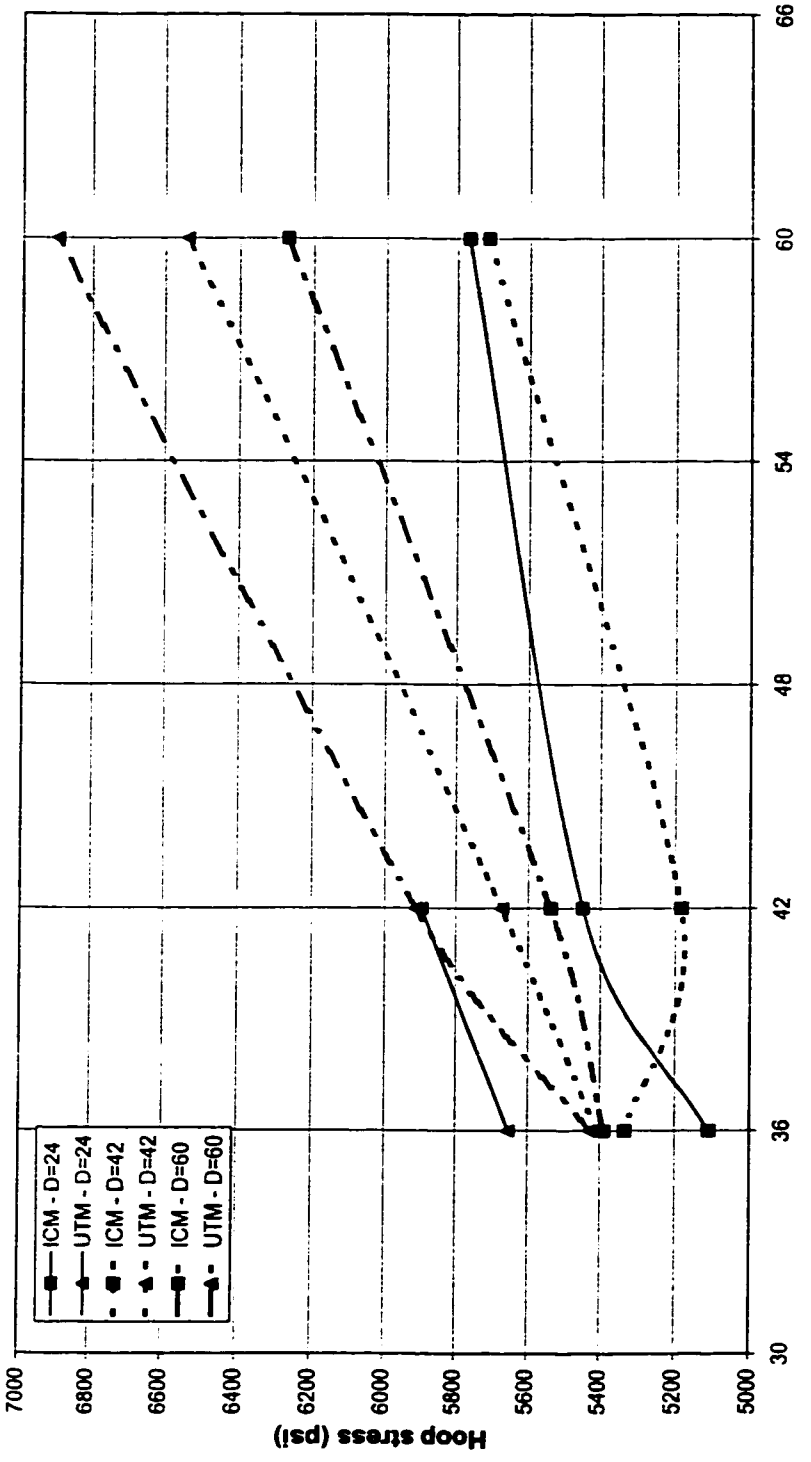

(h) R_b = 300 ft, θ = 8°

Figure A-4 (Contd.)

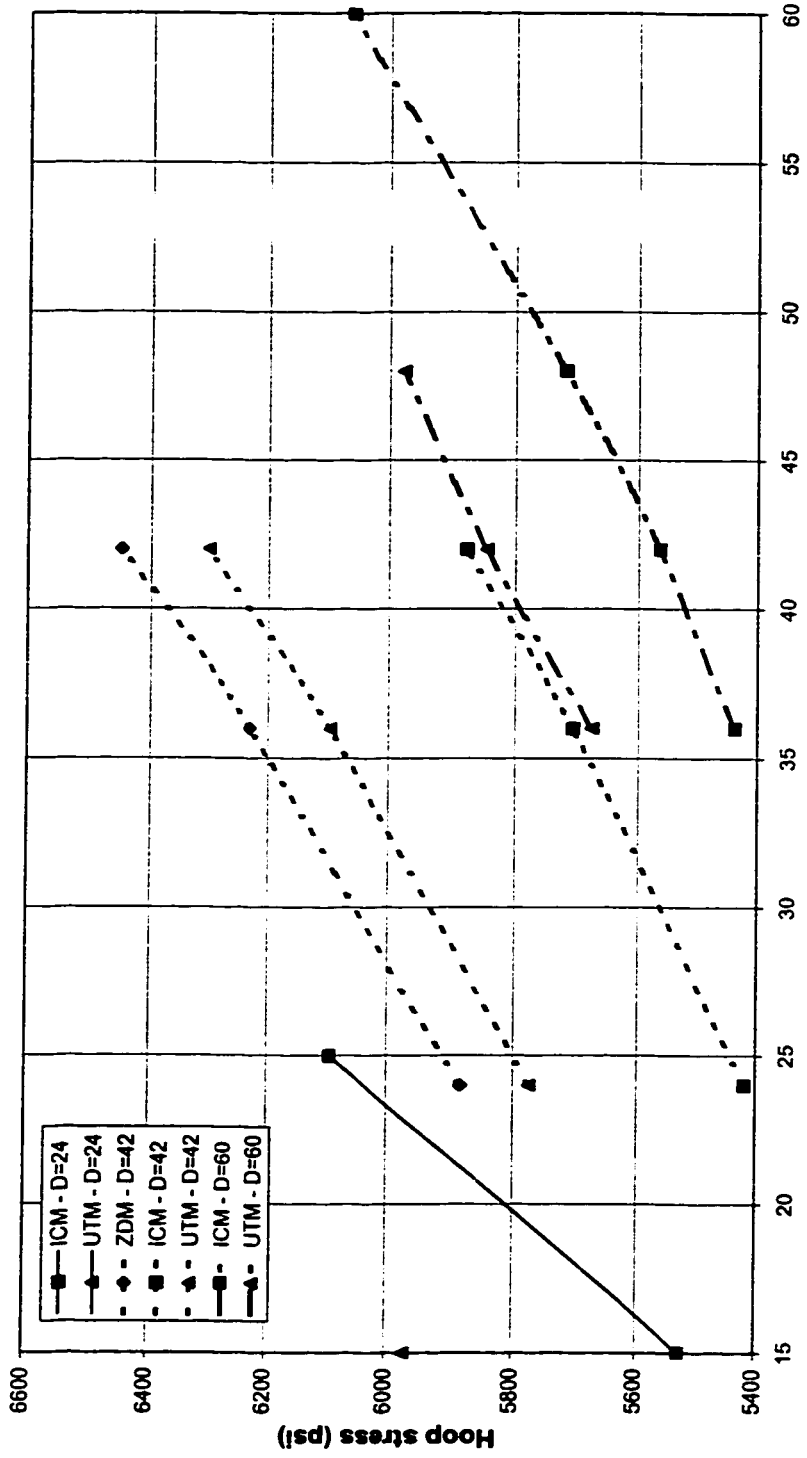

(i) R_b = 700 ft, $\theta = 8^\circ$

Figure A-4 (Contd.)

APPENDIX B

STRESSES IN THE HORIZONTAL BENDS

Table B-1 Maximum principal stresses corresponding to runs listed in Table 5-6

S. No.	D (in)	H_c (in)	R_b (ft)	θ (Degrees)	Maximum pipe principal stress (psi)					
					Installation Condition Method			Ultimate Temperature Method		
					Stress	x / θ_x	α	Stress	x / θ_x	α
1	24	24	50	15	22,952.57	1.9°	172.7°	24,248.73	1.9°	172.7°
2	42	24	50	15	30,435.45	1.3°	-172.5°	29,476.41	1.3°	-172.5°
3	60	24	50	15	36,953.23	3.7°	-172.4°	32,593.35	3.7°	-172.4°
4	42	24	300	15	22,990.85	0.6°	-157.6°	Not Found		
5	42	24	690	15	Not Found			Not Found		
6	42	24	50	45	11,369.26	3.7°	-86°	14,344.09	3.7°	-86°
7	42	24	50	85	9,975.13	534 in	-127.4°	10,679.48	3.5°	-70.5°
8	42	24	50	89	10,071.49	534 in	-127.4°	10,776.70	534 in	-127.4°
9	42	24	50	90	Not Solved			Not Solved		
10	24	48	50	15	Not Found			Not Found		
11	42	48	50	15	Not Found			Not Found		
12	60	48	50	15	Not Found			Not Found		

Table B-2 Maximum longitudinal stresses corresponding to runs listed in Table 5-6

S. No.	D (in)	H_c (in)	R_b (ft)	θ (Degrees)	Maximum pipe longitudinal stress (psi)					
					Installation Condition Method			Ultimate Temperature Method		
					Stress	x / θ_x	α	Stress	x / θ_x	α
1	24	24	50	15	22,154.01	1.9°	-158°	23,467.83	1.9°	-158°
2	42	24	50	15	30,427.50	1.3°	-172.5°	29,469.38	1.3°	-172.5°
3	60	24	50	15	36,952.55	3.7°	-172.4°	32,593.35	3.7°	-172.4°
4	42	24	300	15	22,241.87	0.6°	-157.6°	Not Found		
5	42	24	690	15	Not Found			Not Found		
6	42	24	50	45	9,170.75	3.7°	-144.5°	11,686.67	3.7°	-144.5°
7	42	24	50	85	6,405.28	534 in	-97.4°	8,182.06	534 in	-97.4°
8	42	24	50	89	6,456.69	534 in	-97.4°	8,197.29	534 in	-97.4°
9	42	24	50	90	Not Solved			Not Solved		
10	24	48	50	15	Not Found			Not Found		
11	42	48	50	15	Not Found			Not Found		
12	60	48	50	15	Not Found			Not Found		

Table B-3 Maximum hoop stresses corresponding to runs listed in Table 5-6

S. No.	D (in)	H_c (in)	R_b (ft)	θ (Degrees)	Maximum pipe hoop stress (psi)					
					Installation Condition Method			Ultimate Temperature Method		
					Stress	x / θ_x	α	Stress	x / θ_x	α
1	24	24	50	15	13,022.00	1.9°	-99°	13,737.62	1.9°	-99°
2	42	24	50	15	20,373.75	3.7°	-97.8°	19,712.19	3.7°	-97.8°
3	60	24	50	15	26,588.48	3.8°	-97.7°	23,326.15	3.8°	-97.7°
4	42	24	300	15	8,644.49	1.9°	-98°	Not Found		
5	42	24	690	15	Not Found			Not Found		
6	42	24	50	45	11,168.28	3.7°	-100.9°	13,691.42	3.7°	-100.9°
7	42	24	50	85	8,161.37	10.6°	-100.5°	10,211.35	10.6°	-100.5°
8	42	24	50	89	7,717.21	11.1°	-100.8°	9,568.63	11.1°	-100.8°
9	42	24	50	90	Not Solved			Not Solved		
10	24	48	50	15	Not Found			Not Found		
11	42	48	50	15	Not Found			Not Found		
12	60	48	50	15	Not Found			Not Found		

APPENDIX C

MICROSOFT EXCEL MACROS FOR THE AUTOMATION OF DATA FILE PREPARATION AND POST-PROCESSING

C.1 Introduction

The worksheets and the charts available in Microsoft Excel make it suitable for the data processing tasks such as the pre and post processing of the finite element analyses. Excel provides the facility of preparing macros to automate its tasks. These are programs, developed in *Visual Basic for applications*, which have a direct access to all Excel components.

The chances of errors and mistakes increase a lot if the huge data processing task of preparing the data file of the 3D buried pipe bend model and post processing its results is carried out manually. Excel macros are therefore prepared to automate the process. This increased the efficiency and reliability of the finite element analyses process carried out for the parametric study.

C.2 Macros for Data File Preparation

Two separate macros were prepared, one for the data file preparation of the horizontal bend models, and the other for the vertical bend models. An outline flowchart of the macros is shown in Figure C-1. The macros get their input from the worksheets, which are prepared as shown in Table 4-1. Only the basic data, which includes pipe diameter, D/t ratio, cover depth, bend radius, bend angle, etc. are required to be provided in the data worksheet. The macro calculates the data that is obtained using the basic data and fills the corresponding fields in the worksheet. The

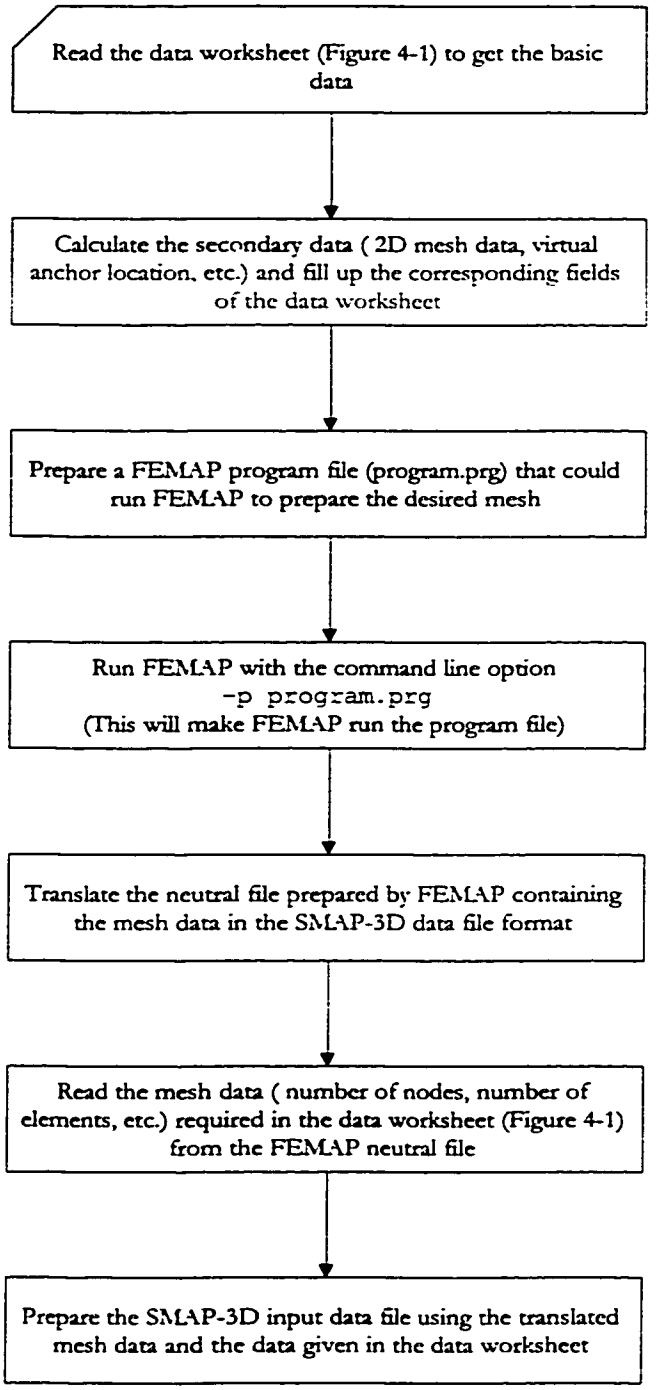

Figure C-1 Flow chart of the macros that prepare the SMAP-3D input data file for the buried pipe bend models

macro runs FEMAP using a FEMAP program file, which is prepared according to the mesh parameters given in the worksheet. The macro translates the FEMAP neutral file and prepares the SMAP-3D input data file using the translated data and the data given in the worksheet.

C.3 Macros for Post-processing

Macros were prepared to get load – displacement curves from the SMAP-3D output files. The macro prepared for the vertical bend models gives a curve similar to that shown in Figure 5-1. Similarly, the macro prepared for the horizontal bend models gives curves similar to those shown in Figure 5-10. After each finite element run, the macro is executed to obtain the curves, which are then visually investigated to see if a stable solution is obtained.

Additional macros were prepared to get the results according to ICM and UTM. The vertical bend macro prepares tables similar to the one shown in Table 5-2. Similarly the horizontal bend macro prepares tables similar to that shown in Table 5-6. These macros also prepare the maximum stress tables as shown in Appendices A and B.

NOMENCLATURE

A = arching factor

A_c = surface area per unit length of a pipe

A_s = material area along the pipe cross-sectional

B_d = trench width at the grade level

C = cohesion of a soil.

C_d = Marston's soil load coefficient

C_k = a factor used in the calculations of k_h

D = pipe outer diameter

E = modulus of elasticity

F = force generated against uplift/lateral movement of a buried pipe

f = pipe-soil friction force per unit length of the pipe

F_m = maximum force generated against uplift/lateral movement of a buried pipe

F_{max} = maximum axial force in a pipe

G_f = specific gravity of the pipe contents

G_s = specific gravity of the continuum element

H = depth of pipe center below grade

H_c = depth of pipe crown below ground surface

I = moment of inertia of the pipe cross-section

K = coefficient of lateral soil stress

K_o = coefficient of lateral soil stress at rest

k = soil modulus of subgrade reaction

k_h = modulus of horizontal subgrade reaction

k_v = modulus of vertical subgrade reaction

L_{inf} = influence length of a pipe connected to a bend

L_{va} = distance of virtual anchor from the end of the straight pipe

n = porosity of soil/continuum element

N_h = dimensionless factor to quantify the strength of buried pipe against lateral movement

N_v = dimensionless factor to quantify the strength of buried pipe against uplift

p = pipe internal pressure

P_c = confining pressure of soil weight on pipe

p_i = vertical pressure on a buried pipe at the crown

p_v = the free-field vertical stress at the elevation of the pipe crown = γH_c

r = radius to pipe wall center line

R_b = pipe bend radius

R_e = radius used for the circular extrusion of L_{va}-L_{inf} length in the case of vertical buried pipe bend mesh

R_ψ = location on the longitudinal axis of the pipe, corresponding to the angle ψ.

S_{eff} = Total effective stress in the pipeline as defined in API-RP 1102 (1993)

t = pipe thickness

W_p = weight of a pipe and its contents per unit length of the pipe

W_s = earth load per unit length of a pipe

(x_b,y_b) = location on the pipe longitudinal axis where bend joins straight pipe with respect to the mesh global coordinate system

(x_c,y_c) = location of pipe bend center with respect to the mesh global coordinate system

(x_i,y_i) = location on the pipe longitudinal axis at the end of influence length with respect to the mesh global coordinate system

y = depth below grade

Y = vertical displacement of the buried pipe

Y_f = vertical displacement associated with maximum uplift force F_m

y_p = depth below the pipe center at the apex of a pipe bend

Z = horizontal displacement of the buried pipe

Z_f = horizontal displacement associated with maximum uplift force F_m

ΔT = temperature change

Ω = effective length parameter

α = coefficient of thermal expansion

β = pipe/soil system characteristic

ϕ = angle of internal friction of a soil

γ = unit weight of the soil

γ_f = unit weight of the contents of a pipe

γ_p = unit weight of the pipe material

γ_s = unit weight of the shell element

γ_w = unit weight of water = 62.43 pcf = 0.03613 pci

μ = coefficient of friction between the soil and the pipe material

ν = Poisson's ratio

θ = angle of a pipe bend

σ_l = net longitudinal stress in a constrained pipe, positive in compression.

σ_p = Poisson's effect stress in a constrained pipe, positive in compression

σ_T = temperature stress in a constrained pipe, positive in compression

ψ = angle used in locating a section of nodes to be moved from circular extrusion to a position along the actual longitudinal axis of the pipe

REFERENCES

Abduljauwad, S. N. (1999). "Interaction of Buried Pipeline with Surrounding Soils." *Proceedings of the Fifth Saudi Engineering Conference* Civil Engineering, College of Engineering & Islamic Architecture, Umm Al-Qura University, Makkah, Kingdom of Saudi Arabia, 3, 259-269.

Al-Ghamedy, H. N. (1997). "Analysis and Design of Pipeline Stiffened-Anchor Plate/Flange." *International Journal of Pressure Vessels and Piping* 72, 131-137.

Altaee, A., and Boivin, R. (1995). "Laterally Displaced Pipelines: Finite Element Analysis." *Proceedings of the 14th International Conference on Offshore Mechanics and Arctic Engineering* Part 5 (of 6), ASME, New York, 209-216.

Altaee, A., Fellenius, B. H., and Salem, H. (1996). "Finite Element Modeling of Lateral Pipeline-Soil Interaction." *Proceedings of the 15th International Conference on Offshore Mechanics and Arctic Engineering* Part 5 (of 6), ASME, New York, 333-341.

Antaki, G. (1997). "A Review of Methods for the Analysis of Buried Pressure Piping." *Welding Research Council Bulletin 425* September.

API-RP 1102 (1993). *Steel Pipelines Crossing Railroads and Highways* American Petroleum Institute, Washington, D.C.

ASME-B31.1 (1992). "Appendix VII-Nonmandatory Procedures for the Design of Restrained Underground Piping." *Power Piping* ASME, New York.

ASME-B31.4 (1992). *Liquid Transportation Systems for Hydrocarbons, Liquid Petroleum Gas, Anhydrous Ammonia, and Alcohols* ASME, New York.

ATV (Abwassertechnische Vereinigung e. V.) (1988). *Regelwerk-Abwasser-Arbeitsblatt A 127* Richtlinien fur die statische Berechnung von Entwasserung-Skanalen und leitungen, Germany.

Audibert, J. M. E., and Nyman, K. J. (1977). "Soil Restraint Against Horizontal Motion of Pipe." *Journal of Geotechnical Engineering Division* ASCE, 103, GT10, October, 1119-1142.

Badi, S. S., and Salmon, D. C. (1997). "Three-Noded Curved Isoparametric Soil Interface Element." *Computers and Structures* 65 (2), 205-212.

Bathe, K. J. and Almeida C. A. (1982). "A Simple and Effective Pipe Elbow Element-Linear Analysis." *Journal of Applied Mechanics* 47, 93-100.

Burns, J. Q., and Richard, R. M., (1964). "Attenuation of Stresses for Buried Cylinders." *Proceedings, Symposium on Soil Structure Interaction University of Arizona*, 378-392.

CANDE (1989). *CANDE-89 Culvert ANalysis and DEsign computer program* User's Manual, Report No. FHWA-RD-89-169, Author: Musser, S. C., Federal Highway Administration, VA.

CGL (Committee on Gas and Liquid Fuel Lines) (1984). *Guidelines for the Seismic Design of Oil and Gas Pipelines Systems* American Society of Civil Engineers, New York, New York.

Chiou, Y. J., and Chi, S. Y. (1993). "Limit Loads of Buried Pipes in Inelastic Soil Medium." *Journal of Engineering Mechanics* ASCE, 119 (5), 938-954.

Chua, K. M., and Lytton, R. L. (1985). *Design of Large-Diameter Flexible Pipes In Trench: The Design and Results of the Factorial Analysis* Research Report, Project RF488800 Texas Transportation Institute, Texas A & M University, College Station, Texas.

Chua, K. M., and Lytton, R. L. (1989). "Viscoelastic Approach to Modeling Performance of Buried Pipes." *Journal of Transportation Engineering* ASCE, 115 (3), May, 253-269.

Dar, S. M., and Bates, R. C. (1974). "Stress Analysis of Hollow Cylindrical Inclusions." *Journal of Geotechnical Engineering Division* ASCE, 100, GT2, February, 123-138.

De Melo, F. J. M. Q., and De Castro, P. M. S. T. (1992). "A Reduced Integration Mindlin Beam element for Linear Elastic Stress Analysis of Curved Pipes Under Generalized In-Plane Loading." *Computers and Structures* 43 (4), 787-794.

Dickin, E. A. (1994). "Uplift Resistance of Buried Pipelines in Sand." *Soil and Foundations* 34(2), June, 41-48.

Duncan, J. M. (1979). "Behavior and Design of Long-Span Metal Culverts." *Journal of Geotechnical Engineering* ASCE, 105, GT3, 399-418.

Duncan, J. M., Byrne, P., Wong, K. S., and Mabry, P. (1980). *Strength, Stress- Strain and Bulk-Modulus Parameters for Finite Element Analysis of Stresses and Movements in Soil Masses* University of California, College of Engineering, Berkley, California, Report No. UCB/GT/80-01.

Einstein, H. H., and Schwartz, C. W. (1979). "Simplified Analysis for Tunnel Supports." *Journal of Geotechnical Engineering* ASCE, 105, GT4, 499-518.

FEMAP (1996 a). *FEMAP User's Manual* Version 4.5 for Windows, Enterprise Software Products, Inc.

FEMAP (1996 b). *Introduction to FEA Using FEMAP* Enterprise Software Products, Inc.

Findlay, G. E., and Spence, J. (1979). "Stress Analysis of Smooth Curved Tubes with Flanged End Constraints." *International Journal of Pressure Vessels and Piping* 7,83-103.

Gabriel, L. H., and Dabaghian, L. (1967). "An Analytical Experimental Method for Determining Interfall Tractions for Buried Structures Subjected to Static Loads." *Highway Research Record* 185,51-72.

Gerbault, M. (1985). "Cacul des canalisations circulaires semi-rigides." *Annales des l'Institut du Batimentet des Travaux Publics* No. 439 Série Théories et Méthodes de Calcul 278, Paris, France.

Gerbault, M. (1995). "Soil-Structure Interaction Model." *Proceedings of the 2nd International Conference on Advances in Underground Pipeline Engineering* ASCE, New York, 42-53.

Goodling, E. C. Jr. (1997). "Quantification of Nonlinear Restraint on the Analysis of Restrained Underground Piping." *Proceedings of the 1997 ASME Pressure Vessels and Piping Conference* Pressure Vessels and Piping Division, ASME, New York, PVP v 356, 107-116.

Gresnight, A. M., and van Foeken, R. J. (1995). "Strength and deformation Capacity of Bends in Pipelines." *International Journal of Offshore Mechanics and Polar Engineering* ISOPE, 5(4), 294-307.

Heger, F. J., Liepins, A. A., and Selig, E. T. (1985). "SPIDA: An analysis and Design System for Buried Concrete Pipe." *Proceedings of the International Conference on Advances in Underground Pipeline Engineering* ASCE, 143-154.

Hetenyi, M. (1946). *Beams on Elastic Foundation* University of Michigan Press, Ann Arbor.

Hibbett, H. D. (1974). "Special Structural Elements for Piping Analysis." *ASME Special Publication, Pressure Vessels and Piping: Analysis and Computers* Editors: Tuba, I. S., Selby, R. A., and Wright, W. B., ASME, New York, 1-10.

Hoëg, K. (1968). "Stresses Against Underground Structural Cylinders." *Journal of Soil Mechanics and Foundations Division* ASCE, 94, SM4, July, 833-857.

Hose, D. R. and Kitching, R. (1993). "Behaviour of GRP Smooth Pipe Bends with Tangent Pipes Under Flexural or Pressure Loads: A Comparison of Analysis by Conventional and Finite Element Techniques." *International Journal of Mechanical Sciences* 35(7), 549-575.

Hsu, T. W. (1996). "Soil Restraint Against Oblique Motion of Pipelines in Sand." *Canadian Geotechnical Journal* 33(1), 180-188.

Hsu, T. W. (1993). "Rate Effect on Lateral Soil Restraint of Pipelines." *Soils and Foundations* 33(4), 159-169.

Jeyapalan, J. K., Ethiyajeevakaruna, S. W., and Boldon, B. A. (1987). "Behaviour and Design of Buried Very Flexible Plastic Pipes." *Journal of Transportation Engineering* 113 (6), 642-657.

Jeyapalan, J. K., Thiyaggaram, M., Saleira, W. E., and Magid, B. A. (1989). "Analysis and Design of RPM and Other Composite Underground Pipelines." *Journal of Transportation Engineering* ASCE, 115 (3), May, 219-231.

Jeyapalan, J. K. (1990). "Advances in Pipeline Material and Design in Europe and North America." *Proceedings of the International Conference on Pipeline Design and Installations* ASCE, March, 1-16.

Kafka, P. G., and Dunn, M. B. (1956). "Stiffness of Curved Circular Tubes with Internal Pressure." *Trans. ASME* 78, 247-254.

Karadeniz, H. (1997). "An Interface Beam Element for the Analysis of Soil-Structure Interactions and Pipelines." *Proceedings of the seventh International Offshore and Polar Engineering Conference* Part 2 (of 4), ISOPE, Colorado, 286-292.

Karman, Th von (1911). "Über die Formänderung dünnwandiger Rohre, insbesondere federnder Ausgleichrohre." *Zeitschrift des Vereines deutscher Ingenieure* 55 (45), 1889-1895.

Katona, M. G., Smith, J. M., Odello, R. S., and Allgood, J. R., (1976). *CANDE - A Modern Approach for the Structural Design and Analysis of Buried Culverts* Report No. FHWA-RD-77-5, Federal Highway Administration, Washington, D. C.

Kondner, R. L., and Zelasko, J.S. (1963). "A Hyperbolic Stress-Strain Formulation for Sands." *Proceedings, 2nd Pan-American Conference on Soil Mechanics and Foundation Engineering* Brazil, I, 289-324.

Kulhawy, F. H., Trautmann, C. H., Beech, J. F., O'Rourke, T. D., McGuire, W., Wood, W. A. and Capano, C. (1983). "Transmission Line Structure Foundation for Uplift-Compression Loading." *Research Report EL-2870*, Electric Power Research Institute, Palo Alto, California.

Leonards, G. A., Juang, C. H., Wu, T. H., and Stetkar, R. E. (1985). "Predicting Performance of Buried Metal Conduits." *Transportation Research Record* 1008, TRB, National Research Council, Washington, D.C., 42-52.

Lucher, U. (1966). "Buckling of Soil-Surrounded Tubes." *Journal of Soil Mechanics and Foundations Division* ASCE, 92, SM6, November, 211.

Mackenzie, D., and Boyle, J. T. (1992). "A Simple Pipe Bend Element for Piping Flexibility Analysis." *International Journal of Pressure Vessels and Piping* 51 (1), 85-106.

Marston, A., and Anderson, A. O. (1913). *The Theory of Loads on Pipes in Ditches and Tests of Cement and Clay Drain Tile and Sewer Pipes* Bulletin No. 31 Iowa Engineering Experiment Station, Ames, Iowa.

Marston, A. (1930). *The Theory of External Loads on Closed Conduits in the Light of the Latest Experiments* Bulletin No. 96 Iowa Engineering Experiment Station, Ames, Iowa.

Mohri, Y., Tsurumaru, Y., and Asano, I. (1990). "Measured Performance and Numerical Analysis of Buried Pipes." *Proceedings of the International Conference on Pipeline Design and Installations* ASCE, March, 535-545.

Moore, I. D., and Booker, J. R., (1987). "Ground Failure Around Buried Tubes." *Rock Mechanics and Rock Engineering* 20, 243-260.

Moore, I. D. (1989). *Review of Buried Plastic Pipe Design* Report No. 039.05.89, The University of Newcastle, Australia.

Mouser, G. F. (1979). "Basic Pipe Stress Evaluation Summary." *Transportation Engineering Journal of ASCE* Proceedings of the American Society of Civil Engineers, 105(TE4), 349-359.

Natarajan, R. and Blomfield, J. A. (1975). "Stress Analysis of Curved Pipes with End Constraints." *Computers and Structures* 5, 187-196.

Nayman, K. J. (1984). "Soil Response Against Oblique Motion of Pipes." *Journal of Transportation Engineering* 110(2), 190-202.

Ng, P. C. F., Pyrah, I. C., and Anderson, W. F., (1997). "Prediction of Soil Restraint to a Buried Pipeline Using Interface Elements." *Numerical Models in Geomechanics* Proceedings of the Sixth International Symposium, NUMOG VI, 469-487

Ohtsubo, M., and Watanabe, O. (1977)."Flexibility and Stress Factors of Pipe Bends-An Analysis by the Finite Ring Method." *Journal of Pressure Vessel Technology* ASME, 99, 281-290.

Ovesen, N. K. (1964). "Anchor Slab, Calculation Methods and Model Tests." *Bulletin 16* Danish Geotechnical Institute, Copenhagen, Denmark.

Pardue, T. E., and Vigness I. (1951). "Properties of Thin Walled Curved Tubes of Short Bend Radius." *Trans. ASME 73, 77-84.*

Peng, L. C. (1978). "Stress Analysis Method for Underground Pipe Lines, Part 1 and 2" *Pipeline Industry* April and May.

Poorooshasb, F., Paulin, M. J., Rizkalla, M., and Clark, J. I. (1994). "Centrifuge Modeling of Laterally Loaded Pipelines." *Transport Research Record* 1431, TRB, National Research Council, Washington, D.C., 33-40.

Prevost, R. C., and Kienow, K. K. (1994). "Basics of Flexible Pipe Structural Design." *Journal of Transportation Engineering* ASCE, 124 (4), July/August, 652-671.

Rajani, B., Zhah, C., and Kuraooka, S. (1996). "Pipe-Soil Interaction Analysis of Jointed Water Mains." *Canadian Geotechnical Journal* 33(3), 393-404.

Rodabaugh, E. C., and George, H. H. (1957). "Effect of Internal Pressure on Flexibility and Stress Intensification Factors of Curved Pipe or Welding Elbow." *Trans. ASME* 79.

Row, R. K., and Davis, E. H. (1982). "The Behavior of Anchor Plates in Sand." *Geotechnique* 32(1), March, 25-41.

SAES-L-051 (1996). "Construction Requirements For Cross-Country Pipelines," *Saudi ARAMCO Engineering Standard* Saudi Arabian oil Company (Saudi ARAMCO), Saudi Arabia.

Seed, R. B., and Duncan, J. M. (1985). "Earth Pressure and Surface Load Effects on Buried Pipelines." *Proceedings of the International Conference on Advances in Underground Pipeline Engineering* ASCE, 320-329.

Selig, E. T. (1988). "Soil Parameters for Design of Buried Pipelines." *Pipeline Infrastructure* Proceedings of the Conference sponsored by the Pipeline Division of ASCE, Editor: Bennett, B. A., 99-116.

Shinokawa, T., and Mitsui, Y. (1993). "Application of Boundary Element Method to Geotechnical Analysis." *Computers and Structures* 47 (2), 179-187.

SMAP-3D (1999). *SMAP-3D, Structure Medium Analysis Program* User's Manual, Version 4.0, Comtech Research, Clifton, Virginia.

Spangler, M. G. (1941). *Structural Design of Flexible Pipe Culverts* Bulletin No. 153 Iowa Engineering Experiment Station, Ames, Iowa.

Spangler, M. G. (1948). "Underground Conduits-an Appraisal of Modern Research." *Trans. ASCE* 113, 316.

Spangler, M. G., and Handy, R. L. (1982). *Soil Engineering* Fourth Edition, Harper & Row Publishers, New York, 727-798.

Thomson, G., and Spence, J. (1983). "Maximum Stresses and Flexibility Factors of Smooth Pipe Bends with Tangent Pipe Terminations Under In-Plane Bending." *Journal of Pressure Vessels Technology* 105, 329-336.

Trautmann, C. H., O'Rourke, T. D., and Kulhawy F. H. (1985 a). "Uplift Force-Displacement Response of Buried Pipe." *Journal of Geotechnical Engineering Division* ASCE, 111(9), September, 1061-1076.

Trautmann, C. H., and O'Rourke, T. D. (1985 b). "Lateral Force-Displacement Response of Buried Pipes." *Journal of Geotechnical Engineering Division* ASCE, 111(9), September, 1077-1092.

Vesić, A. S. (1971), "Breakout Resistance of Objects Embedded in ocean bottom." *Journal of Soil Mechanics and Foundation Division* ASCE, 94(SM9), 1183-1205

Vigness, I. (1943). "Elastic Properties of Curved Tubes." *Trans. ASME* 105-120.

Watkins, R. K. (1985). "Longitudinal Stresses in Buried Pipes." *Proceedings of the International Conference on Advances in Underground Pipeline Engineering* ASCE, 408-416.

Weiß, E., Lietzmann, A., and Rudolph, J. (1996). "Linear and Nonlinear Finite-Element Analyses of Pipe Bends." *International Journal of Pressure Vessels and Piping* 67 (2), 211-217.

Whatham, J. F. (1986). "Pipe Bend Analysis by Thin shell Theory." *Journal of Applied Mechanics* 53, 173-180.

Winkler, E. (1867). *Die leher von der elasticitaet and festigkeit* Prag, Dominicaus (Czechoslovakia), 182.

Yin, J. H., Paulin, M. J., Clark, J. I., and Poorooshasb, F. (1993). " Preliminary Finite Element Analysis of Lateral Pipeline/Soil Interaction and Comparison to Centrifuge Model Test Results." *Proceedings of the 12th International Conference on Offshore Mechanics and Arctic Engineering* Part 5 (of 6), ASME, New York, 143-155.